LABORATORY STUDIES OF THE MECHANICS OF STREAMS FLOWING OVER A MOVABLE BED OF FINE SAND

Thesis by

Norman Herrick Brooks

In Partial Fulfillment of the Requirements

for the Degree of

Doctor of Philosophy

California Institute of Technology

Pasadena, California

1954

ACKNOWLEDGMENTS

The writer would like to express his appreciation for the encouragement and generous assistance offered by Professor Vito A. Vanoni throughout the course of the research.

During the academic year, 1952-53, the writer carried on the research with the aid of a National Science Foundation Predoctoral Fellowship.

ABSTRACT

A laboratory study was made of the characteristics of streams flowing over a loose bed of fine sand in order to determine what factors govern the equilibrium rate of transportation of fine sand in suspension. Twenty-two experimental runs were performed in a 40-foot tilting flume for various conditions with bed sand of two different sizes (0.10 mm and 0.16 mm). Each run represented a uniform open-channel flow in equilibrium with the sand bed.

It was found that more than one equilibrium flow velocity and sediment discharge existed for a given depth, slope, and size of sand because of the extreme variability of channel roughness. At low velocities, the large irregular dunes which formed on the stream bed made the bed friction factor over six times larger than the friction factor for the smooth sand beds obtained at higher flow rates. Thus the transportation rate could not be expressed as a unique function of the bed shear stress, the channel geometry, and properties of the sand as has been supposed in all previous theories for the equilibrium transportation rate of suspended load.

By using the mean velocity and the depth (or the water discharge and sediment discharge) as independent variables, and slope as a dependent variable, an orderly qualitative relationship between the pertinent variables was obtained.

Because of the importance of the dunes in the mechanics of sediment-laden streams, a special study was made of their characteristics and the mechanisms of their formation and movement. The studies also included some theoretical and experimental investigations of the distribution of velocity and suspended sediment within the flow for runs with a smooth bed.

TABLE OF CONTENTS

TABLE OF CONTENTS

TABLE OF CONTENTS

TABLE OF CONTENTS

INTRODUCTION

Rivers are among the most important natural resources available for man's use, and must be developed wisely if the full benefit is to be derived from them. Since a river is not simply a flow of water, but a flow of water and sediment together, any study of river mechanics which considers only the water is inadequate. Even though the total discharge of sediment is usually very small compared with the water discharge, the sediment creates some difficult engineering problems in river control. Because flowing water has the capacity to transport sediment in varying amounts depending on the hydraulic conditions, a stream which is disturbed from its equilibrium by works of man may either erode or deposit sediment.

For example, when a dam is placed across a river, the sediment load is trapped in the reservoir with a resulting loss of storage. In addition, the stream bed may aggrade above the level of the reservoir in the approach reach where the stream is decelerated and thus has reduced transporting power. In the past, towns upstream from a reservoir, and apparently at a safe elevation, have been subjected to flood stages at normal river flow. Furthermore, downstream from a dam, the water will erode its bed to obtain a new sediment load, and may reduce the bed elevation so much that power plants no longer have sufficient tail-water elevation to prevent cavitation, and water diversion points for irrigation are left high and dry.

Consequently, intelligent management of rivers depends on a knowledge of the fundamental laws governing the transportation of sediment by flowing water, as well as ordinary laws of hydraulics for the flow of water by itself. Great progress has been made in the study of sediment transportation, but there are many phenomena which are not yet understood.

A stream moves sediment in several different ways. Relatively large grains move very close to the bed, by rolling and sliding, and are commonly referred to as the bed load. Smaller particles, of sand size, are lifted off the bed by the turbulent eddies and carried considerable distances before falling back to the bed, where they may come to rest, move further as bed load, or be resuspended.

The material which is carried in suspension in the stream is called suspended load. Although the individual particles do not stay suspended indefinitely, still there is a steady average concentration of suspended material at any level in the stream. Very fine materials, such as silts and clays, move almost entirely in suspension, except in special cases where the bed of the stream may also be of this very fine material. If no appreciable amounts of this fine material are found in the stream bed, this part of the suspended load is called the wash load, for the amount of it transported depends primarily on the amount supplied to the stream.

The distinction between the bed load and the suspended load near the bed is not sharply defined, because physically there are all gradations between rolling, or sliding, and suspension close to the bed. In sediment transportation theories the separation of the two is a matter of convenience and is not intended to be a rigorous division.

A more extensive general description of sedimentation problems and existing theory may be found in Reference 1.

One of the outstanding problems needing further study is the relationship of the suspended load to the bed material, bed configuration, and the hydraulics of the stream, for sizes of sediment found both in suspension and in the bed in significant quantities. The presence of material in

the bed indicates that the stream is loaded to its capacity, for it is unable to transport all the material of that size that is available. Theories developed to date yield satisfactorily only the relative distribution of sediment concentrations over the depth of the flow, but not the absolute concentrations or the total suspended sediment discharge. To show how limited the development of suspended sediment transportation theories has been, the problem might be roughly compared to the problem of turbulent flow in a pipe. It would be as if only the relative velocity distribution were known for a given pipe size and hydraulic gradient, without any knowledge of how the total discharge is related to the other variables.

The author devoted his research to laboratory studies of this problem of relating the absolute suspended load concentration to the other pertinent variables, for a stream flowing over a movable bed of fine sand. Actually, suspended sediment and the dunes which sometimes form on the movable bed have a profound effect on the hydraulics of the stream, as well as vice versa; hence the experimental research might better be considered an investigation of the mechanics of the stream as a whole.

A review and some extensions of suspended load theory will be taken up in Chapter I before the experimental work is described in later chapters in order to give the reader a better idea of exactly what the problem is.

In Chapter III, the apparatus and the various procedures used to obtain the fundamental experimental data are described. The sand characteristics are reported in Chapter IV. The methods for calculating the average and maximum bed shear, and the friction factor for the bed are explained in Chapter V. The experimental results are reported in Chapter VI, and some discussion of the results comprises Chapter VII. The conclusions are summarized in Chapter VIII.

The various letters and symbols used will be defined when they are first used, but for the convenience of the reader the notation has been summarized in Appendix A. The reference numbers used throughout the text refer to the numbered items in the list of references at the end of the text. Tables and figures are numbered consecutively from the beginning, but the equations are numbered separately for each chapter. In each equation number, the numeral preceding the decimal point refers to the chapter number, and the number following the decimal point is the serial number in that chapter.

The sediment terminology used herein generally follows the standard definitions given in Reference 2.

CHAPTER I

SUSPENDED SEDIMENT TRANSPORTATION THEORIES

In this chapter some of the basic suspended sediment transportation theories will be reviewed and extended. It will be shown that our present knowledge of the mechanics of streams flowing over movable beds of fine sand is so inadequate that more laboratory studies are needed before a realistic theory of suspended load transport can be formulated. The experimental studies performed by the author and described in later chapters will show that some widely held assumptions are erroneous.

The rate of suspended sediment transportation in a two-dimensional stream is the integral of the product of the sediment concentration and the stream velocity over the depth. The equations for the distribution of sediment concentration and some related problems will be examined in Sec. A, B, and C, and the problem of obtaining the suspended load discharge by integration will be considered in Sec. D.

A. DERIVATION OF THE SUSPENDED LOAD EQUATION

The suspended load equation is the name which will be used for the equation giving the distribution of the suspended sediment concentration over the depth in a two-dimensional stream. In this section this equation will be derived from the theory of turbulent diffusion.

Sediment may be carried in suspension in a flowing stream of water because of the turbulence naturally present. Without the turbulent diffusion of particles upward in the flow, the particles would eventually all settle to the bed of the stream. At any point in a two-dimensional flow in steady state, the rate of subsidence of the particles must be exactly balanced by the rate of upward diffusion. Hence, in order to derive an

equation for the distribution of suspended sediment, something must be known about the turbulent diffusion of discrete particles in a flowing stream.

Burgers (3) has shown from the statistical theory of turbulence that, in a field of homogeneous turbulence, the rate of diffusion or flux of particles, N, through a unit area in a dilute suspension is Ficklan and can be expressed as

$$N = -\epsilon_s \frac{dc}{dy} \tag{1.01}$$

where y = position (which will hereafter be considered the distance from the bed of a stream);

c = concentration of suspended particles at position y averaged over a period of time long enough to eliminate the turbulent fluctuations; and

ϵ_s = turbulent diffusion coefficient for the particles.

If the particles are very small, and have the same density as the fluid, then $\epsilon_s = \epsilon_o$, the diffusion coefficient for fluid particles or molecules. In the statistical theory of turbulence formulated by Taylor (4), it may be shown that ϵ_o is the integral of the Lagrangian correlation coefficient of the velocities of the fluid elements, $v(t)$, in the y-direction, or namely

$$\epsilon_o = \int_o^\infty \overline{v(t - t')\, v(t)}\; dt' \tag{1.02}$$

This expression applies strictly only to turbulence which is homogeneous, whereas the turbulence in a stream certainly is not. Nevertheless, Eq. 1.01, allowing ϵ_s to be variable, has been shown to be a reasonably good approximation by the experimental work of Vanoni (5) and Ismail (6)

on the distribution of suspended sediment in channels.

Eq. 1.02 is quite unworkable for ordinary purposes, making it necessary to find a simpler method of evaluating ϵ_o approximately for engineering applications. Burgers (3) showed further that the eddy viscosity in the Boussinesq equation for the shear stress in a turbulent flow is essentially a diffusion coefficient for momentum. The Boussinesq equation may be written as

$$\tau = \epsilon_m \frac{d(\rho u)}{dy} = \rho \epsilon_m \frac{du}{dy} \qquad (1.03)$$

where τ = Reynolds shear stress, or simply the flux of momentum,

ϵ_m = kinematic eddy viscosity or diffusion coefficient for momentum,

ρ = mass density of fluid, and

u = local mean stream velocity.

The momentum diffusion coefficient ϵ_m can be easily evaluated from the velocity profile for a two-dimensional or axially symmetric flow where the shear stress is a linear function of the distance from the wall. It may reasonably be expected that the diffusion coefficient for sediment ϵ_s is roughly proportional to the diffusion coefficient for momentum, ϵ_m, except in regions of small or zero shear as in the center of a pipe, (see Ismail (6)). It is convenient then to define a dimensionless coefficient β as

$$\beta = \frac{\epsilon_s}{\epsilon_m} \qquad (1.04)$$

Carstens (7) attempted to derive some information about β from an application of the Navier-Stokes equations to the motion of a small spher-

ical particle in an oscillating fluid. The author disagreed with Carstens in a published discussion (8), a reprint of which is included as Appendix B. Briefly, the discussion contended that since the properties of the diffusion are largely dependent on the nature of the turbulent motions of the fluid, no valid information about ϵ_s can be deduced purely on the basis of the equations for motion of a particle in a parcel of fluid undergoing simple harmonic motion.

From Burgers' work (3) it may be inferred that $\epsilon_s < \epsilon_m$ ($\beta<1$) and $\epsilon_s > \epsilon_m$ ($\beta>1$) are both physically plausible, and that generally $\epsilon_s < \epsilon_o$ and $\epsilon_m < \epsilon_o$.

With this background on turbulent diffusion, it is now possible to derive an equation for the variation of suspended sediment concentration with depth for two-dimensional flow. For a steady condition, the flux N defined by Eq. 1.01 in the positive y or upward direction must be just balanced by the rate of subsidence, i.e.

$$- \epsilon_s \frac{dc}{dy} = wc \qquad (1.05)$$

where w is the settling velocity of the particles. By Eqs. 1.04 and 1.03

$$\epsilon_s = \beta\epsilon_m = \beta \frac{\tau}{\rho \frac{du}{dy}} \qquad (1.06)$$

The variable shear stress may now be expressed in terms of the distance y from the bed, the total depth d, and the shear stress τ_o on the bed as

$$\tau = \tau_o \left(1 - \frac{y}{d}\right) \qquad (1.07)$$

The velocity gradient du/dy may be very conveniently derived from the von Karman universal velocity defect law (9)

$$\frac{u - u_{max}}{u_*} = \frac{1}{k} \ln \frac{y}{d}, \tag{1.08}$$

as $$\frac{du}{dy} = \frac{u_*}{ky} \tag{1.09}$$

wherein k = universal constant, and

$u_* = \sqrt{\frac{\tau_o}{\rho}}$ = shear or friction velocity.

This equation has been shown by Vanoni (10) to fit observed velocity profiles in open channels quite well.

Substituting Eqs. 1.07 and 1.09 into Eq. 1.06,

$$\epsilon_s = \beta k u_* y \left(1 - \frac{y}{d}\right). \tag{1.10}$$

Putting Eq. 1.10 into Eq. 1.05 and rearranging

$$\frac{dc}{c} = - \frac{w}{\beta k u_*} \frac{dy}{y \left(1 - \frac{y}{d}\right)} \tag{1.11}$$

With the change of variable

$$H = \frac{d - y}{y}, \tag{1.12}$$

$$dH = - \frac{d}{y^2} dy,$$

Eq. 1.11 simplifies to

$$\frac{dc}{c} = z \frac{dH}{H}, \tag{1.13}$$

or $$\frac{d (\ln c)}{d (\ln H)} = \frac{d (\log_{10} c)}{d (\log_{10} H)} = z \tag{1.14}$$

in which

$$z = \frac{w}{\beta k u_*} \tag{1.15}$$

Since z may usually be considered constant, integration of Eq. 113 yields

$$c \left(\frac{y}{d-y} \right)^z = \text{constant.} \tag{1.16}$$

Taking $c = c_a$ at $y = a$ as a boundary condition, the constant in Eq. 1.16 is $c_a \left(\frac{a}{d-a}\right)^z$, and Eq. 1.16 may be rewritten in the form commonly used in the literature, i.e.,

$$c = c_a \left(\frac{d-y}{y} \cdot \frac{a}{d-a}\right)^z . \tag{1.17}$$

But since a is any arbitrary level, it is sometimes convenient to let $a = d/2$ and c_{md} = concentration at mid-depth, making Eq. 1.17

$$c = c_{md} \left(\frac{d-y}{y}\right)^z \tag{1.18}$$

Either Eq. 1.17 or 1.18 will be called the suspended load equation. Eq. 1.17 was first given by Rouse (11) with a slightly different derivation using mixing length theory.

When c is plotted against (d-y)/y on logarithmic scales, Eq. 1.18 or 1.17 is a straight line with slope z. If for any reason, such as hindered settling rates at large concentrations, z may not be considered a constant over the depth, the curve will no longer be a straight line, but from the differential equation, Eq. 1.14, it is apparent that the slope of the curve at any point is still z as defined by Eq. 1.15.

The behavior of the suspended load equation near $y = 0$ and $y = d$ and the evaluation of the boundary condition will be discussed at length in Sec. C, after some consideration of the problem of nonuniformity of particles.

B. MODIFICATION OF THE SUSPENDED LOAD EQUATION FOR SUSPENSIONS OF NONUNIFORM PARTICLES

In this section, it will be shown how the equations for the diffusion of suspended sediment given in Sec. A can be applied to suspensions of

nonuniform particles. Throughout Sec. A it was presumed that all the particles have identical settling velocity; since this is an idealization never achieved in actuality, it is useful to see how much effect the settling velocity distribution of the particles may have on the suspended load equation and the slope of the concentration profile.

(1) General Frequency Distribution Function for Settling Velocity. First of all, it will be shown that the fundamental differential equation for the diffusion, Eq. 1.05, can be written in terms of the mean settling velocity, W, if the particles are not uniform. Let the frequency distribution function for the settling velocity, w, at any level y be defined by a function $\Phi(w,y)$ such that

$$\int_0^\infty \Phi(w,y)\,dw = c(y) \qquad (1.19)$$

where c(y) is the total concentration at the level y. By definition then, $\Phi(w,y)\Delta w$ is the concentration of particles, by weight, having settling velocity between $w - \frac{\Delta w}{2}$ and $w + \frac{\Delta w}{2}$ at level y.

Eq. 1.05 may now be applied to particles in the very small range $\left(w_1 - \frac{\Delta w}{2}\right) < w < \left(w_1 + \frac{\Delta w}{2}\right)$ to give the following:

$$\epsilon_s \frac{\partial}{\partial y}\left[\Phi(w_1,y)\right]\Delta w + w_1\Phi(w_1,y)\,\Delta w = 0.$$

The total derivative has been changed to a partial derivative because Φ is a function of two variables. Dividing by Δw, and dropping the subscript from w_1, since the relation applies for all w,

$$\epsilon_s \frac{\partial \Phi}{\partial y} + w\Phi = 0 \qquad (1.20)$$

Now to find the differential equation for the total concentration of all

the nonuniform particles, integrate Eq. 1.20 with respect to w

$$\int_0^\infty \epsilon_s \frac{\partial \Phi(w,y)}{\partial y} dw + \int_0^\infty w \Phi(w,y)\, dw = 0. \qquad (1.21)$$

From Eq. 1.10 it is seen that ϵ_s is independent of w provided β is constant for all w; for a limited range of w values, this is approximately true. Therefore, the first integral in Eq. 1.21 becomes

$$\int_0^\infty \epsilon_s \frac{\partial \Phi}{\partial y}\, dw = \epsilon_s \frac{d}{dy} \int_0^\infty \Phi(w,y)\, dw = \epsilon_s \frac{dc(y)}{dy}$$

by Eq. 1.19. The second integral in Eq. 1.21 is by definition the total concentration, c(y), multiplied by the weighted arithmetic mean of w, which will be designated W(y).

The final result is then

$$\epsilon_s \frac{dc}{dy} + W(y)\, c = 0, \qquad (1.22)$$

which differs from Eq. 1.05 only in that W, the mean value of w, is now a function of y. Hence the integration of Eq. 1.22 will not be the same as before, but all the substitutions and changes of variables of Eqs. 1.06 through 1.15 are still valid. In particular it may be noted that Eq. 1.14 becomes

$$\frac{d(\ln c)}{d(\ln H)} = Z(y) \qquad (1.23)$$

where now Z is defined as

$$Z(y) = \frac{W(y)}{\beta k u_*} \qquad (1.24)$$

Consequently, even for a nonuniform suspension, the slope of the c-H curve on logarithmic paper at any point is directly proportional to the weighted arithmetic mean of the settling velocities. This result is true irrespective of the nature of the distribution function $\Phi(w,y)$.

To find the total concentration, $c(y)$, at any elevation, one might seek to integrate Eq. 1.22. However, this is not yet possible because the function $W(y)$ is still unknown, and cannot be determined without knowledge of the distribution function $\Phi(w,y)$ for at least one value of y. Actually, since Eq. 1.20 is linear in $\Phi(w,y)$ the total concentration distribution, $c(y)$, for a given settling velocity distribution could also be found by superposition of solutions of Eq. 1.20.

(2) Normal Distribution Function for Settling Velocity. It will now be hypothesized that the frequency distribution of the settling velocity, w, at some level y = a follows the normal distribution function

$$\Phi(w,a) = \frac{c_a}{\sigma\sqrt{2\pi}} e^{-\frac{1}{2}\left(\frac{w - W_a}{\sigma}\right)^2} \tag{1.25}$$

wherein $W_a = W(a)$ = mean settling velocity at y = a,

σ = standard deviation of the settling velocity at y = a, and

$c_a = c(a)$ = total concentration at y = a.

The constants in Eq. 1.25 are such that

$$\int_{-\infty}^{\infty} \Phi(w,a)\, dw = c_a \tag{1.26}$$

If σ is small compared with W_a, the probability of having a negative w by Eq. 1.25 is extremely small; thus it is allowable to use $-\infty$ as the lower limit for convenience instead of 0, even though negative settling velocities may be impossible.

Now, the solution to Eq. 1.20, found for any particular value of w by analogy with Eqs. 1.05 and 1.17, is

$$\Phi(w,y) = \Phi(w,a) \left(\frac{d-y}{y}\,\frac{a}{d-a}\right)^{z} \tag{1.27}$$

where, as in Eq. 1.15, $z = \frac{w}{\beta k u_*}$. Substituting Eq. 1.25 for $\Phi(w,a)$ and

$$H = \frac{d-y}{y}, \quad H_a = \frac{d-a}{a} \tag{1.28}$$

into Eq. 1.27,

$$\Phi(w,y) = \frac{c_a}{\sigma\sqrt{2\pi}}\, e^{-\frac{1}{2}\left(\frac{w - W_a}{\sigma}\right)^2} \left(\frac{H}{H_a}\right)^{z} \tag{1.29}$$

Since the exponent z is a function of w, it will be necessary to simplify the algebra as follows:

$$\left(\frac{H}{H_a}\right)^{z} = e^{z \ln (H/H_a)} = e^{\frac{w}{\beta k u_*} \ln (H/H_a)} = e^{Bw}, \tag{1.30}$$

where $$B = \frac{\ln (H/H_a)}{\beta k u_*} . \tag{1.31}$$

Eq. 1.29 then simplifies to

$$\Phi(w,y) = \frac{c_a}{\sigma\sqrt{2\pi}}\, e^{Bw - \frac{1}{2}\left(\frac{w-W_a}{\sigma}\right)^2} \tag{1.32}$$

Now complete the square in the exponent as follows:

$$Bw - \frac{1}{2}\left(\frac{w-W_a}{\sigma}\right)^2 = -\frac{-2\sigma^2 Bw + w^2 - 2w W_a + W_a^2}{2\sigma^2}$$

$$= -\frac{w^2 - 2w(\sigma^2 B + W_a) + (\sigma^2 B + W_a)^2 - \sigma^4 B^2 - 2\sigma^2 B W_a}{2\sigma^2}$$

$$= -\frac{1}{2}\left(\frac{w - W_a - \sigma^2 B}{\sigma}\right)^2 + \frac{1}{2}\sigma^2 B^2 + B W_a$$

Substituting for the exponent in Eq. 1.32, the result is

$$\phi(w,y) = \frac{c_a}{\sigma\sqrt{2\pi}} e^{\frac{1}{2}\sigma^2 B^2 + BW_a} e^{-\frac{1}{2}\left(\frac{w - W_a - \sigma^2 B}{\sigma}\right)^2} \qquad (1.33)$$

From the second exponential factor it may be deduced that w is normally distributed with standard deviation σ for all y, but with a variable mean value

$$W(y) = W_a + \sigma^2 B$$

Simplifying on the basis of Eqs. 1.31 and 1.24,

$$W(y) = W_a \left(1 + \frac{\sigma^2}{W_a^2} \frac{W_a}{\beta k u_*} \ln \frac{H}{H_a}\right), \text{ or}$$

$$W(y) = W_a \left(1 + \frac{\sigma^2}{W_a^2} Z_a \ln \frac{H}{H_a}\right) \qquad (1.34)$$

where, as in Eq. 1.28, $H = \frac{d - y}{y}$.

To illustrate the use of Eq. 1.34, consider the following example. For a sieve fraction in a $\sqrt{2}$ sieve series, a reasonable estimate for the standard deviation of w for fine sand is $\sigma = 0.2\, W_a$. A common value for the exponent is $Z_a = 1.0$, and for convenience let $a = d/2$. Then

$$W(y) = W_a\left[1 + .04 \ln \left(\frac{d - y}{y}\right)\right] ;$$

at $y = .05d$, $W(.05d) = 1.12\, W_a$; and at $y = .95\, d$, $W(.95d) = .88\, W_a$. Hence the mean settling velocity drops 21% between the levels $y = .05\, d$ and $y = .95\, d$.

There are now two alternatives for finding the distribution of the total concentration, c(y). The first way, which is the simplest, is to substitute Eq. 1.34 into Eqs. 1.23 and 1.24, thus obtaining

$$\frac{d(\ln c)}{d(\ln H)} = Z(y) = Z_a \left(1 + \frac{\sigma^2}{W_a^2} Z_a \ln \frac{H}{H_a}\right) . \qquad (1.35)$$

Hence, as y increases (and H decreases) the slope Z(y) decreases in exactly the same manner as W(y). Integrating Eq. 1.35 directly with respect to ln H, or ln H/H_a, and adjusting the constants so that $c = c_a$ at $H = H_a$, the final result is

$$\ln \frac{c}{c_a} = Z_a \ln \frac{H}{H_a} + \frac{1}{2} \frac{\sigma^2}{W_a^2} Z_a^2 \left(\ln \frac{H}{H_a}\right)^2 \qquad (1.36)$$

Eq. 1.19, the definition of $\phi(w,y)$, shows that c(y) can also be found by integrating $\phi(w,y)$ as expressed in Eq. 1.33 with respect to w. It may be readily shown that the result is identical to Eq. 1.36.

To show the order of magnitude of the deviation of Eq. 1.36 from the simple suspended load equation, Eq. 1.17, consider again the example given for showing the variation of W(y). With $\frac{\sigma}{W_a} = 0.2$ and $Z_a = 1$ at $a = d/2$, Eq. 1.36 becomes

$$\ln \frac{c}{c_a} = \ln H + 0.02 (\ln H)^2$$

$$\log_{10} \frac{c}{c_a} = (\log_{10} H) (1 + 0.046 \log_{10} H) . \qquad (1.37)$$

Eq. 1.37 is plotted in Fig. 1 along with Eq. 1.18 for $z = 1$. For this example the differences between the precise equation, Eq. 1.37, and the approximation Eq. 1.18 are rather small except extremely close to $y = 0$ and $y = d$.

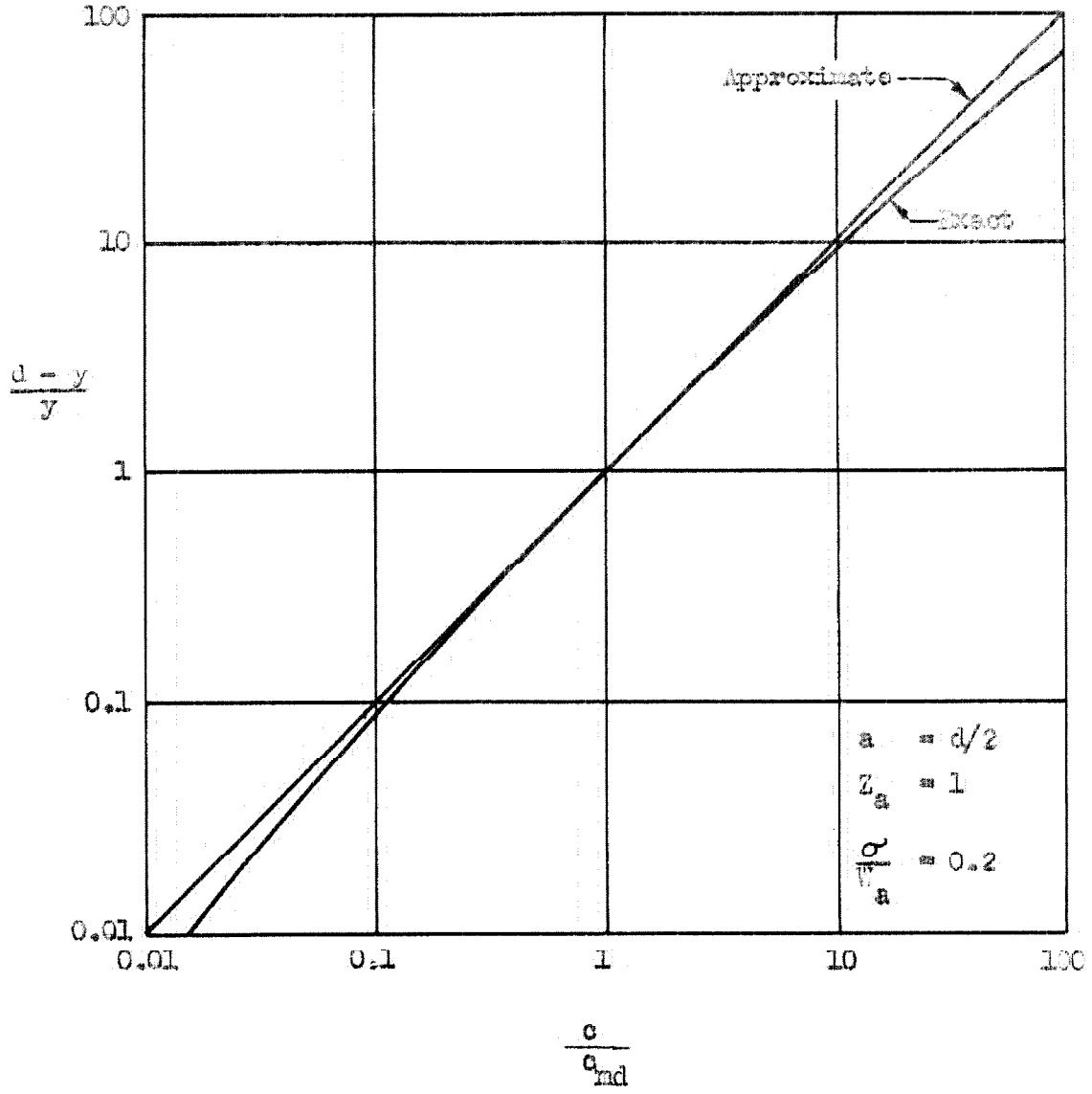

Fig. 1. Comparison of exact suspended load equation for a suspension with normally distributed settling velocities (Eq. 1.37) with approximate equation based on mean settling velocity only (Eq. 1.18) for the numerical values indicated.

The following conclusions may be drawn. First, even if an experimentally determined concentration profile, plotted as in Fig. 1, cannot be represented by a straight line, the slope of the tangent to the curve at any point is still directly proportional to the mean settling velocity at that point by Eq. 1.24.

Secondly, the simple suspended load equation (Eq. 1.18) can be used with reasonable accuracy for the analysis of a suspended sediment distribution provided individual sieve fractions in a $\sqrt{2}$ or $\sqrt[4]{2}$ series are considered separately. The use of larger sieve intervals is not recommended, for the errors involved in using Eq. 1.18 increase rapidly with increasing standard deviation of the settling velocities, as may readily be demonstrated from Eqs. 1.35 or 1.36.

C. THE BOUNDARY CONDITION FOR THE SUSPENDED LOAD EQUATION

The suspended load equation (Eq. 1.17 or 1.18) is clearly inadequate near the bed, for as $y \to 0$, $c \to \infty$. This singularity results from the fact that $\epsilon_s = 0$ at the bed by Eq. 1.10, making dc/dy in Eq. 1.05 become infinite. This difficulty at the bed makes it impossible to use a simple boundary condition at $y = 0$.

Physically however, it could have been expected that the suspended load equation would not be valid right down to the bed surface because the gradients of velocity and concentration become so large that the diffusion very close to the bed surface cannot be described by the Fickian relationship, Eq. 1.01. In fact, when y is no longer large compared with the scale of the turbulence, the use of differential calculus is not justified at all. Moreover, the logarithmic velocity law, Eq. 1.08, breaks down very close to the boundary. For a hydrodynamically smooth boundary, there

is a zone of essentially laminar flow known as the laminar sublayer, and for a hydrodynamically rough wall, the velocity becomes irregular very close to the individual roughness projections.

Very near the water surface the situation is much the same, and the suspended load equation cannot be expected to give accurate results. From Eq. 1.18, it may be seen that $c = 0$ at $y = d$ for all $z > 0$; however, for very fine material, such as silt or clay, it is easily observed that the concentration is not zero at the surface, as it should be by Eq. 1.18.

Lane and Kalinske (12) avoid this difficulty at the bed by taking ϵ_s in Eq. 1.05 equal to $\bar{\epsilon}_s$, the average value of ϵ_s given by Eq. 1.10. Since the distribution of ϵ_s is parabolic the average value is two-thirds of the maximum or

$$\bar{\epsilon}_s = \frac{1}{6} \beta k u_* d.$$

Assuming $k = 0.4$ and $\beta = 1$, and using $\bar{\epsilon}_s$, they obtained from the integration of Eq. 1.05

$$c = c_a \, e^{-\frac{15\, w}{u_*} \frac{y-a}{d}} \qquad (1.38)$$

in which c now approaches a definite limit as $y \to 0$. This is merely an artificial device for obtaining the limiting concentration at the bed, for no additional information about the mechanism of diffusion at the bed has been added; moreover, Eq. 1.18 is still preferred to Eq. 1.38 because it fits observed data better than Eq. 1.38.

Vanoni (5) has shown through extensive experimental investigations that the suspended load equation gives the relative concentration distribution quite well. In order to find the absolute concentrations some way must be found to evaluate c_a in Eqs. 1.17 or 1.38, or c_{md} in Eq. 1.18.

In the last analysis, the actual amount of material carried by a stream depends on the interchange mechanisms between the flow and its bed; as it has been pointed out, this is not a simple diffusion process, so more information or assumptions are needed to complete the theory.

Two methods for evaluating the constant c_a in the suspended load equation have been suggested. Lane and Kalinske (13), the first to study the problem, developed a bed pickup theory based on a comparison of the turbulent fluctuations of the vertical velocity near the bed with the settling velocity of the particles. However, their theory took no account of the hydrodynamic nature of the flow at the bed surface, as expressed by the bed Reynolds number

$$R_b = \frac{Du_*}{\nu} \tag{1.39}$$

in which D is the grain size, and ν is the kinematic viscosity. For clear flow, when R_b is less than about 5, the bed is hydrodynamically smooth, and when greater than 30, hydrodynamically rough. Since the mechanism of entrainment must certainly depend on R_b, Kalinske and Hsia (14) discarded the original theory in favor of the more general dimensionless relationship

$$\frac{c_a}{c_b} = f\left(\frac{w}{u_*}, \frac{Du_*}{\nu}\right) \tag{1.40}$$

where c_b = concentration of sediment of size D in the bed, and

c_a = concentration of same size sediment in the stream close to the bed.

Experimental data obtained by Hsia (14) and Pien (15) along with some miscellaneous field data were used in an attempt to define the func-

tion in Eq. 1.40. Since Hsia's experiments, which provided the most extensive data, were conducted in a flume with a movable bed of very fine silica flour, the relationship for the sand sizes is still not very well defined, and needs to be verified.

Furthermore, for sand the distance a from the bed at which the concentration is c_a by Eq. 1.40, needs to be carefully defined, inasmuch as the concentration changes very rapidly with y close to the bed. The Lane and Kalinske theory is weak at this point, because in their analysis this important distance is not defined. They suggest (12) that their simplified suspended load equation, Eq. 1.38, be used in conjunction with Eq. 1.40, by taking $a = 0$, and $c_a = c_o$; but for the more accurate equation, Eq. 1.17, a cannot be taken as 0. Anyway, there is no need to discuss their theory further, because it will be shown later from the experimental results that Eq. 1.40 is a completely inadequate approach for determining the equilibrium load of a stream.

A second approach has been proposed by Einstein (16). He arbitrarily assumes that all the bed load of a given grain size D moves within a "bed layer" of thickness 2D. He then assumes further that the constant c_a in the suspended load equation, Eq. 1.17, for $a = 2D$, or the top of the "bed layer", is equal to the average concentration of the bed load in the bed layer. The bed load is calculated by Einstein's bed load function, and the velocity with which the grains move is assumed to be proportional to u_*. Dividing the bed load per unit width by this velocity gives the amount of moving material per unit area of the bed, and dividing this quantity by 2D yields the concentration in the bed layer which is used as c_a.

Einstein has given only meager experimental evidence to justify

these somewhat cryptic assumptions. He asserts that flume experiments which he performed with sand mixtures verified his theory, but he failed to report any of the basic experimental data whatsoever. Therefore, it is impossible for anyone else to judge how well his theory checks his observations, and also precludes the possibility of checking any other sediment transportation theories with the data which he obtained. Moreover, in the short section of his report devoted to the flume experiments, he makes no statements at all with particular reference to the suspended load. The size analysis of the sediment used is not even reported.

This investigator felt that the approaches of Lane and Kalinske, and Einstein both had serious weaknesses and a certain amount of arbitrariness, and that further progress in relating the suspended load concentrations to the bed material could not be made until more information was obtained experimentally. Consequently, the research upon which this thesis is based was devoted primarily to further investigation of the mutual interactions between a flowing stream and a movable bed of fine sand. Some interesting results were obtained which show that the problem of determining the suspended load is more complex than previously realized because of the changing bed configuration. Unfortunately, a great deal more experimental work will have to be performed before the mechanics of streams carrying suspended load can be understood, and a reliable suspended load theory can be developed.

D. INTEGRATION FOR THE SUSPENDED LOAD DISCHARGE

Another problem of interest in two-dimensional suspended load theory is the development of a simple way in which the total suspended load discharge may be found from the concentration and velocity distributions

without resorting to numerical integration. The term, "suspended load discharge", as used in this thesis, means the total rate of transportation of sediment in suspension. The problem has been considered by both Lane and Kalinske (12), and Einstein (16), but both analyses need clarification, especially when they are applied to the integration of the load from measured concentration and velocity profiles.

The rate at which sediment is carried through a unit area normal to the stream is $\overline{c(y,t)\ u(y,t)}$. In this expression $c(y,t)$ and $u(y,t)$ are taken as the instantaneous values of concentration and stream velocity respectively, and the bar signifies average value with respect to time. If $\bar{c}$ and $\bar{u}$ are the time mean values of c and u, and c' and u' are the turbulent fluctuations, then

$$\begin{aligned}\overline{c(y,t)\ u(y,t)} &= \overline{(\bar{c} + c')(\bar{u} + u')} \\ &= \bar{c}\,\bar{u} + \bar{u}\,\overline{c'} + \bar{c}\,\overline{u'} + \overline{c'\,u'} \\ &= \bar{c}\,\bar{u} + \overline{c'\,u'}\end{aligned}$$

because $\overline{u'} = 0$ and $\overline{c'} = 0$. Since it may reasonably be assumed that the correlation between u' and c' is small, the term $\overline{c'u'}$ will be neglected. Moreover, the bars will be dropped from $\bar{c}$ and $\bar{u}$ to be consistent with the previous sections where c and u always refer to the time average values.

The total suspended load discharge per unit width, q_s, may now be expressed for a two-dimensional channel as the integral

$$q_s = \int_0^d cu\ dy. \qquad (1.41)$$

(1) Integration Using the Suspended Load Equation. In this section it will be shown how Einstein's procedure (16) for evaluating the integral for q_s (Eq. 1.41) can be made more general and more susceptible to general application.

If the velocity follows the von Karman velocity defect law, Eq. 1.08, rewritten as

$$u = u_{max} + \frac{u_*}{k} \ln \frac{y}{d}, \tag{1.42}$$

then by integration, the average velocity over the depth d is

$$\bar{u} = \frac{1}{d} \int_0^d \left(u_{max} + \frac{u_*}{k} \ln \frac{y}{d}\right) dy = u_{max} - \frac{u_*}{k} \tag{1.43}$$

Rewriting Eq. 1.42 with $\bar{u}$ instead of u_{max},

$$u = \bar{u} + \frac{u_*}{k} \left(1 + \ln \frac{y}{d}\right). \tag{1.44}$$

Now if the concentration distribution fits the suspended load equation, Eq. 1.18, then q_s by Eq. 1.41 becomes

$$q_s = c_{md} \int_0^d \left(\frac{d-y}{y}\right)^z \left[\bar{u} + \frac{u_*}{k} \left(1 + \ln \frac{y}{d}\right)\right] dy \tag{1.45}$$

Certain difficulties are now apparent. The integral above is improper because the integrand becomes infinite at the lower limit. It may be shown mathematically that the integral converges only for $z < 1$; for $z \geq 1$, the integral diverges to negative infinity.

Clearly the mathematical behavior of the expressions for c and u for y very near 0 has no physical meaning. The concentration actually must always remain finite, and the velocity approaches 0, not $-\infty$, as indicated by the logarithmic equation; in fact, it has been pointed out already that neither the suspended load equation nor the logarithmic velocity law was ever expected to apply right down to y = 0. Evidently, then, the lower limit y = 0 in Eq. 1.45 must be replaced by some small, but finite, physically reasonable value of y_o.

Before discussing further what the lower limit y_o should be, it will be convenient to simplify Eq. 1.45 by the change of variable $\eta = y/d$, giving:

$$q_s = c_{md}\,\bar{u}d \int_{\eta_o}^{1} \left(\frac{1-\eta}{\eta}\right)^z \left[1 + \frac{u_*}{k\bar{u}}\,(1 + \ln\eta)\right] d\eta \qquad (1.46)$$

where $\eta_o = y_o/d$ is now the lower limit. By writing $\bar{u}d = q$, the discharge per unit width, and separating into two integrals, Eq. 1.46 can be simplified to

$$\frac{q_s}{q\,c_{md}} = \left(1 + \frac{u_*}{k\bar{u}}\right) \int_{\eta_o}^{1} \left(\frac{1-\eta}{\eta}\right)^z d\eta + \frac{u_*}{k\bar{u}} \int_{\eta_o}^{1} \left(\frac{1-\eta}{\eta}\right)^z \ln\eta\, d\eta \qquad (1.47)$$

Fortunately, Einstein (16) has calculated and tabulated the values of these two integrals, which he designates as

$$J_1(z, \eta_o) = \int_{\eta_o}^{1} \left(\frac{1-\eta}{\eta}\right)^z d\eta \qquad (1.48)$$

and

$$J_2(z, \eta_o) = -\int_{\eta_o}^{1} \left(\frac{1-\eta}{\eta}\right)^z \ln\eta\, d\eta \qquad (1.49)$$

Thus Eq. 1.47 may be simply rewritten as

$$\frac{q_s}{q\,c_{md}} = J_1(z, \eta_o) + \frac{u_*}{k\bar{u}}\left[J_1(z, \eta_o) - J_2(z, \eta_o)\right] \qquad (1.50)$$

The left hand member, $\frac{q_s}{q\, c_{mc}}$, is the ratio of the suspended load discharge concentration, q_s/q, to the mid-depth concentration, c_{md}. If it is preferred to use c_a instead of c_{md}, then c_{md} may be replaced by $c_a(\frac{a}{d-a})^z$.

Eq. 1.50 is a perfectly general result which can be easily used in all cases where c follows the suspended load equation, and u the von Karman logarithmic velocity defect law. The parameters involved are essentially a slope and an intercept for each of the profiles; for the concentration, the intercept used is the mid-depth concentration c_{md}, and the slope is z on a logarithmic graph of c vs. $\frac{d-y}{y}$; for the velocity, the intercept is $\bar{u} = u(.37d)$ = average velocity, by Eq. 1.44, and the slope is $\frac{2.3u_*}{k}$ on a graph of u vs. $\log_{10} y$. Except for some assumption regarding η_o, absolutely no other information or assumption is needed.

Einstein (16) derived an expression equivalent to Eq. 1.50, but the constants have been so arranged and assumed that the basic relationship is obscured. His expression can be used conveniently only when $k = 0.4$, the lower limit is the same as the reference level (i.e. $\eta_o = a/d$,) and u_* and the apparent roughness of the surface are known. A further annoyance is the fact that he constructed charts, not of the simple integrals J_1 and J_2, but of I_1 and I_2 defined as

$$I_1 = 0.216 \frac{\eta_o^{z-1}}{(1-\eta_o)^z} \int_{\eta_o}^{1} \left(\frac{1-\eta}{\eta}\right)^z d\eta \qquad (1.51)$$

and

$$I_2 = 0.216 \frac{\eta_o^{z-1}}{(1-\eta_o)^z} \int_{\eta_o}^{1} \left(\frac{1-\eta}{\eta}\right)^z \ln \eta \, d\eta \qquad (1.52)$$

The factor 0.216 is simply an empirical constant used by Einstein in his theory; it is of no use here. Since double interpolation can be avoided

by using Einstein's charts for I_1 and I_2 instead of his tables for J_1 and J_2, it is more convenient to rewrite Eq. 1.50 in terms of I_1 and I_2 as follows:

$$\frac{q_s}{q\, c_{md}} = \frac{1}{0.216} \frac{(1-\eta_o)^z}{\eta_o^{z-1}} \left[I_1 + \frac{u_*}{k\bar{u}} (I_1 - I_2) \right] \qquad (1.53)$$

It is understood that I_1 and I_2 are functions of z and η_o. The charts of I_1 and I_2 are not reproduced here, but may be found, as mentioned above, in reference 16.

The factor $\frac{u_*}{k\bar{u}}$ may also be expressed in terms of the friction factor f by means of the Darcy-Weisbach formula as applied to channels, (17), namely

$$\frac{\bar{u}}{u_*} = \sqrt{\frac{8}{f}} \; ; \qquad (1.54)$$

hence

$$\frac{u_*}{k\bar{u}} = \frac{1}{k} \sqrt{\frac{f}{8}} \; . \qquad (1.55)$$

There are four possible ways to choose the lower limit $\eta_o = \frac{y_o}{d}$. Since the particles can scarcely be suspended closer to the bed than two particle diameters, Einstein (16) suggests using $\eta_o = \frac{2D}{d}$. In some cases this may be reasonable, but in other cases it is clearly not. If the sand bed is hydrodynamically smooth, then it is quite possible that the level $y_o = 2D$ will be well within the laminar sublayer. For clear flow, the thickness of the laminar sublayer is $\delta = \frac{11.6\,\nu}{u_*}$, but with sand in suspension producing marked reduction of k on the velocity profile equation, (Eq. 1.44), and an unknown effect on the kinematic viscosity near the bed, it is impossible as yet to define the thickness of the laminar sublayer exactly. However, if the investigator would like to assume that

$y_o = \delta \doteq \frac{11.6\nu}{u_*}$ as a lower limit, then $\eta_o \doteq \frac{11.6\,\nu}{u_* d}$. It should be noted, however, that in a sediment laden flow, the velocity at $y_o = \delta$ will generally not be $11.6\, u_*$ as the theory for clear flow predicts. Within the laminar sublayer the amount of transport is probably negligible.

Another possibility for η_o is to take it as the level for which $u = 0$ by an extrapolation of the logarithmic velocity profile. Admittedly, the formula does not apply all the way to $u = 0$, but on the other hand, it is quite possible that the velocity as determined from the fitted profile at $y_o = 2D$ will be negative. Thus if $\eta_o = \frac{2D}{d}$ is used as the lower limit, the suspended load integral may actually include some negative load contributions very close to the bed. However, if the level η_o corresponding to $u = 0$ is used, then the maximum possible value of $\int_o^1 cu\, dy$ will be obtained, and no negative values of the integrand cu will be included. In this case, Eq. 1.44 yields

$$0 = \bar{u} + \frac{u_*}{k}(1 + \ln \eta_o)$$

Solving for η_o,

$$\eta_o = e^{-k\frac{\bar{u}}{u_*} - 1}$$

Still another possibility for η_o is to let it be the level at which the concentration, by extrapolation of the fitted suspended load equation, becomes equal to the concentration of the bed material of the same size, c_b, expressed as weight per unit volume. Thus

$$c_b = c_{md}\left(\frac{1 - \eta_o}{\eta_o}\right)^z$$

and since $\eta_o << 1$,

$$\eta_o \approx \left(\frac{c_{md}}{c_b}\right)^{\frac{1}{z}} .$$

It would certainly be physically unreasonable to use a smaller lower limit than this, as is sometimes the case using $\eta_o = \frac{2D}{d}$, for then the integration would include values of $c > c_b$.

The four possibilities outlined above may now be summarized as follows:

$$\text{(a)} \quad \eta_o = \frac{2D}{d} \qquad \text{(Einstein bed layer)} \qquad (1.56)$$

$$\text{(b)} \quad \eta_o = \frac{11.6}{u_* d} \qquad \text{(Estimated laminar sublayer)} \qquad (1.57)$$

$$\text{(c)} \quad \eta_o = e^{-k\frac{\bar{u}}{u_*} - 1} \qquad u(\eta_o) = 0 \ . \qquad (1.58)$$

$$\text{(d)} \quad \eta_o \approx \left(\frac{c_{md}}{c_b}\right)^{\frac{1}{z}} \qquad c(\eta_o) = c_b \ . \qquad (1.59)$$

Perhaps the most reasonable choice of the four is the <u>largest</u> η_o because it has been shown that it is physically unreasonable to go lower than any one of the four. Further investigation is needed to determine whether or not this is a satisfactory approach.

Nonetheless, choice (c) warrants special attention. As Eq. 1.50 stands, $\frac{q_s}{q\, c_{md}}$ is a function of the three parameters η_o, z, and $k\frac{\bar{u}}{u_*}$; but by Eq. 1.58 η_o is a function of $k\frac{\bar{u}}{u_*}$, making it possible to represent Eq. 1.50 on a single chart. Fig. 2 was constructed on this basis from the values of the integrals J_1 and J_2 given by Einstein (16).

The use of Fig. 2 may be illustrated by the following example. From a measured velocity profile for a wide stream 3 ft deep, it is found that $\bar{u} = u(.37d) = 3.5$ ft/sec. The slope of the velocity profile = 1.25 ft/sec

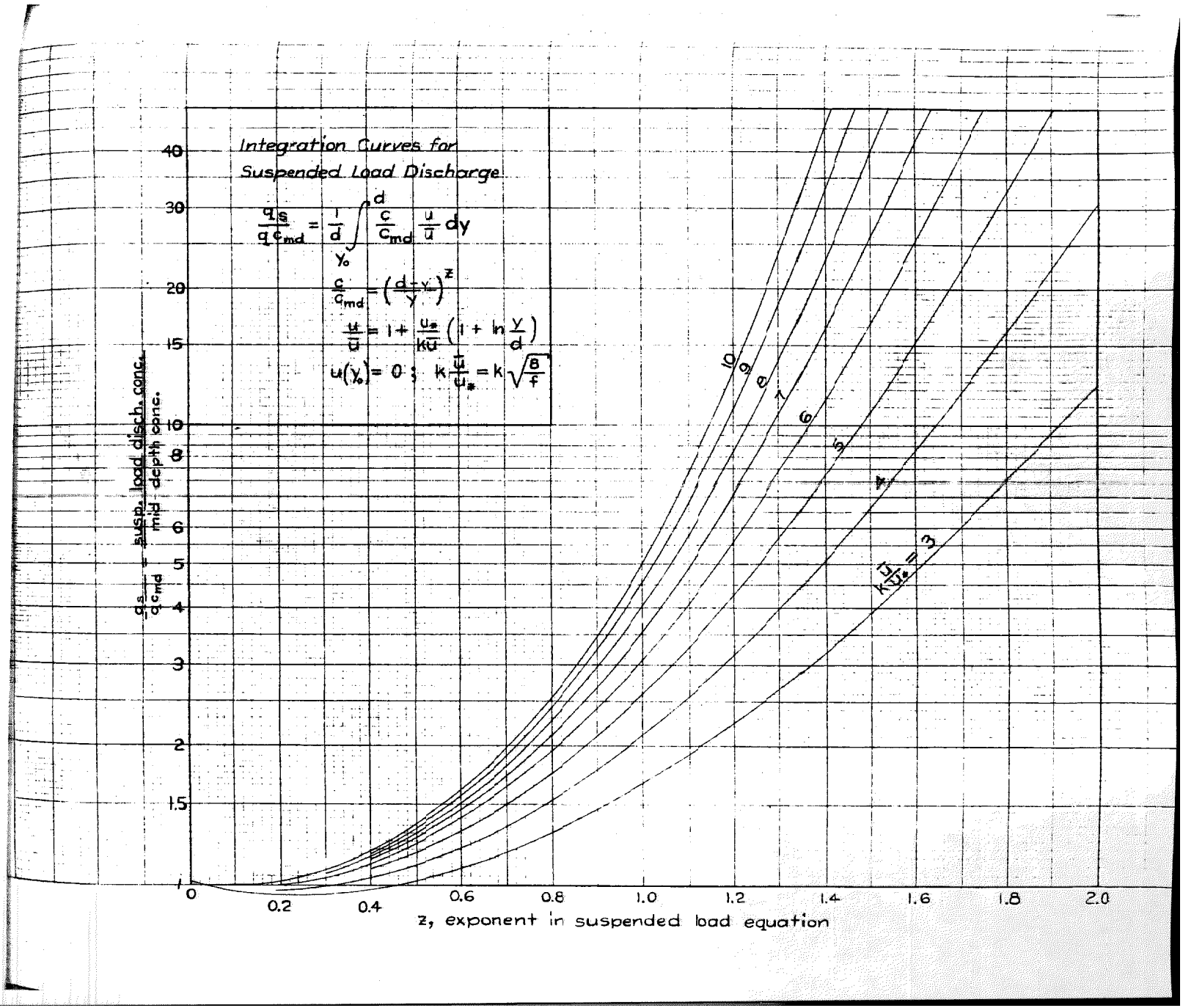
Integration Curves for
Suspended Load Discharge
$\frac{q_s}{q c_{md}} = \frac{1}{d}\int_{y_o}^{d} \frac{c}{c_{md}} \frac{u}{\bar{u}} dy$
$\frac{c}{c_{md}} = \left(\frac{d-y}{y}\right)^z$
$\frac{u}{\bar{u}} = 1 + \frac{u_*}{k\bar{u}}\left(1 + \ln\frac{y}{d}\right)$
$u(y_o) = 0 \; ; \; k\frac{\bar{u}}{u_*} = k\sqrt{\frac{8}{f}}$
$\frac{q_s}{q c_{md}}$ = susp. load disch. conc. / mid-depth conc.
z, exponent in suspended load equation
$\frac{\bar{u}}{u_*} = 3$
10
9
8
7
6
5
4
40
30
20
15
10
8
6
5
4
3
2
1.5
1
0
0.2
0.4
0.6
0.8
1.0
1.2
1.4
1.6
1.8
2.0

per cycle of 10 = $\frac{2.3u_*}{k}$; therefore $\frac{u_*}{k} = 0.54$. In addition, when c is plotted on logarithmic paper vs. $\frac{d - y}{y}$, the slope of the line of best fit is z = 1.1, and the line intersects $\frac{d - y}{y} = 1$ at $c = c_{md} = 0.05$ gr/l. = 50 ppm.

$$k\sqrt{\frac{8}{f}} = k\frac{\bar{u}}{u_*} = \frac{3.5}{0.54} = 6.5$$

$$z = 1.1$$

By Fig. 2,

$$\frac{q_s}{qc_{md}} = 4.5,$$

and hence

$$\frac{q_s}{q} = 4.5\ c_{md} = 4.5\ (50) = 225 \text{ ppm.}$$

Since the discharge per unit width is

$$q = \bar{u}\ d = (3.5)(3) = 10.5 \text{ cfs/ft}$$

the suspended load discharge per unit width is

$$q_s = \frac{225}{10^6} \times 10.5 \times 62.4 = 0.15 \text{ lb/ft/sec}$$

It may be observed from Fig. 2 that for $z < 0.3$, $\frac{q_s}{q\ c_{md}}$ may be considered equal to 1.0 for all practical purposes. The slight drop below 1.0 for the curves for the smaller values of $k\frac{\bar{u}}{u_*}$ at small z is artificial, and results from two slight inconsistencies, as follows:

(a) In the derivation of $\bar{u}$ in Eq. 1.43, the lower limit is taken as 0, whereas in the integration for q_s (Eq. 1.46) the lower limit is y_o defined as the level for which $u(y_o) = 0$. When z is 0, the q_s integral reduces to the same form as the $\bar{u}$ integral, but there is a difference in the lower limits. When $k\frac{\bar{u}}{u_*}$ is large, η_o by Eq. 1.58 becomes very small,

and the discrepancy is not noticeable; for example, if $k\frac{\bar{u}}{u_*} = 10$, then Eq. 1.58 gives

$$\eta_o = e^{-9-1} = .000045.$$

But if $k\frac{\bar{u}}{u_*}$ were only 3, then

$$\eta_o = e^{-3-1} = .018.$$

Thus for small values of the parameter $k\frac{\bar{u}}{u_*}$, the difference in lower limits has a noticeable effect because the integral of the velocity profile with lower limit 0 can be a few per cent less than the same integral with lower limit $y_o = \eta_o d$.

(b) The mid-depth level $y = d/2$ is not exactly halfway between the upper and lower limits, d and y_o. Here again the error is negligible except when $k\frac{\bar{u}}{u_*}$ is small and η_o is of the order of 1 per cent.

For a given z in Fig. 2, the ratio $\frac{q_s}{q\, c_{md}}$ increases when $k\frac{\bar{u}}{u_*}$ (or $k\sqrt{\frac{8}{f}}$) increases. This relationship is partly the result of changing the shape of the velocity profile, and partly the effect of reducing the lower limit η_o. The latter is especially important for the larger z values, for which the concentration profile is very steep and most of the suspended load moves near the bed; in this case, a small change in the η_o value can change the value of the q_s integral a large amount. In fact, since the value of η_o based on $u(\eta_o) = 0$ may not be the best value anyway, considerable error can be expected when $\frac{q_s}{q\, c_{md}}$ gets very large on the chart. Consequently, the curves have not been extended for $\frac{q_s}{q\, c_{md}} > 50$, or for $z > 2$.

It should be remembered that the choice of η_o is such that the values on Fig. 2 represent the maximum possible values of $\int_o^1 cu\, dy$ for each case. If further investigation reveals that some other choice

of η_o is more desirable than $u(\eta_o) = 0$, then q_s may be found directly from Eq. 1.53 with the aid of the charts for I_1 and I_2 given by Einstein (16). In any event, very close to the lower limit, extrapolation of the profiles for c and u is relied upon.

(2) Integration Using Lane and Kalinske's Simplified Suspended Load Equation. Lane and Kalinske (12) integrated the product cu (Eq. 1.41) for the same logarithmic velocity distribution u, but using their simplified version (Eq. 1.38) of the suspended load equation based on a constant diffusion coefficient $\bar{\epsilon}_s$. Here again the expressions they give are too specific (i.e., $k = 0.4$, $\beta = 1$), and it will be useful to show how their results can be generalized to be easily applied to any measured velocity profile, and sediment distribution following Eq. 1.38.

First, Eq. 1.38 will be rewritten without assuming the values of k and β

$$c = c_a \, e^{-\frac{6w}{\beta k u_*}\frac{y-a}{d}}$$

Letting $\frac{w}{\beta k u_*} = z$ as before,

$$c = c_a \, e^{-6z\frac{y-a}{d}} \qquad (1.60)$$

The factor $15\frac{w}{u_*}$ in Eq. 1.38 is equivalent to 6z.

The best comparison of Eq. 1.60 with the more accurate suspended load equation, Eq. 1.18, can be made by taking $a = \frac{1}{2}d$, $c_a = c_{md}$. Eq. 1.60 becomes

$$\frac{c}{c_{md}} = e^{-6z\left(\frac{y}{d}-\frac{1}{2}\right)} \qquad (1.61)$$

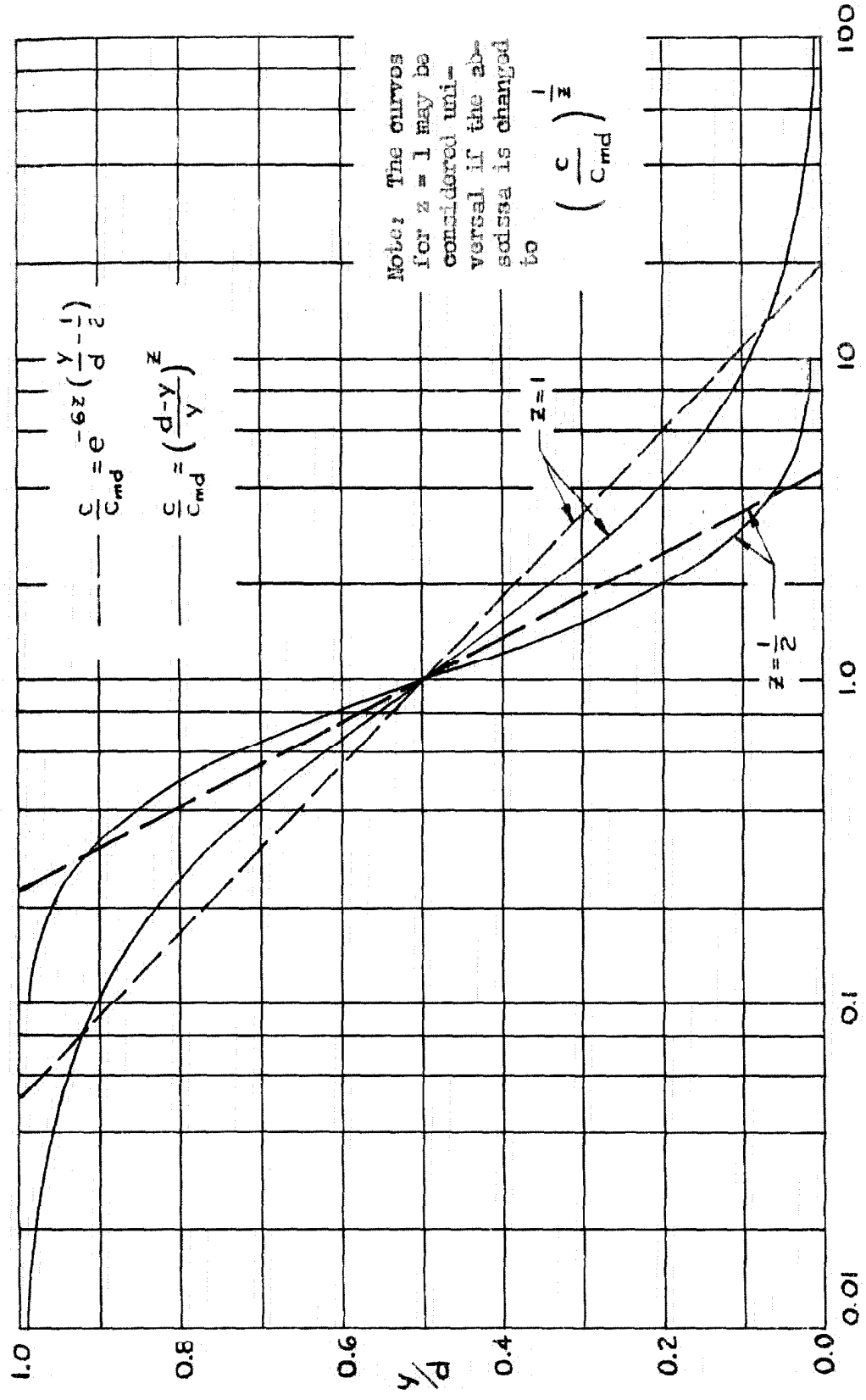

Fig. 3. Comparison of suspended load equations. (Figs. 1.10 and 1.21)

Both equations are plotted in Fig. 3 for z = 1/2 and z = 1. Over most of the lower half of the flow the Lane and Kalinske equation (Eq. 1.61) gives too large a value of c/c_{md}; deviation becomes progressively larger as z increases. The slope of Eq. 1.61, which is a straight line on Fig. 3, is

$$m' = -\frac{2.30}{6z} \tag{1.62}$$

units of y/d per cycle of 10 in c/c_{md}.

Substituting Eq. 1.44 for u and Eq. 1.60 for e into Eq. 1.41,

$$q_s = \int_0^d c_a \, e^{-6z\frac{y-a}{d}} \left[\bar{u} + \frac{u_*}{k}\left(1 + \ln\frac{y}{d}\right)\right] dy \tag{1.63}$$

Letting $\eta = \frac{y}{d}$, and $q = \bar{u}\, d$ and rearranging,

$$\frac{q_s}{q} = c_a \, e^{6z\frac{a}{d}} \, P \tag{1.64}$$

where $$P = \left(1 + \frac{u_*}{k\bar{u}}\right) \int_0^1 e^{-6z\eta} \, d\eta + \frac{u_*}{k\bar{u}} \int_0^1 e^{-6z\eta} \ln\eta \, d\eta \tag{1.65}$$

Carrying out the integration

$$P = \frac{1}{6z}\left\{\left(1 - e^{-6z}\right)\left(1 + \frac{u_*}{k\bar{u}}\right) + \frac{u_*}{k\bar{u}}\left[-.5772 - \ln 6z + Ei(-6z)\right]\right\}$$

wherein Ei(-6z) is the exponential integral in the standard form

$$Ei(-6z) = -\int_{6z}^{\infty} \frac{e^{-\theta}}{\theta} \, d\theta$$

The function P is numerically the same as the P integral plotted by Lane and Kalinske (1, 12), but with different parameters. They give

$$P = P\left(t, \frac{n}{d^{1/6}}\right)$$

where $t = \frac{w}{u_*}$, and

n = roughness coefficient in Manning equation.

Since they assumed k = 0.4 and β = 1.0 in their derivation, then in case $k \neq 0.4$ or $\beta \neq 1.0$, t may be replaced by 0.4z or $-\frac{2.30}{15m'}$ by Eq. 1.62,

in which m' is the slope of the concentration profile. Likewise, when they used $k = 0.4$ and the Manning equation, they obtained

$$\frac{u_*}{k\bar{u}} = \frac{1}{0.4} \frac{\sqrt{g}\ n}{1.49\ d^{1/6}} \quad ;$$

so working back again

$$\frac{n}{d^{1/6}} = 0.105 \frac{u_*}{k\bar{u}}$$

In summary, then, the same numerical values for P in the chart constructed by Lane and Kalinske can be used on a general problem by simply relabeling the abscissa $0.4z$ in place of t and the curves $.105 \frac{u_*}{k\bar{u}}$ in place of $\frac{n}{d^{1/6}}$. All the needed information can now be obtained directly from velocity and concentration profiles.

Although the second integral in Eq. 1.65 is improper, it still converges for all values of z. There is no difficulty in choosing a lower limit as far as the integration is concerned, but this does not mean that a better result can be obtained by using Lane's and Kalinske's simplified suspended load equation and the P integral, than with the original equation and Einstein's J_1 and J_2 integrals (Eqs. 1.48 to 1.50).

For an illustration of the use of the P integral to find q_s, consider the example already used to illustrate the use of Fig. 2. The calculations are as follows:

$$z = 1.1; \quad 0.4z = 0.44$$

$$k\frac{\bar{u}}{u_*} = 6.5; \quad .105 \frac{u_*}{k\bar{u}} = .016$$

Therefore, by Eq. 1.64, with $a = d/2$,

$$\frac{q_s}{q\, c_{md}} = e^{3z} P$$

$$P = P(0.44, .016) = 0.12 \text{ by the graph in Reference (12) or (1, p. 802)}$$

$$e^{3z} = e^{3.3} = 27.1$$

Hence

$$\frac{q_s}{q\, c_{md}} = 27(0.12) = 3.25.$$

In the previous case $\frac{q_s}{q\, c_{md}} = 4.5$ by Fig. 2. The two results should not be expected to agree because they are based on different equations. As z gets larger, the difference in results by the two methods increases.

In this section an attempt has been made to show that the problem of finding the suspended load discharge from concentration and velocity distributions is quite separate from the problem of determining just what these distributions should be. Only two basic assumptions are made: (1) that the velocity profile can be reasonably well fitted by a straight line on semi-logarithmic graph paper, and (2) that the concentration profile is a straight line either when c is plotted against $\frac{d-y}{y}$ on logarithmic paper, or when log c is plotted against y/d. Integration formulas derived by Einstein (16) and Lane and Kalinske (12) have been rearranged to show that basically the only necessary information is the slope and an intercept from each of the concentration and velocity profiles. Although it is believed that the concentration distribution will usually fit the ordinary suspended load equation (Eq. 1.18) better than the simplified one (Eq. 1.61) based on a constant diffusion coefficient (Eq. 1.61), integration formulas with the latter have still been included for completeness.

CHAPTER II

OBJECTIVES AND GENERAL OUTLINE OF EXPERIMENTS

As pointed out in Chapter I, the major problem today with suspended sediment transportation theories is that only the relative distribution of sediment concentration in a two-dimensional stream can be predicted with any assurance by means of the suspended load equation (Eq. 1.18). The boundary condition for this equation, which is needed to obtain absolute concentrations, is very difficult to specify because it depends on the complex mechanisms of interchange of particles between the stream and the bed. But these mechanisms are by no means universal, as supposed by the Lane and Kalinske theory (13), for they are radically altered by changes in the configuration of the sand bed. Under some conditions the bed may be quite smooth, while under different hydraulic conditions the same bed may become covered with rugged, irregular dunes. Consequently, any investigation to determine the boundary condition for the suspended load equation leads directly back to a more fundamental investigation of the mechanics of a sediment-laden stream as a whole. The present investigation has brought to light some important facts about streams carrying suspended load, but little progress could be made in a formal way toward evaluating c_a in the suspended load equation.

There were three major objectives of the experiments.

(1) To determine experimentally what some of the relationships are among the various basic variables, such as depth, velocity, friction factor, and suspended load for a stream flowing over a movable bed of fine sand.

(2) To study the bed configurations with special reference to the part they play in the mechanics of a sediment-laden stream.

(3) To check the suspended load equation, the von Karman logarithmic velocity law, and the integration formulas derived in Chap. I for flows over a movable bed; and to compare the values of the von Karman constant k and the ratio of diffusion coefficients, $\beta = \epsilon_s / \epsilon_m$ with the previous results of other investigators.

At first the attention of the author was fixed primarily on the third objective, but when dunes were encountered it was soon realized how much influence they have on the hydraulics of streams carrying fine sand in suspension. Subsequently, more emphasis was placed on the first two objectives, because it is useless to try to devise a means for determining the boundary condition for the suspended load equation until there is more understanding of what actually happens at the bed surface under various conditions. An investigation of the velocity and sediment concentration profiles was conducted only for the runs for which the sand bed was flat, and was not attempted for any of the runs with dunes because of the very difficult experimental problems involved.

Twenty-two runs were made in a laboratory flume 40 feet long with a movable bed of fine sand of either of two different sizes. The first sand, with mean sedimentation diameter of 0.16 mm was used for Runs 2 to 13, and the second, with mean sedimentation diameter of 0.10 mm, was used for Runs 21 to 30. Each run represented a stable uniform flow of water over a sand bed in equilibrium in the open channel. Six runs were also made with clear water for various special purposes, and are distinguished from the other runs by "C", i.e., Runs C1 to C4, C6, and C7.

The measurements for the runs of the second series, Runs 21 to 30, were slightly more accurate than for the runs of the first series, Runs 2 to 13, because some of the experimental procedures were being tested and improved during the first series. Furthermore, the data for the earliest runs in which dunes were encountered, Runs 5, 8, 9, 10, and 11, are the least accurate of all the runs, for at the time they were made, the importance of studying the dunes had not been fully realized. Nevertheless, the conclusions drawn from the first series were just the same as for the second more accurate series.

The apparatus and various procedures used in obtaining the fundamental data will be now described in the next chapter.

CHAPTER III

APPARATUS AND PROCEDURE

A. THE 40-FOOT TILTING FLUME

The general arrangement of the 40-foot tilting flume is shown in Figs. 4 and 5. The water flows from left to right in the open channel section, down and through the pump at the right hand end, then back through the return pipe and the diffuser to the upper end of the channel. The circuit is completely closed, so that the sediment as well as the water is recirculated by the pump. The flume itself is constructed of two 10-inch steel channel beams bolted to a base plate, as shown in the cross section in Fig. 4, leaving an inside width of 10 1/2 $\pm$ 1/16 inches (0.875 $\pm$ .005 feet). The inside surfaces are painted with a bitumastic paint and are fairly smooth. The flume is supported together with all accessories by a stiff truss, which pivots about one end, and is raised and lowered by a jack at the other. The slope may be read directly from a scale adjacent to the jack.

The pump, just under the downstream end of the flume, is of the axial flow type with a 9-inch impeller which may be driven at any speed from 120 rpm to 1050 rpm by an electric motor and variable speed drive. (See Fig. 5) The maximum capacity of the system is about 1.0 cubic foot per second (cfs), although the largest used in any experimental run was only 0.5 cfs.

The return pipe was originally of 6-inch diameter, but it was quickly found that the flow velocities were usually so low that large amounts of sand were deposited in the pipe where it was useless. The only way in which the bed of the flume could be kept covered with the full

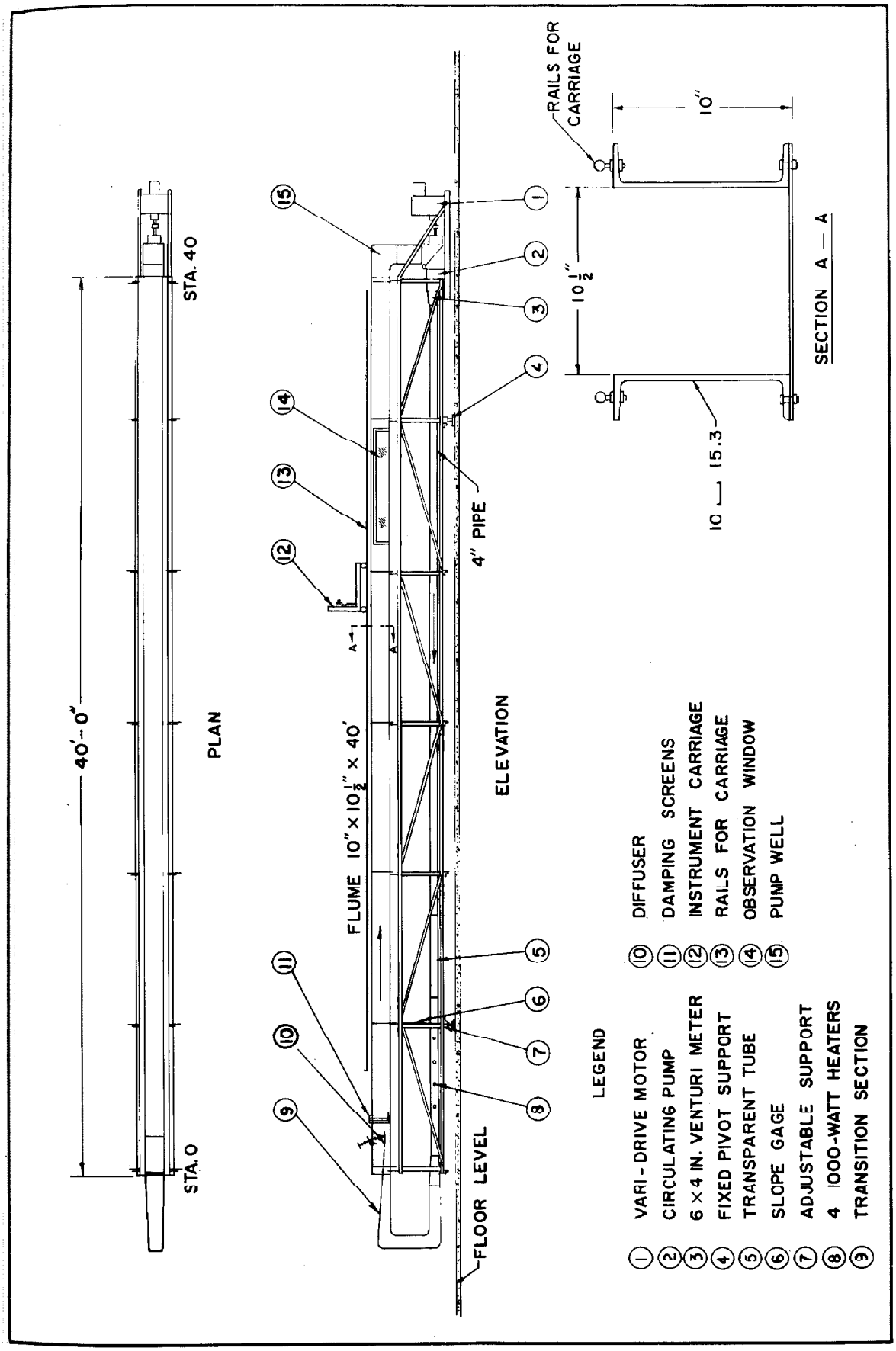

Fig. 4. Schematic diagram of the flume.

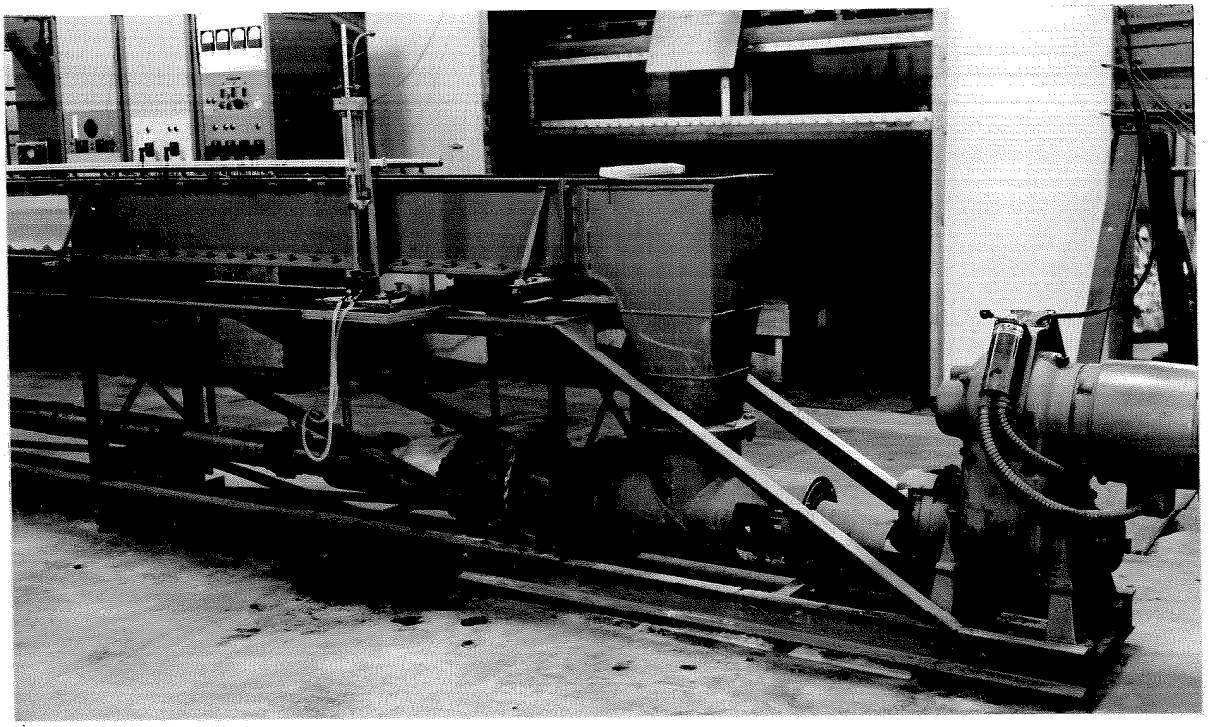

Fig. 5. Downstream end of the flume.

amount of sand was by using a smaller return pipe to make the velocity high enough to keep it scoured clean. Hence, after Run 2, the 6-inch pipe was replaced with a 4-inch pipe, which was satisfactory down to discharges of 0.20 cfs, the lowest discharge used. The cross-sectional area of the 4-inch pipe is equivalent to a depth of 0.10 ft in the rectangular flume section; therefore, since 0.155 ft was the smallest depth used, the mean velocity in the return pipe was always at least 55 per cent more than in the channel, and for the great majority of the cases, it was double the mean channel velocity.

As a further check on storage in the return pipe, a 50-inch-long transparent lucite tube of 4-inch inside diameter was inserted in the return circuit after Run 7. (See Fig. 4) After that it was easy to observe directly how much, if any, deposition there was in the 4-inch pipe. Unfortunately, although the storage was reduced to a negligible amount in the 4-inch pipe itself, still in the vicinity of the pump, the diffusers, and elbows in the return circuit, the cross section was larger and some deposition did occur. As a result, the mean thickness of the sand bed in the flume varied somewhat from run to run, even though the amount of sand in the system was unchanged.

B. ENTRANCE DISTURBANCE AND DAMPING SCREENS

In some of the runs, especially those with high discharges, excessive scour of the sand bed occurred near the entrance. Presumably some large scale turbulence was being generated in the elbows and transition sections at the upper end of the flume, in spite of the gradual transitions and the vanes in the last turn.

Since Dryden (18) has shown that turbulence generated in a wind tunnel can be very effectively damped with fine screens, some sections of window screening (16 openings per inch), supported with coarse hardware cloth, were inserted as damping screens vertically in the flow at the very beginning of the open channel section. The large scale eddies were damped out, but of course, a great deal of new small scale turbulence was generated by the screens. Since the small eddies naturally die out very quickly, this new turbulence was harmless. Unfortunately, these screens were not tried until Run 21a. In all the subsequent runs (23 to 30), from one to five screens were used, depending on what was most effective in establishing a uniform condition in the shortest length. The beneficial effect of the screens was shown very well by a comparison of Runs 21 and 21a. Run 21a was made in an attempt to reproduce Run 21 exactly, but with three screens added at the upstream end. In Run 21, the sand bed did not attain its full depth, and the flow did not reach equilibrium until about station 20, or 18 ft downstream from the entrance (station 2), whereas in Run 21a, equilibrium was already established at station 8. However, in the equilibrium reach the characteristics of the flow were practically identical - that is, the measured slope, friction factor, and total load were the same for the same given depth and discharge in the two runs. (For data, see Chap. VI, Sec. A). Hence, the previous runs are believed to be perfectly valid, although the entrance conditions were perhaps not as good as they could have been.

For Run 29, with discharge at its maximum value, .52 cfs, even with five screens, the sand bed and depth did not become uniform until station 18; without the screens the run would have been impossible, for the major length of the flume would have been consumed by entrance and outlet dis-

turbances. However, the equilibrium once established was very stable, and the run was found completely acceptable.

C. HEATERS FOR TEMPERATURE CONTROL

During the course of the investigations, it was found that the temperature of the water had a significant effect on the amount of sediment transport. So, to control the temperature, four 1000-watt immersion heaters were finally installed in the 4-inch pipe near the upstream end of the flume after Run 13. Three of the heaters were wired for either 110 or 220 volts, so that they could each be switched on to either 250 or 1000 watts. With this arrangement the power input could be easily regulated by 250 watt steps up to 2500 watts, with additional combinations totalling 3000, 3250, and 4000 watts. In general, a temperature difference of 10°C between water and air could be maintained with an input of about 2500 watts. If the heat input exceeds the total losses by 250 watts, the temperature of the water will rise only about 0.2°C in 30 minutes, because of the large volume of water in the system. Consequently it was very easy to maintain the temperature at 25.0° ± 0.2°C for Runs 21 to 30 by operating the switches manually without a thermostat.

D. MOVABLE CARRIAGE, POINT GAGE, AND FLUME SLOPE GAGE

Within the flume, positions and elevations were determined with a point gage (a brass rod with a sharp point) mounted on a carriage which moves on rails attached to the top flange of the channel beams. The carriage could be rolled continuously all the way from station 6 to station 37 (feet from upstream end of the flume). With thumb screws on the carriage, the point gage could be located anywhere in the cross section and

its position could be read to the nearest .001 ft, with verniers, in both the vertical and transverse directions. The carriage was equipped with easily interchangeable mounts, so that a Pitot tube or point sampler could be used in place of the point gage. All three were adjusted to have exactly the same position for the same readings on the scales.

The carriage readings and the slope gage on the truss were checked jointly against a static water surface several times before and during the experiments. Readings of the water surface by the point gage were made at one foot intervals along the flume, and the actual slope was determined from the straight line of best fit on a graph of these readings. It was found necessary to apply a correction of -.00005 to the slope gage readings. Deviations of individual readings from the fitted straight line were corrected either by realignment of the tracks, or by application of corrections (to nearest .001 ft) to all subsequent readings at the few stations where small corrections were necessary.

With the correction of -.00005, the slope of the tracks could be determined from the slope gage with a maximum error less than $\pm$ .00003. However, the error in measuring the slope of the energy grade line for any run was usually considerably larger because of the difficulty in measuring the elevation of a moving water surface and adjusting the flume to precisely the correct slope to make the flow uniform in depth. The problem of determining the slope of the energy line will be discussed in Sec. K. The point gage was adjusted to read .000 plus or minus a few thousandths of a foot anywhere on the steel bed of the flume. However, this was simply for convenience, since the rails, as checked against a static water surface, were still used as the primary reference. Slight irregularities in the bed were of no consequence anyway when the bed was covered with

sand, and were taken account of only for Runs C1 to C4, C6, C7, which were made without sediment.

E. VELOCITY MEASUREMENTS IN THE FLUME

Flow velocities could be measured in several ways. For measuring point velocities in the flume cross section, a 3/16-inch Prandtl type Pitot tube with a coefficient of 1.00 (19) was used with a water and air vertical differential manometer which could be read, with care, to the nearest .0005 ft. With this small sized Pitot tube, it was necessary to allow one to two minutes between readings for the manometer to reach equilibrium, because every change of reading would require a small amount of water to flow out of one column and into the other column through the Pitot tube openings.

To increase the sensitivity, and cut down the time between readings, a diaphragm strain gage connected to a potentiometer was tried in place of the manometer; but the strain gage was so sensitive that it responded to many turbulent fluctuations of the velocity, making it difficult to measure the time average velocity. Since the average velocities were of more interest than fluctuations in this investigation, and also since the manometer was a much simpler instrument, it was used instead of the strain gage.

The sand in suspension did not cause any difficulty in the operation of the Pitot tube, provided a few precautions were observed. The manometer and Pitot tube were always filled full with clear water before the tube was inserted into a flow containing sediment, so that it would not be necessary to draw water into the tube to fill the manometer or bleed the air. In general velocity profiles were taken starting near the

surface and working toward the bed, so that as the manometer adjusted itself to lower and lower readings, the dynamic head column would drop, forcing water out of the end opening of the Pitot tube, thereby minimizing the entrapment of sediment in the tube. There was little tendency for the static head slot to become plugged, but occasionally during prolonged velocity measurements small amounts of clear water were forced out through both openings of the tube to clean out whatever sediment may have collected.

Since the average mass density of the water and sediment mixture, ρ_s, is slightly greater than the density of clear water, ρ_w, a small error is introduced in the readings of velocity head. If it is assumed that the suspension behaves dynamically like a homogeneous fluid of the same average density, ρ_s, then

$$\frac{1}{2}\rho_s u^2 = \rho_w g \Delta h,$$

where

u = velocity

Δh = manometer reading in feet of clear water

g = acceleration due to gravity.

Consequently

$$\frac{u}{\sqrt{2g\Delta h}} = \sqrt{\frac{\rho_w}{\rho_s}} \qquad (3.01)$$

Hence $\left(\sqrt{\frac{\rho_w}{\rho_s}} - 1\right)$ is the relative error introduced by neglecting the density difference. The concentration very rarely exceeded 20 grams per liter (gr/l) at any point where the velocity was measured; hence for concentrations less than 20 gr/l and for a specific gravity of the sand of 2.65, $\rho_s \leq 1.0125\ \rho_w$ and

$$0 > \left(\sqrt{\frac{\rho_w}{\rho_s}} - 1\right) > -.006.$$

At worst, then, the simply calculated velocity would be only 0.6 per cent too large. It was decided to neglect corrections for density completely since these large concentrations occurred only close to the bed where the scour caused in the bed by the proximity of the Pitot tube introduces a further uncertainty in the velocity measurement.

For most of the runs with smooth bed (i.e., Runs 2, 3, 4, 6, 7, 21, 29, C1-C4, C6) vertical velocity profiles on the centerline of the flume were taken with the Pitot tube. They were usually made at about station 26 or wherever it appeared from the water surface and bed profiles (see Sec. H and I) that the flow was most nearly uniform and in equilibrium. In several of the runs (2, C1-C4) additional horizontal or vertical profiles were made, and in Runs 29 and C6 a number of detailed velocity traverses were made in order to calculate the total discharge and the coefficient for the Venturi meter. (See Sec. F)

When the bed was covered with dunes it was practically impossible to obtain velocity profiles. Not only is the velocity profile greatly complicated by the presence of the dunes, which generate large eddies, but also the velocity distribution is unsteady because the dunes progress downstream and change their shape continually. Consequently, even at a fixed point in the flow the velocity will fluctuate a great deal with time, especially near the bed. This is well illustrated by Run 5 where 60 velocity measurements over a period of 100 minutes were made at a single point in the flume about 0.040 ft above the average bed elevation. The velocity ranged all the way from 1.46 to 2.08 ft/sec, and frequently changed more than 10 per cent in one or two minutes.

No further Pitot tube measurements were made for Run 5, and none at all for Runs 8 to 13. However, for Runs 23 to 28 and 30 of the second series, the mean velocity on the centerline at approximately mid-depth was determined from a series of Pitot tube readings, for comparison with the average velocity calculated on the basis of the Venturi meter. Consistent results were obtained for all these runs.

The surface velocity for Runs 24 to 30 was measured by timing the motion of 1/4-inch chunks of cork floating on the surface. The float velocities were consistent with Pitot tube velocities with perhaps a slight tendency to be 2 or 3 per cent faster than the surface velocity estimated from the Pitot tube readings near the surface for Run 29. However, it is known that surface floats generally move slightly faster than the water; since the water surface is sloping, the weight of the float has a component in the downstream direction, which can be balanced only by the drag resulting from a slightly higher velocity of the float. Some rough calculations of these forces showed that the discrepancy observed is at least of the right order of magnitude. For larger floats, the velocity difference would be more. It is believed, then, that the Pitot tube coefficient must be very close to the theoretical value 1.00.

The extent of the velocity measurements made for each run is summarized in Table 1 in Sec. 0.

F. DISCHARGE MEASUREMENT BY VENTURI METER

The mean velocity in the cross section was calculated from the discharge measured by the Venturi meter immediately downstream from the pump in the return pipe. (See Figs. 4 and 5) The Venturi tube was formed by a standard bell-shaped 6 by 4-inch pipe reducer with straight nipples welded

to both ends. The two piezometer holes drilled in the nipples were of 1/8-inch diameter and spaced 8 inches apart. There was no expanding section following the contraction because 4-inch pipe was used downstream from the Venturi meter. The head was measured on another water-air differential manometer to the nearest .001 ft. The area ratio was 0.44, a value considered satisfactory for Venturi meters.

The discharge coefficient, C, of the Venturi meter was determined from a measured discharge, using the equation:

$$Q = C \frac{A_2 \sqrt{2gh_v}}{\sqrt{1 - \left(\frac{D_2}{D_1}\right)^4}} \qquad (3.02)$$

in which

Q = discharge

A_2 = area of contracted section

g = acceleration due to gravity

h_v = differential piezometric head

D_1 = diameter of approach = 6.065 in.

D_2 = diameter of contraction = 4.026 in.

The discharge was obtained by double integration of the velocity "surface" drawn on the basis of point velocity measurements in the flume cross section. For Run C6, without sediment, the discharge, calculated from 44 velocity measurements distributed over one-half the cross section, was 0.471 cubic feet per second; with h_v = 0.400 ft, the discharge coefficient was C = 0.944. This value is lower than usual for Venturi meters, probably for two reasons. First, the location of the Venturi just downstream

from the pump was not desirable, but there was no other feasible location. Secondly, the radius of the reverse curvature of the bell reducer is so short that some separation may occur in the throat, causing the pressure in the throat to be too small. Nevertheless, it was felt that the coefficient was fairly reliable, and it was used as the basis for computing the discharge in all the runs.

Unfortunately, the meter was not installed until after Runs 2 and C1 to C4 had been completed, so that there was no total discharge measured for these runs.

As in the case of the Pitot tube, the density effect on the Venturi meter is very small. The mean concentration never exceeded about 7 gr/l, so by Eq. 3.01 it is seen that the error is 0.2 per cent or less, and may be neglected.

Nevertheless, there was still some question about the effect of suspended sediment on the discharge coefficient for it has been observed that sand in suspension can alter the velocity profiles and friction losses. Therefore, near the end of the experimental program the discharge coefficient C was calculated again for Run 29, for which the average concentration of sediment in the discharge was 3.6 gr/l. The discharge, 0.521 cfs, was calculated from velocity measurements at 69 different points in one cross section of the flume. The head differential was $h_v = 0.483$ ft, making $C = 0.950$, compared with 0.944 determined previously for Run C6. This is considered an excellent check, since the difference, 0.6 per cent, is well within the experimental error involved in calculating the discharge for an open channel flow.

The Reynolds number has a slight effect on the discharge coefficient, but the range of Reynolds number, R_v, attained in the present experiments, was small. Defining Reynolds number for the Venturi meter as

$$R_v = \frac{QD_2}{A_2 \nu} ,$$

where ν = kinematic viscosity and the other quantities are as previously defined, R_v = 167,000 for Run C6 and R_v = 206,000 for Run 29. The smallest R_v for any of the runs was for Run 10, R_v = 77,000; and the largest was for Run 29, just mentioned. Thus, the total variation is less than a factor of three, and the coefficient may be considered as a constant for all practical purposes. No calibration was attempted for a run with one of the smaller Reynolds numbers, because the velocities in the channel were of the order of 1 ft/sec and could not be measured very accurately with the Pitot tube and manometer.

Another more serious difficulty caused by the sand was the deposition of sand in the meter at low discharges. During Run 24, with discharge of Q = 0.265 cfs, the Venturi was removed for inspection; there was just a trace of sand in the 6-inch section and no sand in the 4-inch section. Later, for Run 25 with Q = 0.20 cfs, it was found that about 2 per cent of the area of the 6-inch section was blocked with sand, while just a trace was found in the 4-inch section. From Eq. 3.02 it can be shown that the actual discharge in this case was only 0.5 per cent more than calculated.

Thus the meter performed satisfactorily with .10 mm sand, and probably also with the .16 mm sand, down to discharges of 0.20 cfs, but smaller discharges were not used because it was feared that appreciable deposition would occur in the 4-inch section causing much larger errors in the manometer readings.

Considering all the sources of error, it is estimated that the probable error in the discharge measured with the Venturi meter is 1 per cent or less.

G. MEASUREMENT OF SEDIMENT CONCENTRATION

For all runs a number of one liter flow samples were taken to measure sediment concentrations. The sand was carefully removed from the samples by filtration, and then oven-dried and weighed to within 1 per cent or less, or to the nearest milligram for sample weights under 0.1 gr. The samples were usually taken consecutively in groups of three at each point in order to get an indication of sampling errors and random fluctuations.

Two samplers were used, one for measuring point concentrations in the channel and the other for measuring the average concentration in the discharge in the well over the pump.

(1) Point Sampling. When the sand bed was smooth, and the bottom elevation was constant, point samples were taken in groups of three at various levels in the flow on the centerline at approximately station 26, in order to determine a suspended sediment concentration profile (distribution over the depth). This was done for the same runs for which velocity profiles were taken, namely Runs 2, 3, 4, 6, 7, 21, and 29.

Dunes on the bed in some of the runs made it impossible to measure concentration profiles, as well as velocity profiles. Hence, no point concentrations were measured at all for Runs 5, 8 to 13; and for Runs 23 to 28, and 30, point samples were taken only at mid-depth on the centerline for comparison with the samples of the discharge.

The tip of the point sampler was formed by flattening the end of a 3/16-inch brass tube into a tip with a vertical opening of .040 in. and horizontal opening of .217 in. (See Fig. 6) A very narrow tip was needed because the sand concentration gradients were large; but .040 in. is only about 7 diameters of the 0.16 mm sand, so it could not feasibly have been any smaller. The edges of the tip were filed to make them sharp, and the tube was bent in a right angle 2 3/4 in. from the tip, so that the tip projects upstream from the vertical shank which supports the sampler on the movable carriage mount.

The rate of sampling was regulated to make the velocity of flow into the tip of the sampler equal to the stream velocity at the same point measured with the Pitot tube. The area of the tip was known, so that the number of seconds required to draw a one liter sample could be calculated for any given velocity. In this way the disturbance to the stream was minimized, and the samples should be truly representative of the flow at the sampling point.

Vanoni (5) has shown in a similar case that if the sampling velocity is only 75 per cent of the stream velocity, then the average sample concentration of sediment is 9 per cent too high. If the flow into the sampler is too slow, there will be some curvature of streamlines away from the tip; since the sand particles are denser than the water, they are not as easily deflected and too many particles are drawn into the tip, thereby giving too high a concentration in the sample. If the sampling is too fast the converse is true.

A piece of flexible tygon tubing attached to the brass sampler was used to siphon the samples out into bottles on a platform or elevator, which could be raised or lowered to change the head on the siphon. (See

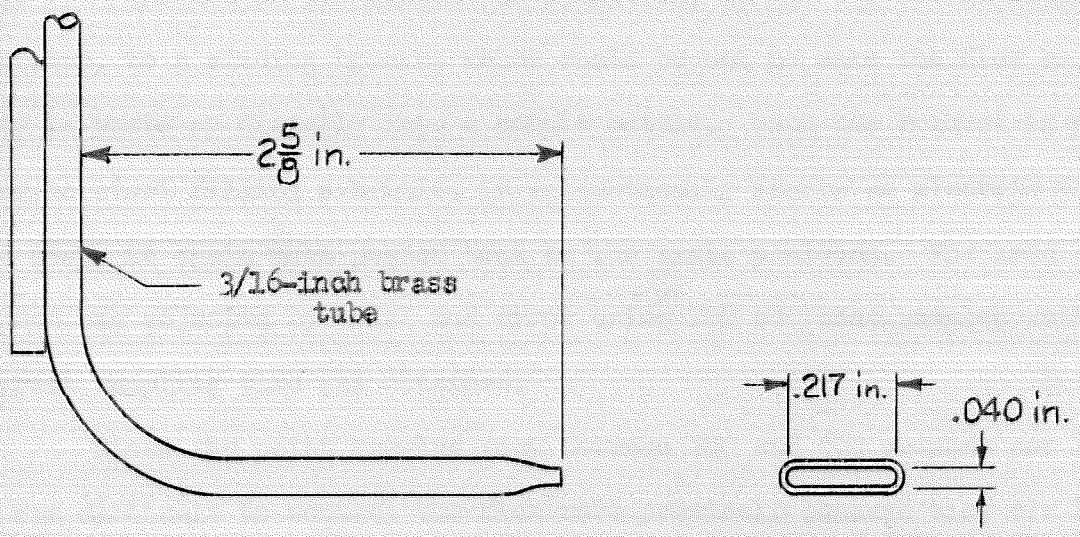

Fig. 6. Point Sampler

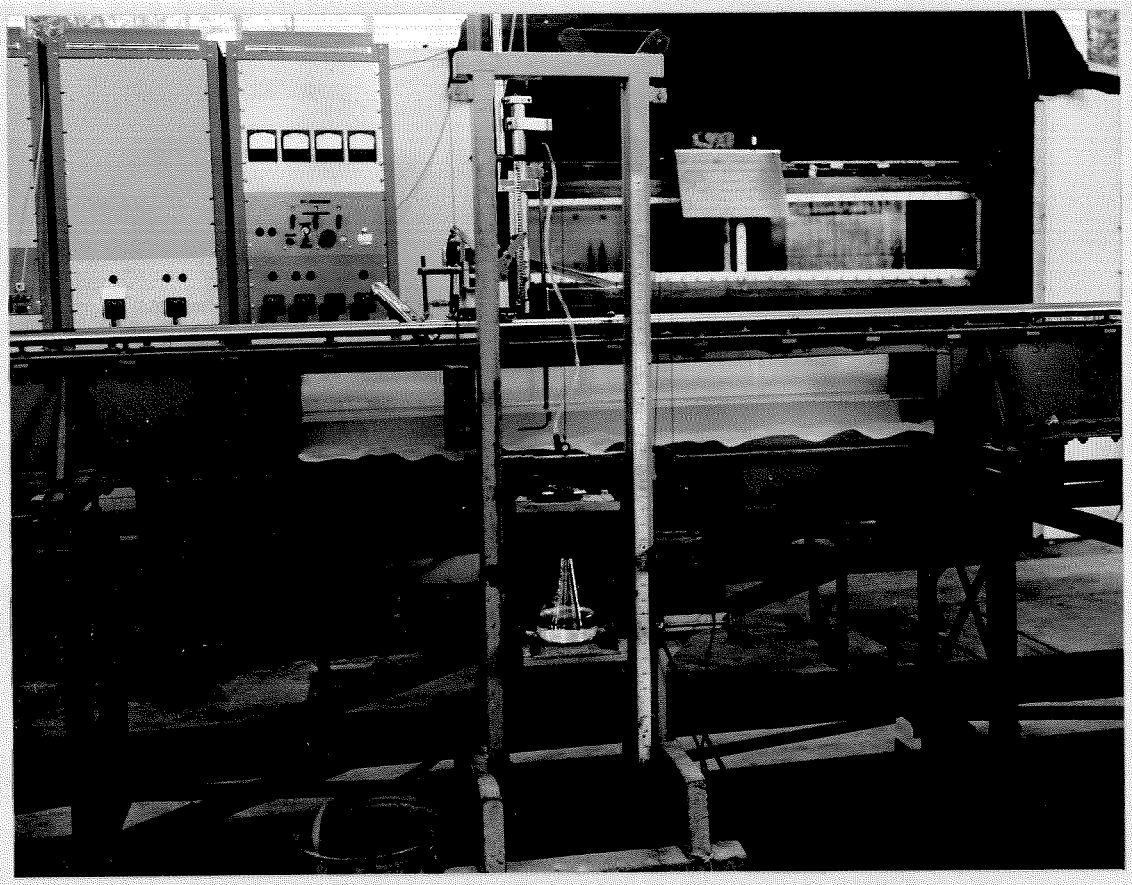

Fig. 7. Setup for point sampling in the stream.

Fig. 7) The end of the siphon was connected, at the top of the bottle elevator, to a sliding bracket which could be set to make the flow go either to waste or directly into a sample bottle. When the bracket is pushed over to start filling a bottle, it automatically starts an electric timer, and stops it again when pushed back to the waste position. The head on the siphon was adjusted by trial and error using 100 cc test samples until the correct sampling time was obtained.

Since the point samples took between 200 and 600 seconds per liter, it was difficult to control the flow rate precisely because tiny air bubbles tended to collect on the sides of the sampling tube and increase the resistance to the flow. Furthermore, it was impractical to discard the samples when the total time was slightly in error, because of the time required to repeat the sample.

Therefore, a simple analysis of the effect of the sampling velocity was made for the point samples of the runs with 0.16 mm. sand for which the actual sampling velocity was more than 5 per cent too slow or too fast. The concentration obtained for each of these samples was compared with the average for the corresponding group of three samples taken for each point (including the sample in question) and the ratio of the individual to the mean concentration is plotted on Fig. 8 as a function of the ratio of the average velocity in the tip of the sampler to the stream velocity. The concentration ratios are necessarily somewhat biased because the means are not statistically independent of the sample being checked, but the over-all distribution of points should be indicative of the general trend.

As expected, the samples for which the velocity was too small tended to have slightly too much sediment and vice versa, but the scatter of points is considerable, and the random fluctuations almost mask the effect of

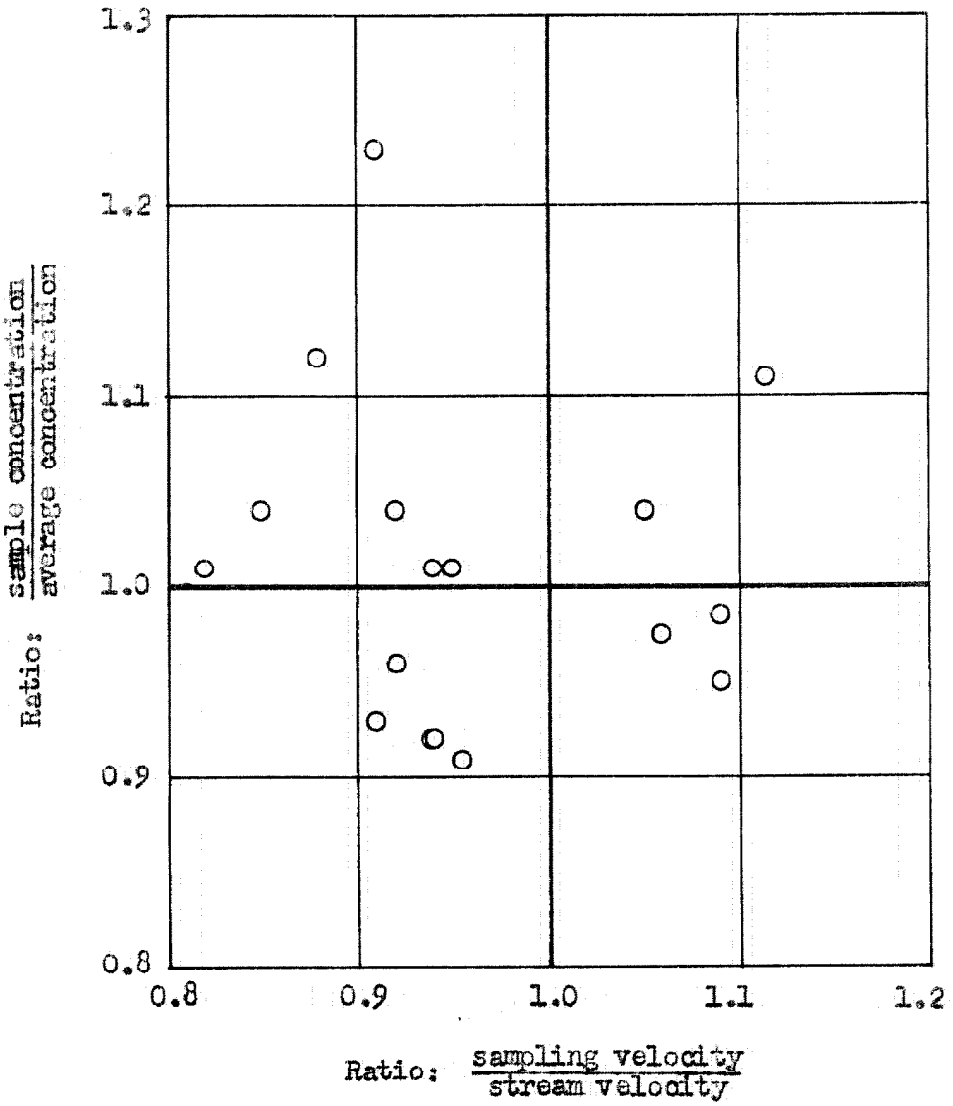

Note: A large number of points for which the velocity ratio is between 0.95 and 1.05 have been omitted.

Fig. 8. Effect of error in sampling velocity on sample concentration for 0.16 mm sand (Runs 2, 3, 4, 6, and 7).

slightly erroneous sampling velocity completely. For the smaller sized sand (0.10 mm) the effect should be even less. Hence individual errors in sampling time up to 10 per cent were tolerated provided the mean sampling time for the group of three was within a few per cent of the correct value.

Deposition of sand in the sampling tube was a problem in both the point sampling and the discharge sampling. Transparent tygon tubing was used to convey the sample from the metal samplers to the collection bottles so that it was possible to see the sand travelling in the tubing. It was observed that dunes would form unless the flow velocity in the tubing was high enough to prevent any deposition at all, or unless the tubing was steeply inclined. All trouble was easily eliminated for the point sampler because the water flowed vertically two feet up from the tip in the sampler tube, and then steeply down again through small tygon tubing, to the sample bottles. (See Fig. 7) Different lengths of tubing were used as required so that there would not be too much slack in the tubing. As a further precaution at the time of sampling the sampler was allowed to run to waste for two or three minutes, not only to fill the sampler with water from each new sampling point, but also to establish a new steady rate of sediment transportation in the sampler and connecting tube. This was necessary because the sediment on the average, once past the tip, did not travel through the sampling system quite as fast as the water. However, the relatively long sampling times helped to average out any remaining fluctuations artificially induced by the sampler.

(2) Discharge Sampling. Samples of the discharge were taken at the end of the flume for all runs except Run 2. The sampler consisted of a copper tube of .302-inch inside diameter with a half loop on one end.

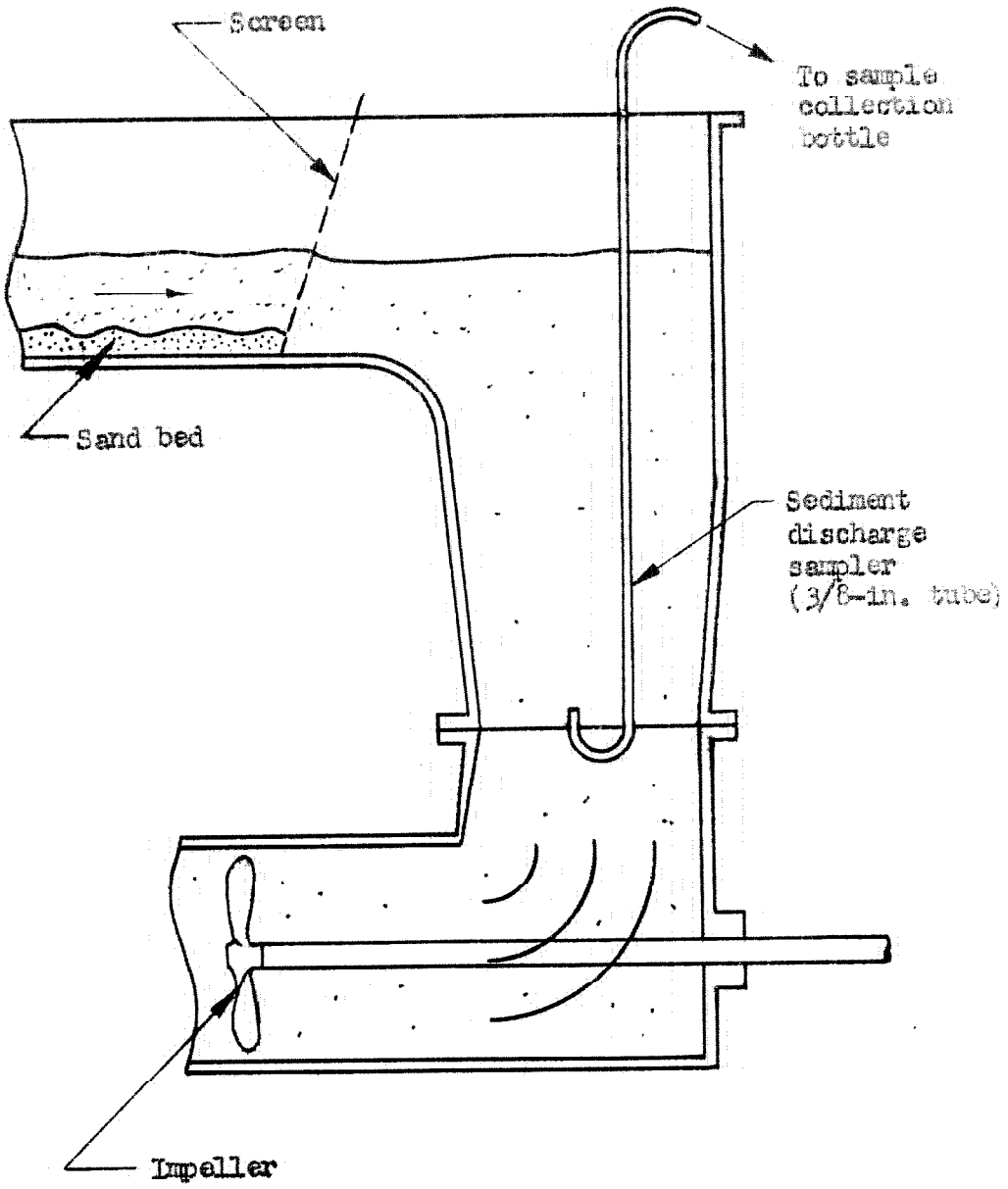

Fig. 9. Longitudinal section of flume at downstream end, showing position of sediment discharge sampler.

The end with the loop was submerged, with the opening facing up, about 20 inches below the water surface in the pump well, as shown by Fig. 9. It was believed that the sediment would be reasonably well distributed in this 9.5-inch diameter cross section of the flow just over the pump, but to be sure that the sample would be representative, the tip was moved around gently to different parts of the cross section during sampling. The head on the siphon was adjusted to make the velocity in the sampler entrance equal to the calculated mean velocity of flow at the sampling cross section. The bottle elevator and timer previously described were also used here.

For these discharge samples, the required sampling time ranged from 68 to 176 seconds, so that it was easier to control the rate of flow than in the case of the point samples; but on the other hand, because the sampling times were shorter, there was considerably more random fluctuation between samples. The fluctuation must have been due partly to the inevitable nonuniformity of sampling in the cross section, as well as to the real fluctuations in the load itself.

Sand storage in the sampler caused difficulty with the sampling of the discharge when the sampling velocities were the lowest and when the concentrations were small (of the order of 1 to 2 gr/l). Originally, the samples from the end tank were taken one at a time, and spaced over an interval of time (Runs 3 to 7, and 9). Between samples the flow in the sampler was stopped, and the sampler was left in the water; before taking the following samples, the siphon was started again, and run long enough to flush out the sand entrapped in the open upturned end between samples. Dunes were avoided in the tygon tubing connecting the sampler to the bottle elevator, as in the case of point samples.

The flushing procedure was checked in Run 8 by running two samples, one immediately after the other, each time the flow was established in the sampler. Three pairs were taken: the average of the first samples of each pair was 1.52 gr/l, while the average of the second samples dropped slightly to 1.39 gr/l. The sampling time was 91 seconds. There must have been a slight surplus of sediment in the U-turn at the bottom of the sampler at the beginning, but the discrepancy was not at all serious for this relatively high sampling rate.

However, for Run 10, with sampling time of 167 seconds and a very light load, the average concentration of the first sample of each of four pairs taken in the same way as Run 8, was 0.38 gr/l, whereas the second samples of the pairs showed only 0.21 gr/l. This was the only run with such exceptionally large differences. Because of the uncertainty and the fact that the latter figure is probably more representative of the true average concentration, the mean concentration for this run is reported as just 0.2 gr/l. Subsequently, the sampler was always removed from the water and blown out when not in use between groups of samples, and more time was allowed for the flow in the sampler to reach equilibrium before each set of samples was started. Furthermore, after Runs 11 and 12, where the samples were still taken in pairs, practically all the discharge samples were taken in groups of three, and as a general rule the total number of these samples taken was increased to about 10. Better results were thus obtained, although a slight tendency for the first sample of a set to be larger than the others still persisted. For example, Run 13 gave the following results for five groups of three each: average first sample, 1.35 gr/l; average second sample, 1.04 gr/l; average third sample, 1.25 gr/l. The sampling time was 158 seconds. It was later found that this trend could be com-

pletely removed by shifting the sampler tip around in the cross section during the initial flow adjustment period in exactly the same way as was done during the actual sampling.

Another cause of fluctuation of the samples was the occasional sloughing of small blobs of sand from the sand bed at the very edge of the pump well. It was discovered during Run 21a that this could be prevented if a piece of window screen (16 openings per inch) was placed vertically in the flow an inch or two from the end of the steel bed of the flume, as shown in Fig. 9. The turbulence induced by the screen was sufficient to prevent the formation of a sand bed between the screen and the falling off point; hence there was no more sloughing at the edge. The improvement due to the screen is shown by the following comparison of the six end samples for Run 21 without the screen with six more for Run 21a with a screen. Run 21a was intended to be an exact reproduction of Run 21, but with a screen at the downstream end as well as three damping screens at the upstream end as described in Sec. B.

Sediment Discharge Concentration, gr/l

	Run 21 (without screen)	Run 21a (with screen)
Average of 6 samples	4.85	4.93
Standard deviation	0.59	0.32

It is quite obvious that the screen reduces the random fluctuations considerably, without affecting the mean. In fact, it is probably just accidental that the means agree so well.

Because of the various kinds of errors involved, and the variable nature of the runs, it is not possible to give a blanket figure for the probable error of the concentration measurements. It is as low as 1 per cent for some of the average point concentrations measured in the central region of the channel, but as much as 5 to 10 per cent for some of the average sediment discharge concentrations. Individual sample concentrations may sometimes be unreliable.

H. WATER SURFACE PROFILES

To determine the depth and especially the slope of the stream accurately, it was necessary to measure the water surface and bed elevations over the entire length of the flume. The graphs of these measurements will be called water surface or bed profiles. All the measurements were made with the point gage mounted on the movable carriage and set on the centerline of the channel.

If the water surface was smooth and glassy, as it rarely was, then its elevation at any point could be easily determined to the nearest .001 ft by lowering the point gage until it just touched the surface and a meniscus was suddenly formed on the point. With small ripples or waves on the surface the point gage was adjusted so that when the carriage was wheeled back and forth about a foot the point gage would make contact with the water for about half of the distance. Since the meniscus, once formed, would not break until the point of the gage was raised a few thousandths of a foot above the surface, it was necessary to bias the point gage setting so that the meniscus would be in contact slightly more than half the time. The small surface ripples were usually induced by the entrance, slight irregularities in the walls, or sand ripples or dunes on the bed, and tended to be

more or less stationary. Consequently, the instantaneous average elevation found over a short distance is more reliable than a time average at a fixed point.

The elevations were read from the scale on the carriage, with corrections, if any, and were recorded directly to the nearest .001 ft on a graph of point gage readings vs. station along the flume. Measurements were usually made at one or two-foot intervals, depending on the accuracy desired and the scatter of the points. A typical water surface profile for a run with only small ripples on the water surface is reproduced in Fig. 10 for Run 27. The other curves on Fig. 10 will be explained in the following sections.

If the total heights of the ripples or waves were not more than .010 ft then the probable error in the measured elevations is less than .001 ft. However, in a number of runs, especially those with the highest Froude numbers (> 0.7), the height of the standing waves often reached .020 ft and in a few exceptional cases, .050 ft.

In those cases, where the mean elevation could not be easily estimated by eye, the elevations of a typical trough and crest in the vicinity of each station were measured. Since the height of the waves was still small compared with their wavelength (usually of the order of one foot), the average of the crest and trough elevations is a good first approximation for the mean elevation. Unavoidably, though, one wave may not be representative of a group passing slowly by a given station. Thus, many measurements along the flume are needed to obtain a reliable mean water surface profile. A profile for a wavy condition is shown in Fig. 11.

Since the waves always kept moving slightly it was useless to try to plot the exact positions of any particular waves; therefore, points for

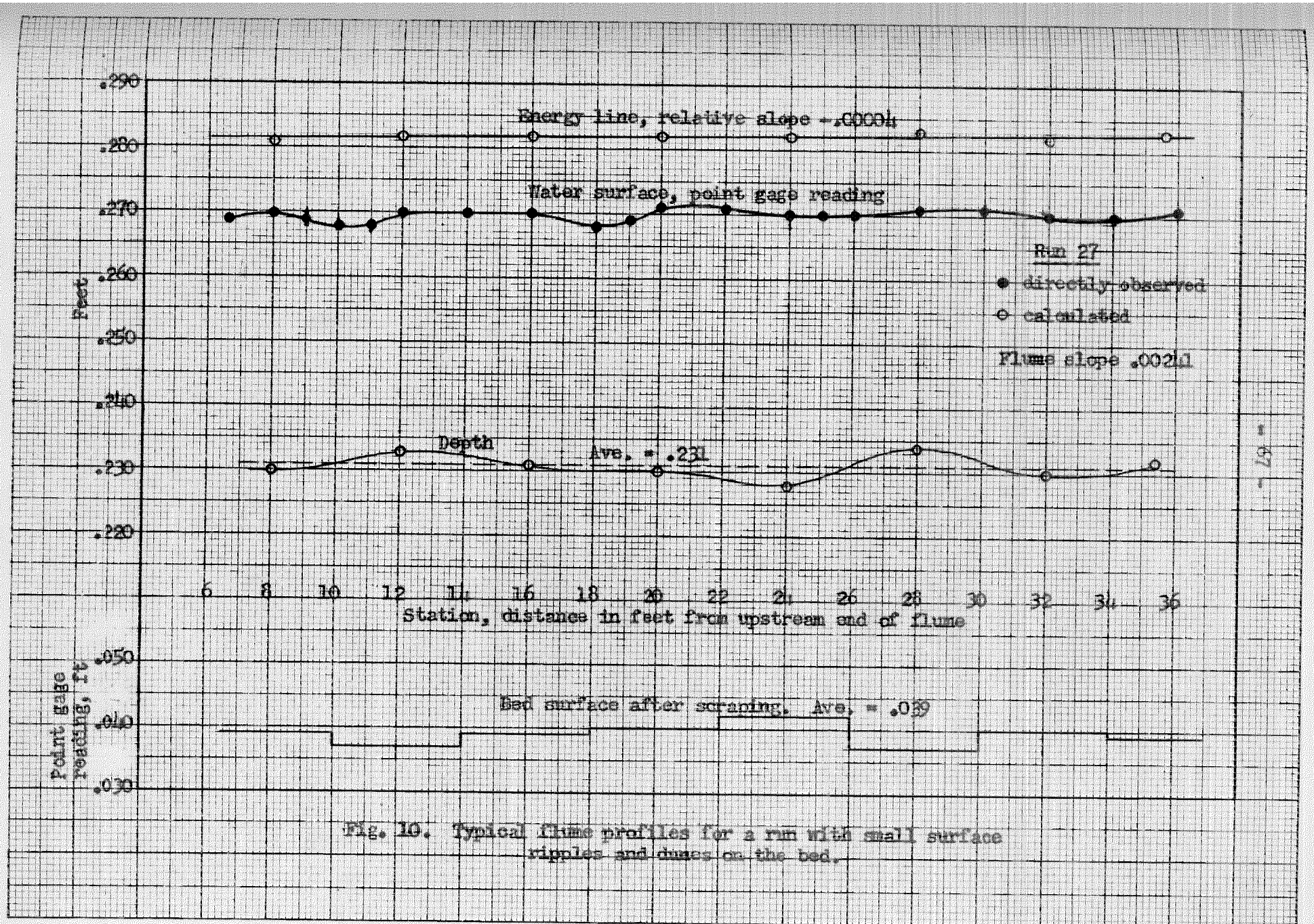

Fig. 10. Typical flume profiles for a run with small surface ripples and dunes on the bed.

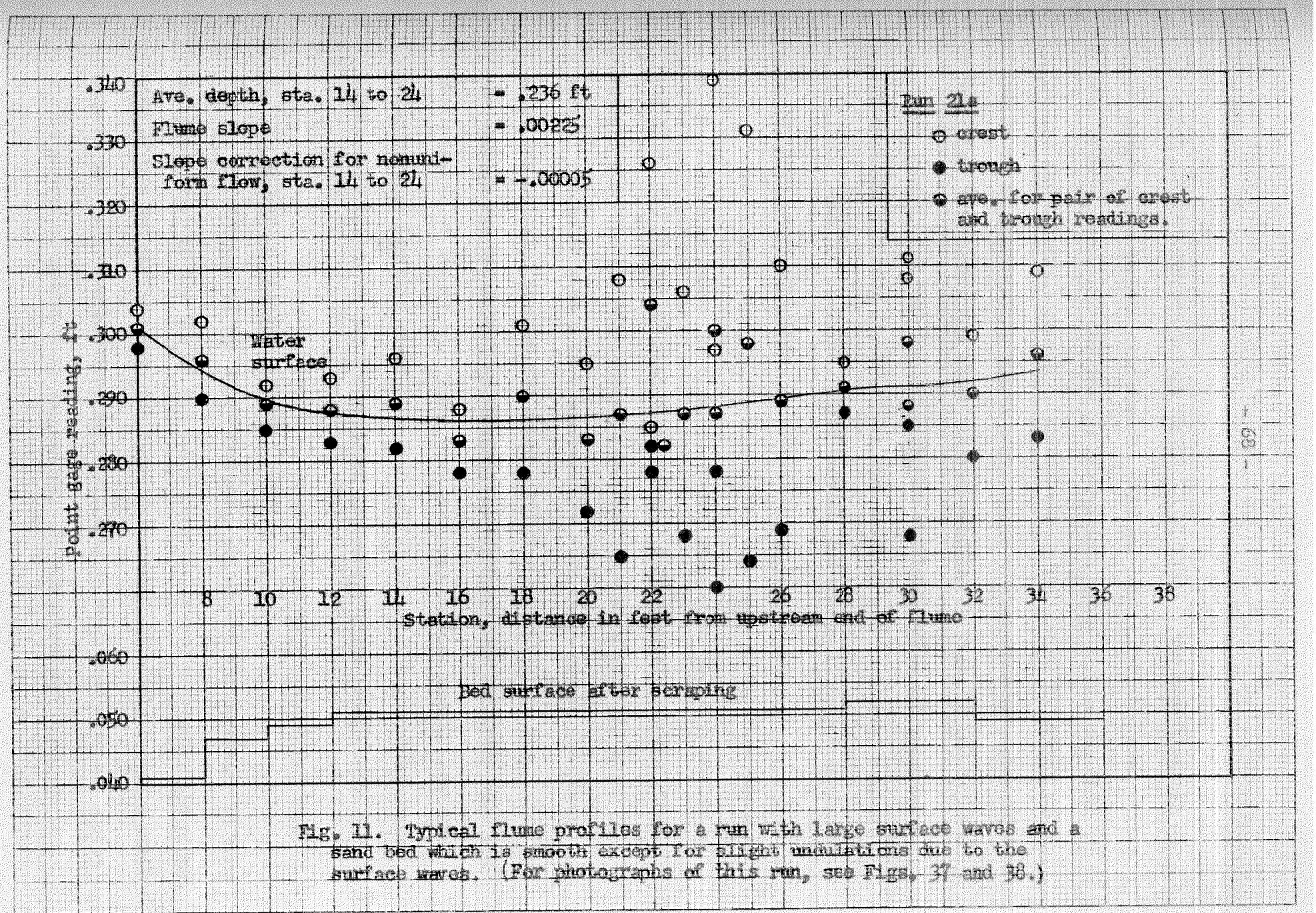

Fig. 11. Typical flume profiles for a run with large surface waves and a sand bed which is smooth except for slight undulations due to the surface waves. (For photographs of this run, see Figs. 37 and 38.)

a crest and an adjacent trough were both plotted on the same abscissa on the graph of point gage readings vs. station. The calculated mean points were also plotted, and the profile of the mean water surface was then plotted through these points. The scatter of the points is rather large, but it is believed that a smooth curve drawn through them is reasonably reliable. In viewing the water surface profiles in Figs. 10 and 11, the reader should note that the zeros on the vertical scales are suppressed and that the relative distortion of the vertical and horizontal scales is 1:200. The bed profiles, depth curves, and energy lines are explained in the next three sections.

One or more water surface profiles were made in this way for each of the following runs: 2, 3, 4, 6, 7, 21, 21a, 23 to 30, with sediment; and C1 to C4, C6, and C7 with clear water. Unfortunately for the other runs, 5 and 8 to 13, only a mean water surface with a possible error of several thousandths of a foot was recorded. In these cases, the flume slope was adjusted so that the water surface was parallel to the flume, and the average was determined by running the carriage back and forth over the whole length of the flume. There were no large surface waves. Accurate water surface profiles would have been useful in obtaining more accurate measures of the depth and the slope of the energy grade line.

I. BED ELEVATION PROFILES AND MEAN DEPTH

In addition to the water surface profiles, it was necessary to have bed profiles. If the tip of the point gage is lowered to measure the elevation of the bed surface when the flume is running, it simply erodes a small hole in the bed. Furthermore, the visibility is very poor with any appreciable amount of sediment in suspension. It was necessary, then, to stop

the flume in order to take any measurements at all. If the pump is stopped suddenly, several large waves travel up the flume, but the bed configuration is practically undisturbed by the passage of the waves overhead. This was checked both visually and with motion pictures. The sand in suspension which settled to the bed increased the bed elevation slightly, usually less than .0005 ft, and always less than .0015 ft. A correction for this was necessary only in Runs 21 and 29.

Point gage readings to the nearest .001 ft could be made on a sand surface under water with the aid of an intense oblique beam of light from a flashlight attached to the end of the carriage. The light was focused on the bed under the point gage and the gage was lowered until the point just touched its own shadow, thereby indicating contact with the bed. The accuracy of the technique was tested in the window section of the flume where it was possible to look into the flume with one's eye at the level of the bed.

In the earliest runs with sediment, Runs 2, 3, 4, 6 and 7, the sand bed of the stream was flat except close to the walls. The bed elevation was measured at the center of the channel without disturbing the sand. The depth at the centerline, which is just the difference between the water surface and bed elevations, was found to be reasonably representative of the whole width when the bed was smooth. From the depth profile along the flume, a reasonable value of the mean depth at the sampling station was estimated.

For Runs 5, 8, 9, 10, 11, with the bed covered with dunes, the mean elevation for the whole flume was estimated to the nearest .005 ft from some scattered measurements and the knowledge of how much sand there was in

the system. The mean depth, computed as the difference between the estimated mean water surface and bed elevations, was subject to errors up to ± .005 ft. Since more accuracy was desired, this procedure was changed after Run 11.

A bed scraper was built for leveling the dunes to find the mean sand elevation in a given reach. This device is shown in Fig. 12 along with the carriage and point gage. The frame slides on the rails on top of the flume and the straight-edged, double-bladed scraper is supported by two vertical 5/16-inch rods. Each rod is threaded on top and can be raised or lowered independently by turning a wing nut. The rods are spring loaded so that the scraper is held firmly in the position set by the nuts.

To level the bed, the scraper was pushed back and forth over a given reach and adjusted between passes until all the sand that was originally within a given reach was redistributed to make a perfectly flat surface with no sand left over. The elevation of this artificially formed surface was measured with the point gage on the center line, so that it was unnecessary to keep the blade of the scraper precisely leveled in the transverse direction. Even if one end of the scraper happens to be set slightly higher than the other, the center elevation must still be the average elevation. This independent adjustment of the two ends was very helpful in the leveling process because frequently in the case of dunes there would be, by chance, a little more sand on one side of the channel than the other in a short reach.

Since the sand is originally in a very loose state, measurements of the density of the sand in place before and after scraping showed that the density or the volume is virtually unchanged. (The sand density measurements will be described in Chap. IV, Sec. C.) Consequently, the measured

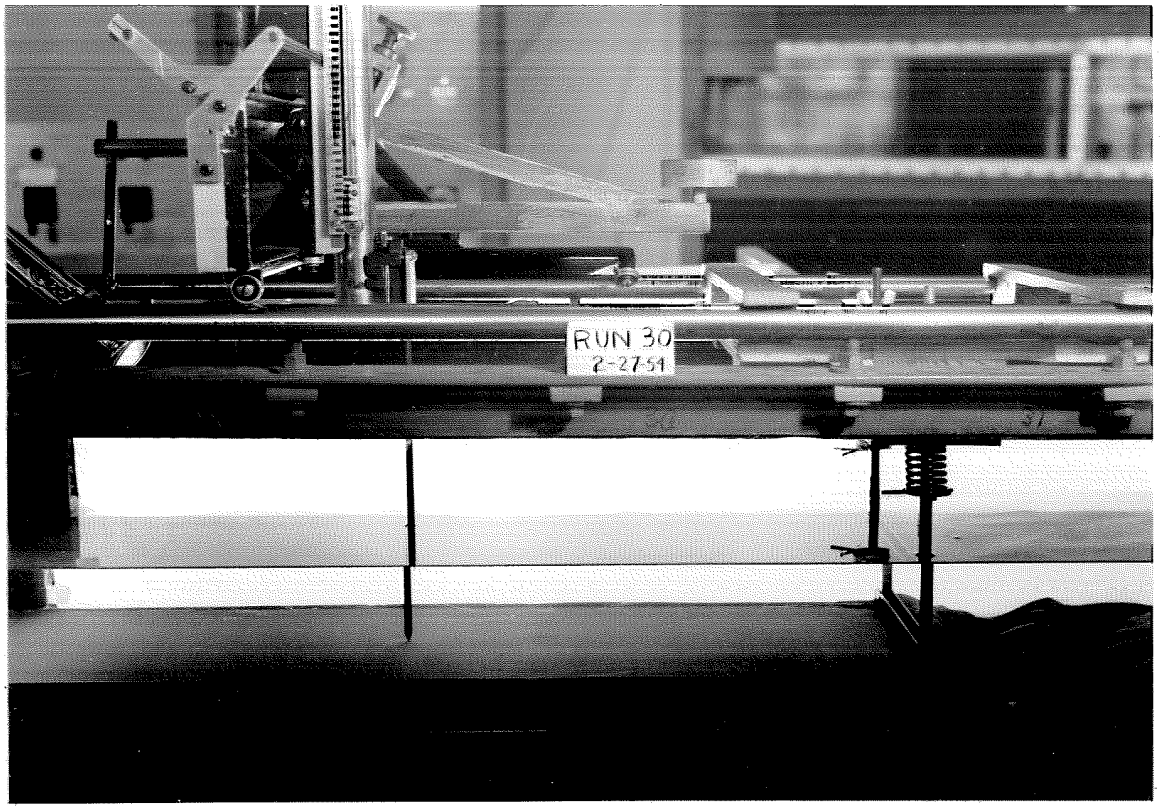

Fig. 12. Scraper for leveling the bed, and point gage mounted on carriage for measuring the mean bed elevation. (Water still).

average elevation must be very close to the true mean sand elevation of the configuration before scraping.

To determine the bed profile, the bed was scraped in reaches or sections of either 2, 3, or 4 feet, depending on how irregular the bed appeared and how much variation there was between adjacent reaches. Sections shorter than two feet were not used because they are too short in relation to the wavelength of the dunes to get a good sample. For example, if a reach is only two and one-half wavelengths long, the mean bed elevation will depend quite a bit on whether there are three troughs and two crests, or two troughs and three crests included in the interval being scraped. Two typical scraped bed profiles are shown in Figs. 10 and 11.

In some of the runs, long sand waves going through the system caused the water surface and bed profiles to fluctuate cyclically over a period of a few hours. Hence it was a general procedure to take the bed profile immediately following a water surface profile in order to be sure that the points should correspond to exactly the same flow condition.

Taking a bed profile with the scraper destroys the bed configuration and sometimes several hours are needed to regenerate it. For Runs 21 to 30, one or more preliminary sets of water surface and bed profiles were taken to establish an equilibrium flow and then when the final run was made a water surface profile was measured during the last ten or fifteen minutes of the run. The pump was shut off just as soon as the profile was finished. Photographs and measurements of the dune size were made, and finally the bed was leveled for the bed profile.

A depth profile was obtained by plotting the difference between the mean bed and water surface elevations at each station. The mean depth was calculated for the part of the flume in which the flow was judged to be ap-

proximately uniform and in equilibrium and was used as the basis for calculating the shear and mean velocity for Runs 21 to 30. For Runs 12 and 13, bed profiles were obtained with the scraper, but no detailed water surface profiles were made. The depth in these two cases was based on the measured average water surface and the mean of the bed elevations.

In conclusion, for the runs with movable sand bed, good water surface profiles were obtained for Runs 2, 3, 4, 6, 7, and 21 to 30, and good mean bed profiles with the scraper for Runs 12, 13 and 21 to 30. The other runs were all deficient in one respect or another as outlined above. The set of Runs 21 to 30, with 0.10 mm. sand, should be considered more accurate than the first set, Runs 2 to 13 with 0.16 mm. sand, which suffered somewhat while the author was learning good experimental techniques.

J. DEPTH REGULATION

The depth of flow was regulated by the amount of water used in the system, inasmuch as the only place in the system where the water storage is variable is in the open channel section itself. This is quite different from an open circuit system where the water is supplied from a reservoir and the depth of flow is controlled by the discharge, the slope, and the roughness (or a downstream control in a short flume). For a given discharge, depth is an independent variable and slope is a dependent variable in a closed circuit flume, whereas in an open circuit flume the situation is reversed.

The relative volume of water in the flume was determined by the static water level at some particular flume slope setting. A stationary point gage at the upstream end of the flume was used to measure this level to the nearest .001 ft.

Fluctuations of the distribution of sand in the system made it impossible to establish a fixed relationship between depth and amount of water. But the depth for any given run could be maintained constant by keeping the amount of water in the flume constant. For every liter removed in the process of sampling, a new liter of water was added at the same time. For long runs, replenishments had to be made also for evaporation and leakage through the packing around the shaft of the pump. Such close control on the amount of water is necessary because one liter is equivalent to .001 ft of depth.

K. SLOPE OF THE ENERGY GRADE LINE.

The energy slope of the flow is almost always one of the most difficult quantities to measure, because the actual drop in the distance of a laboratory flume is very small. In these experiments the slope ranged from .0013 to .0035; if the section of uniform flow is twenty feet long, the corresponding drop is only .026 to .070 ft.

In the runs without complete water surface and bed profiles (Runs 5, 8 to 13), the slope of the flume itself (which was also the slope of the water surface) was taken as the slope of the energy line. Actually, the water surface slope is the true energy slope only if the bed is parallel to the water surface; otherwise the velocity head varies, since the depth varies. No bed profiles were made for Runs 5, 8, 9, 10, and 11, but by visual inspection of the bed configuration this correction was judged to be small. For Runs 12 and 13, bed profiles were made with the scraper, and a small correction (-.00015) was made for bed slope in Run 12. The maximum possible error in the slope values for this group of runs is probably about $\pm$.0002, because of errors in determining the slope of the water surface,

and the unknown factor of the bed slope.

In the other runs, for which there were both water surface and bed profiles, it was possible to calculate the specific energy, e, at points every few feet along the flume.

In coordinates referred to the rails of the flume, e is defined as:

$$e = y'_s + \alpha \frac{U^2}{2g}$$

wherein U = mean velocity in the entire cross section,

g = acceleration due to gravity, and

y'_s = elevation of water surface by the water surface profile.

The velocity head coefficient α, was taken as 1.00, since a few per cent error in α has a negligible effect on the slope.

Depending on the spacing of the bed measurements, e was calculated and plotted at 2, 3, or 4 foot intervals, and then a straight line was fitted to the points by eye in the working region of the flume. The slope of the energy line, S, is the sum of the slope of the flume, S_f, and the slope of the energy line relative to the flume. An effort was made to keep the relative slope as small as possible, usually $\pm$ .0001 or less.

In some of the runs a simpler, although equivalent, calculation was made in case the water surface and bed profiles were fairly straight although not quite parallel. If x is the distance along the flume, then, as stated above:

$$S = S_f - \frac{de}{dx} = S_f - \frac{d}{dx}\left(y'_s + \frac{U^2}{2g}\right).$$

Now if q is the discharge per unit width, and y'_b is the bed elevation, the depth, d, is $(y'_s - y'_b)$ and

$$U = \frac{q}{y'_s - y'_b} .$$

Hence

$$-\frac{d}{dx}\left(\frac{U^2}{2g}\right) = -\frac{q^2}{2g}\frac{d}{dx}\frac{1}{(y_s' - y_b')^2} = +\frac{U^2}{g(y_s' - y_b')}\left(\frac{dy_s'}{dx} - \frac{dy_b'}{dx}\right) .$$

In open channel hydraulics, the Froude number F is defined as

$$F = \frac{U}{\sqrt{gd}} = \frac{U}{\sqrt{g(y_s - y_b)}} ,$$

so finally

$$S = S_f - (1 - F^2)\frac{dy_s'}{dx} - F^2\frac{dy_b'}{dx} . \qquad (3.03)$$

The slope of the flume is read from the slope gage, and the slopes of water surface and bed relative to the flume ($\frac{dy_s'}{dx}$ and $\frac{dy_b'}{dx}$) are obtained from the profiles. In all cases, $S \doteq S_f$ so that the last two terms of Eq. 3.03 actually represent just a small correction to S_f.

It is interesting to note from Eq. 3.03 that the relative importance of the bed and water surface slope is governed by the Froude number; that is, as $F \to 1$, $S \to (S_f - \frac{dy_b'}{dx})$, (the absolute bed slope), and as $F \to 0$, $S \to (S_f - \frac{dy_s'}{dx})$, (the absolute water surface slope).

For Runs 2, 3, 4, 6, 7, 21 to 30, and C2, C3, C4, and C6, for which the energy line was plotted or S was determined by Eq. 3.03 above, the probable error is estimated to be less than .00005 or roughly 2 per cent of an average value for the slope.

L. OBSERVATIONS OF BED CONFIGURATION

When the first runs with dunes were encountered it was decided that it would be worth while to make some quantitative observations of the bed configurations and to record them permanently with photographs. Rough measurements were made of dune wavelength, height, and velocity of movement;

but because the dunes on the bed were usually so highly irregular, (as shown by the photographs in Ch. VI, Sec. B), it was very difficult to define these quantities and their average values objectively. Hence, the reported values should be considered as approximate, for they are not the result of tedious precise measurements on randomly selected dunes. The observations are intended only to give relative order of magnitudes and to help show how the bed configuration is related to the other variables, especially channel roughness. Some of the particular problems encountered in measuring the height, wavelength, and velocity of dunes will be discussed in the following paragraphs.

Dune height, although apparently a straightforward measurement, defies precise definition. First, the troughs just upstream and just downstream from a crest are usually not at the same depth, so that the height on the front is different from the height on the back. Furthermore, the crests are not truly two-dimensional; the lateral extent is often only a fraction of the flume width, the line of the crest is never straight, and the crest elevation varies considerably along the top of the dune, often dropping to zero at the ends. Should the maximum or average crest height be used? If so, should its elevation be compared with the deepest part of the trough, which frequently is off to one side, or should the trough elevation just downstream or upstream be used?

In addition, there is the perplexing problem of deciding how big a little hump of sand has to be before it warrants being called a dune, and being included in finding the average dune height. And conversely, how large must a depression in the sand be before it is allowed the distinction of being a genuine trough? This question is particularly bothersome in the case of a large mound of sand with two peaks separated only by a very shal-

low dip; in a case like this, is it one dune or two, and what should the dune height be considered?

The foregoing questions illustrate some of the impasses encountered in measuring dune height. In general, the author tended to measure heights from the highest point of the crest to the lowest point of the trough; average dune heights were estimated from a selection of representative looking dunes. Frequently, the highest dune was located and measured, because it is a more objective measure than the average dune height.

Inside the flume the elevations of crests and troughs were measured with the point gage; next to the window they were measured with a scale. Usually the dune heights in the central region are about the same or slightly smaller than the heights next to the window. The dune height was measured most frequently next to the window, because it could be done without stopping the flow.

Measuring the dune wavelength was subject to some of the same difficulties as measuring the height. The usual procedure was to measure, several times during the progress of a run, the total length of a sequence of about ten dunes next to the wall. From the photographs it is apparent that it was often hard to decide what should be counted as a dune. The procedure was to omit a small crest if it appeared more or less accidental, and include it if it seemed to have a definite connection with the rest of the configuration in the channel. The average wavelength was determined by averaging all the results. Note was frequently made of the range of values and any obvious relation of wavelength to dune height in individual cases.

From the photographs it may be seen that the wavelength at the wall may be either a little larger or smaller than the wavelength in the central region. In general, the wavelength was measured at the wall, as was the

height, because it was unnecessary to stop the flow.

The average velocity of travel of the dunes downstream was measured by following several representative crests and troughs at the window for a few minutes. Since the dunes would frequently change shape drastically or disappear before going even one foot, they could not be followed for long distances. Here again the average values reported for dune velocity should be considered only approximate; the sampling of dunes was meager and the velocity near the wall is probably less than the dune velocity in the central region. Because of the reduced visibility of the sediment-laden water and the difficulty of measuring distances on the bed inside the flume when the water was running, it was possible to measure dune velocities only at the wall.

M. PHOTOGRAPHS

Several photographs were taken for all the runs except Runs 2, 3, 4, and 7, to record the bed configuration or the character of the water surface (wavy, ripply, smooth, etc.). Some were taken overhead looking down, and others through the side windows. Some of the best photographs are included in Chap. VI, Sec. B. (Figs. 27 to 38).

For the overhead pictures, the water was stopped and allowed to settle. It was not generally feasible to drain the water off, because many puddles remain after draining and one or two days' wait is required for the bed to dry up enough to look natural again. When the photographs were taken through the water, the light was scattered some by a small amount of colloidal matter in suspension, resulting in less than normal contrast between the light and dark regions. The light was supplied by a flash bulb mounted in a reflector about 18 inches above the bed, and facing downstream.

Thus the light areas in the photographs are always the upstream faces of the dunes, and the shadows are the downstream faces. The overhead photographs of the bed are all mounted so that the light is coming from the reader's left, and the downstream direction is to the right.

The window pictures were taken either with the water running or still, depending on the visibility in the flow. The bed was lighted with two photoflood lamps behind the opposite window. A steel tape, marked in inches, was placed in all these pictures to give the scale and provide coordinates for reference. For some of the runs, groups of pictures were taken at measured intervals of several minutes to show the change and rate of movement of the configuration. Values of dune height, wavelength, and velocity obtained from the photographs were used to supplement or check the values measured directly.

Some time lapse and high speed motion pictures were taken for the purpose of studying the motion of the dunes. The observations from them will be explained later, in Chap. VI, Sec. B.

N. ESTABLISHING UNIFORM FLOW IN EQUILIBRIUM; REPRODUCIBILITY

Before making final measurements for a run it was first necessary to establish uniform flow in equilibrium with its sand bed. With a movable bed this was far from easy because of the changing configurations of the bed (smooth or rippled), and the frequent tendency for the sand to spread itself unevenly throughout the length of the flume. Equilibrium as used hereafter implies (1) that the depth of flow stays constant over a working section of the flume, and (2) that the pattern and distribution of sand on the bed has stopped changing.

Originally, it was believed that the rate of transport and the flow velocity would be uniquely determined by the size of sediment, the size of channel, and the shear stress on the bed, which in turn depends simply on the depth, width, and slope of the stream. As far as this author has been able to ascertain, every previous investigator of sediment transportation phenomena has assumed this hypothesis to be true; therefore, it was quite a surprise to find that the relationship is not unique. A further discussion will be included with the experimental results in Chap. VI, Sec. A.

This false assumption led to immediate difficulty in programming the runs to be made in the flume. The three main quantities which could be regulated were depth, d, discharge, Q, and the slope of the flume, S_f. The width is fixed and the sediment load cannot be controlled directly. An attempt was made at first to select various depths and slopes to be run for each of the sand sizes; but in the course of the experiments it was found that for some depth-slope combinations, there are two, or maybe even more, different equilibrium discharges and sediment loads. These are possible because of the tremendous variations in the roughness of the channel due to the appearance of dunes of various sizes.

Over quite a range of conditions, the slope changes very little, so that equilibria are hard to define sharply on the basis of a given slope. Furthermore, small changes in discharge, made to adjust to a given slope, can produce significant changes in the other variables, like total load and bed configuration. Sometimes it was not always possible to determine immediately even whether or not an adjustment of discharge was toward or away from equilibrium. Consequently many hours could be wasted trying to obtain an equilibrium by adjusting the discharge to match a given depth-

slope combination.

On the other hand, by fixing the rate of flow and the depth, it was possible to make the final adjustment in the slope quite simply. If the first approximation for the slope was in error, the amount of adjustment required could be figured by measuring the slope of the energy grade line relative to the flume. The adjustment of the slope of the flume would then cause only slight changes in the equilibrium. The slope of the energy line was really already determined, so in effect the inclination of the flume itself is just being adjusted to this slope, with the only net change to the flow being very minor redistribution of depths over the length of the flume. The rapid convergence of this adjustment process is well illustrated by Run 24 and the two corresponding preliminary runs, as follows:

	Prelim. A	Prelim. B	Final Run
S_f = slope of the flume	.0023	.0030	.0029
S = slope of the energy line	.0030	.0029	.0028
d = mean depth of flow, ft	.223	.223	.226
Q = discharge, cfs	.265	.265	.265

It is quite clear that a good estimate of the equilibrium slope of the energy line can be made even when the flume slope is badly off as in Prelim. A. The slight drop of S from .0029 for Prelim. B to .0028 for the final run can be attributed in part to the slight increase in depth.

The time required to reach equilibrium depended on the sediment load and the amount of adjustment of the bed configuration required. With high loads, less than one-half hour was required, but with light load up to four hours was sometimes needed. The final configuration of the bed was

found to be independent of the initial bed configuration, whether flat or in dunes, evenly or unevenly distributed in the flume. The initial condition affected only the amount of time required to reach equilibrium.

The reproducibility of the runs was excellent. This was well demonstrated in Run 28, where two water surface and bed profiles were taken on two different days. Scraping the bed for the first bed profile erased the dunes and ripples, so that the dunes had to be regenerated and equilibrium reestablished before any other measurements, including the second set of profiles, could be made. The two sets of profiles were practically identical, indicating that the equilibrium achieved was stable, well-defined, and reproducible. The calculated mean depths, velocities, and slopes for these cases were practically identical, as shown by the following tabulation:

	First Day	Second Day
d = depth, ft	.285	.284
U = mean velocity, ft/sec	1.31	1.32
S = slope	.00245	.00242

Other runs gave similar evidence of being very stable.

O. SUMMARY OF PROCEDURE

To establish uniform flow over a sand bed in equilibrium, it was found most feasible to select the depth and discharge and to adjust the slope to make the flow uniform. After running the flume long enough to ensure that the equilibrium was well established, various measurements and observations of water surface and bed elevation, velocity, sediment concentration, bed configuration, and other items were taken. The extent of the data obtained and some of the procedures used for each of the runs is summarized in Table I.

Table 1

SUMMARY OF PROCEDURE

Run Numbers	2	3	4 7	5	6	8 9 10 11	12 13	21	21a	23	24 25 26 27 28 30	29	C1 C2 C3 C4	C6	C7
Bed Condition:															
Smooth	x	x	x		x			x	x	x		x			
Dunes				x		x	x				x				
No sediment													x	x	x
Temperature:															
Not controlled	x	x	x	x	x	x	x						x	x	x
Controlled at 25°C.								x	x	x	x	x			
Velocity by Pitot tube:															
Vertical centerline profile	x	x	x		x			x				x	x	x	
Other vertical or horiz. "	x											x	x	x	
Mid-depth, centerline only										x	x				
Discharge:															
Measured by Venturi		x	x	x	x	x	x	x	x	x	x	x	**	x	x
Sediment Samples:															
Various depths on centerline	x	x	x		x			x				x			
Mid-depth, centerline only										x	x				
Discharge samples		x	x	x	x	x	x	x	x	x	x	x			
Water Surface Elevations:															
Estimated over-all average				x		x	x								
Detailed profile	x	x	x		x			x	x	x	x	x	x	x	x
Sand Bed Elevations:															
Flat bed - centerline profile	x	x	x		x			x	x	x		x			
Average estimated				x		x									
Scraped for profile							x	x	x	x	x	x			
General character of water surface and bed observed:	x	x	x	x	x	x	x	x	x	x	x	x	x	x	x
Bed Configuration Measurements:															
Wavelength of dunes*				x		x	x	x	x	x	x	x			
Height of dunes*						x	x	x	x	x	x	x			
Velocity of dunes*				x		x	x	x	x	x	x	x			
Photographs:															
Through window - still										x	x	x			
" " -water in motion				x	x	x	x	x	x	x	x	x			
Bed from overhead - still				x	x	x	x	x	x	x	x	x			

*Dunes or ripples near wall if bed is smooth in center, or meanders in bed
**For Run C1, the discharge was found by integration of velocity distrib.

CHAPTER IV

SAND CHARACTERISTICS

Fortunately, the uniform sands previously prepared and used by Vanoni (5) for suspended load investigations were still available and were used in these experiments, making it unnecessary to prepare new sand. Ismail (6) has also used these same sands. Two different uniform sands were used: Sand No. 1 with mean sedimentation diameter of 0.159 mm for Runs 2 to 13, and Sand No. 2 with sedimentation diameter 0.103 mm for Runs 21 to 30. Settling velocity measurements made on these sands by Vanoni were used as will be explained in more detail below.

A. SEDIMENTATION DIAMETER AND FALL VELOCITY FOR SAND GRAINS

The basic characteristics of sediment in all suspended load studies is its settling or fall velocity, w, in the transporting fluid. It is a complex function of the size, shape, and density of the particles, the density and viscosity of the fluid, and the concentration of particles in suspension. The size and shape of a sand particle are hard to describe geometrically, but the net effect of the size and shape on settling may be conveniently indicated by the sedimentation diameter, D_s. The sedimentation diameter of a particle is by definition the diameter of a sphere of the same density as the particle which has the same fall velocity in the same fluid at the same temperature.

McNown and Malaika (20) have made some measurements of drag on various small spheroidal, cylindrical, prismatic, and conical bodies at very small Reynolds numbers. From their results, it may easily be demonstrated

for all the various shapes tested and for Reynolds numbers in the Stokes range (< 0.1) that the sedimentation diameter depends only on the size and shape of the body itself, and not on the properties of the fluid or the difference in densities. In the absence of any direct evidence to the contrary, it seems quite reasonable to assume that the same is also approximately true for sand grains even at somewhat higher Reynolds numbers. In the present experiments, the highest particle Reynolds number, based on fall velocity and sedimentation diameter, was about 4.

For sand grains settling in water, the variation in Reynolds number is due entirely to temperature change, and in all practical cases this variation is less than a factor of 2 or 3. Thus, even though it may be found that the sedimentation diameter of a given particle changes somewhat over a wide range of Reynolds numbers, still it is believed that the assumption of constant sedimentation diameter will be found to be fairly good for the purpose of making temperature corrections of fall velocity.

Since the sands used were predominantly quartz (specific gravity 2.65), with only a trace of heavy minerals, the chart prepared by Rouse (1) for the fall velocity of quartz spheres in water at various temperatures was used. It is based on calculations from the well-defined drag coefficient - Reynolds number diagram for spheres. From the measured settling velocity of any sand grain in water at a known temperature, the sedimentation diameter, or the diameter of a quartz sphere having the same fall velocity, may be read from the chart.

McNown and Lin (21) have shown that the settling velocity of uniform sized particles decreases markedly as the concentration of the particles increases. This effect is called hindered settling because of the interference of the flow patterns established by each falling particle. As

a particle subsides, the surrounding water must flow upward; but when there are a great many particles settling, more water must be displaced upward through a constricted cross section. Hence the fall velocity is reduced. Although their analysis applies strictly only to suspensions of small identical spheres, it undoubtedly gives a good first approximation for a fairly uniform suspension of natural sand grains.

Table 2, based on an interpolation of McNown and Lin's results, gives the reduction in the settling velocity as a function of concentration for quartz spheres of diameter 0.103 mm. in water at 25°C. These values are the corrections which will be used for Sand No. 2. Since point concentrations as large as 28.5 gr/l were measured, it is important that hindered settling be taken into account in analyzing the experimental results.

Unfortunately, the analysis of McNown and Lin does not extend to high enough particle Reynolds numbers to permit tabulation of reductions in fall velocity for Sand No. 1 also. Nevertheless, the trend in their results for increasing Reynolds numbers indicates that the percentage reductions would not be as large.

B. MEAN SEDIMENTATION DIAMETER FOR A MIXTURE

The problem of finding a mean sedimentation diameter for a sand mixture has been handled in essentially the same way as done by Vanoni (22). First a sieve analysis of a sample was made with a fourth root of two series of standard Tyler laboratory sieves, which were shaken for 10 minutes in a Tyler Rotap machine. For each sieve fraction, Vanoni had found a mean sedimentation diameter, D_{s_i}, from directly measured fall velocities of a number of randomly selected sand grains. Results of his which are used here are tabulated in Table 3. Note that for the small sieve sizes the

Table 2

Effect of Concentration on the Fall Velocity of Quartz Spheres in Water

(based on McNown and Lin)

Diameter = 0.103 mm Temperature = 25°C

Concentration gr/l	Fall Velocity ft/sec	Per cent Reduction
0	.0300	0
0.1	.0299	0.2
1	.0290	3
5	.0275	8
10	.0264	12
20	.0250	16
30	.0242	19

Table 3

(after Vanoni)

Relation between Sedimentation Diameter and Sieve Diameter

Tyler Sieve No. Retained on	Sieve Openings Next Above	Ret. on	Mean Sieve Diam.	D_{s_i}, Mean Sed. Diam.	w_i, Fall Velocity at 20°C
	mm	mm	mm	mm	cm/sec
80	.208	.175	.191	.198	2.38
100	.175	.147	.161	.168	1.86
115	.147	.124	.135	.153	1.61
150	.124	.104	.114	.129	1.21
170	.104	.088	.096	.107	0.89
200	.088	.074	.081	.096	0.74
250	.074	.061	.067	.086	0.61

mean sedimentation diameter is substantially larger than the mean sieve diameter.

The average settling velocity, w, at 20°C, for any mixture is calculated as the weighted arithmetic average of the sieve fraction settling velocities, w_i; that is

$$w = \sum_i w_i p_i , \qquad (4.01)$$

where p_i is the fraction of the total weight of sand in the i^{th} sieve fraction, and $\sum p_i = 1$. The mean sedimentation diameter D_s is then taken as the sphere diameter corresponding to w, instead of the weighted mean of the individual D_{s_i} as Vanoni suggested. However, with the sands being fairly uniform, the calculated mean sedimentation diameter is practically the same by either method.

Since we are directly concerned with settling velocity, it seems more reasonable in general to average the fall velocity instead of the sedimentation diameter. Furthermore, w, as defined above, fits conveniently into an energy dissipation formula. If c is the total concentration of a dilute suspension, expressed as weight per unit volume, the rate of energy dissipation per unit volume due to the quiescent settling is simply

$$E = \sum_i w_i (cp_i) = c \sum_i w_i p_i = cw . \qquad (4.02)$$

This equation will be used in a later chapter.

Values of the mean settling velocity of a mixture at other temperaturesmay be found by using the mean sedimentation diameter and the fall velocity chart for quartz spheres (1). Theoretically, it might be better to find first the individual w_i at different temperatures using the D_{s_i}, and then apply Eq. 4.01 again; but for the well-sorted sands used, the result by either method is nearly identical.

It should be noted here that the use of a mean sieve diameter, a mean sedimentation diameter, or a mean settling velocity for a sieve fraction is theoretically unsound. Basically, a sieve is supposed to trap all the sand grains in a certain size range. Suppose, for the moment, that it is possible to define the size of the grains precisely, and that the sieve makes a clean-cut separation of sizes. Now the average size of the material caught on a sieve will be precisely the average of the upper and lower size limits only if the distribution of sand sizes within the sieve interval is symmetrical. The distribution curve for a sieve interval, under the restrictive assumptions above, is simply a segment of the over-all size distribution curve.

In a sieve interval, the distribution is nearly symmetrical only if (1) the sieve interval considered is near the center of the over-all size distribution or (2) the sieve interval is very small compared to the size range of the sample. But if a particular sieve size is substantially smaller than the mean size of the whole sample, then the average size of the material caught on that sieve will be biased toward the upper limit of the sieve interval, or the size of the sieve above. The converse is true when the sieve size is larger than the mean.

For example, consider the sieve analysis of Sand 1 plotted on Fig. 13: 97.6 per cent of the sand passed the 80 mesh sieve with 0.175 mm opening, and only 55 per cent passed the next sieve, 100 mesh with 0.147 mm opening. The median size of the sand in this interval is represented by the 76.3 per cent point on the curve, which corresponds to .155 mm. On the other hand, the average of the upper and lower limits is .161 mm, or 4 per cent too high. If a larger sieve spacing had been used, such as in the $\sqrt{2}$ series, the discrepancy could have been much more serious.

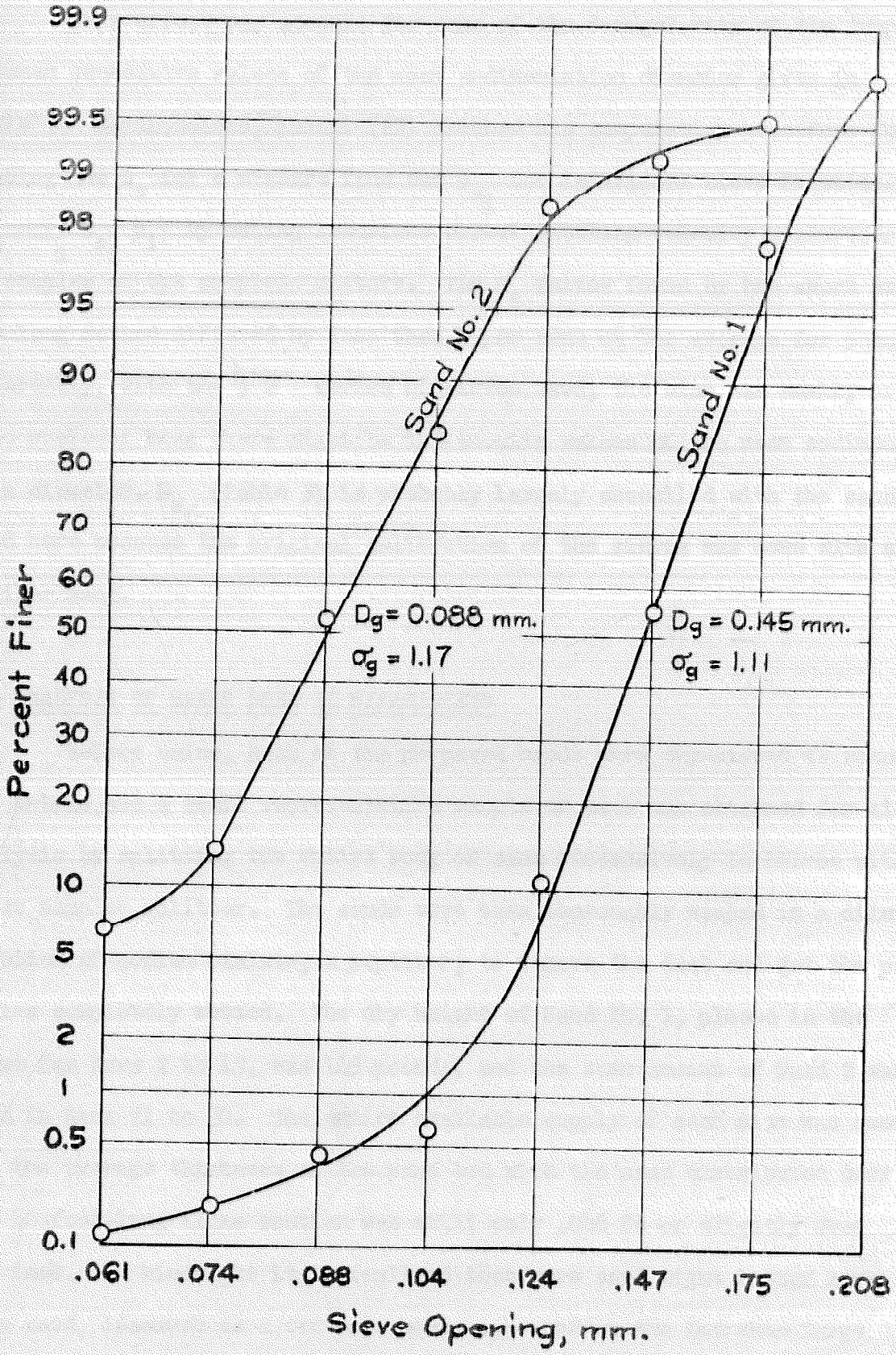

Fig. 13. Sieve Analysis of Sands Used

This effect may account for some of the irregularity of the jumps between successive values of the mean sedimentation diameter given in Table 3. Nevertheless, Vanoni (22) checked his computation procedure for finding the D_s for a mixture from the D_{s_i} for individual sieve fractions ($D_s = \sum_i D_{s_i} p_i$) by making laborious direct settling velocity measurements on samples of the complete mixture. The D_s values found by the short and the long method differed by less than 1 per cent on the average for 5 cases. Apparently, with the $\sqrt[4]{2}$ series of sieves used, the bias was small, or else whatever bias there might be in Vanoni's values of the mean sedimentation diameter, D_{s_i} (Table 3), is probably largely cancelled with the sands used here because the original calibration of the sieves was done with a similar sand.

C. ANALYSIS OF SANDS USED IN EXPERIMENTS

Before using, each of the prepared sands were dry-sieved to remove any debris, and a small representative sample of each was obtained for sieve analysis by splitting the entire body of sand successively in halves with a Jones sampler splitter. The sands were then thoroughly washed in a dilute solution of sodium oxalate, a peptizer, to remove the dust and get the particles completely wetted. The dry weight of Sand No. 1, placed in the flume for Runs 2 to 13, was 145 pounds, and the same amount of Sand 2 was used in Runs 21 to 30. The entire available supply of each size was used, but the average thickness of the sand bed with the sand distributed over the 40-foot-long flume section was still only .046 ft or slightly over 1/2 inch. In hindsight it is realized that more sand might better have been used, inasmuch as a few bare spots appeared on the bed when large dunes were formed. The possible effect of these bare spots will be dis-

cussed in Chap. VI, Sec. B (3).

The sieve analysis of the two sands used are plotted on logarithmic probability paper in Fig. 13, as suggested by Otto (23). Since the logarithms of the sand sizes are approximately distributed according to the normal error law, the sieve analyses plot as straight lines except for the tails. Thus the geometric mean is the median (by weight) or the 50 per cent size, D_{50}, and the geometric standard deviation, σ_g, is the ratio of D_{50} to D_{16}, the size for which 16 per cent of the sand is finer. Table 4 summarizes the main properties of the sands used.

Table 4

Summary of Sand Properties

	Sand No. 1	Sand No. 2
Geometric mean sieve diameter, D_{50}, mm	.145	.088
Geometric standard deviation, σ_g	1.11	1.17
Mean sedimentation diameter, D_s, mm	.159	.103
Mean settling velocity (20°C), w, cm/sec	1.69	0.83
Ave. density in place in flume, gr/cc	-	1.46
Main constituent	Quartz	Quartz
Specific gravity	2.65	2.65
Amount used in the flume, lb	145	145

A very slight decrease in size has resulted from the extensive use of these sands; Vanoni originally reported the geometric means as .147 mm and .091 mm for the two sands, while the corresponding values just prior to these investigations were .145 mm and .088 mm. There has also been a slight increase in the geometric standard deviation.

The dry weight of sand per unit volume in place under water on the bed of the flume was measured for Sand No. 2. With the sand bed flat, the

depth of the sand layer was measured carefully with the point gage. A short piece of 3-inch-diameter thin-walled brass tube, 1 1/2 in. long, was sharpened on one end and pushed down through the sand to the steel bed. The volume of sand thus enclosed was determined from the cross-section area of the tube and the depth of the sand layer.

The sand inside the cutter was easily removed by siphoning since the top of the cutter was beneath the water surface. The siphoned water was filtered, and the sand dried and weighed. The calculated density in place ranged from 1.43 to 1.50 gr/cc for five determinations, with an average of 1.46 gr/cc or 91 lb/cu ft. This is a typical value for loose uniform sand. Consequently, it is presumed that the density of Sand No. 1, which was not measured, was approximately the same.

CHAPTER V

CALCULATION OF BED SHEAR AND FRICTION FACTOR

A. DEFINITION OF SHEAR

One of the most difficult, but most important quantities to determine for a flowing stream is the shear stress exerted on the bed. This shear is the force which causes loose granular material to roll and slide along the bed of a stream. Furthermore, the internal shear stress in the water generates turbulence which enables the stream to carry sediment in suspension. The intensity of the turbulence and the strength of the turbulent diffusion are directly related to the shear.

Even if the bed of a stream is a flat surface, the bed shear stress at any point varies with time because of the turbulent fluctuations of the local stream velocity. C.M. White (24) has shown that these shear fluctuations can be of the order of magnitude of 100 per cent. However, of necessity, only the time average shear will be considered here.

If the stream bed is not smooth but is covered with obstacles, such as dunes or large particles, part of the resisting force will be due to increased pressure on upstream faces of obstacles, and reduced pressure in the wake behind them. Looking at the stream as a whole, it is impossible to separate the direct shear from the components of the normal forces parallel to the stream. Thus, the term, shear stress (or shear), as used hereinafter will refer to the resultant of all normal and tangential stresses acting on the bed in the direction of flow, and averaged over an area large compared with the obstacles. This is the usual way that the shear is defined by the hydraulic engineer, but it will be shown later that this measure of shear is inadequate to determine uniquely the sediment transporta-

tion rate of fine materials. For a given total shear stress, more sediment is entrained from a flat smooth surface than from a surface covered with dunes, because in the latter case only a small part of the shear is actually tangential stress effective for moving sediment.

For a channel with a uniform flow, the shear force on the bed is equal to the downstream component of the weight of the water. If the cross section area of the stream is A, the unit weight of water is γ, and the slope of the stream is S, then the shear force per unit distance in the direction of flow is γAS; if the wetted perimeter is p, the average stress, $\bar{\tau}_o$ at the boundary is

$$\bar{\tau}_o = \frac{\gamma AS}{p} = \gamma rS. \qquad (5.01)$$

The hydraulic radius r is defined as A/p.

If a stream is very wide with constant depth, d, then at an appreciable distance from the side walls the flow is two-dimensional and the shear stress is

$$\tau_o = \gamma dS. \qquad (5.02)$$

Unfortunately, the laboratory flume used was not wide enough to make the flow two-dimensional in the central region. The shear at the center in this case is larger than the average, γrS, but smaller than γdS, the maximum possible. Some discussion of the distribution of shear in rectangular open channels with uniform roughness is now in order.

B. SHEAR DISTRIBUTION ON THE BOUNDARIES OF RECTANGULAR CHANNELS OF UNIFORM ROUGHNESS

In elementary hydraulics it is assumed that the shear is uniform around the periphery, and equals γrS. This assumption is exactly true only in the case of axial symmetry, as in flow in a circular pipe, or two-

dimensional flow. In all other cases the shear varies in some manner which depends on the turbulent structure of the stream. At present so little is known about turbulence in three-dimensional channels even in the absence of suspended sediment, that a good analytical solution to the shear distribution problem is not yet possible. The discussion which follows in this section is necessarily confined to clear flow.

(1) Theoretical Solutions. Nevertheless, the Bureau of Reclamation (25,26) has recently attempted an analytical solution of the problem, using severe assumptions which makes the results subject to some doubt. The essential points of their derivation and the restrictions on it, may be summarized as follows:

Let x = distance in the horizontal direction transverse to the flow

y = distance in the vertical direction

τ_x = shear stress acting in the direction of flow on a vertical plane

τ_y = shear stress acting in the direction of flow on a horizontal plane.

First they show, quite correctly, that equilibrium of forces in the direction of the stream requires

$$\frac{\partial \tau_x}{\partial x} + \frac{\partial \tau_y}{\partial y} = \gamma S \,, \qquad (5.03)$$

γS being the downstream component of the weight of a unit volume of water. It is then assumed that there exists some scalar function $\Psi(x,y)$ such that

$$\tau_x = -B \frac{\partial \Psi}{\partial x} \,, \quad \tau_y = -B \frac{\partial \Psi}{\partial y} \qquad (5.04)$$

where B is some constant. Substituting Eq. 5.04 into Eq. 5.03 a Poisson partial differential equation is obtained:

$$\frac{\partial^2 \Psi}{\partial x^2} + \frac{\partial^2 \Psi}{\partial y^2} = -\frac{\gamma S}{B} \qquad (5.05)$$

The boundary conditions are (1) $\tau_y = 0 = \frac{\partial \Psi}{\partial y}$ at the free surface, and (2) $\Psi = 0$ on the wetted perimeter. Condition (2) is equivalent to taking $\tau = 0$ at the boundary on all planes perpendicular to the boundary and parallel to the axis of flow.

Eq. 5.05 is then solved either by classical mathematical methods, yielding solutions in the form of infinite series, or by the method of finite differences, or with a membrane analogy. Very good solutions to this equation may be obtained by these methods, but the important question here is whether the Poisson differential equation even applies to the physical situation. Since there is no known physical basis whatever for Eq. 5.04, the solution for Ψ and the calculated values of the shear at the boundaries must be checked against experimentally determined values of shear for a wide range of conditions before any confidence can be put in either the basic equation or the solution. The Bureau of Reclamation report (26) does not give any verification of the shear values calculated, although at first glance they appear qualitatively reasonable. The Bureau's calculations will be compared with some experimental results in the next subsection.

In this same Bureau of Reclamation report (26) a further assumption is made regarding the velocity distribution u (x,y), namely that $\Psi = Ku^n$, where K and n are constants. The value $n = 4$ appears to give the best fit for comparison with observed velocity distributions. This assumption has no bearing on the problem of the shear distribution, and does not make Eq. 5.04 any more tenable. In fact, a comparison with the theory of turbulent flow proposed by von Karman (27) for the case of a wide rectangular channel is illuminating. On the basis of his similarity hypothesis,

von Karman derives

$$\tau = k^2 \rho \frac{u'^4}{u''^2} \tag{5.06}$$

where k is the von Karman universal constant (about 0.4), ρ is the mass density, and u' and u'' are the first and second derivatives of the velocity with respect to y. On the other hand, Eq. 5.04 with the substitution $\tau = Ku^n$ reduces for two-dimensional flow to

$$\tau_y = \tau = -B \frac{d}{dy}(Ku^n) = -KB\, n\, u^{n-1}\, u' \tag{5.07}$$

The results are quite different. Since Eq. 5.06 is based on assumptions which have a definite physical basis in relation to the nature of turbulent flow, and Eq. 5.07 is not, Eq. 5.06 is preferred and can easily be shown from measured velocity distributions to be much more accurate. Eq. 5.07 does not lead to the simple power law for the velocity distribution as implied by Lane (25).

(2) Experimental Determinations. The shear distribution on the boundaries of a channel can be approximately determined from a measured velocity distribution, using the logarithmic velocity formula of von Karman (27). For two-dimensional or axially symmetric flow, von Karman gives the velocity distribution, u, in terms of the shear velocity $u_* = \sqrt{\tau_o/\rho}$ and the distance from the wall, y, as

$$u = \frac{u_*}{k}\left(\ln \frac{u_* y}{\nu} + C_1\right) \tag{5.08}$$

for a hydrodynamically smooth wall, and

$$u = \frac{u_*}{k}\left(\ln \frac{y}{K_s} + C_2\right) \tag{5.09}$$

for a rough wall, where K_s is a characteristic length for the roughness

elements. When u is plotted against $\log_{10} y$, the slope, m, of the straight line profile in units of velocity per cycle of 10 is

$$m = \frac{2.30u_*}{k} \quad . \tag{5.10}$$

The assumptions made are: (1) that Eqs. 5.08 and 5.09 also apply near the wall or bed of a prismatic channel where τ_o and u_* are variable; and (2) that the value of k is the same everywhere in the flow. The value of y for each point is taken as the distance to the closest solid boundary. Consequently, by plotting the velocity profiles at various points normal to the periphery and measuring the slope m for each, the relative distribution of u_* can be found by Eq. 5.10. The value of k is still considered unknown, but may be found by integrating the shear in the following way:

The boundary shear τ_o at any point is

$$\tau_o = \rho u_*^2 = \rho \frac{k^2}{2.30^2} \, m^2 \tag{5.11}$$

and the average value is, by Eqs. 5.11 and 5.01,

$$\bar{\tau}_o = \rho \frac{k^2}{2.30^2} \, \overline{m^2} = \rho g r S \tag{5.12}$$

If an over-all shear velocity is defined as

$$U_* = \sqrt{\bar{\tau}_o / \rho} = \sqrt{g r S} \tag{5.13}$$

then

$$\frac{k^2}{2.30^2} \, \overline{m^2} = U_*^2 \tag{5.14}$$

and

$$k = \frac{2.30 \, U_*}{\sqrt{\overline{m^2}}} \quad . \tag{5.15}$$

Substituting Eq. 5.15 into Eq. 5.10,

$$\frac{u_*}{U_*} = \frac{m}{\sqrt{\overline{m^2}}} \qquad (5.16)$$

Although this result may be applied to any shaped channel, the subsequent discussion is confined to rectangular open channels.

For Runs C1 and C6, two runs with clear flow and smooth boundaries, the velocity distribution was measured in sufficient detail to find the shear distribution by Eq. 5.16. The walls and bed were smooth. In each case the analysis was made for only half the channel, since velocity measurements showed that the flow was symmetrical about the centerline. The vertical and horizontal velocity profiles are shown in Fig. 14 and the values of the velocity on which they are based are tabulated in Appendix D. More data on Runs C1 and C6 may be found in Table 7 in Chapter VI.

All the profiles except one in each case were straight lines on semi-logarithmic paper with the only significant deviations occurring for (1) points near the surface, (2) points on a horizontal profile which are actually closer to the bed than the wall, or (3) points on a vertical profile which are closer to the wall than the bed. Curiously, the two profiles which were definitely not straight were both the vertical profiles, 0.30 ft from the centerline, or 0.14 ft from the wall. They could both be fitted quite well with a broken line with the turning point at about 0.035 feet above the bed with the lower line having the smaller slope. It is believed that this is the result of some large scale secondary circulation in the stream which has a fairly fixed pattern. In these two cases the slope used was the slope of the straight line which gives best fit over the entire profile, excluding the retarded zone near the surface.

To utilize Eq. 5.16 it was necessary first to find $\sqrt{\overline{m^2}}$. This

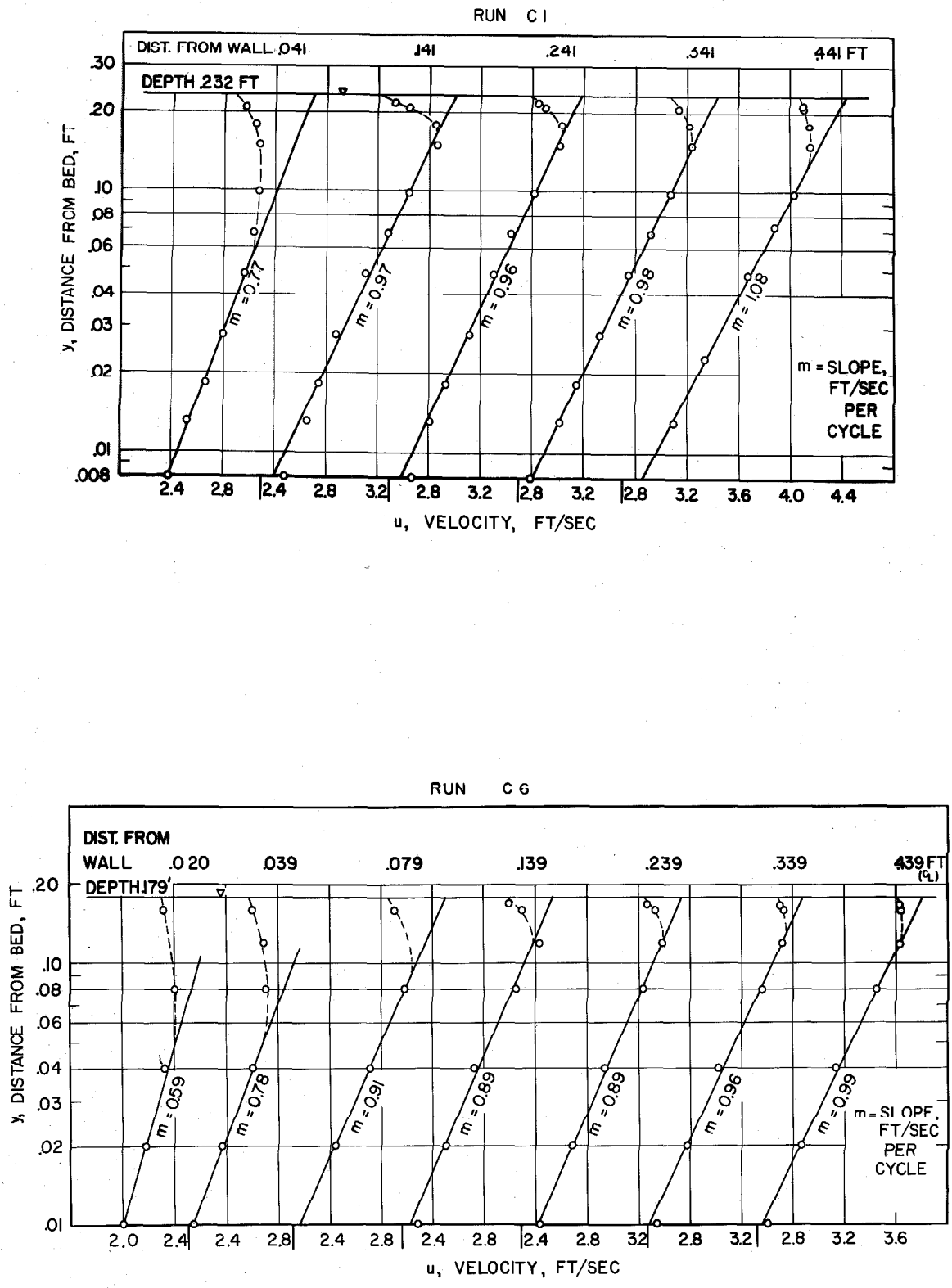

Fig. 14a. Vertical velocity profiles for Runs C1 and C6

was done by plotting m^2 around the boundary, and integrating the area under the curve by Simpson's rule to get the average. The values of k obtained by Eq. 5.15 were 0.395 and 0.365 for Runs C1 and C6 respectively. The shear distributions finally obtained are plotted in Fig. 15 in terms of u_* / U_*, the ratio of local shear velocity to the root-mean-square shear velocity, or $\sqrt{g r S}$.

For comparison, the shear distribution calculated by the Bureau of Reclamation (26) and reported by Lane (25) has also been plotted in the coordinates of Fig. 15 for width-depth ratio of 4. For Run C1 the width-depth ratio is 3.75 and for Run C6, 4.9. The agreement between the experimental and theoretical curves is surprisingly good.

All the curves show a maximum shear in the center, but the Bureau curve is a little too high in the central part of the bed and too low near the corner and along the wall. In fact, there is no a priori reason why the shear should be zero in the corner; hence the experimental curves were not made to pass through zero.

There are several limitations on the method illustrated above for finding the shear distribution experimentally. First of all, it is rather difficult to determine the profile slope values accurately, because they are very sensitive to small errors in the measurement of velocity or distance from the wall. Near the corner, the slope values are especially hard to measure because the logarithmic law applies for such a small part of the profile due to the interference of the adjacent wall. Furthermore, the large number of measured velocities required, especially near the boundaries, makes it a tedious procedure.

It is interesting to note that the discharge calculated from a

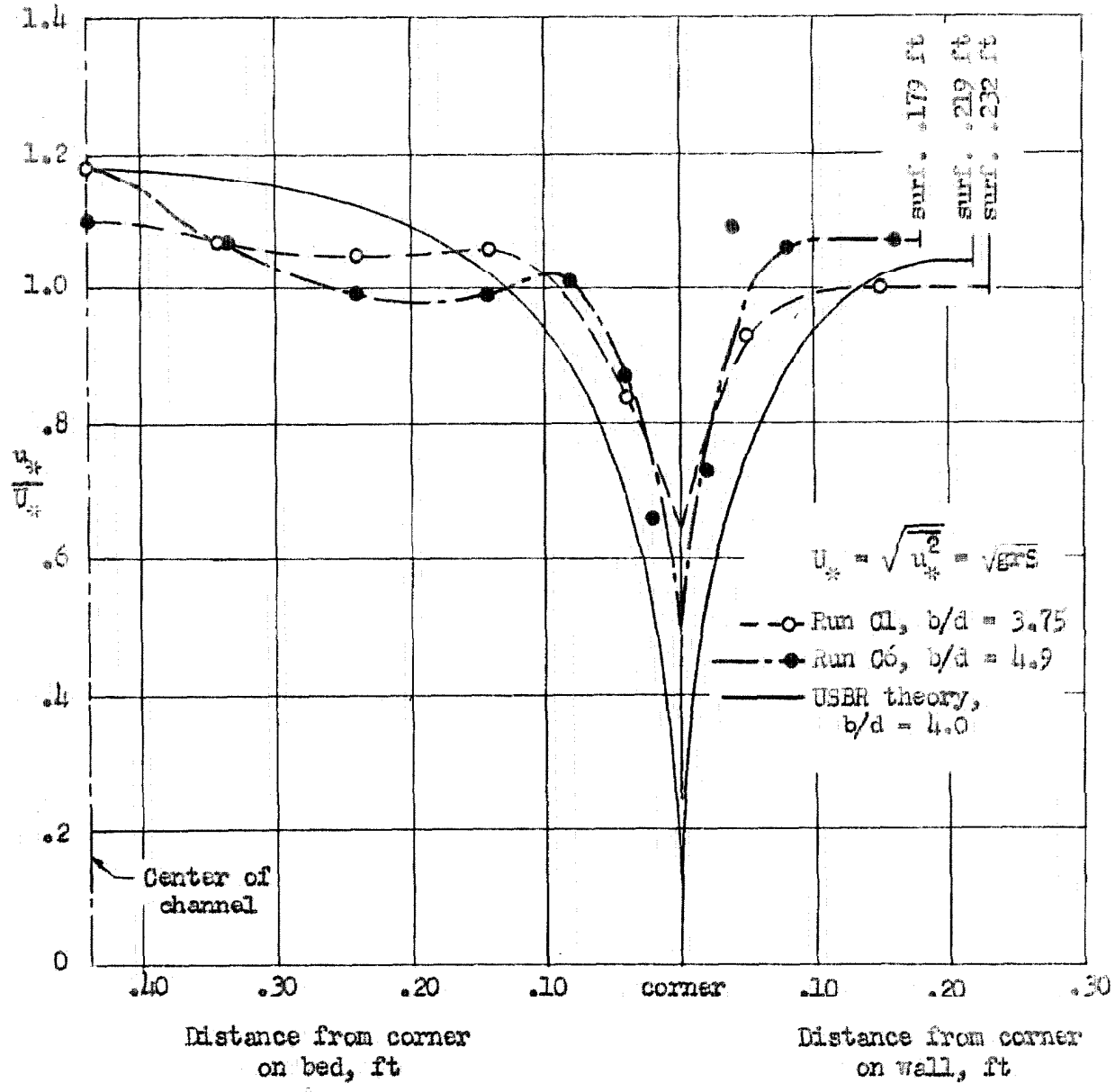

Fig. 15. Shear velocity distribution for clear flow in a rectangular channel of uniform roughness.

given set of velocity measurements is far more accurate than the shear distribution calculated from the same velocity measurements. This results from the fact that the discharge calculation is an integration of velocity, whereas the shear distribution depends on slopes or essentially differentiations of the velocity field.

Since many of the Pitot tube measurements are fairly close to the wall, some of the velocities are subject to a small but undetermined error. The wall causes too much constriction to the flow around the nose of the Pitot tube, resulting in too low a pressure at the static pressure opening and thus too high a measured velocity.

A further limitation is the possible error in the assumption that von Karman's equations can be applied. Certainly his similarity hypothesis breaks down when the velocity u becomes a function of two variables, and the walls upset the symmetry of the turbulent flow pattern. It is encouraging, though, that the profiles generally are straight, but it is still an assumption that the slopes are proportional to the boundary shear and that k is fixed for a given flow.

The scatter of points in Fig. 15 shows that the experimental errors are rather large. Hence the curves should be considered only approximate. It is even doubtful whether the inflection of the u_* / U_* curves in the bed section is a real effect.

Keulegan (28) has also studied the distribution of shear in rough rectangular channels with Bazin's data. Using experimentally derived values of $k = 0.40$ and $C_2 = 8.5$ in the velocity equation, Eq. 5.09, he computed the boundary shear velocities, u_*, from single velocity measurements, instead of from slopes of velocity profiles. Some minor adjustment of his results is needed, however, because the average value of $(u_* / U_*)^2$ found

by integration over the boundary is only .90 to .98 for the six cases tabulated instead of 1.00. Consequently, the reported values of the parameter u_* / U_* must be, on the average, from 1 to 5 per cent too low. This may be the result of $k = 0.40$ being 1 to 5 per cent too high. Nonetheless, Keulegan's results are substantially in agreement with the two experimentally determined shear distributions in Fig. 15.

Available experimental data on shear distribution are so few and the errors are so large that it is still impossible to predict exactly just what the shear distribution will be in any given case. The method outlined above is still an indirect approach, and future research would be more valuable if the wall shear stress could be measured directly as a force, as has been done recently by Liepmann and Dhawan (29) for a flat plate in a wind tunnel.

(3) Comparison of Mean Bed and Wall Shear. In this study, the difference between the average bed and wall shear, and the value of the shear at the center of the bed are of particular interest. If $\bar{\tau}_b$ and $\bar{\tau}_w$ are the mean values of the shear stress on the bed and wall, respectively, then

$$\frac{\bar{\tau}_b}{\bar{\tau}_o} = \frac{\overline{m_b^2}}{\overline{m^2}} , \tag{5.17}$$

and

$$\frac{\bar{\tau}_w}{\bar{\tau}_o} = \frac{\overline{m_w^2}}{\overline{m^2}} , \tag{5.18}$$

where m_b and m_w are the slopes of the velocity profiles along the bed and the wall. The corresponding bed and wall shear velocities U_{*b} and U_{*w} may be given by the equations

$$\frac{U_{*b}}{U_*} = \sqrt{\frac{\bar{\tau}_b}{\bar{\tau}_o}} \quad , \tag{5.19}$$

and

$$\frac{U_{*w}}{U_*} = \sqrt{\frac{\bar{\tau}_w}{\bar{\tau}_o}} \tag{5.20}$$

The values of these shear velocity ratios were calculated for Runs C1 and C6 and are tabulated in Table 5. For comparison, the same

Table 5

Average Bed and Wall Shear Velocities, and Maximum Shear Velocity on the Bed

(Clear flow in rectangular channels of uniform roughness)

Source	$\frac{b}{d}$	$\frac{U_{*b}}{U_*}$	$\frac{U_{*w}}{U_*}$	$\frac{u_{*m}}{\sqrt{gdS}}$	f
Run C1	3.75	1.03	0.94	0.96	.0167
Run C6	4.9	0.99	1.01	0.93	.0180
Series 61, Bazin	4.0	1.03	0.92	0.93	.026
" 56, "	4.75	1.03	0.93	0.97	.035
" 57, "	4.75	1.04	0.90	1.01	.060
" 65, "	4.75	1.05	0.87	0.97	.060
" 55, "	6.7	1.02	0.93	0.94	.0175
" 59 "	7.7	1.01	0.94	0.95	.0135
U.S.B.R.	4.0	1.05	0.90	0.97	-

quantities were calculated for the shear distributions given by Keulegan (28) for Bazin's data and the theoretical distribution proposed by the Bureau of Reclamation (26) for width-depth ratio, b/d, equal to 4. In these cases, the reported shear values were averaged directly instead of using Eqs. 5.17 and 5.18; in addition, an adjustment was made in

Keulegan's calculated data by using the actual calculated average value of $(u_* / U_*)^2$ as the relative average shear instead of 1.00 as it should have been. Simpson's rule was used in all cases to obtain average values from plotted curves.

From Table 5 it may be concluded that the average shear velocity for the bed alone (U_{*b}) will only be a few per cent higher than the value $U_* = \sqrt{grS}$ in the range of width-depth ratios listed. There is obviously some discrepancy in Run C6, because $U_{*w} > U_{*b}$ is physically impossible for b/d = 4.9. It must be concluded that either the slopes of the velocity profile are in error, or that the slope is not directly proportional to the shear velocity because of three-dimensional effects such as secondary circulation.

The tabulated values for the Bureau of Reclamation theory agree quite well with the other values, although the difference between the average bed and wall shears is perhaps a little too large.

(4) Maximum Bed Shear. In the fourth column of Table 5, the maximum shear velocity, u_{*m}, which should be at the center of the bed, is compared with the maximum possible for a wide rectangular channel, i.e., $\sqrt{gdS}$. The ratio of these two values is easily found from the relation

$$\frac{u_{*m}}{\sqrt{gdS}} = \frac{u_{*m}}{U_*} \cdot \sqrt{\frac{r}{d}} = \frac{u_{*m}}{U_*} \sqrt{\frac{b}{b + 2d}}$$

No adjustment of the values given by Keulegan was made here, because it was believed that the calculated values of u_{*m} / U_* were probably more accurate than the other reported values of u_* / U_* upon which the integration of the shear stress was based, and found to be slightly in error.

There should be a consistent trend for the maximum shear velocity ratio of Table 5 to approach 1.00 as the channel becomes very wide, but it is apparently masked by the experimental errors, or the effect of other variables, such as channel roughness. In Bazin's data, the higher values are associated with larger friction factors, f, which are also tabulated in Table 5. The Darcy-Weisbach friction factor, f, may be defined for any shaped cross section (30) as

$$f = 8 \left(\frac{U_*}{U}\right)^2 , \qquad (5.21)$$

where U is the average channel velocity and U_* is the average shear velocity, $\sqrt{grS}$.

On the basis of these six series of Bazin's data, Keulegan (28) suggested the formula

$$\frac{u_{*m}}{U_*} = 1 + \alpha \frac{U_*}{U} \cdot \frac{d}{b} \qquad (5.22)$$

where α is a constant equal to about 11. Since there is insufficient evidence to prove or disprove Eq. 5.22, and because it can lead to values of $u_{*m} / \sqrt{gdS}$ greater than 1.00, it will not be used here. Another method for finding the value of u_* at the center of the channel for runs for which only one vertical velocity profile was determined will be described in Sec. D after consideration of the case of nonuniform roughness.

C. BED SHEAR AND FRICTION FACTOR FOR OPEN CHANNELS OF NONUNIFORM ROUGHNESS

In the preceding section, only channels with uniform roughness on the walls and bed were considered. If the wall surface is not as rough as the bed, as was the case in all the experimental runs with a movable sand

bed, then the distribution of shear is altered. As the bed becomes rougher, the shear on the bed increases and the shear on the wall decreases because the bed offers more resistance to flow. In the central region the flow becomes more nearly two-dimensional and the effect of the walls diminishes.

No attempt will be made to derive the entire shear distribution for the case of variable roughness. The method given previously, based on Eqs. 5.08 to 5.16, could still be used provided the value of the von Karman constant k has a fixed value; but when sediment is carried in suspension the value of k is reduced and probably may no longer be considered a constant throughout the flow. For a flow carrying suspended load in a closed rectangular channel, Ismail (6) found that the k value was significantly larger near the upper boundary than it was near the bed, where there was more sediment in suspension.

However, for the present investigation, calculation of the average bed shear and the maximum at the center will be quite sufficient. It will be assumed that the roughness of the bed is uniform and that the wall roughness is different, but also uniform. In such cases, methods for finding the mean bed shear from the over-all average shear have commonly been called "side-wall correction methods", and will be the topic for the remainder of this section.

(1) Existing Side-Wall Correction Methods. Einstein (31) has proposed a method of side-wall correction for finding the mean bed shear, based on the Manning flow equation,

$$U = \frac{1.49}{n} r^{2/3} s^{1/2} \qquad (5.23)$$

where n is the roughness coefficient and the other variables are as pre-

viously defined. Einstein assumed that the cross section area, A, of the stream could be divided into a wall section, A_w, and a bed section, A_b, as illustrated in Fig. 16, and that the Manning equation could be applied to

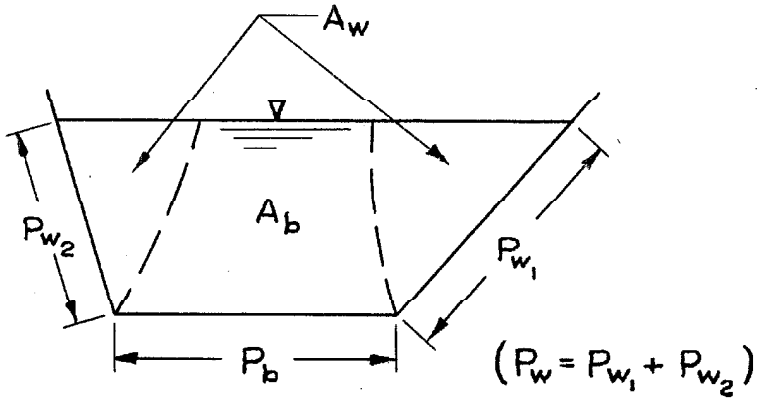

Fig. 16. Definition sketch for side-wall correction methods.

each, using the same slope and mean velocity for each section. Letting the subscript w denote "wall section" and b denote "bed section", Eq. 5.23 gives

$$U = \frac{1.49}{n_b} r_b^{2/3} S^{1/2} = \frac{1.49}{n_w} r_w^{2/3} S^{1/2} \qquad (5.24)$$

wherein the hydraulic radii are defined in terms of the areas A_b and A_w and the wetted perimeters p_b and p_w for the bed and wall sections respectively as

$$r_b = \frac{A_b}{p_b}, \quad \text{and} \quad r_w = \frac{A_w}{p_w} \qquad (5.25)$$

An additional relation which is needed is

$$A = A_b + A_w . \qquad (5.26)$$

Given U, S, A, p_w, p_b, and either n_b or n_w, the remaining five unknowns, r_w, r_b, A_w, A_b, and either n_w or n_b, can readily be found from these five

equations. The shear velocities for bed and wall are then

$$U_{*b} = \sqrt{g r_b S} \; ; \quad U_{*w} = \sqrt{g r_w S} \tag{5.27}$$

This procedure can be used with any other flow equation, although perhaps not quite so easily. However, the Manning equation is poor in the case of hydrodynamically smooth boundaries, such as the side-walls in the present investigation, and the Einstein method will not give good results, especially when the temperature is variable. Johnson (32) pointed this out, and showed the advantage of using the Karman-Prandtl resistance equations in place of the Manning formula. The Darcy-Weisbach friction coefficient f, used in the Karman-Prandtl equations, has a further advantage in that f is dimensionless, whereas the Manning n is not. Therefore, Johnson's method was used in this investigation to correct the bed shear for the effect of the walls.

Although the coefficients in the Karman-Prandtl equations and the corresponding resistance diagram giving f in terms of the Reynolds number and the relative roughness are based on experimental data for flow in pipes, still they may be used with reasonable accuracy for flow in channels. Keulegan (28) has shown that when the hydraulic radius r is used as the characteristic length for the channel cross section, the resistance formulas are practically the same for various shapes of cross section. Hence, if the pipe diameter, D, is replaced by 4r (since $r = D/4$ for a pipe), the pipe resistance diagram may also be used with good approximation for channels.

One good test of any side-wall correction method is to see how well it works in the limiting case of uniform roughness on the whole boundary. By either Einstein's or Johnson's method we find that in this case

$r_b = r_w = r$, and therefore, by Eq. 5.27, $U_{*b} = U_{*w} = U_*$. But it has been shown in Table 5 in Section B that for rectangular channels several times as wide as they are deep that U_{*b} can exceed U_{*w} by 10 per cent, and exceed U_* by several per cent. This slight inconsistency is largely the result of assuming that the mean velocity of flow in the wall section, U_w, is equal to the mean velocity in the bed section, U_b, when it may be expected that U_b is slightly greater than U_w.

O.G. Haywood (33) tried to take some account of the velocity distribution in a method of side-wall correction he proposed. He subdivided the flow as Einstein did into a wall section and a bed section, but as the result of various conflicting assumptions, he arrived at results for which U_{*b} did not even equal $\sqrt{gr_bS}$. His method is thus completely inadequate.

In Appendix C it has been shown how the Johnson method of side-wall correction, using the Darcy-Weisbach formula, can be modified to include U_b/U and U_w/U as parameters, U being the average velocity for the whole channel. Using $U_w/U = 0.9$, a reasonable value estimated from velocity distributions, it was found for all the experimental runs that U_{*b} was never more than 4 per cent larger than the value calculated using $U_w/U = 1.0$. As expected, this difference is of the same order of magnitude as $(U_{*b} - U_*)$ for channels of uniform roughness. As the present studies do not require such precision in U_{*b}, it will be assumed for simplicity that $U_w = U_b = U$; hence the method outlined below is essentially that of Johnson (32). The main usefulness of the equations derived in Appendix C is in determining what error may be involved by taking the velocity in the wall section, U_w, equal to the velocity in the bed section, U_b.

(2) Derivation of Equations for Side-Wall Correction. First it will be convenient to define here a few new terms and to recapitulate some definitions and formulas already given.

S = slope of the energy line

ν = kinematic viscosity

g = acceleration of gravity

U = mean velocity

These quantities apply to either the entire flow, the bed section, or the wall section.

Each of the following quantities and formulas may be used either with subscript b for the bed section or subscript w for the wall section, or without any subscript for the whole channel:

A = area of cross section

p = wetted perimeter

$r = A/p$ = hydraulic radius (5.28)

$U_* = \sqrt{grS}$ = shear or friction velocity (5.29)

$f = 8\,(U_*/U)^2$ = Darcy-Weisbach friction factor (5.30)

$R = 4\,Ur/\nu$ = Reynolds number (5.31)

The following assumptions are made:

1. The cross section can be divided into two sections, one producing shear on the bed and the other shear on the walls. The boundaries between the bed and wall sections are considered surfaces of zero shear, and are not included in the wetted perimeters p_b and p_w.

2. The velocity in the wall section, U_w, equals the velocity in the bed section, U_b. (Cf. Appendix C if this assumption is unsatisfactory).

3. The formulas above for r, U_*, f, and R can be applied to each section as if it were a channel by itself.

4. The roughnesses of the walls and bed are each homogeneous, although different.

The derivation which follows applies to any reasonable shape of open channel section. It may also be extended to cases with more than two types of roughness.

The following fundamental quantities are taken as known variables: U, S, g, ν, p_w, p_b, and A. In addition, the quantities r, U_*, f, and R, for the whole section, may be determined directly by Eq. 5.28 to 5.31. The principal unknowns of interest are U_{*b}, the friction velocity for the bed, r_b, the bed hydraulic radius, and f_b, the bed friction factor.

To solve the problem, f_w must also be known. If the equivalent sand roughness of the side-walls is known, then the value of f_w can be determined with some auxiliary calculations from a generalized pipe resistance or Stanton diagram, such as the one given by Rouse (30). Since the side-walls were hydrodynamically smooth in the present investigations, the procedure which will be outlined for finding f_w will be somewhat simplified by the elimination of the relative roughness as one of the variables. However, the general case can be solved, with the same type of approach.

For smooth walls, f_w will be a function only of the Reynolds number for the wall,

$$R_w = \frac{4\, U_w r_w}{\nu} = \frac{4U\, r_w}{\nu}$$

Inasmuch as r_w is still unknown, rewrite R_w as

$$R_w = R\,\frac{r_w}{r} \quad . \tag{5.32}$$

By Eqs. 5.29 and 5.30

$$g\, r_w S = \frac{f_w}{8}\, U^2 \quad , \tag{5.33}$$

and $$g\,r\,S = \frac{f}{8}\,U^2 \quad . \tag{5.34}$$

Hence $$\frac{r_w}{r} = \frac{f_w}{f} \quad , \tag{5.35}$$

and Eq. 5.32 becomes

$$\frac{R_w}{f_w} = \frac{R}{f} \quad . \tag{5.36}$$

Thus the quantity $\frac{R_w}{f_w}$ can be found directly, but neither R_w nor f_w individually. Consequently, it was necessary to construct a special curve, Fig. 17, giving f as a function of R/f for smooth-walled channels. Fig.17 is based on the graph of f vs. R given by Rouse (30) for the Karman-Prandtl resistance equation for turbulent flow in smooth pipes. Hence, knowing f and R, it was possible to find f_w by Eq. 5.36 and Fig. 17.

Now, the geometry requires that

$$A = A_b + A_w. \tag{5.37}$$

If $r = A/p$ is substituted into Eq. 5.34,

$$A = \frac{p\,f\,U^2}{8\,gS} \quad .$$

Similarly, $$A_b = \frac{p_b\,f_b\,U^2}{8\,g\,S} \quad ,$$

and $$A_w = \frac{p_s\,f_w\,U^2}{8\,g\,S} \quad .$$

Putting these expressions for the area into Eq. 5.37, and cancelling the common factor $U^2/\,2gS$, the result is

$$pf = p_b\,f_b + p_w\,f_w \tag{5.38}$$

Since f_b is the only unknown, the solution is

$$f_b = \frac{p}{p_b}\,f - \frac{p_w}{p_b}\,f_w \quad . \tag{5.39}$$

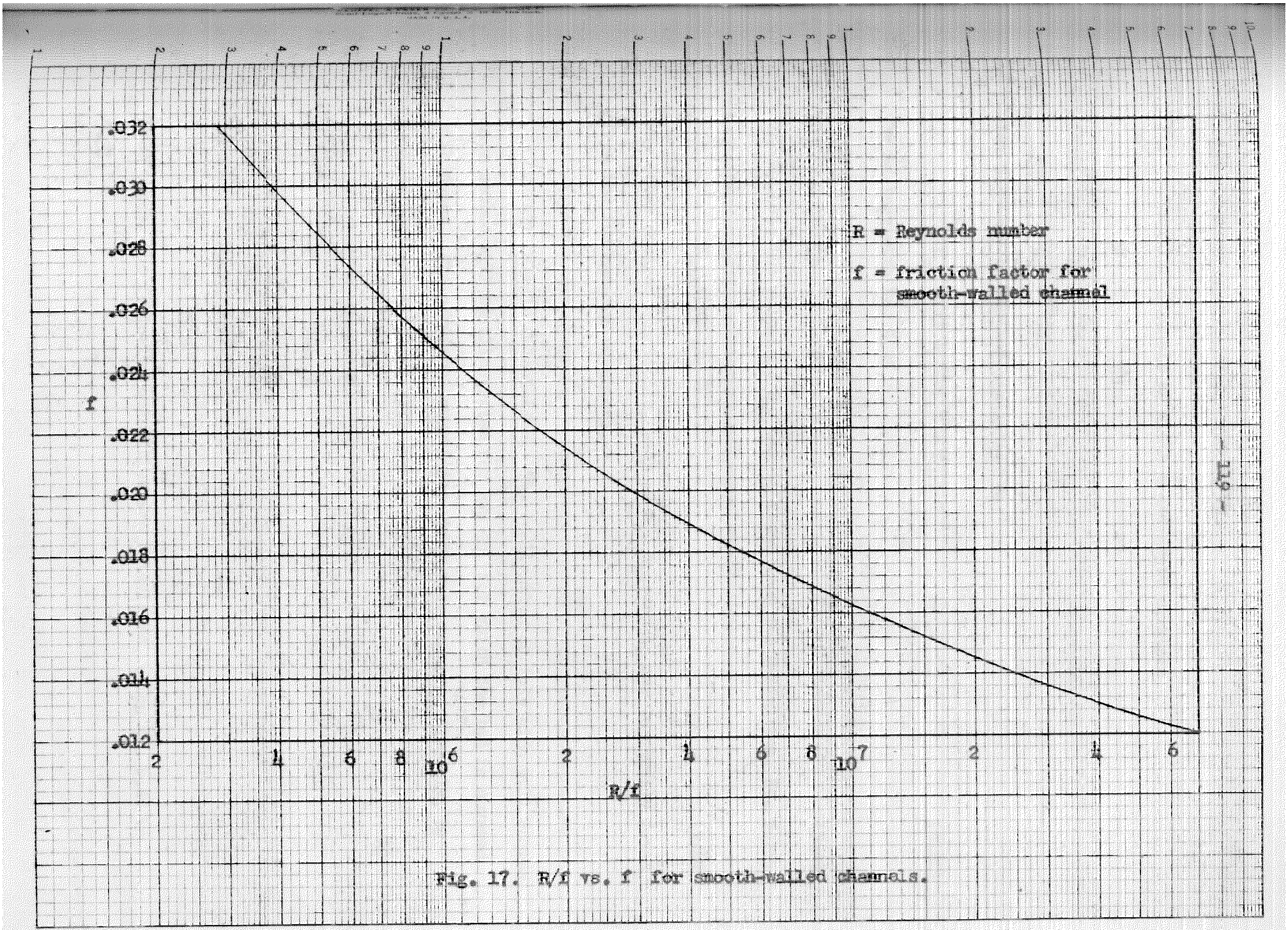

Fig. 17. R/f vs. f for smooth-walled channels.

For rectangular channels of width b and depth d, where

$$p = b + 2d ,$$

$$p_b = b,$$

and $$p_w = 2d,$$

Eq. 5.39 may be further simplified to

$$f_b = f + \frac{2d}{b} (f - f_w) \qquad (5.40)$$

By analogy with Eq. 5.35,

$$r_b = r \frac{f_b}{f} \quad . \qquad (5.41)$$

To complete the solution, U_{*b} may be found from its definition, Eq. 5.29,

$$U_{*b} = \sqrt{g r_b S} \quad . \qquad (5.42)$$

Any other desired quantities, such as r_w, A_w, and A_b may be readily found from the fundamental equations.

(3) Sample Calculation. The application of this side-wall correction method will be illustrated for Run 28, for which the bed is covered with dunes. The pertinent quantities which were measured directly, by methods outlined in Chap. III, are as follows:

$$Q = 0.328 \text{ cfs}$$

$$d = 0.284 \text{ ft}$$

$$b = 0.875 \text{ ft}$$

$$S = .00242$$

$$T = 25^{\circ}C$$

From these, the following quantities are calculated, using Eq. 5.28 to 5.31:

$$A = bd = (0.875)\ (0.284) = 0.248 \text{ sq ft}$$

$$U = Q/A = \frac{0.328}{0.248} = 1.32 \text{ ft/sec}$$

$$p = b + 2d = 0.875 + 2(0.284) = 1.443 \text{ ft}$$

$$r = A/p = \frac{0.248}{1.443} = 0.172 \text{ ft}$$

$$U_* = \sqrt{grS} = \sqrt{(32.2)(0.172)(.00242)} = 0.116 \text{ ft/sec}$$

$$f = 8\left(\frac{U_*}{U}\right)^2 = 8\ \frac{(0.116)^2}{(1.32)^2} = .062$$

$$\nu = 0.965 \times 10^{-5} \text{ ft}^2/\text{sec}$$

$$R = \frac{4\,U\,r}{\nu} = \frac{4(1.32)(.172)}{.965 \times 10^{-5}} = 94{,}000$$

The next step is to find f_w, the friction factor for the smooth walls. By Eq. 5.36

$$\frac{R_w}{f_w} = \frac{R}{f} = \frac{94{,}000}{.062} = 1{,}520{,}000.$$

From Fig. 17, the value $f_w = .0226$ is read from the curve for $R_w/f_w = 1.52 \times 10^6$.

Now by Eq. 5.40,

$$f_b = f + \frac{2d}{b}(f - f_w) = .062 + \frac{2\,(0.284)}{0.875}\ (.062 - .0226)$$

$$f_b = .088$$

And by Eq. 5.41 and 5.42,

$$r_b = r\,\frac{f_b}{f} = 0.172\ \frac{.088}{.062} = 0.244 \text{ ft}$$

$$U_{*b} = \sqrt{gr_b S} = \sqrt{(32.2)(0.244)(.00242)} = 0.138 \text{ ft/sec}$$

The ratio of the mean bed shear stress to the over-all average is

$$\frac{\bar{\tau}_b}{\bar{\tau}_o} = \frac{r_b}{r} = \frac{f_b}{f} = \frac{.088}{.062} = 1.42 .$$

Similarly for the wall

$$\frac{\bar{\tau}_w}{\bar{\tau}_o} = \frac{r_w}{r} = \frac{f_w}{f} = \frac{.0226}{.062} = 0.36 .$$

Since the average bed shear is now almost four times the wall shear, it is clear that a very significant redistribution of shear stresses has been caused by the increased roughness of the bed due to the dunes.

A side-wall correction is obviously indispensable; Johnson's method (32) as used here is the simplest and most reliable one. A slight improvement of the method, allowing for different bed and wall section velocities, has been outlined in Appendix C, but has not been used in calculating the experimental results which are reported in full in the next chapter.

D. METHOD FOR CALCULATING BED SHEAR ON THE CENTER LINE

For the runs in which velocity and sediment concentration profiles were measured on the center line only, it was necessary to know u_{*m}, the shear velocity at the center of the bed, in order to calculate values of the von Karman k, and the diffusion coefficient for sediment. The method of calculating the shear distribution given in Sec. B cannot in general be used because of the variability of k with sediment in suspension. Furthermore, that method is tedious, and detailed velocity distributions for the whole cross section were obtained for only three runs.

For channels several times as wide as they are deep, the value of u_{*m} will be several per cent less than $\sqrt{gdS}$, the shear velocity for two-

dimensional flow, unless the bed is very rough. (Cf. Sec. B (4) and Table 5 for channels of uniform roughness). However, u_{*m} is still more than the average for the bed, U_{*b}.

In the absence of any other objective method for calculating u_{*m}, the following procedure seemed reasonable:

1. Find the friction factor for the bed, f_b, by Eq. 5.40.

2. Determine the mean velocity, $\bar{u}$, on the center line vertical from a measured velocity profile. Since the profile could be fitted with the von Karman logarithmic formula, Eq. 1.44, $\bar{u}$ could be read from the profile at $y/d = 1/e$ or $y = 0.37d$. The slight retardation near the surface was neglected.

3. Calculate u_{*m} from the Darcy-Weisbach formula applied to a central strip, using f_b and $\bar{u}$; i.e.,

$$u_{*m} = \bar{u}\sqrt{f_b/8} \tag{5.43}$$

The complete calculated results are included in the following chapter, but a short summary is given in dimensionless form in Table 6 for the runs where u_{*m} was needed.

As expected, the shear velocity ratios for the runs with sediment, and hence larger f_b, are slightly larger than the clear flow runs for comparable width-depth ratios. For example, for b/d between 3.6 and 3.9, the average value of $u_{*m}/\sqrt{gdS}$ for Runs C1 and C4 is 0.94 and for Runs 3, 4, 7, and 21, it is 0.97.

The previously calculated maximum shear velocity ratios for Runs C1 and C6 in Table 5 were 0.96 and 0.93 respectively compared with 0.95 and 0.96 here. The check is very satisfactory and so it is believed that the error in the values of u_{*m} found from Eq. 5.43 does not exceed a few per cent.

Table 6

Shear Velocity at the Center of the Bed

$$u_{*m} = \bar{u}\sqrt{f_b/8}$$

Run	$\frac{b}{d}$	f_b	$\frac{u_{*m}}{\sqrt{gdS}}$
C1	3.75	.017	0.95
C2	5.1	.0185*	0.99
C3	7.6	.0205*	0.97
C4	3.9	.0195*	0.92
C6	4.9	.0185	0.96
2	3.1	.018**	0.91
3	3.6	.0275	0.97
4	3.7	.023	0.97
6	4.5	.0225	1.00
7	3.6	.0225	0.98
21	3.7	.022	0.95
29	3.1	.019	0.89

*Estimated from resistance diagram; total discharge was not measured for these runs.

**Based on estimated discharge.

CHAPTER VI

EXPERIMENTAL RESULTS

The experimental results will be presented in three interrelated sections. In Section A the characteristics of the stream as a whole will be reported, with particular emphasis on the basic relationships between sediment load and discharge, depth, slope, mean velocity, and other variables which pertain to the entire flow. In Section B, observations of the water surface and bed configuration will be summarized, and illustrated with photographs. In Section C, velocity and sediment concentration profiles, measured for the runs for which the sand bed was smooth, will be compared with the theory in Chap. I. A brief summary is given at the end of each main section, instead of at the end of the chapter.

A. CHARACTERISTICS OF THE STREAM AS A WHOLE

(1) Summary of Data. Each run represented a stable uniform flow in equilibrium with its movable sand bed. Runs were established and the measurements were made according to procedures outlined in detail in Chap. III.

The bed was composed of a uniform fine sand of mean sedimentation diameter $D_s = 0.159$ mm for Runs 2 through 13 and $D_s = 0.103$ mm for Runs 21 through 30. The properties of the sand and the methods of analysis have been described in Chap. IV.

The sand was so fine that the rate of suspended load transport was much greater than the rate of bed load transport, except possibly in Runs 10 and 26 where the total transportation rate was very small. This does not mean that an insignificant amount of material was in motion on the

bed; on the contrary, several layers of sand grains were almost always sliding along the bed, but at a relatively low rate compared with the velocity of the water. If the same amount of material was in suspension, it yielded a much larger transportation rate, (expressed as a weight per unit time passing any cross section) because the sand then traveled at the full speed of the water.

Anyway, the distinction between bed load and suspended load is quite nebulous, and no attempt was made here to make an artificial separation. All the values of transportation rate and discharge concentration reported in this section refer to the entire sediment discharge, bed load included. At the point where the sediment discharge was measured, in the forebay of the pump, all the load was in suspension and was measured as such. Hence, the sediment discharge concentration, by its definition, is the total rate of sediment transportation divided by the discharge, and thus, is not necessarily the same as the average concentration of sediment in suspension in the channel. Measurements of point concentrations in the channel will be reported in Section C.

In Table 7 are tabulated the most important measured and calculated quantities for each flow. In order of their appearance in the table, the items are as follows:

1. Q = discharge, in cubic feet per second (cfs), as measured by the Venturi meter (cf. Chap. III, Sec. F.).

2. d = average depth in feet in the reach of stable flow, determined from water surface and bed profiles (cf. Chap. III, Secs. H and I).

3. $r = \frac{bd}{b+2d}$ = hydraulic radius in feet. (b = width = 0.875 ft for all runs.)

Table 7

Summary of Experiments

Run No.	Q Discharge cfs	d Depth ft	r Hydr. Radius ft	S Slope	U_* Shear Vel. ft/sec	U Average Vel. ft/sec	f Friction Factor	T Water Temp. °C	r_b Bed Hydr. Radius ft	U_{*b} Bed Shear Vel. ft/sec	f_b Bed Friction Factor	No. of Sed.Disch. Samples	$\bar{C}$ Sed. Disch. Conc. gr/l	G Sediment Discharge lbs/min	F Froude No.	Water Surface Condition	Bed Condition	Run No
Clear Water																		
C-1	.695	.232	.152	.0050	.157	3.44	.0167	18	.156	.159	.017	-	-	-	1.27	Smooth	No sand	C-1
C-2	.45 e	.171	.123	.0050	.141	3.0 e	-	18.5	-	-	.0185 e	-	-	-	1.3 e	Smooth	No sand	C-2
C-3	.24 e	.115	.091	.0050	.121	2.4 e	-	18	-	-	.0205 e	-	-	-	1.3 e	Smooth	No sand	C-3
C-4	.32 e	.225	.148	.00125	.077	1.6 e	-	14.5	-	-	.0195 e	-	-	-	0.6 e	Smooth	No sand	C-4
C-6	.47	.179	.127	.0049	.142	3.00	.0180	27	.131	.145	.0185	-	-	-	1.25	Smooth	No sand	C-6
C-7	.435	.241	.155	.00195	.099	2.06	.0183	17	.157	.099	.0185	-	-	-	.74	Small waves	No sand	C-7
Sand Bed, D_{50} = 0.16 mm																		
2	.54 e	.284	.172	.0018	.100	2.15 e	.017 e	17	.174 e	.100	.018 e	0	-	-	.71e	Small waves	Smooth	2
3	.435	.243	.156	.0025	.112	2.04	.024	22	.178	.120	.0275	5*	1.95*	3.1	.73	Waves	Smooth	3
4	.43	.236	.153	.0024	.108	2.08	.022	12.5	.164	.112	.023	5	2.45	3.9	.75	Waves	Smooth	4
5	.28	.18	.13	.0031	.115	1.8	.033	26	.145	.12	.038	5	1.9	2.0	.74	Lge Ripples	Meanders & low dunes	5
6	.345	.195	.135	.0024	.103	2.00	.021	21	.143	.106	.0225	6	2.45	3.1	.80	Lge waves	Smooth	6
7	.435	.243	.156	.0021	.103	2.04	.020	31.5	.170	.107	.0225	7**	2.15**	3.5	.73	Waves	Smooth	7
8	.375	.24	.155	.0023	.11	1.75	.030	27.5	.185	.12	.036	6	1.5	2.1	.63	Ripples	Meanders & low dunes	8
9	.285	.245	.155	.0026	.115	1.35	.059	27.5	.21	.13	.079	12	1.1	1.2	.47	Ripples	Dunes	9
10	.20	.25	.16	.0020	.10	0.93	.095	24	.225	.12	.135	4	0.2	0.15	.33	Smooth	Dunes	10
11	.205	.155	.115	.0033	.11	1.5	.043	26	.135	.12	.050	6	2.7	2.1	.67	Lge Ripples	Meanders & low dunes	11
12##	.37	.30	.178	.0022	.111	1.40	.050	26	.248	.131	.070	6	0.72	1.0	.45	Ripples	Dunes	12##
13	.215	.197	.136	.0035	.124	1.23	.076	26.3	.176	.142	.102	13	1.2	0.93	.30	Lge Ripples	Dunes	13
Sand Bed, D_{50} = 0.10 mm																		
21	.435	.236	.154	.00225	.106	2.10	.0205	25.0	.166	.110	.022	6	4.85	7.9	.76	Waves	Smooth	21
21a	.435	.236	.154	.0022	.104	2.10	.020	25.0	.165	.108	.0215	6	4.9	8.0	.76	Lge waves	Smooth	21a
23	.325	.189	.132	.00245	.102	1.96	.0215	25.0	.141	.106	.023	12	5.1	6.2	.79	Lge waves	Smooth	23
24#	.265	.226	.149	.0028	.116	1.34	.060	25.0	.197	.133	.079	6	4	4	.50	Ripples	Dunes	24#
24#	.265	.17	.12	-	-	1.8	-	25.0	-	-	-	6	7	7	.76	Small waves	Low ripples	24#
25	.20	.187	.131	.0033	.118	1.23	.074	25.0	.168	.134	.095	10	5.3	4.0	.50	Lge Ripples	Dunes	25
26	.20	.279	.170	.0013	.084	0.82	.084	25.0	.245	.101	.12	6	0.19	0.14	.27	Smooth	Dunes	26
27	.20	.231	.151	.00235	.107	0.99	.094	25.0	.207	.126	.13	11	1.35	1.0	.36	Small ripples	Dunes	27
28	.33	.284	.172	.0024	.116	1.32	.062	25.0	.244	.138	.088	12	3.6	4.45	.44	Ripples	Dunes	28
29	.52	.280	.171	.00185	.101	2.13	.0180	25.2	.178	.103	.019	15	3.45	6.7	.71	Smooth	Smooth	29
30	.265	.281	.171	.00215	.108	1.08	.080	25.0	.246	.130	.115	12	1.75	1.7	.36	Small ripples	Dunes	30

e - estimated

* Also 5 samples at 17.5 °C, $\bar{C}$ = 2.1 gr/l ; and 5 at 12.5 °C, $\bar{C}$ = 2.35 gr/l

** Also 7 samples at 28 °C, $\bar{C}$ = 1.8 gr/l ; and 10 at 26° C, $\bar{C}$ = 1.4 gr/l

\# Dual equilibrium due to a long flat sand wave. See text.

\#\# Long flat sand wave present, but data pertains only to rugged dune section.

4. S = slope of the energy line, or the slope of the water surface if the flow was perfectly uniform. Frequently a small correction for non-uniformity was applied as outlined in Chap. III, Sec. K.

5. $U_* = \sqrt{grS}$ = shear velocity for the whole channel, feet per second.

6. $U = Q/bd$ = average velocity of flow for the entire channel, feet per second.

7. $f = 8(U_*/U)^2$ = Darcy-Weisbach friction factor for the whole channel.

8. T = water temperature in degrees Centigrade. During the second sequence, Runs 21 to 30, the temperature was controlled by immersion heaters at 25°C.

9. r_b = hydraulic radius for bed section in feet from side-wall correction procedure, Eq. 5.41.

10. $U_{*b} = \sqrt{gr_bS}$ = shear velocity for the bed section, feet per second.

11. $f_b = 8(U_{*b}/U)^2$ = friction factor for the bed alone, calculated from the side-wall correction procedure, Eq. 5.40.

12. Number of discharge samples on which the average is based.

13. $\bar{C}$ = average sediment discharge concentration in grams per liter. For procedure, see Chap. III, Sec. G (2).

14. $G = 3.74\,\bar{C}Q$ = total sediment transportation rate, or discharge, in pounds per minute. 3.74 is the conversion factor for units.

15. $F = U/\sqrt{gd}$ = Froude number.

16 & 17. Water surface condition and bed condition entries are included here because of their importance in the results. These conditions will be fully explained and illustrated in Sec. B.

In the subheadings, D_s is the mean sedimentation diameter of the bed material. (Cf. Chap. IV). D_s for the sediment load is usually slightly less.

Where entries are missing in Table 7, either the item does not apply or the data were not obtained. Whenever there is a reasonable basis for making good estimates, when the data are missing, estimated values have been entered and designated by "e".

For all the entries in Table 7 only the significant figures are reported. The accuracy of the figures is thus indicated directly; for example, the discharge is reported to the nearest .005 cfs. Of all the runs, Runs 5, 8, 9, 10, and 11 are the least accurate, as shown by the entries for d, r, U_*, r_b, and U_{*b}, which are given only to the nearest 5 units in the third place. Runs 21 to 30 are the most reliable; in these cases the slope was generally measured to the nearest .00005, instead of .0001 as in the previous runs.

Because of the limitations of the flow system, it was not possible to cover a wide range of conditions. Discharges less than 0.20 cfs were not used because of the problem of sand storage in the pipe; depths greater than 0.30 ft were not used because the effect of the walls becomes too large, and difficulty was encountered with the inlet condition. In addition, velocities giving Froude numbers F in excess of 0.80, caused high standing surface waves, which made the flow completely unmanageable. Nonetheless, in spite of these three restrictions, enough conditions were covered to lead to some valuable conclusions, which are believed to be qualitatively valid over a much wider range of conditions. No attempt was made to derive an empirical formula for the transportation rate on the basis of these flume data.

In this chapter, the conclusions drawn refer specifically to the laboratory flume. An attempt was made to understand only what happens in the laboratory flume, leaving the additional complexities of the mechanics of natural rivers in the realm of conjecture and the subject for other research. However, comparison of the laboratory results with a few observations of natural rivers in Chapter VII ("Discussion of Results"), indicates that the conclusions drawn here are probably true to a large extent for streams in general.

(2) Impossibility of Taking Slope or Shear as an Independent Variable. The data given in Table 7 have been plotted in several different ways on Figs. 18 to 25, to make several different conclusions clear.

First of all, from Figs. 18 and 19, it appears that the mean velocity, U, and the sediment discharge concentration, $\bar{C}$, are not uniquely determined by the depth, d, and slope, S. For example, on Fig. 18, the points (U = 2.04, $\bar{C}$ = 1.95) and (U = 1.35, $\bar{C}$ = 1.1) have practically the same d and S values, but quite different velocity and concentration values. This result is completely contrary to present concepts of open channel hydraulics; it is commonly believed that if the depth, width, and slope, and hence the shear, are known in addition to the size of material, that the velocity of flow and the sediment transportation rate can be calculated uniquely.

In applying any flow formula, such as the Manning equation or the Darcy-Weisbach formula to a flow over a movable bed of fine sand, the usual assumption of approximately constant roughness leads to a gross misconception about the relationship of velocity to depth and slope. Actually, the "constant" roughness can change more than any of the other variables, because of the changing bed configuration. For example, increasing the slope of a stream with depth constant is supposed to increase its velocity, but from either Fig. 18 or 19 it is apparent that higher slopes are frequently associated with lower velocities for a given depth. Similarly, if the depth is increased, holding the slope constant, then the velocity should increase, whereas the experimental results show that this is not the case.

Because the walls have a significant and variable effect on the flow, it is perhaps preferable to compare the data on the basis of the hydraulic radius for the bed, r_b, and the bed shear, obtained from the side-

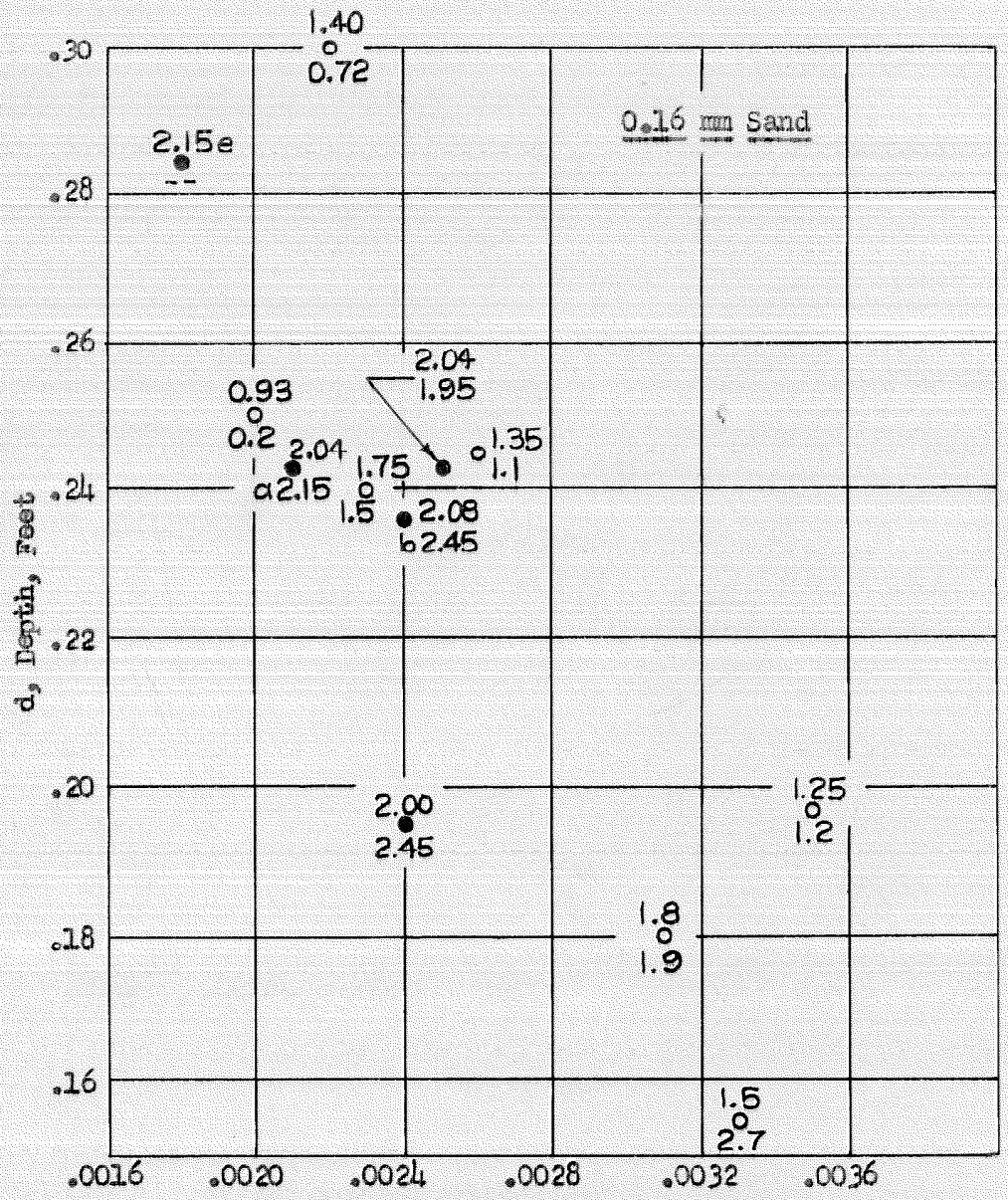

Legend: ● Bed smooth o Bed covered with dunes

Upper figure: U = mean velocity, ft/sec
Lower figure: C = sed. disch. concentration, gr/l

a: T = 31.5° C.
b: T = 12.5° C.
e: estimated and T = 17° C.

Fig. 18. Velocity and concentration vs. depth and slope for 0.16 mm sand

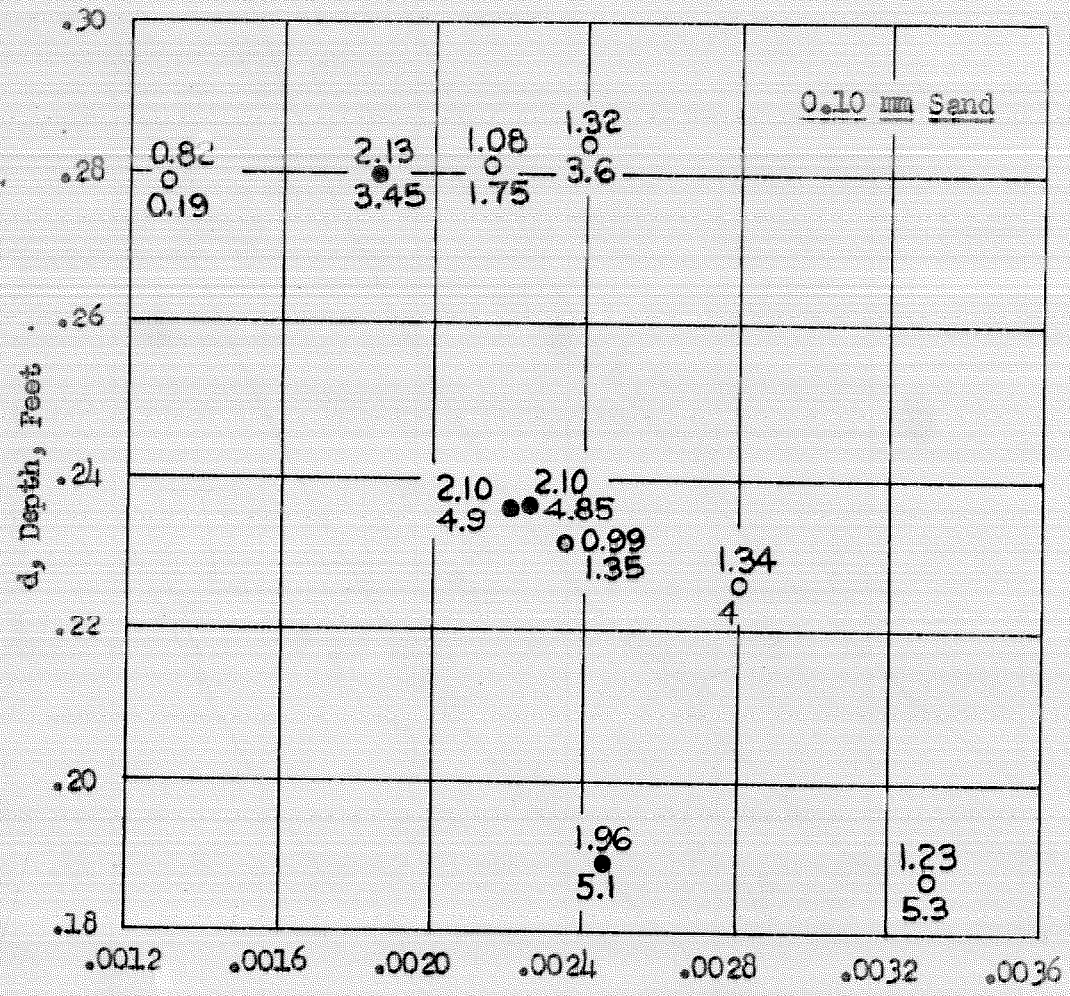

Legend: ● Bed smooth
o Bed covered with dunes

Upper figure: U = mean velocity, ft/sec
Lower figure: $\bar{C}$ = sed. disch. concentration, gr/l

Fig. 19. Velocity and concentration vs. depth and slope for 0.10 mm sand.

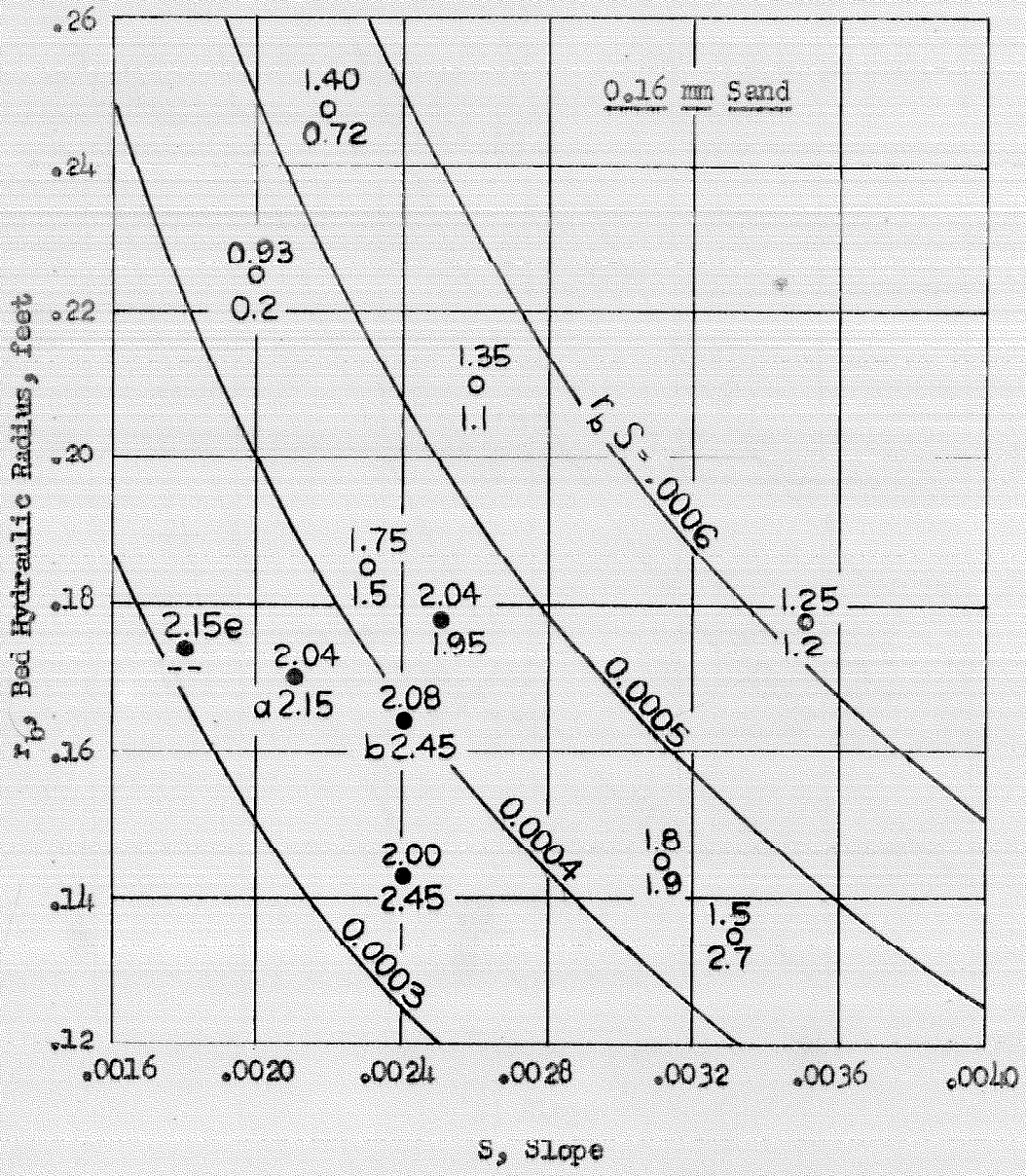

Legend: ● Bed smooth
o Bed covered with dunes or meanders

Upper figure: U = mean velocity, ft/sec
Lower figure: C = sed. disch. concentration, gr/l

a: T = 31.5° C
b: T = 12.5° C
e: estimated, and T = 17° C

Fig. 20. Velocity and concentration vs. bed hydraulic radius and slope for 0.16 mm sand.

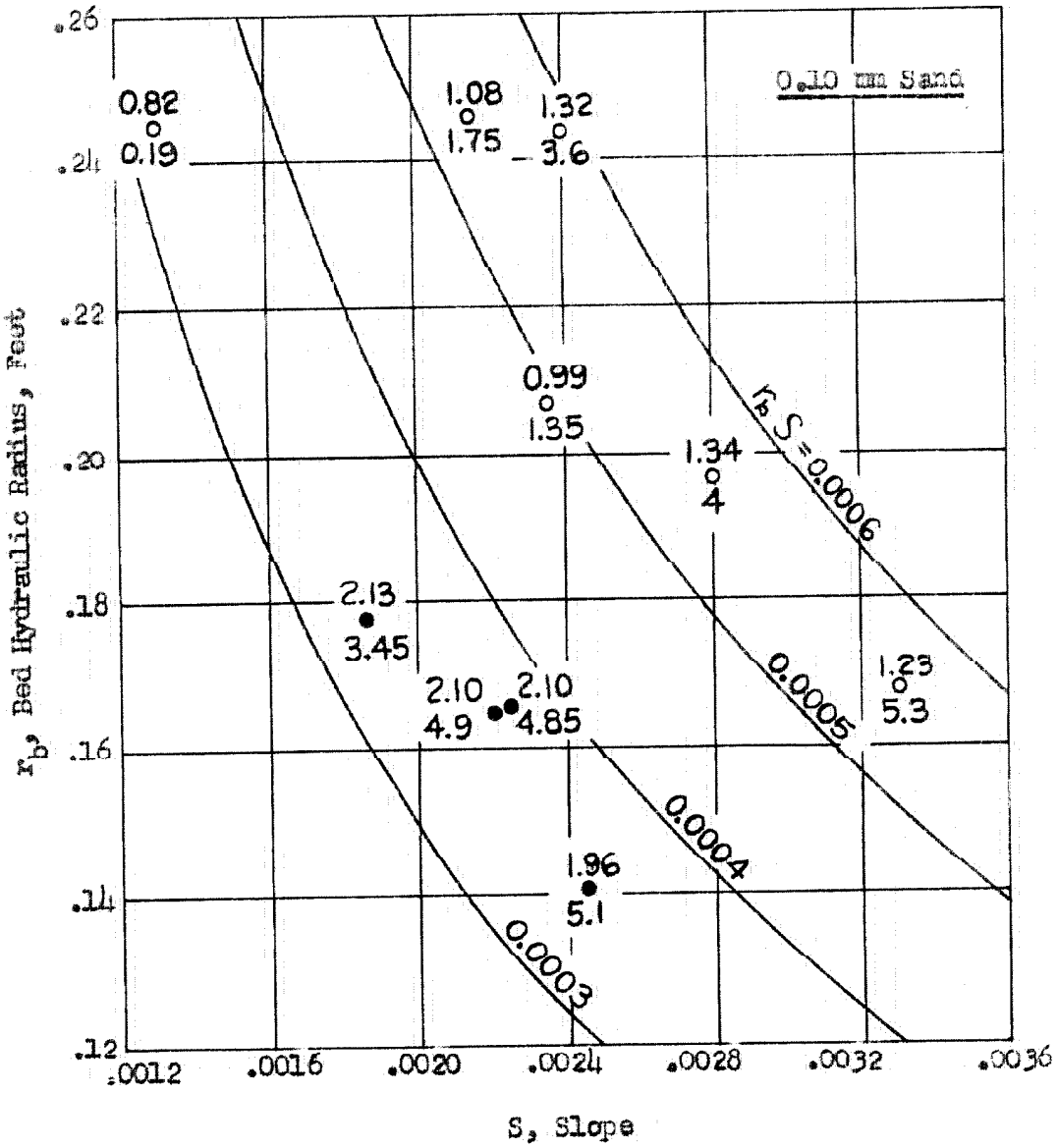

Legend: ● Bed Smooth
o Bed covered with dunes

Upper figure: U = mean velocity, ft/sec
Lower figure: $\overline{C}$ = sed. disch. concentration, gr/l

Fig. 21. Velocity and concentration vs. bed hydraulic radius and slope for 0.10 mm sand.

wall correction computations. (Cf. Chap. V, Sec. C). In Figs. 20 and 21, U and $\bar{C}$ have been plotted again against S and r_b, instead of against S and d. Lines of constant shear, or simply constant r_b S, are also shown. The same conclusions may be drawn. If anything, one might even be led to conclude that the higher concentrations and velocities are associated with the smaller shears, a result completely contrary to widely held beliefs.

However, it may be noticed that there is no longer a direct conflict of points of greatly different velocity at identical r_b and S. This is the result of the limitations on the range of conditions which could be included in the runs. All the points for which the bed was covered with dunes (and U is small) lie to the right of points for which the bed is smooth (and U is higher). There is no doubt that if runs could have been performed at even smaller discharges, the slope values for the runs with rough bed and large slope would have decreased again to the point where there would be a conflict of points with runs having smooth bed.

Fig. 21 shows this effect most clearly. The three points at the top of the chart for rough dune-covered bed show that as U is reduced, S is reduced, because in all three cases the dunes are large and well established, and the roughness does not change radically. By analogy, starting with the point (U = 1.23, $\bar{C}$ = 5.3) at the right in Fig. 21, decreasing the velocity sufficiently would undoubtedly reduce S from .0033 to .0022 for r_b = 0.165 ft. The concentration would be substantially reduced also. But two existing points for smooth bed for the same r_b and S show that U = 2.10 ft/sec, $\bar{C}$ = 4.9 gr/l is also a possible combination. Therefore, the evidence indicates that U and $\bar{C}$ are not uniquely determined by either r_b and S or d and S.

In the range of experiments conducted, it may be noted from Table 7

that the shear velocity for the bed, U_{*b}, has remarkably little variation compared with the velocity or transportation rate. It may indicate that in the range of sediment loads encountered the bed configuration tends to adjust itself in a way which greatly reduces the variation of shear that might ordinarily be expected. This being the case, it is improbable that the suspended load transport of a stream can ever be expressed directly in terms of the shear.

(3) Depth and Velocity as Independent Variables. Since velocity and sediment discharge concentration cannot be expressed uniquely as a function of the slope and either the depth or the hydraulic radius, an attempt was made to find out which quantities could be most logically used as independent variables. It was found that any two variables representing two of the following three groups could be considered as independent: (a) d or r; (b) U or Q; and (c) $\overline{C}$ or G. For Figs. 22 and 23, d and U were used as coordinates and for Figs. 24 and 25, Q and G. These two particular combinations of independent variables seemed most logical and made the results the easiest to interpret.

The sand size is, of course, a very significant variable, but since only two sizes of sand were used, little could be deduced about the effect of the sand size on the sediment load. No information was obtained on the behavior of a graded sand.

Temperature is a variable of secondary importance, which will be discussed in more detail subsequently. However, the temperature had sufficient influence that it was found advisable to regulate it at 25° C for the second series of runs, Runs 21 to 30, to avoid any possible confusion resulting from too many variables changing at once. For the earlier runs,

Runs 2 to 13, with 0.16 mm sand, the range was 21 - 27.5°C, except for three runs; these three cases are specially labeled on all the figures in this section.

For Figs. 22 and 23, U and d are taken as the independent variables and two of the dependent variables, f_b and $\bar{C}$, are written in for each of the plotted points. From these two figures the following fairly definite qualitative conclusions may be drawn:

(a) f_b and $\bar{C}$ are uniquely determined by U and d, for the flume. From these all other quantities listed in Table 7 may be calculated, so that the character of the flow is completely determined by a selection of U and d. This was also borne out by general experience in operating the flume; by choosing the depth and mean velocity, one, and only one, definite equilibrium flow could be obtained. (Cf. Chap. III, Sec. N.)

(b) For a fixed depth, $\bar{C}$ increases as U increases in most cases. Also, f_b decreases markedly as U increases, because of the changes in the bed configuration. For example, in the case of the 0.16 mm sand, Fig. 22 shows that increasing the velocity from about 1.25 to 2.0 ft/sec, for $d \doteq 0.195$ ft, results in a drop in f_b from .102 to .0225 because the dunes are washed away, and the sand bed becomes flat. At the same time, the discharge concentration $\bar{C}$ is increased from 1.2 to 2.45 gr/l.

(c) For a fixed velocity, $\bar{C}$ decreases slightly as d increases. f_b does not appear to depend much on the depth in the limited range studied, except when the bed becomes smooth. In this case, f_b decreases as d increases for fixed U because the Reynolds number increases.

(d) The above conclusions apply equally well for both sand sizes.

(e) For a given d and U, the sediment discharge concentration $\bar{C}$ for the 0.10 mm sand, is roughly 2 to 4 times as much as for the 0.16 mm

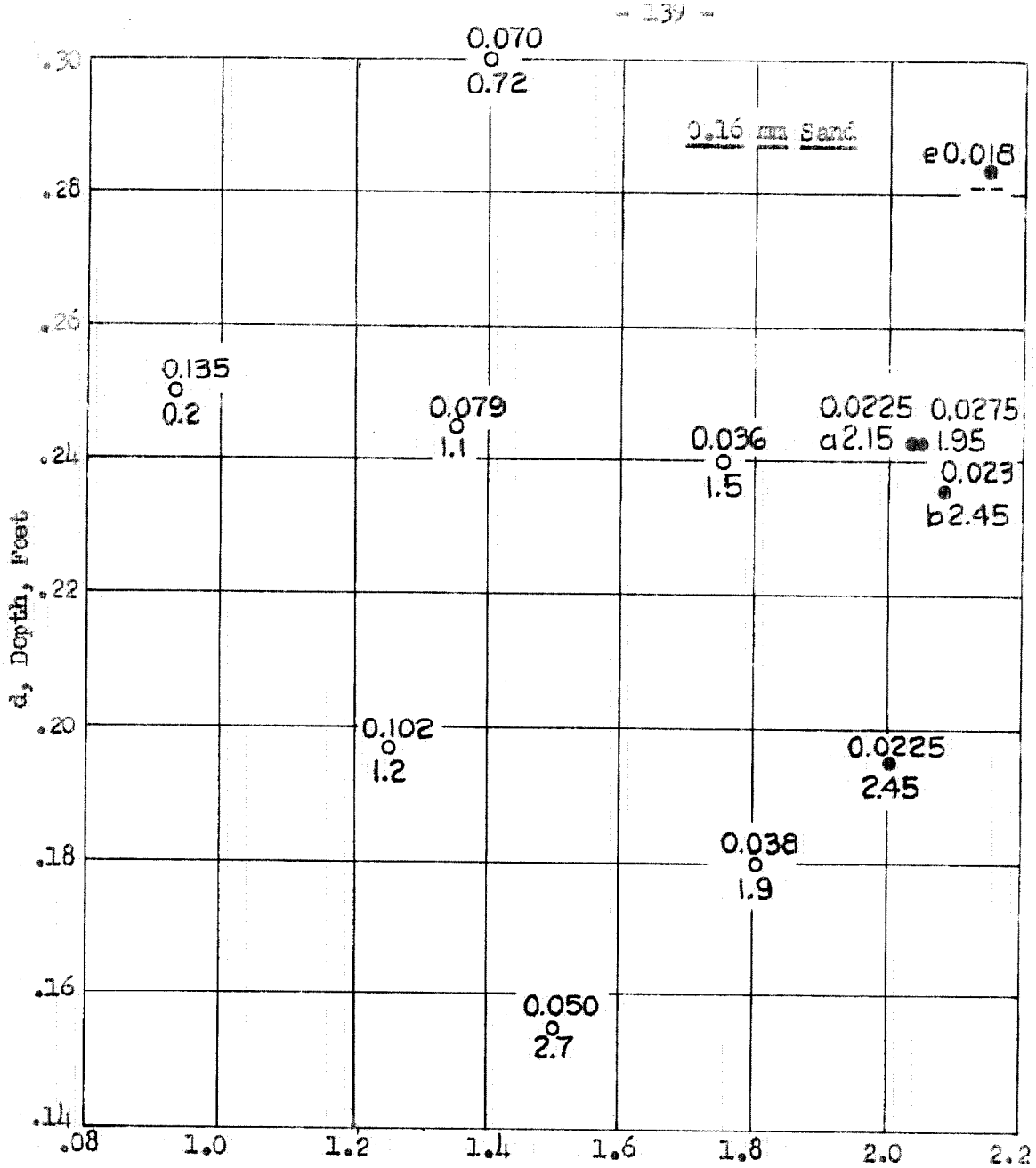

Legend: ● Bed smooth ○ Bed covered with dunes or meanders

Upper figure: f_b = friction factor for the bed

Lower figure: $\overline{C}$ = sed. disch. concentration, gr/l

a: T = 31.5° C.
b: T = 12.5° C.
e: estimated and T = 17° C.

Fig. 22. Bed friction factor and concentration vs. depth and velocity for 0.16 mm sand

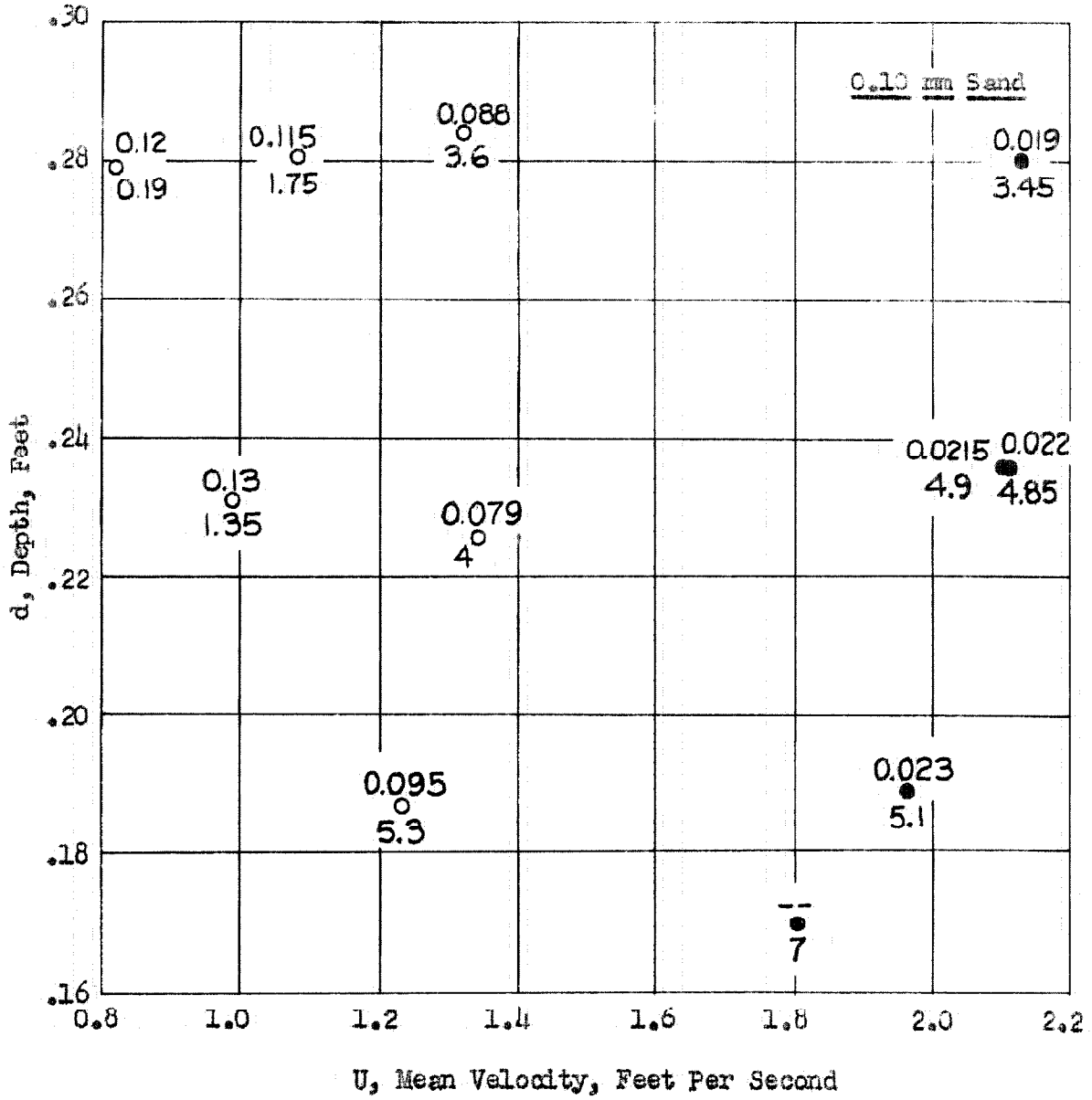

Legend:
- ● Bed smooth
- o Bed covered with dunes

Upper figure: f_b = friction factor for the bed

Lower figure: $\bar{C}$ = sed. disch. concentration, gr/l

Fig. 23. Bed friction factor and concentration vs. depth and velocity for 0.10 mm sand.

sand, in the range of conditions covered.

(f) f_b appears to be numerically the same for both sand sizes for any given d and U. Since f_b may be influenced by the amount of sediment load as well as the dune configuration, no further conclusions may be drawn here regarding the factors governing f_b.

(4) Water Discharge and Sediment Discharge as Independent Variables. Some corollaries of the conclusions above can most easily be deduced by re-plotting the data as in Figs. 24 and 25. The discharge, Q, and the total sediment transportation rate, G, are used as the independent variables, and the values of f_b and d are recorded opposite the plotted points. Note that the scales are logarithmic and that the length of the cycle in the Q scale is just twice that of the G scale. Additional conclusions based on Figures 24 and 25 are as follows:

(a) f_b, d, and all the other variables can be uniquely determined from Q and G. For example, to transport 1.5 lb/min of 0.16 mm sand with a discharge of 0.25 cfs in the laboratory flume, it may be estimated from the neighboring points on Fig. 24 that the required depth will be about 0.19 ft and $f_b = .07$. For the same load of 0.10 mm sand, there follows from Fig. 25 that d = 0.27 ft and $f_b = .12$, with Q = 0.25 cfs, as before. The required slope in each case can be obtained by working back through the side-wall correction equations in Chap. V. Sec. C. It may be noted that in an open circuit flume, Q and G are the only two variables which are independent and can be directly controlled. Everything else adjusts to these values.

(b) Maintaining a constant sediment discharge, G, while the water discharge, Q, is increased, requires that the depth d increase, although not as much as Q. The velocity U also increases.

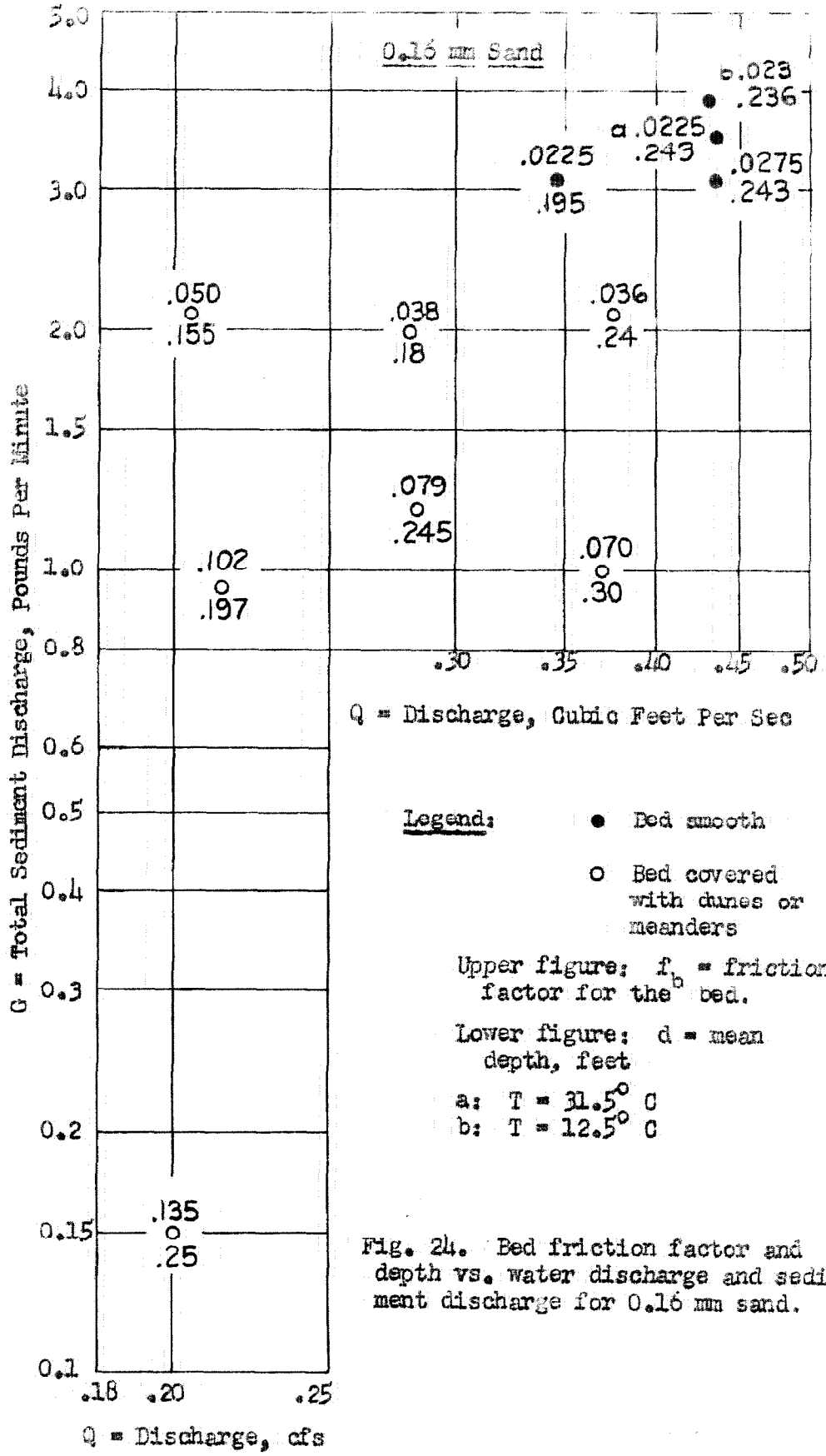

Fig. 24. Bed friction factor and depth vs. water discharge and sediment discharge for 0.16 mm sand.

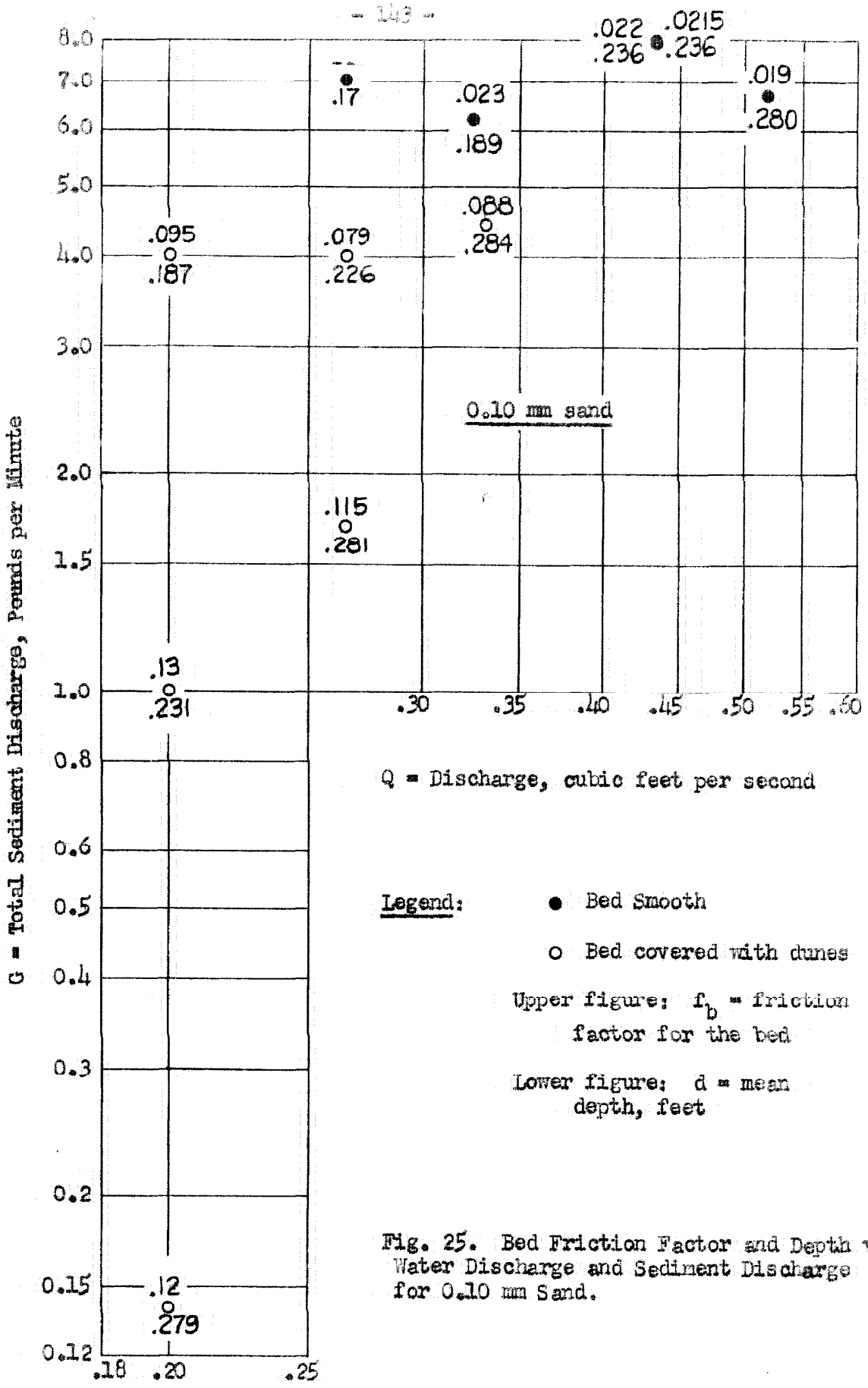

Fig. 25. Bed Friction Factor and Depth vs. Water Discharge and Sediment Discharge for 0.10 mm Sand.

(c) For a constant Q, an increase in G requires a decrease in d. This is a significant conclusion, for it implies that the depth of flow depends on the sediment load for any given discharge; hence, a unique stage-discharge relation did not exist for the laboratory flume. For example, Run 23 and Run 28 have practically identical slopes and discharges (see Table 7), but two different depths, 0.189 ft and 0.284 ft respectively. G for the former is 6.2 lb/min and for the latter 4.45 lb/min.

(d) For a given discharge, Q, the largest f_b values are associated with the smallest sediment transportation rates, G. From Fig. 25 it appears that f_b reaches an upper limit of about .12 or .13 (very large values), and a further decrease in G will not increase f_b any further. Physically, there must be a limit to the roughness of the channel, because the height of the dunes is certainly limited by the depth of the water.

(e) The above conclusions are qualitatively the same for both sand sizes.

(5) Effect of Temperature on Load. The effect of temperature variation on the sediment load was investigated briefly with Runs 3, 4, and 7. With lower temperature, the viscosity of the water is higher, and the settling velocity of the particles is reduced. It may be expected, then, that the sediment will be more easily carried in suspension at lower temperatures, and the load will be larger.

This general trend is borne out by Fig. 26, in which the sediment discharge concentration $\bar{C}$ is plotted as a function of temperature for Runs 3, 4, and 7, including the additional concentration measurements noted in the footnotes in Table 7. All these runs are essentially the same except for the temperature and the load, but inevitably there is also slight

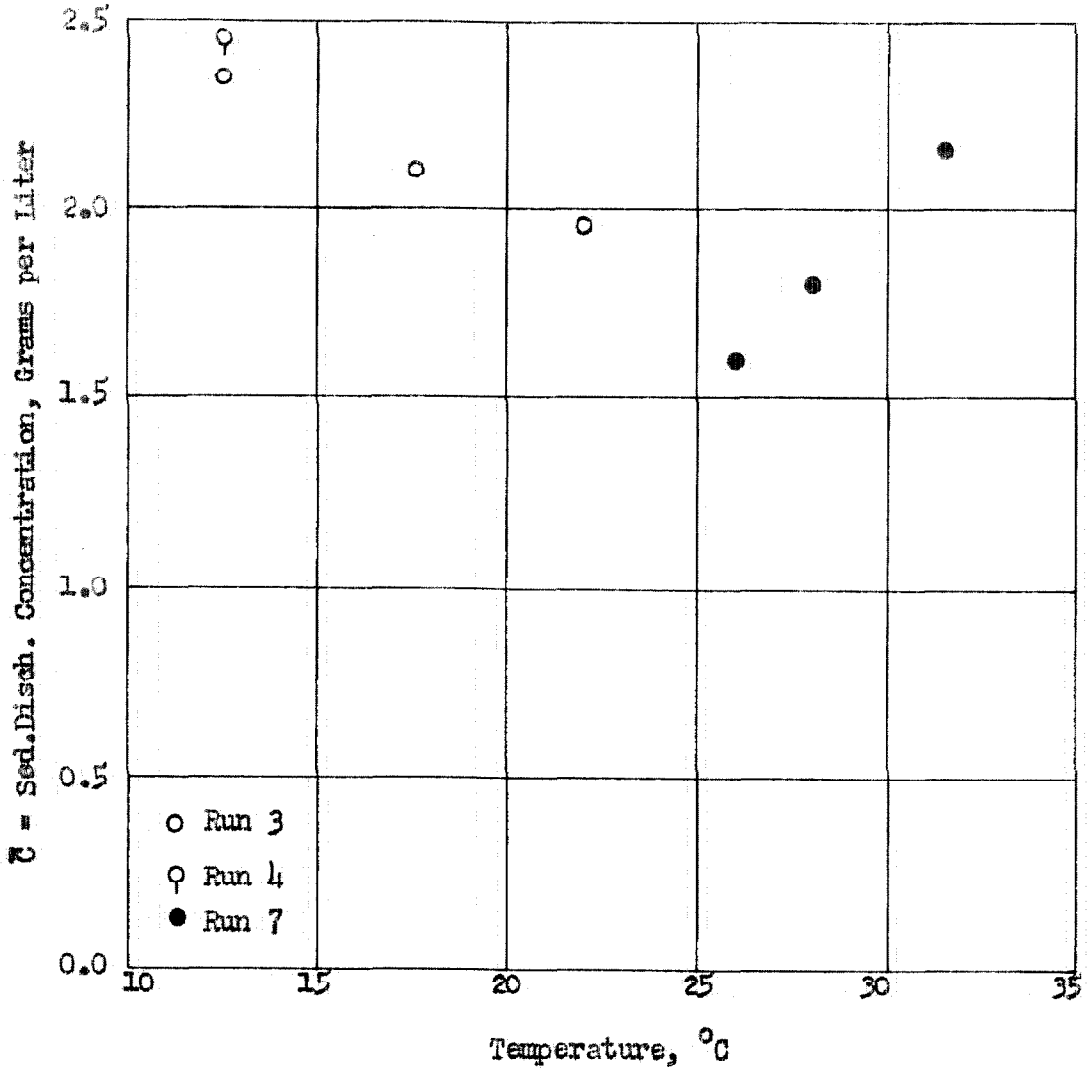

Fig. 26. Variation of Concentration with Temperature for Runs 3, 4, and 7.

variation of the friction factor and the slope also. Except for the last point, the trend of the concentrations is definitely downward as the temperature T increases, with a total drop of about 30 per cent between the values T = 12° and 25°C. It is very puzzling why $\bar{C}$ should suddenly increase again, as T rises to 31.5°C; it may possibly be due to an experimental error. Even though the temperature has quite an appreciable effect, it is still a variable of secondary importance when compared to other variables like depth and velocity. Temperature was measured for all the runs and later controlled for Runs 21 to 30, but no further effort was made to investigate temperature as one of the variables affecting the suspended load.

(6) Summary. Considering the laboratory stream as a whole, the most important results may be summarized as follows:

(a) The velocity and the sediment transportation rate are not unique functions of the shear, or any combination of depth, bed hydraulic radius and slope. This is demonstrated by Figs. 18 to 21.

(b) By using velocity as an independent variable in place of slope, an orderly relation between the various variables was found (Fig. 22, 23). Or, the water and sediment discharges may be considered as the independent variables as in Fig. 24, 25.

(c) At low transportation rates and velocities, the bed friction factor f becomes exceedingly large (up to .13) as the result of large dunes which form on the bed. Since the roughness varies more than any other quantity in a flow equation, the common assumption of constant roughness can lead to gross misconceptions about the hydraulics of a stream flowing over a bed of fine sand.

(d) Various qualitative relationships between d, f_b, U, Q, $\bar{C}$, and G are set forth in subsections (3) and (4) above.

(e) Other things being equal, a decrease in temperature will increase the sediment transportation rate somewhat. However, temperature is the least significant of all the variables mentioned.

B. OBSERVATIONS OF THE WATER SURFACE AND BED CONFIGURATIONS

It has been shown in the previous section that changes in the roughness of the bed have a profound influence on the hydraulics of a stream flowing over a bed of movable sand. In order to reach some understanding of the mechanics of such streams, it is imperative to study the mechanics of the dunes themselves, and the mutual interactions between the dunes and the stream.

For almost all of the runs, some observations and photographs were made of the bed configurations, according to the procedures outlined in Chap. III, Secs. L and M. In general, time prevented the accumulation of a large amount of detailed statistical information on the sizes, shapes, wavelengths, and velocities of the dunes for each run; instead, it was hoped that some rough measurements used in conjunction with photographs would give a good qualitative account of the phenomena. At present the author is still unable to explain completely why dunes behave the way they do, but an attempt will be made to give some objective information about them in this section.

Some observations of the nature of the water surface are also included here, because it, too, has some bearing on the mechanics of sediment-laden streams, especially at flow velocities approaching or exceeding the critical velocity for the channel.

All of the photographs illustrating the experimental results, Figs. 27 to 38, have been grouped together on the following pages to help the reader get an over-all view, while the detailed explanations for the figures are necessarily spread over a number of pages of the text. Except for Fig. 35, the illustrations are drawn entirely from the series with 0.10 mm sand, Runs 21 to 30, for which better photographs were obtained than for the first series. No significant differences in bed configurations were detectable on the basis of sand size alone for the two sands used.

Each illustration represents an equilibrium condition, which prevailed at the time the photograph was taken, or just before the flow was stopped to clarify the water for taking a picture. Practically no disturbance to the configuration resulted from suddenly stopping the pump. The photographs are all mounted so that the downstream direction is to the right, except as noted in Fig. 35.

(1) General Description of Bed and Water Surface Conditions—Photographs. The over-all range of bed and water surface conditions encountered in the course of the experiments will be summarized first before the detailed discussions of the observations are presented.

When the velocity and the transportation rate are low, the dunes which form are fairly large and haphazardly placed. As the velocity increases, the dune wavelength increases slightly, the pattern of the dunes becomes more regular, the dunes move faster, and the friction factor decreases. (See Figs. 27 to 31). With further increase in velocity, a point is reached where the sand no longer spreads itself uniformly through the system, but has a definite tendency to form a long, flat sand wave,

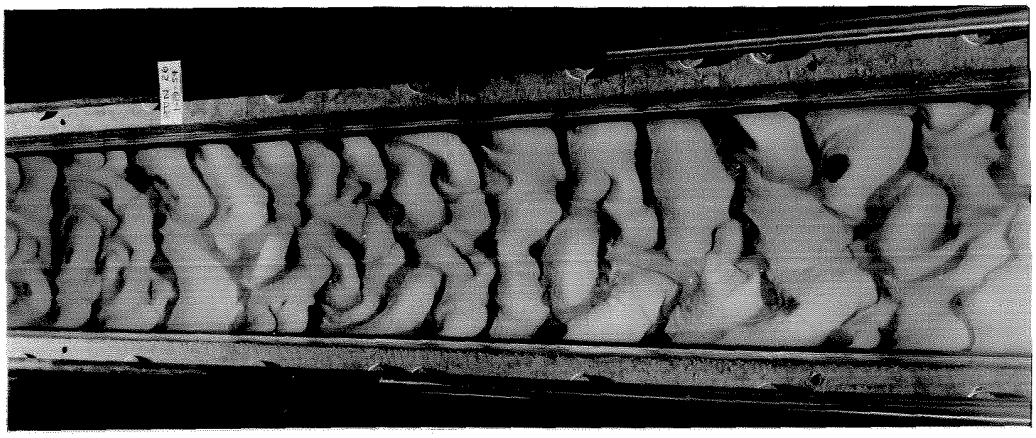

(a) Run 26: d = .279 ft, U = 0.82 ft/sec, f_b = .12, $\bar{C}$ = 0.19 gr/l

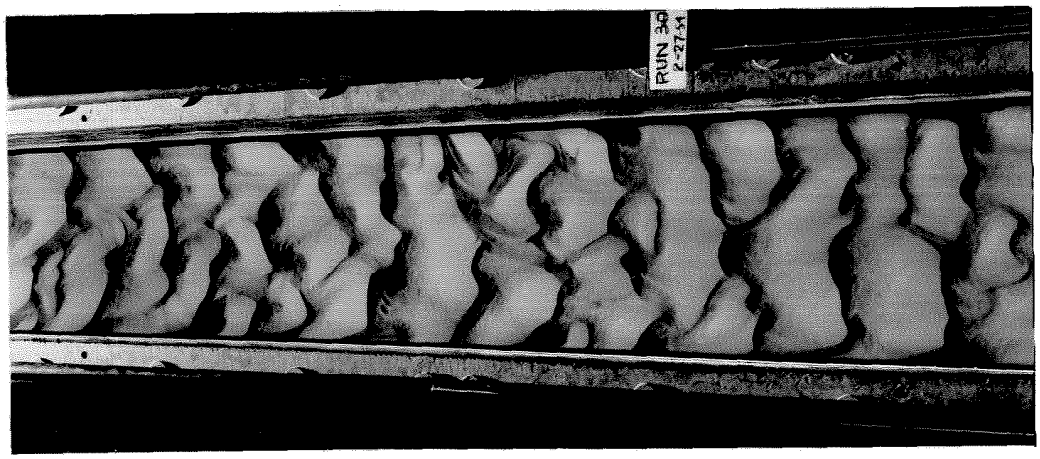

(b) Run 30: d = .281 ft, U = 1.08 ft/sec, f_b = .115, $\bar{C}$ = 1.75 gr/l

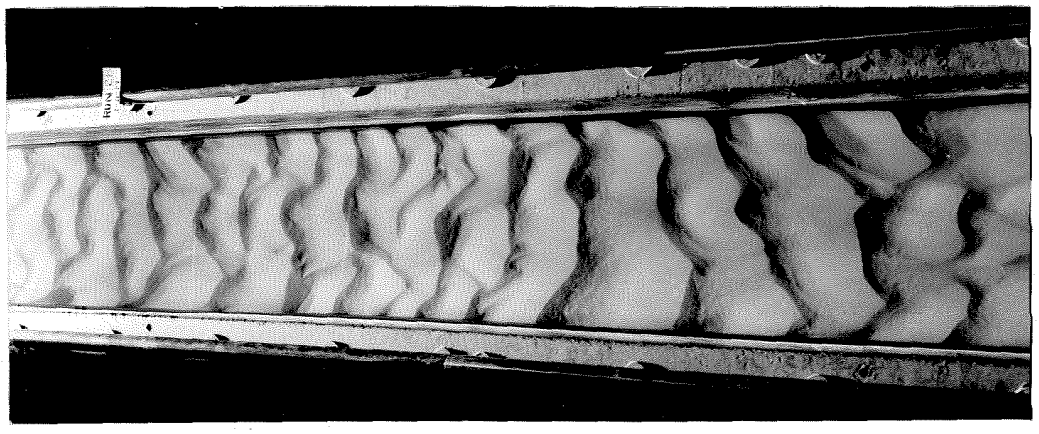

(c) Run 28: d = .284 ft, U = 1.32 ft/sec, f_b = .088, $\bar{C}$ = 3.6 gr/l

Fig. 27. Overhead views of typical bed configurations (water still). Note progressively better alignment of dunes with increasing velocity and sediment concentration, with depth fixed.

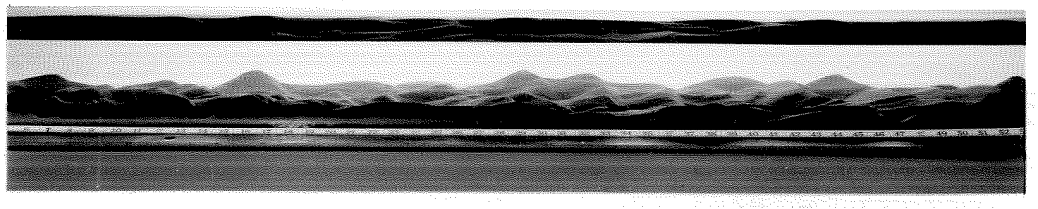

(a) Run 26: d = .279 ft, U = 0.82 ft/sec, f_b = .12, $\bar{C}$ = 0.19 gr/l

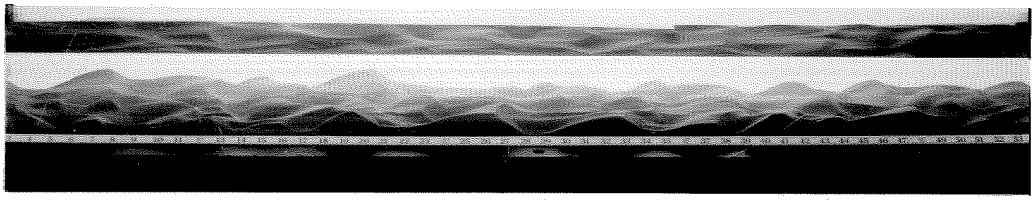

(b) Run 30: d = .28 ft, U = 1.08 ft/sec, f_b = .115, $\bar{C}$ = 1.75 gr/l

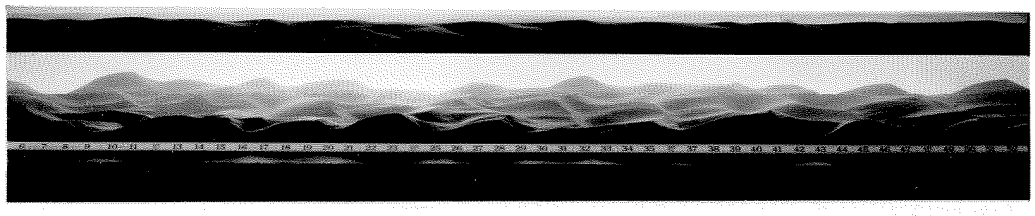

(c) Run 28: d = .284 ft, U = 1.32 ft/sec, f_b = .088, $\bar{C}$ = 3.6 gr/l

Fig. 28. Side views of typical bed configurations (water still), for same runs as shown in Fig. 27.

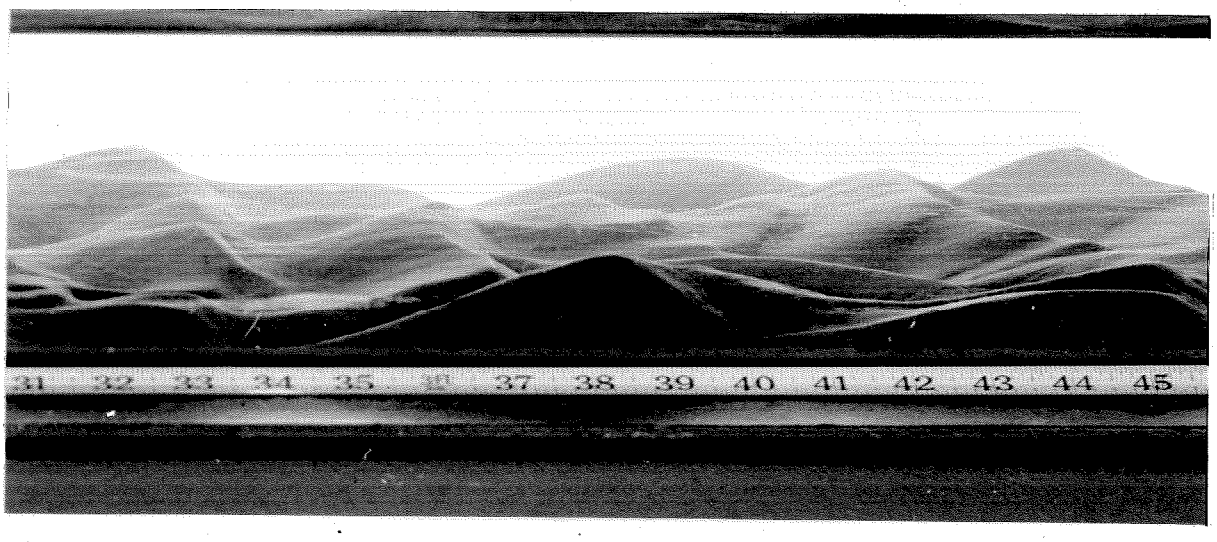

(a) Run 26: d = .279 ft, U = 0.82 ft/sec, f_b = .12, $\bar{C}$ = 0.19 gr/l

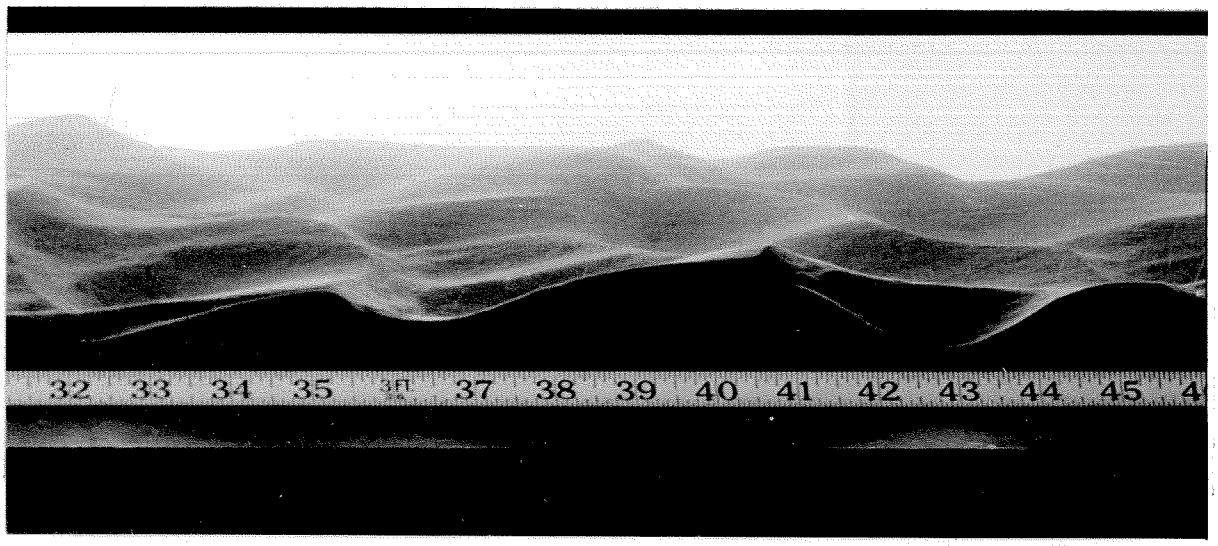

(b) Run 28: d = .284 ft, U = 1.32 ft/sec, f_b = .088, $\bar{C}$ = 3.6 gr/l

Fig. 29. Enlarged views of bed configuration from Fig. 28 (a),(c). Note the more streamlined appearance of the configuration for Run 28.

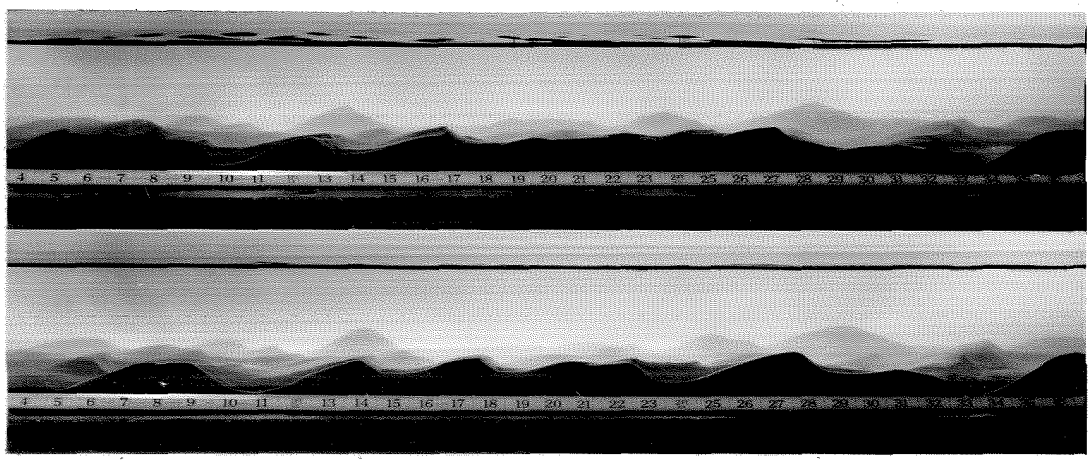

d = .279 ft, U = 0.82 ft/sec, f_b = .12, $\bar{C}$ = 0.19 gr/l
Time elapsed, 10 minutes

Fig. 30. Side views of Run 26 with water flowing showing very slow movement of dunes.

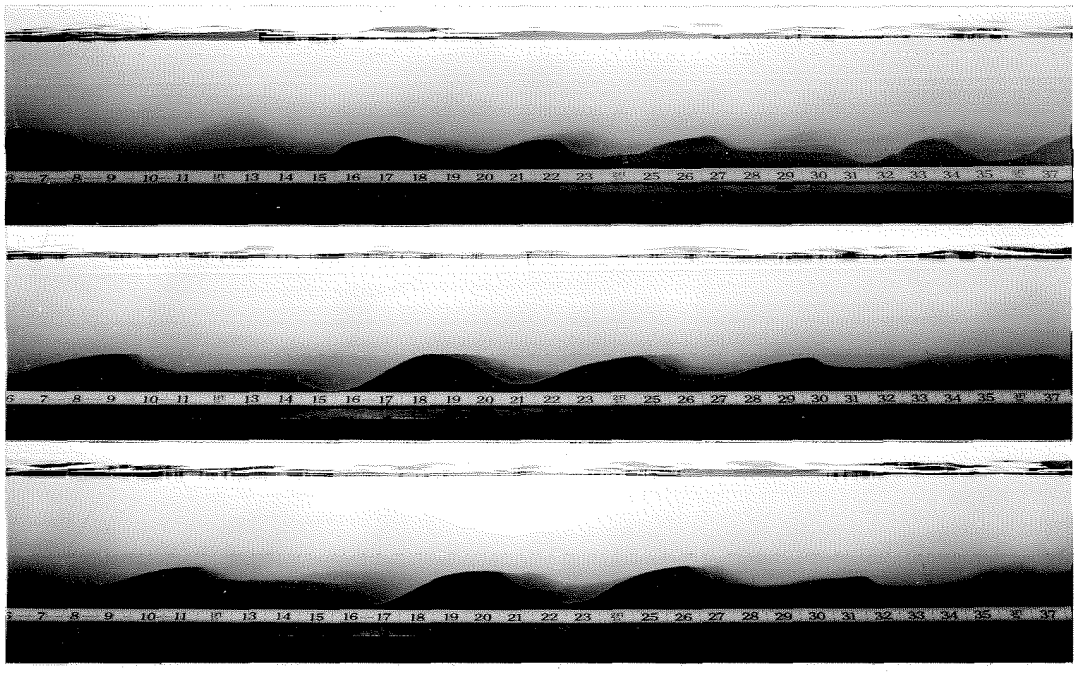

d = .281 ft, U = 1.08 ft/sec, f_b = .115, $\bar{C}$ = 1.75 gr/l
Time elapsed between successive pictures, 6 minutes

Fig. 31. Side views of Run 30 with water flowing, showing more suspended load and more dune movement than Run 26 (Fig. 30).

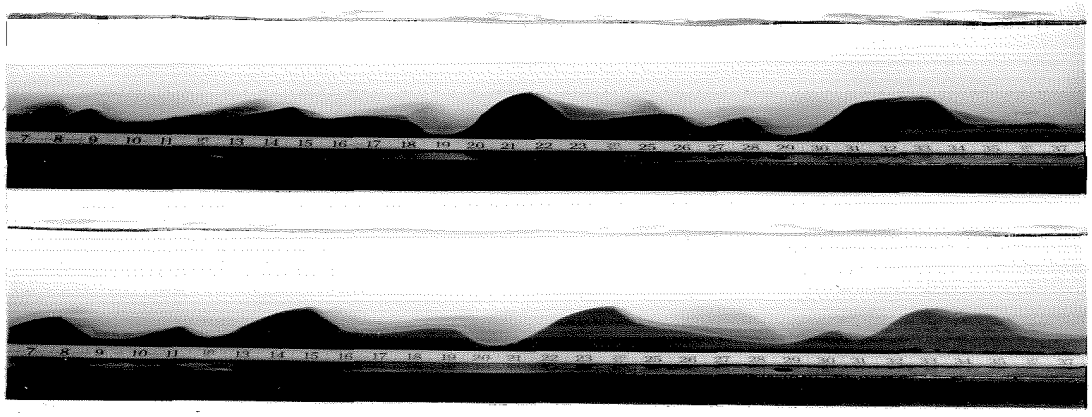

d = .231 ft, U = 0.99 ft/sec, f_b = .13, $\bar{C}$ = 1.35 gr/l
Time elapsed, 6 minutes

Fig. 32. Example of actively-changing dune configuration, Run 27.

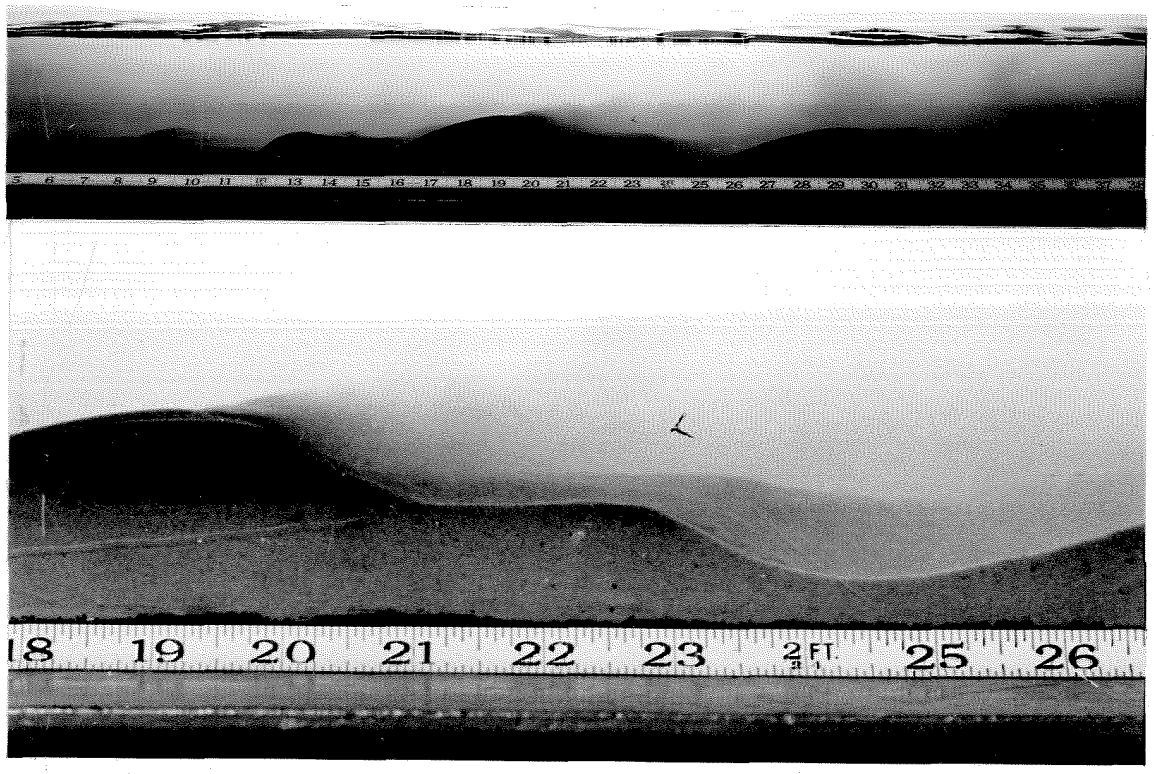

d = .281 ft, U = 1.08 ft/sec, f_b = .115, $\bar{C}$ = 1.75 gr/l

Fig. 33. Very large dune next to wall, Run 30. Note leeside eddy and entrainment of sediment behind crest.

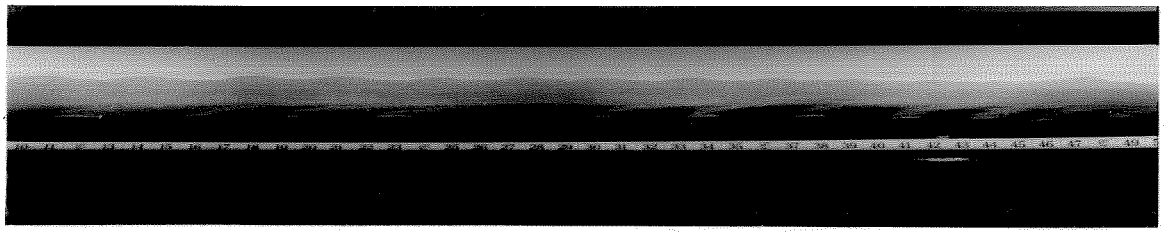

(a) On top of thick sand wave
d = .17 ft, U = 1.8 ft/sec, f_b = - , $\bar{C}$ = 7 gr/l

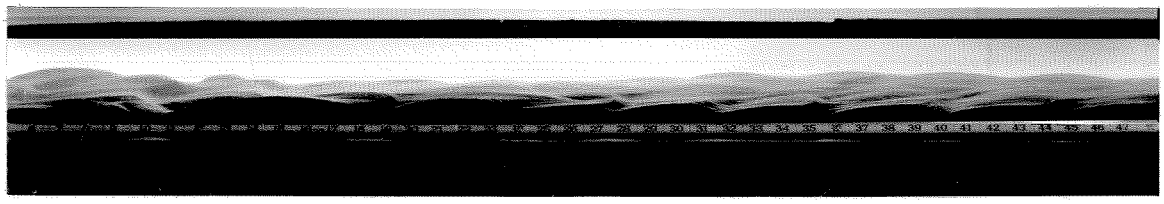

(b) End of sand wave, transition to dune section

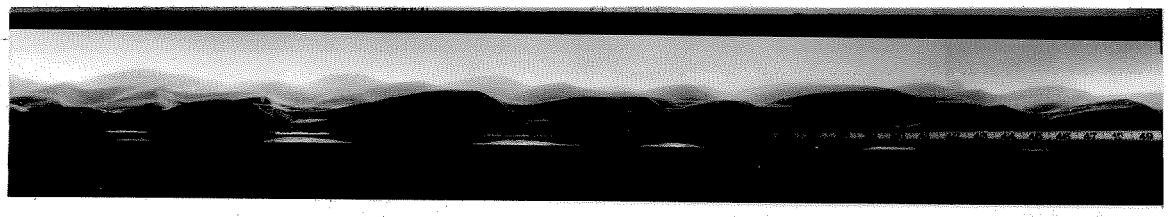

(c) Typical dune configuration away from sand wave
d = .226 ft, U = 1.34 ft/sec, f_b = .079, $\bar{C}$ = 4 gr/l

Fig. 34. Side views of Run 24 at three different times, showing the sand wave moving through the system. The flow was in equilibrium on top of the flat sand wave, as well as over the dune region.

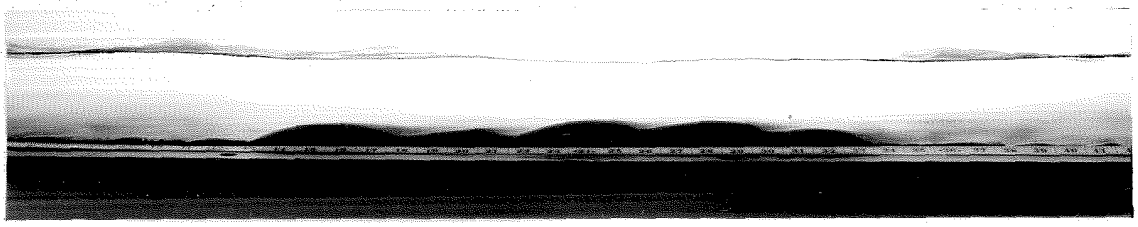

$d = .18$ ft, $U = 1.8$ ft/sec, $f_b = .038$, $\bar{C} = 1.9$ gr/l

In the center of the picture, the thickest part of the sand bed is on the near side of the channel, and at the ends of the picture at the far side.

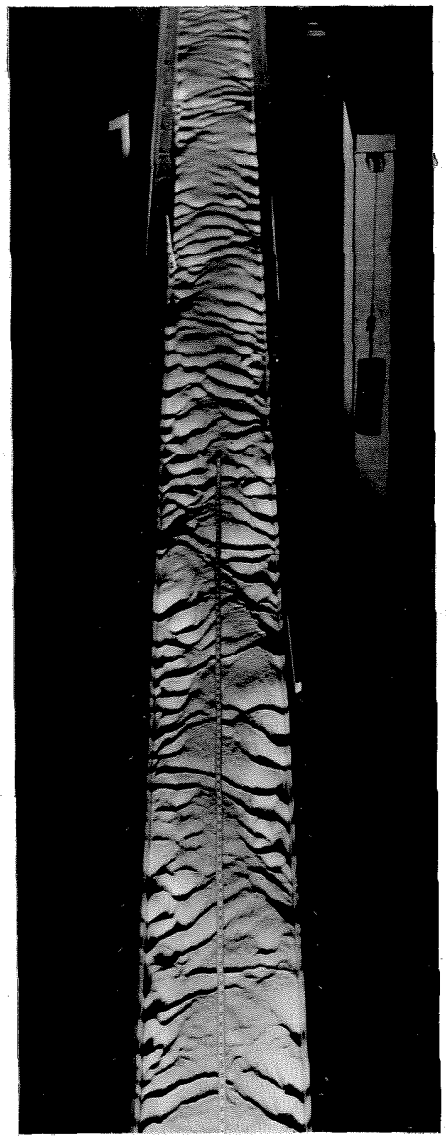

Overhead view showing thick part of bed weaving back and forth (looking downstream).

Fig. 35. Example of meandering bed, Run 5

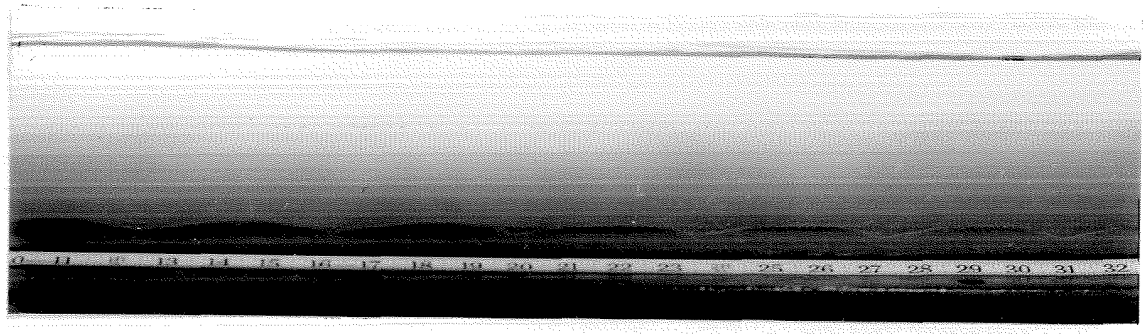

$d = .280$ ft, $U = 2.13$ ft/sec, $f = .0180$, $\bar{C} = 3.45$ gr/l

(a) Side view, water flowing. Note decrease of sediment concentration near water surface.

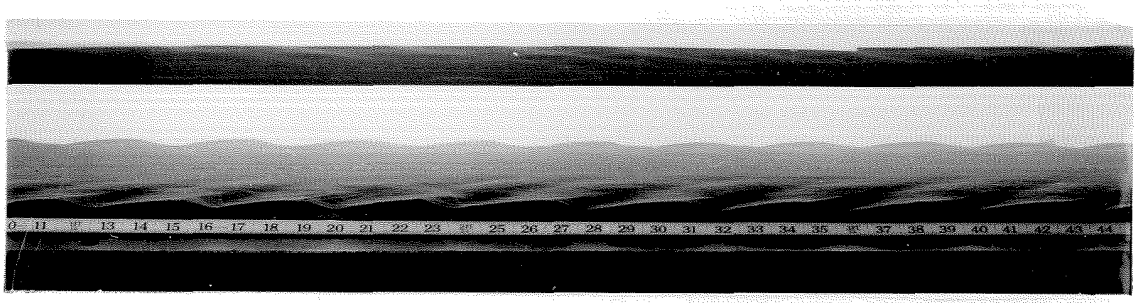

(b) Water still.

Fig. 36. Smooth water surface and bed for Run 29, with velocity high enough to eliminate dunes, but not high enough to induce standing surface waves.

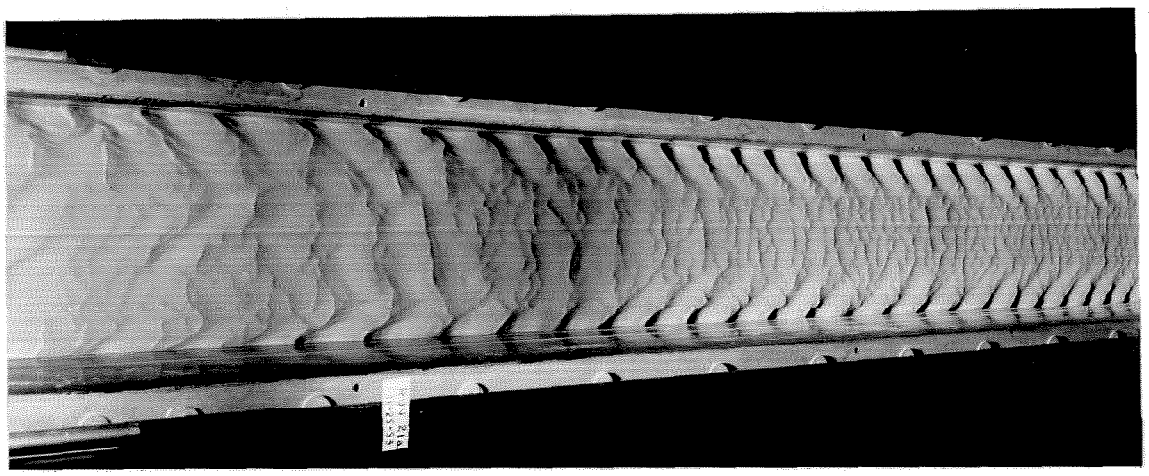

(a) Stations 8 to 15. (Inlet is at Station 2)

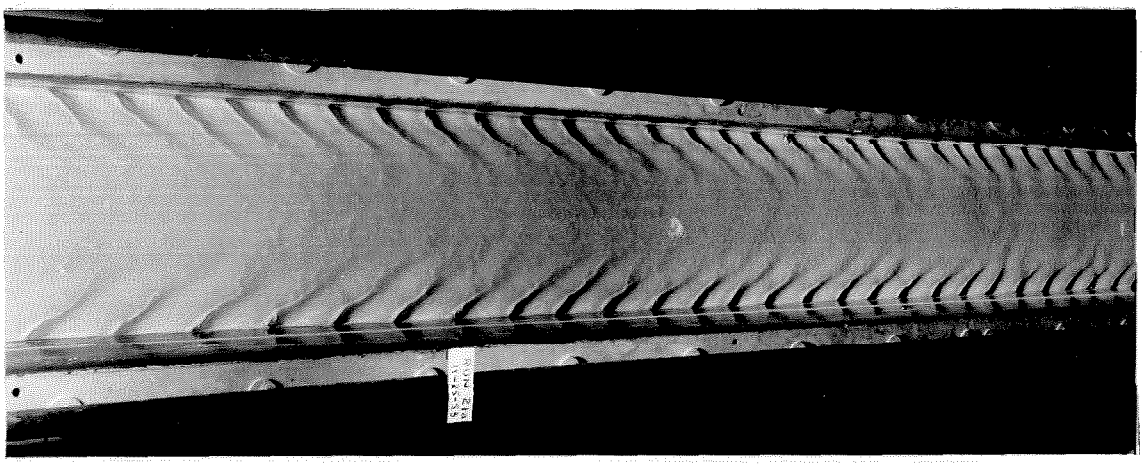

(b) Stations 21 to 27, same time as (a)

$d = .236$ ft, $U = 2.10$ ft/sec, $f_b = .0215$, $\bar{C} = 4.9$ gr/l

Fig. 37. Overhead views of bed, Run 21a, showing entrance disturbance and final equilibrium, which is typical of runs with smooth bed.

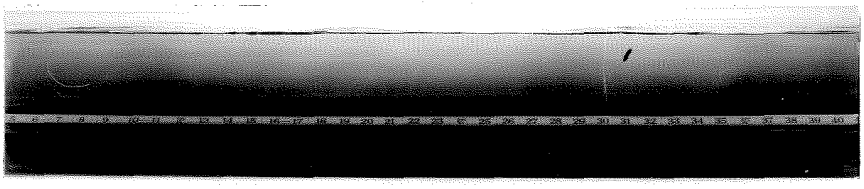

(a) 0 seconds

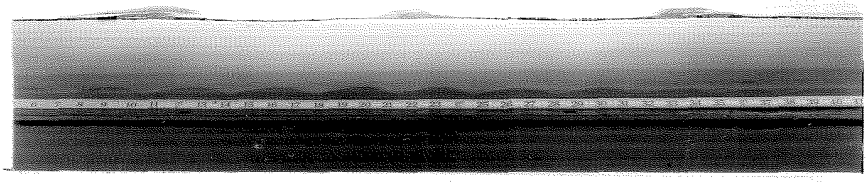

(b) 40 seconds

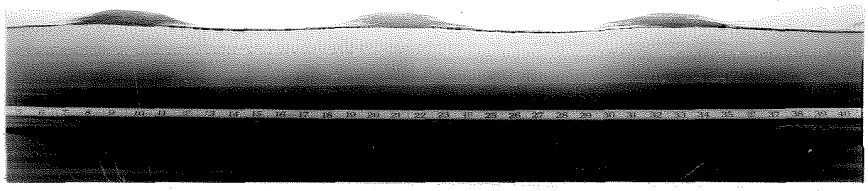

(c) 57 seconds

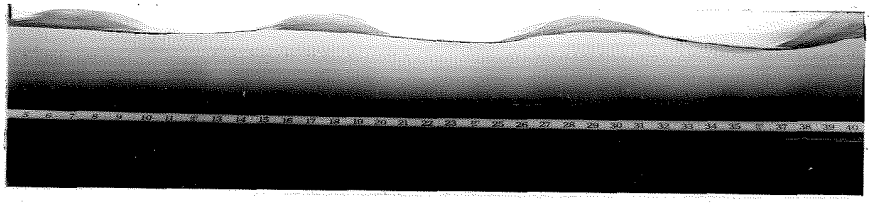

(d) 78 seconds

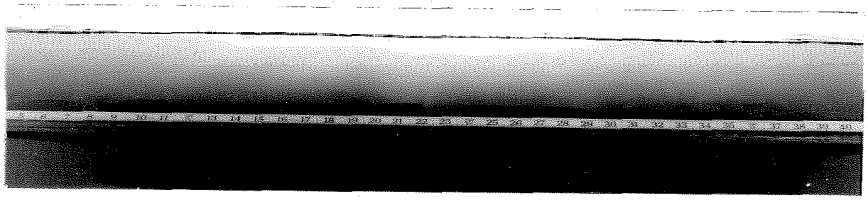

(e) 109 seconds

d = .236 ft, U = 2.10 ft/sec, f_b = .0215, $\bar{C}$ = 4.9 gr/l

Fig. 38. Time sequence showing growth and collapse of standing surface waves, Run 21a.

which has a steady thickness, length, and velocity when equilibrium is established. Run 24 is a good example of this condition, and is illustrated in Fig. 34. Meanders in the sand bed, as shown by Fig. 35, were also observed at this intermediate range of velocities.

At still higher velocities and transportation rates, the sand again spreads itself uniformly throughout the flume, with the surface of the bed now quite smooth except for some small ripples near the wall, as shown in Figs. 36 and 37.

Up to Froude number $F = 0.7$ to 0.75, the water surface is relatively calm. At the lowest $F = 0.27$, (Run 26, Fig. 30), the surface has a glassy smoothness, in spite of large bed irregularities. At higher velocities before the dunes disappear, the surface becomes quite rippled as a result of the disturbance to the flow by the bed. (Fig. 31) But when the Froude number reaches some critical value between 0.7 and 0.75, large standing waves appear and disappear, as demonstrated in Fig. 38. At still higher Froude numbers, the waves get extremely high, sometimes as high as the average depth of flow, and long, low, rapidly-shifting antidunes are formed. No runs were performed at this extreme condition, because it was impossible to ascertain whether the flow was in equilibrium, and most of the usual measurements were impossible. It was also noted, however, that even at velocities substantially above critical (i.e., $F > 1$), the water surface never flattened out again as it would for clear water flow, but continued to be intensely wavy as long as there was a sand bed.

The individual features will now be considered in more detail.

(2) Growth of Dunes from a Flat Surface. If the sand bed is initially flat, then at low velocities, the grains start moving, first mainly

as bed load, and gradually build up a system of dunes. As long as the velocity is sufficient to cause any movement at all, dunes will always form in this fine sand. As the dunes grow, the transporting power of the stream is visibly increased in two ways, even with the velocity of flow kept constant. First, the localized increase of shear stress in the vicinity of the crests causes increased bed load movement there. In addition, many turbulent eddies are formed behind the dunes, which are sometimes strong enough to lift the particles into suspension. When equilibrium is finally reached, perhaps after several hours, the rate of entrainment of particles from the bed is exactly balanced by constant redeposition from the stream. Thus, no particle is truly suspended for all time, but may stop on the bed while other particles move to maintain a steady average concentration of suspended sediment.

The appearance of the dunes cannot be attributed to any outside disturbance. No matter how carefully the bed is smoothed prior to the start of a run, still the dunes will form. Because of the turbulence, the initial movement of the sediment is inherently nonuniform over the bed surface, and slight irregularities develop on the surface. These in turn grow into tiny ripples spaced very close together; they keep growing in height and wavelength until the shear on the crests is large enough to prevent any further deposition and increase in height. If there are some irregularities in the bed at the beginning, the process of dune development is accelerated, but the end result is still completely independent of the initial condition of the bed. It is interesting to note that just <u>one</u> artificial trough in an otherwise flat bed is sufficient to generate a ripple train downstream rather quickly. The initial trough starts an oscillation of some sort in the flow which facilitates the formation of more ripples,

like images of the first one. Consequently, the front of the wave train advances many times more rapidly than the individual ripples, by formation of new ripples on the front. This observation demonstrates quite clearly that the dune configurations are closely interrelated to the internal flow pattern of the stream, for otherwise it would be impossible to propagate a disturbance in the bed downstream so rapidly.

Time-lag color motion pictures were made to show the development of the equilibrium bed configuration of Run 26 (Fig. 27 (a), 28 (a), 29(a), and 30) from an initially flat bed of sand. The frames were taken at 20-second intervals, so that at a projection speed of 20 frames per second, the "time magnification" is 400, and an hour's events in the flume could be shown on the screen in 9 seconds. From the motion pictures it could be seen that the bed changed most rapidly near the beginning, and approached the final configuration asymptotically. The development was by no means a smooth function of time, but rather jerky. While some parts of the bed appeared to change slowly, nearby a depression might be scoured relatively rapidly. It was believed that some sudden change in the flow pattern occurred when an existing pattern had become unstable, and that the bed was locally scoured to make adjustments.

(3) Characteristics of Stable Dune Configurations. Since it is difficult to describe the dune configurations verbally, a number of typical photographs have been included as Figs. 27 to 33 to show the dune characteristics visually. It may be noticed from the photographs that there is considerable variation of sizes, shapes, and wavelengths, and that the pattern is by no means strictly two-dimensional. In spite of the variations, though, the configuration in equilibrium appears to maintain a definite

over-all character; perhaps the best proof of this is the fact that once equilibrium is reached, the slope of the stream and the friction factor remain practically constant, with variations only of the order of magnitude of the experimental errors.

Although all the various details of the figures cannot be described, still some generalizations are possible. Fig. 27 demonstrates, as mentioned previously, that as the velocity is increased, the dune pattern becomes more regular. Runs 26, 30, and 28 all have practically identical mean depths, as noted in Fig. 27. In Run 26, the dune crests are curved, irregularly spaced, and of limited lateral extent. They are sometimes diagonal in the channel instead of perpendicular to the direction of flow, and there is evidence that the flow lines near the bed are tortuous. The "troughs" are often more of the shape of round depressions than lateral troughs.

As the velocity is increased from 0.82 ft/sec for Run 26 to 1.32 ft/sec for Run 28, (Fig. 27(c)), the alignment of the dunes improves and the crests become smoother, resulting in some decrease in the friction factor f. With higher velocity the dune crests are generally more nearly perpendicular to the direction of flow, and the flow near the bed must be straighter. Many of the crests are now continuous across the entire width of the channel. Fig. 29 shows that the dune crests in Run 28 are more rounded than for Run 26 for which the velocity and load were smaller.

The measured heights, wavelengths, and velocities of the sand dunes are summarized in Table 8 for the 10 runs which had stable dune patterns. Three cases where meanders were observed were excluded; in two additional cases, Runs 12 and 24, where there was a solitary long, thick sand wave in the system, all the data pertain only to the rugged, dune-covered reach.

Table 8

SUMMARY OF DUNE MEASUREMENTS

Run No.	d Depth in.	f_b Bed Friction Factor	$\bar{c}$ Sed. Disch. Conc. gr/l	Sand Depth			Dune Height					Wavelength at Wall		Vel. of Dunes at Wall		U Stream Velocity in./min	Run No.
				Maximum		Ave. for channel in.	At Wall		Central Region		h Est. Repres. Height in.	Ave. λ in.	Max. Observed in.	Min. Observed in./min	Max. Observed in./min		
				At Wall in.	Central Region in.		Ave. in.	Max. in.	Ave. in.	Max. in.							
0.16 mm Sand																	
9	2.95	.079	1.1	1.5	1.2	.48 e	-	1.25	-	-	.5	5.3	9	1	2.7	970	9
10	3.0	.135	0.2	1.5	-	.47 e	-	1.4	-	-	.6	4.5	6	0.4	1	670	10
12*	3.6	.070	0.72	1.25	-	.41	-	1	-	-	.5	5.6	11	0.9	2.5	1010	12*
13	2.35	.102	1.2	1.25	1.1	.38	-	1.1	-	-	.5	5.3	8	1	2.5	900	13
0.10 mm Sand																	
24*	2.71	.079	4	-	-	.35	.5	1	.5	1	.5	4.7	8	0.75	1	965	24*
25	2.24	.095	5.3	1.4	1	.40	.6	1.3	.5	1	.5	4.7	8	0.5	1.75	885	25
26	3.35	.12	0.19	1.6	1	.53	.75	1.25	.5	1	.6	4.5	7	0.05	0.175	590	26
27	2.77	.13	1.35	1.6	1.15	.47	.75	1.4	.6	1	.65	4.3	10	0.1	0.4	710	27
28	3.41	.088	3.6	1.5	1.4	.50	.6	1.4	.6	1.4	.6	5.0	8	0.6**	1.25**	950	28
30	3.37	.115	1.75	1.75	1.2	.49	.75	1.6	.6	1.1	.65	4.8	8.5	0.2	0.75	780	30

e - estimated

* - All data pertain only to region with dunes, excluding long flat sand wave.

** Average velocity 0.7 in./min.

The first three items, depth, bed friction factor, and sediment discharge concentration, are taken directly from Table 7, and are included here for comparison purposes. The maximum sand depth, the next item, is the maximum observed height of surface of the sand bed above the steel bed. The maximum sand depth is larger next to the window than in the central part of the flume because there was a general tendency for the sand bed to be slightly thicker on the average near the walls than in the center. The average sand depth was determined from the mean elevation of the bed after it was leveled with the bed scraper described in Chap. III, Sec. I.

The dune heights given in Table 8 must be considered as approximate because of the difficulties in defining the height discussed in Chap. III, Sec. L. The average heights were determined from a number of representative-looking dunes, and are thus subject to errors of judgment of this observer. The maximum dune height is a more objective measure, because the observer simply has to locate the largest dune, and measure the height from the highest point of the crest to the lowest point of either of the two troughs, fore and aft, or possibly to one side. Minimum dune heights have no meaning, inasmuch as bumps or irregularities of any arbitrarily small size can be found.

Maximum and average values of dune height are tabulated for the central region and for the longitudinal cross section of the bed made by the window. In determining the average height for the earlier runs, Runs 9, 10, 12, and 13, no distinction was made between the window section and the central region, although it was sometimes noted that the dunes were slightly higher at the walls. The last column under dune height gives the height, h, which is believed most representative for the flow as a whole.

It is indeed surprising that there is so little variation in the average height, h, considering the variation in depths and velocities represented by the runs tabulated. This is believed to be the result of a shortage of sand in the flume. Since the average amount of sand on the bed of the flume was only about 0.4 to 0.5 inches, it was certainly impossible to have the average height greater than 0.8 to 1.0 in., and it is perhaps possible that the short supply restricted the average height still further. A number of bare spots on the bed in each run showed that the development of the dunes had been stopped somewhat short of the limit. However, the total area of the bare spots, away from the inlet, very rarely amounted to more than a very few per cent of the total area. Naturally, they were the most prominent for the runs for which the bed was the thinnest, i.e., Runs 12, 13, 24, and 25, and are not as numerous for Runs 26, 28, and 30, used for the illustrations. It is recognized that this shortage of sand was a shortcoming of the experiments, but nevertheless it is the opinion of the writer that the resulting limitation on the growth of the dunes was not very great. Furthermore, if the dunes had been even larger, the main conclusions would not be weakened, but would be made even more striking.

Of all the measurements of the bed configuration, the average wavelength, the next item in Table 8, is probably the most reliable. It was usually based on several measurements of 8 or 10 dunes at a time at the window. From the figures it may be observed that the average wavelength in the center of the channel is the same, or perhaps slightly less than at the wall. There was, of course, considerable variation in wavelengths, with the low dunes generally being short and the high dunes long. The maximum observed wavelengths usually associated with very high dunes, have also been tabulated in Table 8 as a matter of interest to show the extremes

possible.

The velocity of the dunes will be discussed in subsection (5) along with mechanisms of dune movement.

(4) Relation of Friction Factor to Dune Configuration. By far the most direct effect of the dunes on the stream hydraulics is the great increase in resistance to flow. The Darcy-Weisbach friction factor, f, for the bed may be expected to depend on the average dune height, h, the average spacing or wavelength, λ, the arrangement and shape of the dunes, and perhaps the suspended load of the stream. Since f_b is a measure of relative roughness, h and λ will be expressed in terms of the depth of the stream, d. In Fig. 39, f_b is plotted as a function of h/d and λ/d with the discharge concentration $\bar{C}$ also recorded under each point. The shape and arrangement are not included as variables because there is no simple way to describe them quantitatively.

In spite of the roughness of the dune measurements, Fig. 39 gives support to the following two conclusions, which are quite naturally to be expected.

(1) With the relative dune height constant, the friction factor increases when the relative spacing or wavelength of the dunes decreases.

(2) With the relative spacing constant, the friction factor increases when the relative dune height increases.

The interesting question of whether the suspended load per se affects the friction factor cannot be resolved on the basis of the experimental data presented here. Any change in the load is always accompanied by some changes in the bed configuration, so the effects of the two cannot be separated without a specially designed experiment. Even in the

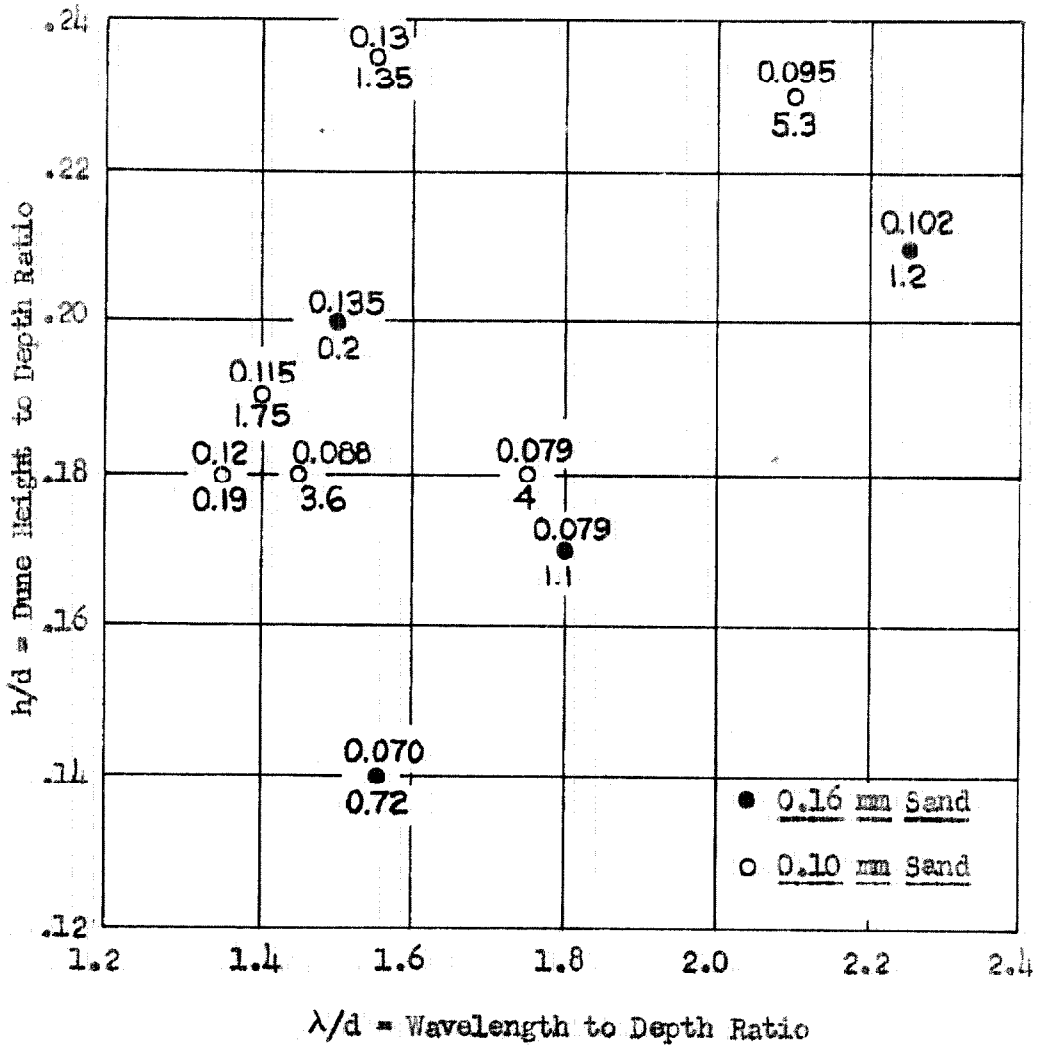

Legend: Upper figure: f_b = bed friction factor
Lower figure: $\bar{C}$ = sed.disch.concentration, gr/l

Fig. 39. Relationship of Bed Friction Factor to Dune Height and Wavelength

case of the two points very close to $h/d = .18$ and $\lambda/d = 1.4$, (Runs 26 and 28), it cannot be concluded that the drop in f_b from .12 to .088 is due to the increase in $\bar{C}$ from 0.19 to 3.6, because there is a noticeable improvement in the alignment of the dunes and smoothing of the crests also associated with the drop in f_b. (Cf. Fig. 27 (a,c) and 29.)

(5) Mechanisms of Dune Movement and Their Relation to the Suspended Load. The measurement of the average velocity with which a dune configuration moves downstream is difficult to define precisely because it is impossible to establish an unbiased reference point in the ever-changing pattern. Dunes are incessantly growing or shrinking, appearing or disappearing, getting longer or shorter, merging or splitting, twisting or turning at varying rates at the same time they move ahead. Just in the course of moving ahead a foot, most dunes will deform so much that they are unrecognizable; occasionally a dune's lifespan is not even long enough to travel a foot! The faster the dunes travel the more quickly they change their shape. Figs. 30 to 32 show the movement of the dunes in short intervals of time as noted. Fig. 32 shows a pattern for Run 27 undergoing an especially rapid alteration. The process is uneven, for at any one time there are some regions deforming much more actively than the neighboring ones. As mentioned in the section on growth of dunes, it is believed that the unevenness may be linked to the changing structure of the large scale eddies.

The velocity of the dunes was measured directly by following individual features for a few minutes by eye, or from examination of photographs taken at intervals. The range of values observed in several meas-

urements for each run is tabulated in Table 8. The largest speed observed is usually greater than twice the smallest. Even for Run 26, illustrated in Fig. 30, where a casual look at the photographs reveals no significant changes in the configuration after ten minutes, a close inspection will show that the amount of advance between pictures varies from about 0.5 to 1.5 in. In the time lapse motion pictures of Run 26, this variation of the rate of movement was shown very clearly; the sand appears practically to flow along with sudden thrusts at various points.

The dune velocity can be used to obtain a rough estimate of the bed load. For example, consider the run with the smallest load of 0.10 mm sand, with average dune velocity of about 0.1 in./min and total measured sediment discharge 0.14 lb/min. The maximum possible bed load discharge may be found by assuming that the entire bed of sand is moved forward at the average rate of 0.1 in./min. Since the average bed thickness is 0.53 in. (see Table 8) and the width of the flume is 10.5 in., the volume rate of transport is 0.1 x 0.53 x 10.5 = 0.56 $in.^3$/min. The specific weight of the loose sand is 90 lb/ft^3 (see Table 4) so that 0.56 $in.^3$/min corresponds to 0.56 x 90/1728 = 0.03 lb/min, the estimated maximum possible bed load discharge. By comparing this figure with the total measured sediment discharge, G = 0.14 lb/min, it may be concluded that even at this very low rate of transport, the suspended load discharge is still the major part. However, a similar calculation for Run 10, the run with the smallest load for the 0.16 mm sand, gives the maximum estimated bed load discharge as 0.18 lb/min against a measured total G of only 0.15 lb/min, indicating that the suspended load discharge for this run is not very significant. For all the other runs, however, the bed load was relatively minor.

An inspection of Table 8 for each of the sand sizes shows that the dune velocity increases as the sediment discharge concentration increases. But it is curious that the dune velocities for the 0.10 mm sand are consistently lower than for the 0.16 mm sand in spite of the larger sediment concentrations for the former. A possible explanation for this observed fact may be found by considering the mechanisms of dune motion.

A dune can progress downstream only by erosion from the upstream face and deposition on the downstream face. In the case of wind-blown sand dunes and larger-sized sediments in water, there is practically no entrainment of sediment from the lee side of a dune; sediment blown over the crest falls out on the lee side and sediment pushed over the crest by bed load movement slides down the lee slope. In either case, the sand is not moved again until the entire dune passes over and the sand particles emerge again on the upstream face.

However, in the case of fine sand in water, the material supplied to the downstream face is not at all dormant. It was observed both by eye and photographically that the turbulent eddies generated in the wake of a dune are strong enough to lift particles out of even the deepest part of the trough up into the stream where they are carried away as suspended load. Thus the amount of deposition on the lee side of the dune, and hence the rate of forward movement, is reduced by the erosion caused by the lee-side eddies. Consequently, with the finer sand it is reasonable to expect that the lee-side eddies will cause more erosion, and hence lower dune velocities than in the case of the 0.16 mm sand. Lower dune velocities actually were observed.

For dunes of any given size, the strength of the lee-side eddies, as indicated by the entrainment of sand, varied considerably; at times the erosion was so severe that it appeared to the naked eye as if an eddy were boring a hole in the bed of a trough. Fig. 33 shows the cloud of sediment raised by a vigorous eddy behind an extraordinarily large dune next to the window. The line of separation of streamlines in back of the dune is sharply defined by the suspended sediment. From the figure it is apparent that the rate of erosion is much less on the upstream face than on the downstream face at the instant the photograph was taken.

From some high speed closeup motion pictures made of the dune motion at low rates of transport, one could observe two principal ways in which the sediment became suspended. One was the erosion in the trough by the lee-side eddies just described. The motion pictures gave the appearance that the trough was being bombed; sometimes the bed would lie almost quiet for a while, and then suddenly a large group of particles would seem to spray up in all directions from some point on the bed, and finally be swept away by the current. The other mechanism was the sweeping of the bed load off the crests of the dunes at sufficient velocity so that with the aid of the turbulence in the wake of the dune, a substantial part of the material could be carried off in suspension a considerable distance downstream, instead of falling to the bed just beyond the crest.

For a flow in equilibrium the rate at which the sediment is lifted into suspension must be just balanced by the rate of redeposition. However, it was not noticed that the particles tended to return to the bed at any particular points. After the particles are swept into suspension in clouds, they are gradually diffused and each grain returns to the bed

by its own devious path. Many of them undoubtedly come down on the upstream faces of the dunes, there to retard the rate at which that face is being eroded in the process of moving the dune forward. Actually, this result is a necessary consequence of the fact that the growth of the downstream face is retarded by the eroding action of the lee-side eddies, for if the progression of the upstream face were not in some way also retarded the dune would soon devour itself!

To summarize the interrelationship of the dune mechanisms and the suspended load, it could be said that the dunes provide an efficient mechanism for getting the fine sand into suspension at low flow rates, and that in so doing the velocity of the dunes is reduced.

(6) Sand Waves and Meanders in the Bed. As the velocity of flow is progressively increased, there comes a point where the sand tends to collect in a single long, flat wave, which travels perpetually through the system. The wave is a long, thick deposit of sand with a flat top, over which the water flows with reduced depth, and increased velocity and sediment load. In the remainder of the flume, the bed is still covered with rugged dunes, and the mean thickness of the sand bed is much less. It is not known whether this is a system effect or a real transportation phenomenon, or a combination.

Solitary sand waves were prominent in Runs 12 and 24, and were also present on a much smaller scale in conjunction with meanders in Runs 5, 8, and 11. No other run for the 0.10 mm sand, in addition to Run 24, was performed for a flow condition that produced a sand wave, simply because there were too many experimental difficulties. However, preliminary runs for

reconnaissance, not reported in detail, showed that this was certainly a common phenomenon. In Fig. 23, the gap in the range of velocities covered between 1.35 and 1.8 ft/sec is due to the fact that runs could not be performed in this range which did not produce a very sizeable sand wave. The essential features of all of them were quite similar to Run 24, which will be described at this point.

Three views of Run 24 are shown in Fig. 34. The middle of the sand wave with its flat bed surface is shown by (a), the transition by (b), and the typical configuration of dunesfor the rest of the flume by (c). The mean thickness of the sand bed in the sand wave is about 0.80 in., while it is only 0.35 in. in the dune section. The dimensions of the wave remained constant after equilibrium was established, even though the wave periodically had to pass through the pump and return pipe.

The flow had apparently reached a new equilibrium on top of the sand wave since the sand depth and surface configuration remained uniform over a section about 8 ft long between the transition regions at the two ends of the wave. All the usual measurements could be made for this section except the slope, because the reach was so short. They are reported in Table 7 along with the data for the dune section, and the relevant figures in Sec. A include a point for this additional equilibrium condition.

At each end of the sand wave the transition section was only about 4 or 5 ft long, indicating that the adjustment between the two separate equilibria was fairly rapid. The wave progressed downstream by continual erosion in the upstream transition region and deposition in the downstream transition region.

The rate of travel of the sand wave should be determined by the difference in the total sediment discharge, G, between the flat section on the wave and the dune region. Inasmuch as G was 7 lb/min over the wave, and 4 lb/min elsewhere, 3 lb/min or 60 in.^{3}/min must be the rate at which material is moved from one end of the wave to the other. But the volume rate of accumulation is also the width of the channel (10.5 in.) times the increase in mean bed thickness (.80 - .35 = .45 in.) times the velocity. The velocity corresponding to the measured load difference is then 60/(0.45 x 10.5) = 13 in./min. However, the actual average rate of advance was only 5.3 in./min. One possible explanation for this inconsistency may be that the sand wave accelerates at the end of the flume where the total load was measured, but there is no other evidence for supposing this. The argument above should be quite sound, because it is based only on a continuity principle for the sand. Further investigation is needed to understand why the calculated and measured velocities are so different.

The velocity of the individual dunes in the rugged section was found to be about 1 in./min or only one-fifth of the sand wave velocity. Consequently, the dunes ahead of the sand wave must have been buried in the "onrush", and new dunes must have appeared behind the sand wave.

The solitary sand wave is a baffling phenomenon; it is not apparent what determines its length and height, or even why it existed at all at some flow rates and not others.

The meanders in the sand bed, illustrated in Fig. 35, were equally puzzling. Here the sand distributes itself nonuniformly <u>across</u> the channel by forming a central ridge which weaves back and forth in the channel. The surface of the bed is covered with small ripples. Definite rhythmic

patterns were observed in Runs 5 and 11 for the 0.16 mm sand, but in the course of the experiments with the 0.10 mm sand, only faint suggestions of meandering were seen. The average wavelengths in Runs 5 and 11 were 3.4 and 3.9 ft respectively. Some meanders also appeared in Run 8, but the pattern was not so well defined. In all three of these cases it may be noted that the Froude numbers were fairly large, ranging from 0.63 to 0.74, but were not quite large enough to induce standing waves on the water surface.

(7) Water Surface Configuration and its Relation to the Bed. The character of the free water surface is largely dependent on the Froude number, F, because gravity is an important force. Consequently, F and the water surface condition are tabulated in adjacent columns in Table 7. At very low F values, around 0.3, the water surface was very smooth, with only a few scattered dimples due to tiny vortices, in spite of the fact that the bed was very rough in these cases (See Fig. 30). As the Froude number increases, the surface becomes more and more sensitive to disturbances to the flow resulting from the dune configuration. (See Figs. 31, 32, and 33). The surface ripples for F values up to about 0.7 reflect directly the wavelength of the bed configuration; in contrast to the large standing waves, the ripples are generally not over 0.015 ft high, and shift about quickly, giving the water surface a ripply appearance - hence, the designation "ripples".

When the Froude number gets up to 0.70 or 0.75, then large standing waves develop. A typical wave train would move very slowly up the stream, with the waves becoming gradually steeper, and finally disappearing rather

suddenly, without breaking. This process is well illustrated by the timed sequence of pictures shown in Fig. 38. At other times, the waves would persist without much change in height; they would move upstream slowly as before, but the waves would gradually die out at the upstream end of the train and new ones would be generated at the lower end. The wavelengths were not carefully measured during the runs, but from the photographs it was found that the wavelength was 10 to 11 in. for Runs 6 and 23, and 11 to 12 in. for Runs 21 and 21a. The heights in exceptional cases exceeded one inch.

The standing waves were always more pronounced at the downstream end of the flume; furthermore, when the turbulence damping screens were used at the inlet, the surface waves were larger and extended farther upstream. It is probable that the wave trains could develop only where uniform flow is well established; with the damping screens the inlet condition is improved, making the reach of uniform flow longer.

Standing waves on the surface tended to erase whatever dunes might otherwise form on the bed. In all cases with wavy water surface, the bed was smooth in the center, with little ripples about 1/4 in. high near the walls only, as shown by Figs. 36 or 37. If the waves were very high, as in Run 23, the bed would be slightly undulated, with the same wavelength as the surface waves.

However, at the largest depth used, d = 0.28 ft, it was found that the sand bed would be leveled by the flow itself even before the Froude number was high enough to make surface waves. Run 29 was the only run performed with the good fortune of having both a smooth bed and smooth water surface, as illustrated in Fig. 36. With depth of d = 0.24 ft, a

smooth bed condition could not be obtained without moderate surface waves, but it was still possible to carry out the usual measurements. At d = 0.19 ft, whenever the bed was smooth, the waves were large, making the flow practically unmanageable. At still smaller depths, it was impossible to obtain an equilibrium flow with a smooth bed, for the waves were so large that small antidunes started to form.

It was concluded, then, that the Froude number, at which the bed becomes smooth, decreases as depth increases. Had a larger flume been used, permitting greater depths, it would have been much easier to establish a number of uniform flow conditions with a flat bed without interference from surface waves.

The foregoing remarks about the waves and the smooth bed apply for Froude numbers up to about 0.8 only. For higher F values, the waves were always too large to permit measuring the depth and the slope with any accuracy, and the shifting pattern made it impossible to measure point velocities and concentrations. At still larger F, the surface waves are accentuated by large, rounded antidunes, and reach heights as great as the mean depth. Occasionally a breaking wave could be seen; others would just disappear.

(8) Summary. At low velocities, dunes will always form on the bed, making the bed roughness very large. As the velocity and transportation rate increase, the dunes become more regular and rounded and the friction factor decreases gradually; long sand waves are formed next, and finally the bed is swept smooth at high velocities and transportation rates, with a pronounced drop in the friction factor. At Froude numbers of 0.7 to 0.75, standing waves appear on the surface.

As the most important observations are illustrated by Figs. 27 to 38, the reader is referred to these figures for a visual review of the phenomena described in this section.

In addition to increasing the roughness of the stream bed tremendously, the dunes provide two efficient mechanisms for getting the bed sand into suspension. At low stream velocities, the particles on the downstream face of the dune may be lifted into the stream by the lee-side eddies. When the velocity is somewhat higher, the bed load material is swept off the crest directly into suspension, and kept in suspension over the trough by the lee-side eddies there.

The dunes were observed to move downstream at velocities from 1/5000 to 1/500 of the mean stream velocity, being the slowest at low transportation rates. For the runs with 0.16 mm sand, they generally moved faster, even though the transportation rate was smaller than it was for similar runs with the smaller sized sand. As the dunes moved, they continuously deformed so much that individual dunes became unrecognizable before traveling even a foot.

C. DISTRIBUTION OF VELOCITY AND SUSPENDED SEDIMENT WITHIN THE STREAM.

In this section the results based on measurements of point velocities and concentrations will be reported. Centerline profiles were obtained only for the runs for which the sand bed was flat, because of the experimental difficulties in determining representative profiles in the presence of an irregular, changing dune configuration. Consequently, the data reported here cover a very limited range of conditions, and perhaps should be taken only as suggestive of what might be found by a more ex-

tensive investigation. Nevertheless, some positive conclusions can be made, especially regarding the reduction of the von Karman constant by the suspended load.

The velocity measurements will be taken up first, in subsection (1), and the concentration measurements in subsection (2). The formulas developed in Chap. I for integration of the suspended load discharge from the measured profiles will be applied to the experimental data in subsection (3).

A discussion of the experimental procedures by which these point velocities and point concentrations were measured, may be found in Chapter III, Secs. E and G (1). All the basic data upon which the curves in this section are based have been tabulated for reference in Appendix D.

(1) Velocity Distribution. Velocity profiles were generally measured only in the center of the flume, where it was believed that the flow would be most nearly two-dimensional. However, detailed velocity traverses were made over half of the entire cross section for Runs C1, C6, and 29.

The velocity contours have been plotted in Fig. 40 for Run 29 to show that the flow is very closely two-dimensional in the central region of the flume, except for the upper third of the depth. Inasmuch as the sand bed in Run 29 was smooth and the depth (0.280 ft) was practically the largest used in any of the runs, the fraction of the cross-sectional area which should be assigned to the walls for the wall shear is as large in this case as for any of the runs. This ratio, A_w/A, may be easily determined from the values of the depth, d, and the bed hydraulic radius, r_b, calculated from the side-wall correction procedure of Chap. V, Sec. C(2)

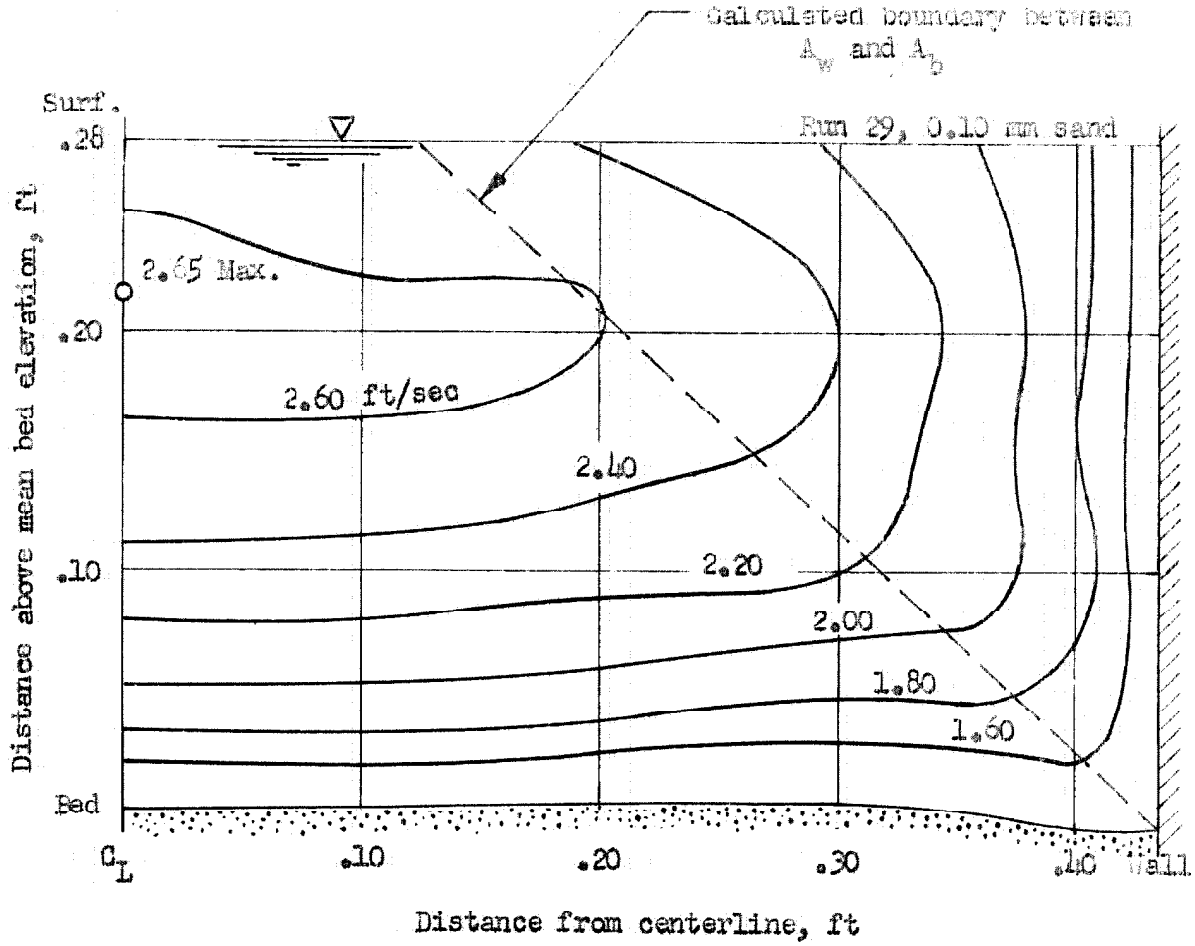

Fig. 40. Velocity contours in cross section of flow for Run 29

as follows:

$$\frac{A_w}{A} = 1 - \frac{A_b}{A} = 1 - \frac{r_b}{d} \quad ,$$

because $A_b = r_b b$ and $A = bd$.

For Run 29, it is found from Table 7 that $r_b = 0.178$ ft and $d = 0.280$ ft; hence, $A_w/A = 0.36$. In Fig. 40, the dashed line shows how the cross section could be divided in this ratio by assuming that the boundary curve between A_w and A_b is a straight line through the corner. From the contours in the figure, this division seems reasonable.

In spite of this large wall area, A_w, the contours are straight and parallel to the bed in the center of the flume. It may also be noted from Fig. 40, that the thickness of the sand bed was not perfectly uniform across the channel; near the wall, there are some small ripples, about .020 ft high (see Fig. 36(b)), which, when leveled out, give a slightly lower than average bed elevation near the corner. The hump in the average bed elevation near the abscissa .300, comes approximately at the limit of the lateral extent of the ripples. This irregularity of the bed near the corner is reflected by the contours nearest the bed.

The velocity measurements over the cross section for Runs C1 and C6 have already been plotted as semi-logarithmic profiles in Fig. 14 for the purpose of obtaining the shear distribution around the boundary of a uniform channel with clear flow. The data upon which those curves were based have also been tabulated in Appendix D. In addition, a few velocity measurements off the centerline for some of the other runs have been included in Appendix D, but are not shown on any of the figures.

The centerline profiles have been plotted semi-logarithmically in Fig. 41 for both the runs with clear flow (Runs C1, C2, C3, C4, and C6)

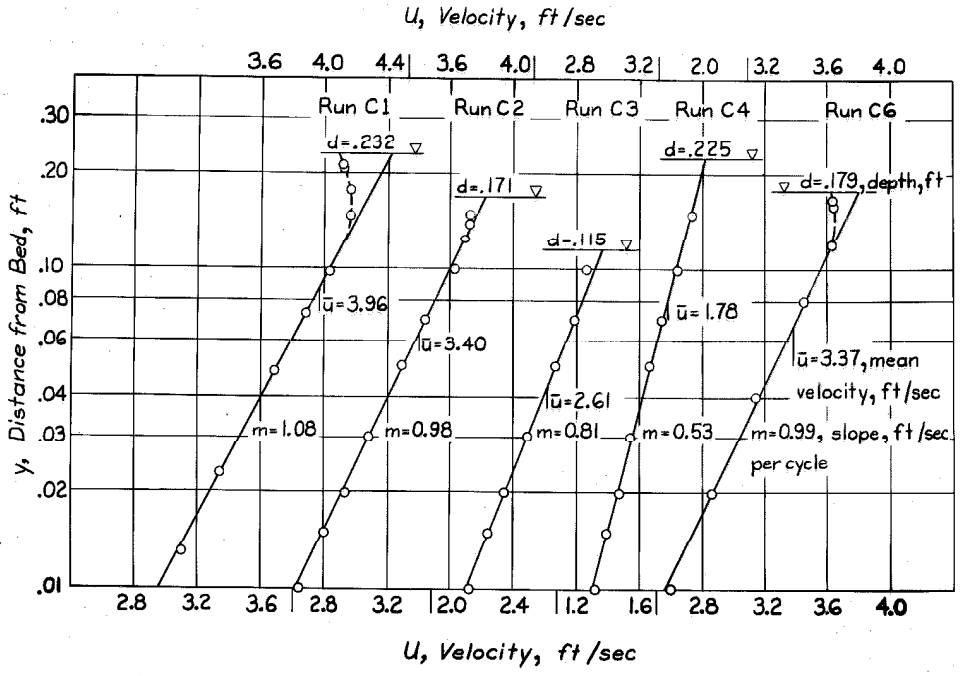

(a) Clear flow

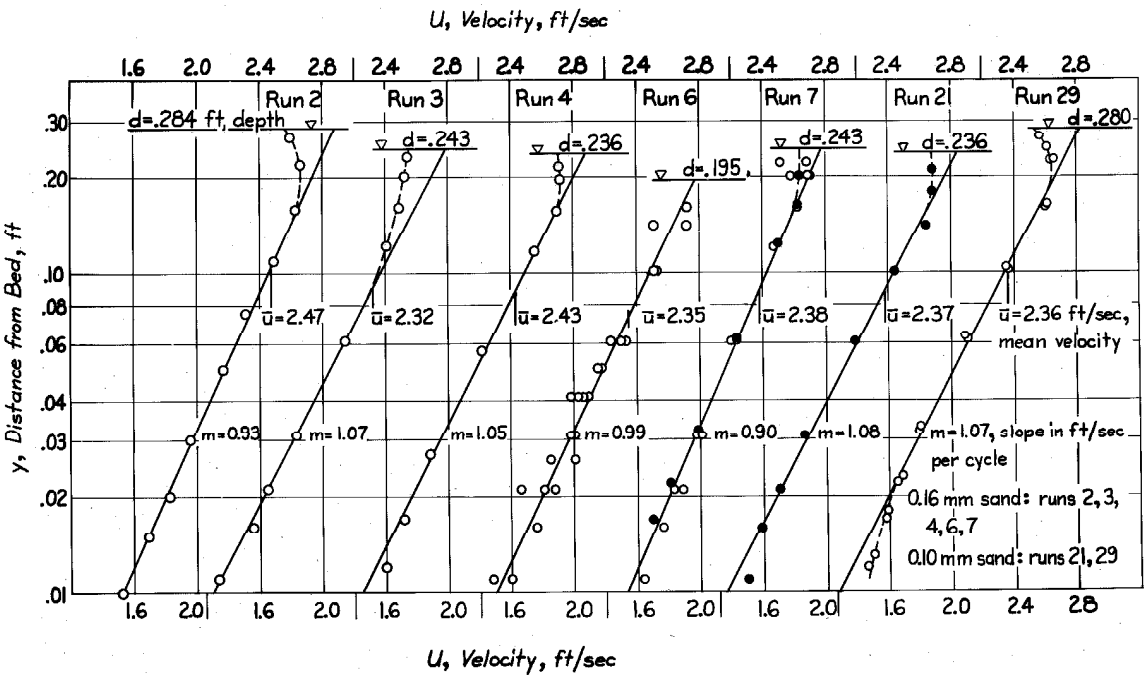

o *water surface smooth, or position of wave crest or trough relative to pitot tube not observed*

● *average of velocity readings under crest and trough of surface wave*

(b) With suspended sediment (sand bed smooth)

Fig. 41. Velocity profiles on the centerline of the flume.

and the runs with a smooth sand bed and suspended load, (Runs 2, 3, 4, 6, 7, 21, and 29). In all cases the velocity distribution can be well approximated by a straight line, except for minor deviations near the surface and also near the bed for the runs with heavy suspended load, (especially Runs 21 and 29). The retardation near the surface is believed to be mainly the effect of the side walls or secondary circulation induced by them, for at the smallest depth (0.115 ft in Run C3), this retardation is very slight.

For some of the runs with sediment, for which velocity profiles are plotted in Fig. 41, there were persistent standing waves on the water surface, because the Froude numbers were all between 0.7 and 0.8. Under the trough of a standing wave, the depth is reduced and all the velocities are increased, and under a crest the opposite is true. If the point velocities are measured without regard to the position of the Pitot tube relative to the surface waves, there is considerable scatter of points, as in Run 6; however, since these are not random errors, a better profile is obtained by taking a pair of readings at every level, one with the Pitot tube under a trough and one under a crest. A good linear first approximation for the true mean velocity is then found by averaging these crest and trough readings. This was done for Runs 7 and 21, where the waves were also large enough to cause substantial fluctuations in the velocity. The plotted means define a more reliable profile.

The straight lines for the velocity profiles may be fitted to the logarithmic law by the proper choice of $\bar{u}$ and k in Eq. 1.44, which is

$$u = \bar{u} + \frac{u_{*m}}{k}\left(1 + \ln \frac{y}{d}\right) \qquad (6.01)$$

The mean velocity, $\bar{u}$, was read directly from the profile at y = d/e, as noted for each one on Fig. 41. The shear velocity on the centerline, u_{*m}, was calculated for each run by the procedure outlined in Chap. V, Sec. D, and has been tabulated in Table 9. The values are generally a little less than $\sqrt{gdS}$, the shear velocity for a wide rectangular channel, or the maximum possible, as may be seen from the tabulated ratio, $u_{*m} / \sqrt{gdS}$.

The value of the von Karman k was calculated from the slope of the profile, m, in feet per second per cycle of 10, from the relation

$$k = \frac{2.30\, u_{*m}}{m} \quad . \qquad (6.02)$$

The measured slopes are given directly on Fig. 41, and the calculated k values are listed in Table 9. The sediment discharge concentration $\bar{C}$ for each run is also included in Table 9 for comparison purposes.

The reduction of k by the suspended load is unmistakable. For the runs with clear flow the k values lie in the narrow range 0.375 to 0.390, with an average of 0.382, which is very close to the commonly accepted approximate value of 0.4. On the other hand, with suspended sediment, k ranges from 0.246 to 0.322. The reduction is clearly significant and certainly cannot be attributed to experimental errors, or the method used to calculate the values of u_{*m}.

Furthermore, it appears, on the basis of the few values found, that k is less for the runs with 0.10 mm sand (Runs 21 and 29) than for the runs with the 0.16 mm sand. This may be either the effect of more suspended load or the difference in sand size. Although the number of runs for which k values could be found was too small to permit any conclusions about the effect of concentration or size, still there is no doubt that

Table 9

von Karman Constant for
Velocity Profiles on the Centerline

Run No.	d Depth ft	f_b Bed Frict. Factor	$\bar{u}$ Mean Profile Vel. on C_L ft/sec	u_{*m} Shear Veloc. on C_L ft/sec	$\frac{u_{*m}}{\sqrt{gdS}}$	k von Karman Const.	$\bar{C}$ Sediment Disch. Conc. gr/l
			Clear Flow				
C1	.232	.017	3.96	.183	0.95	.390	0
C2	.171	.0185e	3.40	.164	0.99	.385	0
C3	.115	.0205e	2.61	.132	0.97	.375	0
C4	.225	.0195e	1.78	.088	0.92	.382	0
C6	.179	.0185	3.37	.162	0.96	.376 (Ave.= .382)	0
			Sand Bed, D_s = 0.16 mm				
2	.284	.018e	2.47	.117	0.91	.290	-
3	.243	.0275	2.32	.136	0.97	.292	1.95
4	.236	.023	2.43	.130	0.97	.285	2.45
6	.195	.0225	2.35	.124	1.00	.288	2.45
7	.243	.0225	2.38	.126	0.98	.322	2.15
			Sand Bed, D_s = 0.10 mm				
21	.236	.022	2.37	.124	0.95	.264	4.85
29	.280	.019	2.36	.114	0.89	.246	3.45

e = estimated

the presence of suspended load does substantially reduce the von Karman constant k.

(2) Sediment Concentration Profiles. The sediment concentration profiles for the center of the flume for the seven runs for which profiles were obtained, are shown in Fig. 42. The concentration, c, has been plotted logarithmically against (d - y) /y, where y is the distance from the bed, in order that the points may be fitted to the two-dimensional suspended load equation (Eq. 1.18) with a straight line. It may be recalled from Chap. I that the slope of the profile, z, is the number of cycles of c per cycle of (d-y) /y, and that

$$z = \frac{w}{\beta k u_{*m}} \quad . \qquad (6.03)$$

To show that the distribution of suspended sediment was approximately two-dimensional, the concentration was measured at a few points off the centerline (see Appendix D). There was little variation of concentration in the horizontal direction compared with the vertical direction. For example, in Run 29, at 0.103 ft from the bed, the concentration was 2.73 gr/l on the centerline and 2.84 gr/l at the same level only 0.035 ft from the wall.

For the lower half of the flow (i.e., (d-y)/y > 1), the plotted points may be fitted well by a straight line, but in the upper half the points deviate, especially for the runs with the 0.10 mm sand. This is to be expected because of the effect of the walls on the velocity distribution and because the assumption, that the diffusion coefficient for sediment, ϵ_s, is proportional to the kinematic eddy viscosity, ϵ_m, is not accurate in regions where the shear and the velocity gradient are both small.

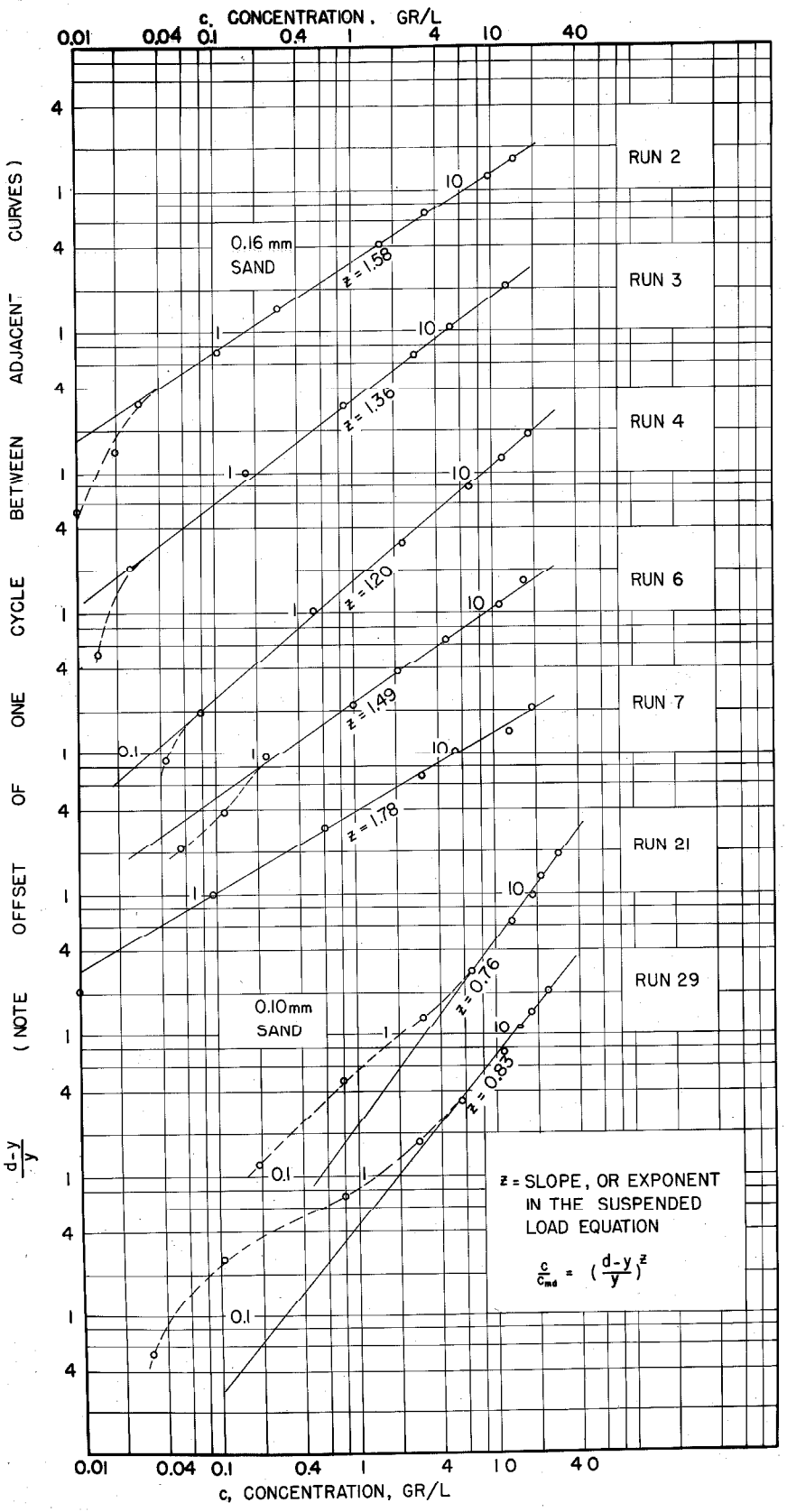

Fig. 42. Sediment concentration profiles on the centerline of the flume.

Secondary circulation and selective sorting of the material can also cause significant deviations in the upper levels. However, since the amount of sand carried above the mid-depth was small compared with the load below mid-depth, it is much more important to have the formula fit the observed concentrations in the lower part than in the upper part.

Since the profiles are best defined by points near the bed, care was taken at the time of the sampling to determine accurately the distance, y, from the bed to the sampling point. For Runs 21 and 29 it was necessary to deduct 0.001 ft from the bed elevations measured in still water to allow for the amount of material that was in suspension when the water was flowing.

The ratio of diffusion coefficients, $\beta = \epsilon_s / \epsilon_m$, may be calculated from Eq. 6.03. The values of u_* and k have already been discussed and are listed in Table 9. The values of z are determined directly from the straight line profiles, and are noted on Fig. 42 and in Table 11. The mean fall velocity, w, for the suspension was found in the manner outlined below.

There are two factors which make the mean fall velocity vary. One is the fact that in a suspension of nonuniform particles, the mean size decreases going toward the surface because the concentration gradients are less for the smaller sized particles. This phenomenon was analyzed at length in Chap. I, Sec. B. Table 10, which demonstrates that effect for Run 29, gives, for five values of y, the mean sedimentation diameters, D_s, which were calculated from sieve analyses of point samples by the method outlined in Chap. IV, Sec. B. There is definitely a regular decrease of D_s as y increases.

Table 10

Variation of Mean Settling Velocity with y for Run 29

y Distance above bed ft	D_s Mean Sed. Diameter mm	% Reduction in w for Conc.	w Fall Velocity (at 25°C) ft/sec
.018	0.098	15	.0235
.033	0.096	13	.0235
.063	0.094	8	.0235
.103	0.091	5	.023
.163	0.085	3	.021
Discharge sample	0.095	6.5*	.0245

Total depth, d = .280 ft. For bed material D_s = 0.103 mm.

*Based on sediment discharge concentration

Table 11

β Values for Sediment Concentration Profiles on the Centerline

Run No.	D_s Mean Sed. Diameter mm	T Water Temp. °C	% Reduction in w for Conc.	w Fall Vel. ft/sec	z Slope of conc. Profile	$\beta = \frac{\epsilon_s}{\epsilon_m}$
			0.16 mm Sand			
2	0.159e	17	a	.0525	1.58	0.98
3	0.157	22	a	.0565	1.36	1.04
4	0.158	12.5	a	.048	1.20	1.08
6	0.160	21	a	.057	1.49	1.07
7	0.163	31.5	a	.070	1.78	0.97
					(Ave.	1.03)
			0.10 mm Sand			
21	0.098	25.0	8	.0255	0.76	1.03
29	0.095	25.2	6.5	.0245	0.83	1.05
					(Ave.	1.04)

e = estimated

a = No basis for calculating, since McNown and Lin (21) analysis does not extend far enough. Estimated to be not more than 4 per cent, thus reducing β values 4 per cent at most.

Very close to the bed, it is believed that D_s is the same as for the bed material. At y = .018 ft for Run 29, D_s is only 0.098 mm compared with 0.103 mm for the bed sand; however, a sieve analysis at y = .011 ft (for Run 21) yielded D_s = 0.102 mm, which is practically the same as for the bed material itself.

Counteracting this decrease in D_s is the hindered settling phenomenon discussed previously in Chap. IV, Sec. A. The per cent reduction of w is the most near the bed where the concentrations are largest. Table 10 shows the per cent reduction in w for Run 29 from Table 2 (Chap. IV, Sec.A). With the aid of a fall velocity chart for quartz spheres (1), the mean settling velocities, given in Table 10, were calculated with the required reduction to show the combined effect of sorting and hindered settling. For the example chosen, the two factors are in perfect balance in the lower part of the flow inasmuch as w remains constant at .0235 ft/sec for all practical purposes up to y = 0.103 ft or 37 per cent of the depth.

If the mean settling velocity had been computed for the bed material instead of from the actual suspended load samples, and no correction for particle interference is made, then w would have been .030 ft/sec for Run 29, or fully 30 per cent higher than actual. Hence, the neglect of these two factors, sorting and hindered settling, can lead to erroneous values of β.

Since making sieve analyses for all the sampling points is a tedious procedure, an approximate method for finding w was devised. A single sieve analysis was made of the composite of the sediment discharge samples, and a reduction corresponding to the discharge concentration was made for the hindrance effect. For Run 29 this approximate method gives

w = .0245 ft/sec, compared to .0235 ft/sec found from sieve analyses for the individual sampling points. It was decided then, pending further investigation, to assume for the other runs that a representative w could be determined in this simplified way.

All the values of D_s and w given in Table 11 were determined on this basis. Unfortunately, the analysis of hindered settling by McNown and Lin (21) does not extend to large enough particle Reynolds numbers to permit determination of the amount of reduction required for the hindered settling for the 0.16 mm sand. Therefore, no correction was included in the calculations, but it is estimated that the corrections are not more than 4 per cent.

From the values of u_{*m}, k, w, and z given in Tables 9 and 11, the values of β, also listed in Table 11, were computed by Eq. 6.03 for each run. Since the variation in the values is small considering the experimental errors involved, the original assumption that ϵ_s is proportional to ϵ_m is borne out. Furthermore, this factor of proportionality, β, has a value close to 1.0 for both sand sizes.

This result was checked in another way for Run 29. From the sieve analyses of the samples at various levels, it was possible to plot the concentration profile for each sieve fraction, as has been done in Fig. 43. It may be noticed right away that the points do not fit a straight line as well as the points for the total concentrations in Fig. 42, because now the effect of the concentration on the fall velocity is not counterbalanced by the sorting. If a smooth curve were plotted through the points, the slope of the tangent z would decrease when (d-y)/y becomes large, indicating by Eqs. 1.14 and 6.03 that the settling velocity w is decreasing

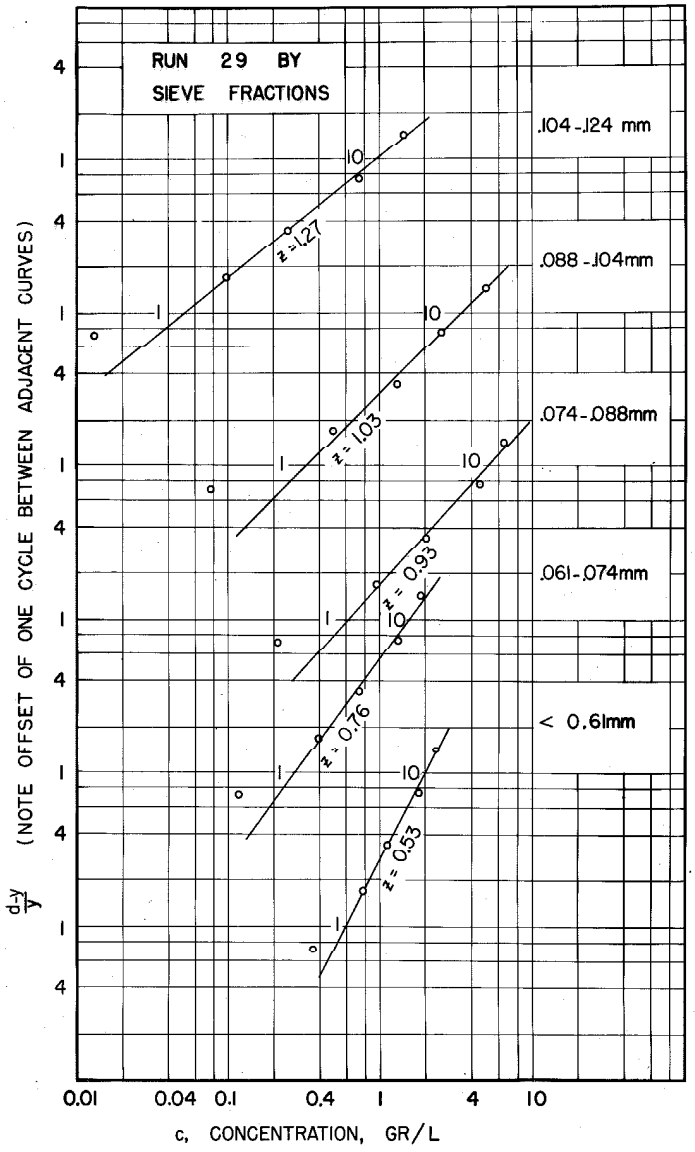

Fig. 43. Sediment concentration profiles for individual sieve fractions on the center-line for Run 29.

as expected. This is evidence, then, for the fact that the good fit of the profiles in Fig. 42 is partly fortuitous. While it is true that the 0.16 mm sand is more nearly uniform in size than the 0.10 mm sand, still it is believed that the points would not fit a straight line so well were it not for the two counteracting factors of sorting and hindered settling.

The value of β for each sieve fraction was obtained approximately by fitting a straight line to the points in Fig. 43, and assuming a uniform correction for the hindered settling of -10 per cent. Table 12 shows

Table 12

Analysis of Concentration Profiles by Sieve Fractions for Run 29

Tyler Sieve No.	Mean Sieve Diam.	% of Sed. Disch.	D_{s_i}, Sed. Diam.**	w_i, Fall Vel.*	z, Slope of Profile	$\beta = \frac{\epsilon_s}{\epsilon_m}$
	mm		mm	ft/sec		
150	0.114	5.9	0.129	.039	1.27	1.10
170	0.096	25.1	0.107	.0285	1.03	0.99
200	0.081	34.5	0.096	.024	0.93	0.93
250	0.067	11.4	0.086	.020	0.76	0.93
Pan	-	22.6	(0.07e)	(.014e)	0.53	(0.94e)
					(Ave.=	0.99)

e - estimated

*For T=25°C, including an estimated 10% average reduction for hindered settling for all sieve fractions.

**By Table 3.

the relevant data and the values of β obtained. The average is 0.99 compared with 1.05 reported in Table 11 for the combined profile for Run 29; the difference may be largely attributed to the use of w = .0245 ft/sec

in Table 11, which was determined from the sediment discharge samples in order to be consistent with the other runs, whereas the actual average value of the settling velocity in the lower part of the flow is shown by Table 10 to be .0235 ft/sec, or 4 per cent less, making $\beta = 1.01$.

Thus, the conclusion that $\beta \neq 1.0$ is verified by the profiles for the individual sieve fractions.

(3) Application of Load Integration Formulas. In Chap. I, Sec. D, a detailed analysis was given for the problem of finding the suspended load discharge per unit width, q_s, by integration of the product of concentration and velocity over the depth. Eq. 1.53, based on the suspended load equation will now be applied to the experimental runs with various choices of the lower limit of integration, η_o.

A rigorous comparison of experimental results with the calculated suspended load discharge is not possible because the measured sediment discharge concentration, $\bar{C}$, includes also the bed load, and because the centerline profiles of concentration and velocity on which the integration is based are not truly representative of the whole cross section. Nevertheless, with the high transportation rates associated with the runs for which profiles were obtained, the bed load is believed to be small. Furthermore, it has been observed that the concentration does not vary substantially going across the channel at any given level. Since most of the load is carried close to the bed anyway, the distortion of the velocity distribution by the walls at the upper levels does not introduce a very large error. Consequently, the order of magnitude of the measured $\bar{C}$ should be the same as the calculated ratio of suspended load discharge to water discharge, q_s/q.

When using any of the integration procedure, it is important to have the suspended load equation fit the observed concentrations well only where the concentrations are large. If the curve deviates large amounts when the concentrations are relatively small, as is often the case in Fig. 42, the error introduced in the total transportation rate is still small.

The results of the calculations are summarized in Table 13 in dimensionless form. In part (a) of the table four values of the lower limit η_o have been listed for each run; they were calculated from Eqs. 1.56 to 1.59, and represent the various physical possibilities for the lower limit of integration. Column 1 is based on Einstein's bed layer concept (16) giving the lower limit at two grain diameters above the bed level $y = 0$. The next column gives the values of η_o corresponding to the upper edge of a hypothetical laminar sublayer. In column 3 η_o is the level at which the velocity is zero by extrapolation of the velocity profile, and in the last column η_o is the level at which the concentration equals the bed concentration by extrapolation of the concentration profile. The values of the dimensionless ratio, q_s / qc_{md}, listed in Table 13 (b), were calculated from z, $k \frac{\bar{u}}{u_*}$, and η_o, and may be compared with the measured ratio $\bar{C}/c_{md}$.

From an inspection of the table, it is clear that the agreement between the values is not perfect, but qualitatively quite good. When the value of the exponent z is small (less than 1) and hence q_s / qc_{md} is small, the agreement of all the values is excellent; for the theoretical calculation it appears that any one of these choices of the lower limit would be satisfactory.

However, for the higher z values (greater than 1.3 or 1.4), the calculated q_s / qc_{md} is significantly larger than the experimentally de-

Table 13

Integration for Suspended Sediment Discharge

$$\frac{q_s}{q\, c_{md}} = \frac{1}{d} \int_{y_o}^{d} \frac{c\, u}{c_{md}\, \bar{u}}\, dy$$

(a) Values of Lower Limit $\eta_o = \frac{y_o}{d}$

Run No.	(1) $\eta_o = \frac{2D}{d}$	(2) $\eta_o = \frac{11.6\nu}{u_{*d}}$	(3) $u(\eta_o) = 0$	(4) $c(\eta_o) = c_b$
2	.00335	.00405	.00082	.00325
3	.0039	.0036	.00255	.00145
4	.0040	.0050	.0018	.0014
6	.0049	.0051	.0018	.00325
7	.0039	.0032	.00084	.0044
21	.0025	.0038	.0024	.00029
29	.00205	.0035	.00235	.00033

(b) Values of the Integral for Various η_o

Run No.	z Profile slope	$k\frac{\bar{u}}{u_*}$	$\frac{q_s}{q\, c_{md}}$ = $\frac{\text{sus. sed. disch. conc.}}{\text{mid-depth conc.}}$ Calculated for η_o as above				$\bar{C}/c_{md}$ (meas. sed. disch. conc.) ÷ c_{md}
			(1)	(2)	(3)*	(4)	
2	1.58	6.1	19.5	18	25	19.5	-
3	1.36	5.0	6.65	6.75	6.75	6.65	9.5
4	1.20	5.3	4.45	4.3	4.7	4.7	4.55
6	1.49	5.3	10.2	10.3	12	11.5	8.45
7	1.78	6.1	43	49	55	39.5	23.5
21	0.76	5.0	1.69	1.70	1.65	1.57	1.62
29	0.83	5.0	1.88	1.86	1.85	1.81	1.82

*Values read directly from Fig. 2.

termined concentration ratio, $\bar{C}/c_{md}$. The discrepancy results from the fact that when z is large, a major part of the load travels very close to the bed where the extrapolated concentration and velocity profiles may not be accurate. None of the choices of the lower limit gives a good value of q_s/qc_{md} when this ratio is large.

It may be noted that the calculated values of q_s/qc_{md} given in the third column (for $u(\eta_o) = 0$) were read directly from Fig. 2, whereas all the others required a laborious calculation based on Eq. 1.53 and Einstein's charts (16) for the integrals I_1 and I_2. Until such time as further investigation of a wider range of conditions shows that some other particular choice of the lower limit is more reasonable, the writer suggests that the chart of Fig. 2 may be conveniently used. For low z values, q_s/qc_{md} by the chart is fully as good as any of the other calculated values, and when z becomes larger, none of the values are very accurate anyway.

It should be remembered that η_o for which $u(\eta_o) = 0$ gives the maximum value of $\int_{\eta_o}^{1} cu\, d\eta$, since the integrand is zero at this lower limit. In Table 13, the few instances where the value of q_s/qc_{md} in the third column is not the largest of the four are the result of slight inevitable errors of calculation.

A further example of the application of Fig. 2 has been included as Table 14 for the individual sieve-fraction concentration profiles for Run 29. (Cf. Fig. 43). The exponent z varies from 0.53 to 1.27, and the values obtained from Fig. 2 compare favorably with the measured ratio of the discharge concentration to the mid-depth concentration for each sieve fraction.

Table 14

Integration of Suspended Sediment Discharge for Individual Sieve Fractions for Run 29

$$k\frac{\bar{u}}{u_*} = 5.05$$

Tyler sieve retained on	150	170	200	250	Pan
z, exponent	1.27	1.03	0.93	0.76	0.53
q_s/qc_{md}, by Fig. 2	5.3	2.82	2.26	1.65	1.22
$\bar{C}/c_{md}$, measured	3.92	2.66	1.92	1.43	1.30

For all the present runs where the sand bed was smooth, the level $\eta_o = 2D/d$ (Table 13, col. 1) is higher than the level for which $u(\eta_o) = 0$ (col. 3), and thus it might be reasoned that the former would be a better choice. However, when the bed becomes covered with dunes, the friction factor increases and the situation is reversed. For example, assume the typical values $f_b = .08$ and $k = .30$; by the Darcy-Weisbach formula (or directly from Eq. 1.55),

$$k\frac{\bar{u}}{u_*} = k\sqrt{\frac{8}{f_b}} = 3.0$$

By Eq. 1.58,

$$\eta_o = e^{-3.0-1} = .019$$

Now η_o is considerably more than 2D/d for any of the runs, and the use of $\eta_o = 2D/d$ in a case like this would include negative values of the integrand in the load integral. Consequently, if it is found that the suspended load equation can be applied reasonably well to flows over dune-covered bed, then the use of η_o for which $u(\eta_o) = 0$ and the chart in Fig. 2 is recommended in place of the lower limit $\eta_o = 2D/d$.

(4) Summary. The main results of this section on velocity and suspended sediment distributions are as follows:

(a) The Prandtl-Karman logarithmic velocity law (Eq. 6.01) and the suspended load equation (Eq. 1.18) fit the measured centerline profiles fairly well, except near the surface.

(b) The von Karman constant k ranged from 0.375 to 0.390 for clear flow, and from 0.246 to 0.322 for flows carrying suspended load, with a smooth sand-covered bed.

(c) From the sediment concentration profiles, the ratio of the diffusion coefficient for sediment to the eddy viscosity, β, was found to be close to 1.0. Careful consideration was given to the effects of sorting and hindered settling on the mean fall velocity of the sediment.

(d) The integration formulas developed in Chap. I were found to be reasonably accurate for $z < 1$, and only qualitatively correct for $z > 1.4$. In view of its reasonable accuracy and its simplicity, the use of the integration chart of Fig. 2 seems justified.

CHAPTER VII

DISCUSSION OF RESULTS

In this chapter, the discussion of the principal results of the experiments will be extended with particular reference to the work of other investigators, and the relationships with other sediment transportation problems will be indicated. Chapter VI, "Experimental Results," already includes a comprehensive discussion and explanation of the mechanics of the streams observed in the laboratory flume.

A. BASIC SUSPENDED SEDIMENT TRANSPORTATION RELATIONSHIPS

The most important result of the experiments is that the velocity and sediment discharge of the laboratory stream could not be expressed as a function of the shear stress or any combination of depth, hydraulic radius, and slope. Because there are such large variations in roughness due to changes in the dune configuration, the standard fixed-bed open channel hydraulics is no longer adequate.

(1). Field Observations of Natural Streams. It is believed that the bed configuration of a natural stream, and hence the depth and velocity with which it flows, are greatly affected by the amount of sediment load the stream must carry. In Chapter VI, Sec. A (4c), it was pointed out that two of the experimental runs had identical discharge and slope, but two quite different depths and sediment discharges. Leopold (34) has reported several similar situations observed on large natural rivers.

For example, Leopold's Figure 28 gives the following information. When Hoover Dam was built on the Colorado River, the sediment

load below Hoover Dam was sharply reduced because of the desilting action of the reservoir behind the dam. At Yuma, Arizona, the annual suspended sediment discharge after the dam closure was only one tenth of what it had been previously. For a typical flow of 12,000 cfs, the depth jumped from about 5 to 9 feet, the velocity decreased from about 5 ft/sec to 3 ft/sec, and the Manning n increased from about .013 to .030 (which corresponds to a five-fold increase in the Darcy-Weisbach f.) The slope did not change, although the stream bed elevation dropped about 8 feet in the first 10 years after construction of the dam. Here is a case where for a given discharge and slope, the stream responded quite differently when the suspended load was reduced. Qualitatively the changes which have occurred are in perfect agreement with the conclusions based on the laboratory data plotted in Figs. 24 and 25 (Chap. VI, Sec. A(4).)

Leopold suggests that the increase in roughness was an effect of the decrease in suspended load. However, it is doubtful if the effect is direct; probably the bed of the stream has become covered with irregular dunes giving increased resistance to the flow. Actually, it is fortunate that the stream can adjust its bed, change the hydraulics of the stream, and thus greatly reduce its transporting capacity; for otherwise, the degradation at Yuma would undoubtedly have been much more severe.

Another example is given by Leopold (34) in his Figure 23, showing the changes in the hydraulic characteristics of the Colorado River at Grand Canyon, Arizona, occurring during the flood of December, 1940 to June, 1941. On the rising stage, the suspended load was very large, and the stream bed aggraded; on the falling stage the load was

much less, and the bed was scoured. For two approximately equal discharges, the following data may be read from two sets of points on his curves:

	Rising stage	Falling stage
Discharge, cfs	13,000	12,000
Suspended load discharge, tons per day	500,000	47,000
Depth, ft	9.5	16.5
Velocity, ft/sec	5	2.6
Gage height, ft	8	7.5
Stream bed elevation, ft	-1	-9
Width, ft	290	290

Presumably the slope of the river was approximately the same in both cases, as the stage was not changing rapidly. Assuming a constant slope, then, it may readily be shown from the Darcy-Weisbach formula (Eq. 5.21) that the f value is 6.5 times as large on the falling stage as on the rising stage; and on the falling stage, when the transportation rate is small, the shear is actually much larger.

A further examination of Leopold's Fig. 23 reveals that for a given depth, the discharge depends on the amount of load. For instance, when the depth is 16.5 ft, the discharge on the falling stage is 12,000 cfs, as indicated in the tabulation above, whereas it is 40,000 cfs, by interpolation, on the rising stage, when the sediment discharge is large.

In this second example also, the observed changes in the Colorado River during the passage of a flood agree qualitatively with

conclusions drawn from the experimental results in Chap. VI, Sec. A. The Colorado River is an especially good example for illustrating these effects because the sediment load, carried mostly in suspension, is large and variable; the bed is predominantly fine sand.

On another point, however, there is an apparent contradiction between Leopold's observations and the results of the flume experiments. From a massive collection of data on natural rivers, he concludes (34, p. 24) that "a wide river having a particular velocity is observed to carry a smaller suspended load than a narrow river having the same velocity and discharge." In other words, for a fixed velocity, the suspended load discharge concentration increases when the depth is increased. This is just the opposite of what has been concluded from the flume experiments where the sand size is held fixed. (See Chap. VI, Sec. A (3c).)

However, Leopold's statement applies to streams as found in their natural condition; it does not mean then that if any given stream were artificially made narrower and deeper that the sediment discharge would increase. Since Leopold compares a number of different streams, the size of the bed material is a variable which is not taken into account. Perhaps it might be construed on the basis of both Leopold's conclusion and the results of the flume experiments that the narrow streams carry more load only because they are typically cut in finer material than the wider streams; but when the bed material is the same, there is evidence in Chap. VI to show that a wide shallow stream would carry more load at a given velocity.

When the sediment size is essentially fixed, the writer's conclusion regarding the effect of depth on concentration is supported by field observations of Hill (35) published in 1926, for the Colorado River at Yuma. A curve given by him shows that as the depth increases from 10 feet to 30 feet, the average silt concentration decreases from about 1.1% to 0.4%, with the velocity remaining constant. Even though the friction factor did not change much for a corresponding laboratory situation, still it may be deduced from Hill's curves that the roughness must have increased to offset the increase of depth in order to keep the velocity of flow effectively constant.

The decrease of sediment concentrations associated with an increase in the temperature of the water is another effect which has been observed for a natural stream as well as in the laboratory flume. Lane, Carlson and Hanson (36) report that on the Colorado River below Parker Dam the suspended load discharge concentration is about 2.5 times as great in the winter when the water temperature is about 50°F, than it is in the summer, when the temperature is about 85°F. Since other conditions are nearly constant because of the regulation of the river by Hoover Dam, there is no doubt that this is mainly a temperature effect. This is more variation than was observed in the flume where, at 54°F the discharge concentration was only 1.4 times as much as it was at 80°F. The increase in the suspended load is believed to be mainly the result of increased fluid viscosity and the consequent reduction of settling velocities at lower temperatures. In the suspended load equation, the exponent z is lowered and the distribution of the suspended sediment is more nearly uniform; thus for a given concentration near the bed, more material will be carried overhead when z is smaller.

On the basis of field data of the kind presented above, this writer concludes that the qualitative relationships found between the transportation rate and the various other variables in the laboratory flume are also true for natural streams with movable beds of fine sand.

(2). Results of other Laboratory Experiments. The multiplicity of the relation between sediment discharge and depth and slope discovered in the present experiments has not been pointed out by any previous investigators, as far as this author is able to ascertain. Either the roughness effect causing this multiplicity has not been noticed or else it has not been nearly so pronounced, if existent at all, for some of the other sand sizes heretofore used in sediment transportation experiments.

With coarse material, the sediment moves primarily as bed load; although dunes have been observed, it is possible that the roughness may not undergo nearly such radical changes. In this case, the bed load transportation would be more or less directly related to the shear, as first suggested by Du Boys, and checked by countless investigators during the past several decades. (See Reference (1).) However, the large scatter of the points in all graphs of bed load transportation rates (which is usually ignored) is evidence that some other effect, such as roughness has not been taken account of. In bed load formulas, notably the Waterways Experiment Station (Vicksburg), the Manning roughness coefficient n has been included in the formula as an independent variable. Einstein's bed load theory (16) takes account of

variable channel roughness in a manner which will be described in detail in the next subsection.

In a very recent report describing laboratory flume experiments on the transportation of Missouri River sand, Straub (37) reaffirms the theory that the bed load discharge depends only on the bed shear. Since the median sieve diameter of his material is 0.18 mm most of this material moves as bed load at low rates of transportation, but at higher rates the suspended load must become appreciable.

Straub states as conclusion (1) "...the tractive force equation of the Du Boys type using the Straub values of the parameters ψ and τ_c agreed well with the experimental results ..."; in other words, the transportation rate is uniquely determined by the shear, regardless of the discharge. However, an inspection of the basic data reveals some large deviations from this conclusion; for example for Test No. III, with a tractive force (bed shear) of 0.0373 lb/ft^2, the transportation rate was 26.5 lb/hr per foot width, whereas for Test No. D - 1, with practically identical tractive force (0.0372 lb/ft^2), the measured transportation rate was 400 lb/hr per foot width, or about 15 times as much. There was a significant difference in the roughness, presumably resulting from changes in the bed configuration. It would appear, then, that an important effect has been neglected.

Since the report states that the load is mainly bed load, it appears that some of the same roughness effects found in the present experiments with finer sand may also be found to apply to streams carrying predominantly bed load.

Straub also concludes from experiments that the tractive force is practically constant for any given transportation rate. This may well be true, but that does not give any assurance that the shear τ_o will not also be the same for other transportation rates as well. It was noted in Chap. VI, Sec. A(2) that there is surprisingly little variation of the shear velocity ($\sqrt{\tau_o/\rho}$) for the experiments performed by this writer. For example, for Runs 26 and 29 (Table 7) the sediment discharges are 0.14 and 6.7 lb/min respectively, in spite of the fact that the values of the bed shear velocity, U_{*b}, are 0.101 and 0.103 ft/sec respectively.

The effect of temperature has also been observed by Straub (37) in his recent laboratory experiments described above. He concludes that the suspended load discharge is 2 to 4 times as much at 40°F as it is at 80°F for the same discharge. As expected, the distribution of suspended sediment in the vertical was more uniform at the low temperature, indicating a lower exponent z and reduced settling velocity.

It is doubtful whether changes in roughness play a very significant part in the mechanics of streams with beds of silt or clay, or the finely ground silica flour used by Hsia (14). It seems that dunes may never become very large in this material because it is so easily moved by flowing water even at very low velocities. For nine different flows over a bed covered with this extremely fine material, Hsia found that the Manning n varied only from .0119 to .0098, with one of the highest values being for the run with the smallest sediment discharge concentration (0.64%) and the smallest n for the run with the largest concentration (11.1%). He found that the transportation rate did have a direct relation to the bed shear, increasing when the shear increased.

Hsia described the bed with the terms "ripples", "rugged and irregular", and "smooth" successively as the velocity increased, although his roughness values indicate that the changes in the bed configuration were not nearly as significant as they were in the present experiments and did not result in two different discharges and transportation rates being possible for the same depth and slope.

Consequently, the results of the writer's investigations should not be construed as contradicting the results of these previous experiments on the transportation of extremely fine suspended load.

(3). Evaluation of Theories for Suspended Load Discharge. From the forgoing discussion and the experimental results presented in Chap. VI, Sec. A and B, it is evident that any workable theory must include a way in which to determine the stream roughness, for it is not adequate to assume that it is constant.

The bed interchange theory advanced by Lane and Kalinske (13) (and described briefly in Chap. I, Sec. C) is simplified by consideration of the pickup mechanism from a flat bed surface only, whereas it has been observed that the existence of dunes greatly facilitates the suspension of bed material as explained in Chap. VI, Sec. B(5). Thus, a more general theory is needed which takes account of the changing bed configuration and its effect on the pickup mechanism.

Einstein and Barbarossa (38) have made a significant attempt to analyze river channel roughness. A basic implication of their approach is that there is a definite stage-discharge relationship for a stream, and that there will be a particular roughness associated with each

point on the rating curve. This is equivalent to assuming that there is a unique relation between depth, slope and discharge, irrespective of the sediment load. There is now strong evidence both from the field and the laboratory, indicating that this is not a basically correct physical law. It may appear true for any particular natural stream, inasmuch as it is not easy to isolate the effects of the various variables until something unusual happens to the stream, such as being dammed.

The analysis of Einstein and Barbarossa appears consistent because their basic curve for finding the channel roughness is based on stream data calculated from a stage-discharge curve for each stream. Consequently, their analysis will probably be found adequate for applying to the natural streams from which it was derived, but of limited help in predicting what changes would occur in the stream whose equilibrium is drastically upset by manmade works.

Einstein's basic transportation theory (16) is based on this analysis of roughness. An examination of his theory will reveal that for a given bed material, there is only one equilibrium rate of flow and sediment transportation rate corresponding to each combination of bed hydraulic radius and slope. Experiments performed by this writer show that this is certainly not true for fine sand in the laboratory flume, and it is the opinion of the writer, with some substantiating evidence from Leopold (34), that this assumption is not always correct for natural rivers either. Therefore, it is believed that Einstein's basic approach to the determination of channel friction and suspended load discharge will have to be modified.

Blench (39) in his regime theory for canals has avoided consideration of basic quantities such as the shear. Since his analysis is purely empirical, it may be that he has arrived at some results which are just as reasonable as those of other investigators, who have assumed that transportation of suspended sediment depended on the shear. However, it is difficult to evaluate his work because he has not reported any of the basic data, but only some of the constants in various empirical equations.

In view of the complexity of suspended load phenomena, it is no wonder that there has been considerable difficulty in finding a reasonable theory for determination of the suspended load transporting capacity of streams flowing over movable beds. This author has no basic theory to propose, and has sought only to establish some basic facts with which to evaluate existing theory. At present, there is great need for more good information on exactly what happens in such streams; without it sediment transportation theory will remain a jumble of approximate theories based on a great variety of different assumptions.

B. DUNES AND CHANNEL ROUGHNESS.

(1) Field Observations on Large Natural Streams. As pointed out in Chap. VI, dunes play a very important role in the mechanics of streams flowing over a movable bed of fine sand because they cause extreme variations in the channel roughness.

The maximum size of the dunes is probably governed largely by the scale of the turbulence, and hence the size of the stream. Some observations of large natural rivers indicate that the dunes formed in beds of fine material are of approximately the same size relative to the depth as the dunes in the laboratory. Lane and Eden (40) who summarized some infor-

mation obtained in the lower Mississippi River, reported sand waves or dunes up to 20 ft high in 100 feet of depth at Vicksburg, and 13 ft high in 30 feet of depth at Bullerton. The ratio of depth to average dune height for the laboratory dunes is shown by Fig. 39 to be about 4 to 5 for the runs with the largest dunes, or substantially the same order of magnitude as these large Mississippi River sand waves. However, in the Mississippi River the wavelength-to-height ratio was commonly of the order of 50 to 100, whereas in the laboratory runs it was of the order of 10.

Some recent observations by the Missouri River Division of the Corps of Engineers (41) showed how rugged and irregular the bed of a river can be. In a sediment transportation study reach on the Missouri River near Omaha, periodic soundings of the sandy bottom have shown that the character of the bed surface is quite changeable, being smooth at some times or places and rugged and irregular, much like the bed of the flume, at other times or places. A number of examples show that the elevation of the bottom of the stream changes by as much as six or seven feet in distances of less than 50 feet in a flow 10 to 15 feet deep on the average.

Hence, although it was not possible to make a thorough analysis of large river dunes, the evidence indicates that the size of dunes in fine material is more or less proportional to the depth of flow. Since the dune size is relative, the Darcy-Weisbach f, which is a function of the relative roughness, should be used to characterize a dune configuration instead of the Manning n, which is directly related to the actual size of the roughness elements by Strickler's formula. If the channel roughness for the laboratory runs had been reported as the Manning n, the values obtained would not seem at all large compared with values obtained for natural riv-

ers; a bed surface covered with dunes 0.5 in. high in a flow 3 in. deep is very rough, whereas in a flow 5 ft deep, the same bed configuration would be considered relatively smooth.

(2) Dune Mechanisms. The mechanisms which cause the formation of dunes and sand waves have not been well understood. The observations of the author indicate that the turbulence generated in the wake of the dunes prevents the trough from filling up, and maintains a balance between the erosive power of the stream in the trough and over the crest, where the Bernoulli effect gives the stream locally increased transporting power.

von Karman (42) suggests that sand ripples in the desert arise from the stratification of the flow, with a dense, sediment-carrying layer of air close to the ground. He hypothesizes that the gravity force acting on this layer as it slides down the lee face accelerates the fluid sufficiently to give it the necessary erosive power to keep the trough scoured out. However, since observations of subaqueous dunes show that the turbulence generated by the ripples is a far more important factor, the writer believes that it is also an important factor for wind-blown ripples and small dunes.

Anderson (43) has proposed a theory relating subaqueous sand waves to water surface waves in open channels. One of his results is a relationship between the wavelength-depth ratio and the Froude number; as the Froude number increases, the wavelength increases also by his equation. As the Froude number F approached one in the flume, and standing waves developed, as shown in Fig. 38, it was observed that the low undulations in the bed are directly related to the surface waves. Langbein (44) has shown that F ≈ 1 is critical for the formation of these low symmetrical sand

waves, which are called antidunes when they get large enough to move upstream and cause the surface waves to break.

Nevertheless, the character of these sand waves is quite different from the dunes which are observed at lower velocities. To be sure, the water surface is ripply as the result of the dunes on the bed; but the dunes are not caused by the surface ripples. This is clearly demonstrated by the fact that similar dunes form in closed channels. They were observed, incidentally, in the transparent section of the return pipe in the flume circuit, and have also been reported by Ismail (6) and Craven (45), among others. Furthermore, at very low Froude numbers, such as F = 0.27 for Run 26, the water surface was observed to be practically smooth in spite of very large dunes on the bed.

Therefore, unless the Froude number is near the critical value one, it appears that the surface waves or ripples cannot be the cause of the sand dunes. However, the experimental data used by Anderson, and also the data obtained in the present investigations, do indicate that the wavelength does increase when the Froude number increases. However, two factors, an increase in velocity and a decrease in depth, cause the Froude number, as well as the transportation rate, to increase; hence, it still cannot be concluded that the gravity surface wave phenomena affect the bed configuration at low Froude numbers.

In relating the friction factor to the bed configuration, it is important to consider the wavelength as well as the height, as demonstrated by Fig. 39 in Chap. VI, Sec. B (4). Morris (46) has made a recent study of types of conduit roughnesses, and shows that it is not possible to characterize all different types of roughness by a single length, such as the commonly used Nikuradse sand roughness.

This writer strongly recommends the use of the Darcy-Weisbach friction factor, f, for open channels with a movable bed, instead of the Manning or Kutter n, or the Chezy C, because f, which is the only dimensionless coefficient, is essentially the same as for pipe flow and is directly related to skin friction coefficients in boundary layer theory.

C. TURBULENCE CHARACTERISTICS OF SEDIMENT-LADEN FLOWS

(1) von Karman Constant. In the present experiments it was found that the von Karman k was significantly reduced by the suspended load. (cf. Chap. VI, Sec. C (1)). The values ranged from 0.375 to 0.390 for five runs with clear flow, and from 0.246 to 0.322 for seven runs with sediment. Similar reduction of k values by the suspended fine sand was also found in the laboratory by Vanoni (5, 47) for open channel flow, and by Ismail (6) for closed channel flow. Both Vanoni's and Ismail's data show that k decreases as the concentration increases. This trend could not be verified conclusively by the writer because of the limited number of runs for which k was determined.

A recent study by the Missouri River Division of the U. S. Corps of Engineers (48) showed that the average k value, based on 291 determinations in the study reach of the Missouri River near Omaha, was about 0.26. Because of the difficulty of measuring the slope of the river accurately, and the variability of the suspended load, the values varied considerably, with 90 per cent of the values between 0.15 and 0.48. For the St. Clair River, a nonalluvial stream, the average of 100 k values was 0.43, with 90 per cent of the values in the range 0.31 to 0.59. Here again the slope measurement posed a difficulty, but the average of a large number of values should still be reliable.

Although it is generally agreed that the suspended sediment, at least in the sand sizes, causes a reduction in k, it is not clear exactly what the cause is. Vanoni (47) has ascribed the reduction to the damping of the turbulence by the suspended sediment, but Laursen (49) contends that the effect is due to increased roughness. While it may be true that large roughness elements will reduce the k value, certainly this cannot be taken as an explanation for the decrease of k while the friction factor f also decreases in Vanoni's experiments. The present investigation also demonstrates that a change in friction factor is not necessarily associated with a change in k; for example, from Table 9, page 185, it is seen that for Run C6 with clear flow, $k = 0.376$ and $f_b = .0185$, while for Run 29 with 0.10 mm sand, $k = 0.246$ and $f_b = .019$.

Kalinske and Hsia (14), in their study of the transportation of silica flour (median sedimentation diameter 0.011 mm), found that the k value was not noticeably reduced by the suspended sediment, although the k value varied from 0.32 to 0.44. However, since the rate of energy dissipation by a turbulent suspension of particles is approximately γw per unit volume (cf. Eq. 4.02), a small concentration of coarse material probably has as much effect on the turbulence characteristics as a large concentration of very fine material. Thus, the results of Kalinske and Hsia do not need to be taken as a contradiction of the finding by Vanoni (5) and others that k is reduced by fine sand in suspension.

(2) Turbulent Diffusion Coefficient for Sediment. The ratio $\beta = \epsilon_s / \epsilon_m$ has been found in this investigation to be close to 1.0. Ismail (6) found that β was 1.5 for the 0.10 mm sand and 1.3 for the 0.16 mm sand, but his values are in error for two reasons. First of all, for the

shear velocity on the centerline, he used the average value for the whole closed channel (10.5 in. wide by 3 in. high) instead of the maximum shear velocity u_{*m} which should occur at the center of the channel (cf. Chap. V, Sec. B). It is estimated, then, that the u_{*m} values used by Ismail were 8 per cent too small, resulting in k values also 8 per cent too small by Eq. 6.02. Eq. 6.03 shows that the calculated value of β will then be 18 per cent too large.

Secondly, he did not correct the settling velocity for the selective sorting in the flow and the hindered settling effect. On page 190 it has been pointed out that the neglect of both of these factors can result in a settling velocity 30 per cent too large for the 0.10 mm sand. Combining these two corrections (in Eq. 6.03), it is possible that his values of β for the 0.10 mm are fully 50 per cent too large, indicating that β should also be near 1.0 for his data.

Laursen (49) has stated that experiments at the Iowa Institute of Hydraulic Research have shown values of β greater than one, even when the sorting and concentration effects are taken into account. However, to the knowledge of this writer, no data have yet been published.

Since the turbulent diffusion of heat is analogous to the diffusion of particles and momentum, the eddy conductivity ϵ_c should be of the same order of magnitude as ϵ_s and ϵ_m in a turbulent shear flow. For uniform flow between parallel plates, Page, Schlinger, Breaux and Sage (50) found that the ratio ϵ_m / ϵ_c varied from 0.7 to 0.9; or, expressed inversely, to be analogous with β, ϵ_c / ϵ_m varies from 1.4 to 1.1. Although the agreement between the experimentally determined β (1.0) and their value of ϵ_c / ϵ_m is not exact, it is reasonable; since the actual diffusion mechanisms are not exactly the same anyway, there is no reason to expect ϵ_c to be identical to ϵ_s, as pointed out by Burgers (3).

CHAPTER VIII

SUMMARY OF CONCLUSIONS

Most of the conclusions which are summarized below are based on a comprehensive laboratory investigation of the characteristics of streams flowing over a movable bed of fine or very fine sand in a laboratory flume. Two sizes of sand were used as bed material, one with mean sedimentation diameter of 0.16 mm and the other with mean sedimentation diameter of 0.10 mm. The sediment load was carried almost entirely in suspension for all the runs with one or two exceptions.

The principal conclusions may be summarized as follows:

(1) For the laboratory flume it was found that neither the velocity nor the sediment discharge concentration can be expressed as a single-valued function of the bed shear stress, or any combination of depth and slope or bed hydraulic radius and slope. This finding is contrary to the almost universally-held assumption that the suspended sediment transporting capacity of a stream can be uniquely related to the geometry of the stream cross section, the slope of the channel, and the size of the bed material. All present theories, based on this erroneous assumption, were found to be inadequate.

(2) The difficulty in relating the velocity and concentration to the bed shear arises because the changeable bed configuration causes extremely large variations in the channel roughness. For the 0.10 mm sand the Darcy-Weisbach friction factor for the bed varied from .019 for a run for which the velocity was high and the sand bed was swept smooth, to .13 for a run for which the velocity was low and the bed became covered with a

stable pattern of large irregular dunes.

(3) When either mean velocity and depth, or water discharge and total sediment discharge are used as the pair of independent variables for the flume data, all other quantities are uniquely determined by what appears to be an orderly and logical relationship between all the various variables.

(4) From the data obtained in the laboratory flume with 0.10 mm and 0.16 mm sand, the following qualitative relationships were found:

(a) When the mean velocity of the stream U increases, with no change in the depth, d, the bed friction factor f_b decreases, and the total sediment discharge concentration $\bar{C}$ generally increases.

(b) When d is increased, holding U constant, $\bar{C}$ decreases slightly, and f_b does not change appreciably in the range of conditions covered. Field evidence supports this conclusion.

(c) For a given d and U, f_b seems to be numerically the same for both sand sizes used. The bed configurations also appeared the same.

(d) For a given d and U, the discharge concentration $\bar{C}$ for the 0.10 mm sand was 2 to 4 times as large as $\bar{C}$ for the 0.16 mm sand.

(e) If the water discharge Q is to be increased without changing the total sediment discharge G, then an increase in d is required, although this increase is relatively less than in Q.

(f) For constant Q, an increase in G requires a decrease in d. Field observations indicate that this relationship is also true for some large rivers.

(g) For a given slope and discharge, it was found that two depths of flow were possible. When the sediment discharge is small, the depth is large, the velocity is small, and the bed is rough; and when the sediment

discharge is large, the depth is small and the bed of the laboratory channel is smooth. Field data show that this conclusion applies to natural streams as well.

(h) For a given Q, the largest bed friction factors are associated with the lowest transportation rates G.

(i) A decrease in temperature causes an increase in the suspended load discharge, other things being equal. This effect has also been observed in other laboratory investigations and in the field for streams flowing over a bed of fine sand.

(5) At the lowest velocities and transportation rates, the dunes were the most irregular, having the shortest wavelengths and the sharpest crests. At somewhat larger velocities the alignment of the dunes improved and the crests became more rounded; the friction factor was reduced. A further increase in velocity induced the formation of long solitary sand waves 8 to 10 ft long, which travel perpetually through the system. Meanders in the bed were also observed for some of the runs. Finally, at the highest velocities tested, the sand bed became smooth and uniform.

(6) Froude numbers of about 0.7 were critical for the formation of standing waves on the water surface in the flume.

(7) The turbulence generated in the wake of a dune is largely responsible for throwing bed material into suspension at low transportation rates and prevents the trough from filling up.

(8) The dunes move downstream at speeds of the order of 1/5000 to 1/500 of the mean stream velocity. The dune velocity was somewhat higher for the runs with the 0.16 mm sand than for the runs with the 0.10 mm sand, in spite of the fact that the transportation rates were larger for the lat-

ter. This observation can be explained in terms of the entraining action of the lee-side eddies.

(9) The von Karman logarithmic velocity law was found to fit observed centerline velocity distributions very well in most cases. For clear flow the von Karman constant k ranged from 0.375 to 0.390, and for sediment-laden flow from 0.246 to 0.322.

(10) From theoretical considerations, it was shown that the suspended load distribution theory can be extended to suspensions of nonuniform particles. If the suspended sediment distribution is analyzed by sieve fractions in a standard $\sqrt{2}$ or a $\sqrt[4]{2}$ series, the simple suspended load equation, based on a uniform settling velocity, can be used with good approximation.

(11) The suspended load equation was found to fit the measured suspended sediment distributions on the centerline of the flume for the runs with smooth bed, for at least the lower half of the flow. From these distributions it was calculated that the ratio of the diffusion coefficient for sediment to the eddy viscosity was close to 1.0. Careful consideration was given to the effect of hindered settling and the reduction of the mean size in the suspension by selective sorting.

(12) A simple method for integrating the product of the velocity and the concentration over the depth to obtain the suspended load discharge was developed from the logarithmic velocity distribution and the suspended load equation. (See Fig. 2). From the laboratory runs it has been shown that the method is fairly accurate for values of the exponent z in the suspended load equation less than one, and only qualitatively correct for z values greater than 1.4.

(13) A method for finding the boundary shear distribution for clear flow in a channel of uniform roughness from measured velocity distribution has been outlined, and applied to two of the experimental runs. The maximum shear was found at the center of the bed and the minimum shear in the corners.

REFERENCES

1. Rouse, Hunter. Engineering Hydraulics. Proc. Fourth Hydr. Conf. Iowa Inst. of Hydr. Research. June 12-15, 1949. Chap. XII. pp. 769-857.

2. "Report of the Subcommittee on Sediment Terminology". Trans. Amer. Geophys. Un. Vol. 28, No. 6, 1947, pp. 936-938.

3. Burgers, J. M. "On Turbulent Fluid Motion". Mimeographed Notes. Calif. Inst. of Tech. 1951.

4. Taylor, G. I. "Diffusion by Continuous Movements". Proc. London Math. Soc. Series 2, Vol. 20. 1921-22, p. 196-211.

5. Vanoni, Vito A. "Transportation of Suspended Sediment by Water". Trans. Amer. Soc. Civ. Engrs. Vol. 111, 1946, pp. 67-133.

6. Ismail, Hassan. "Turbulent Transfer Mechanism and Suspended Sediment in Closed Channels". Trans. Am. Soc. Civ. Engrs. Vol. 117, 1952, pp. 409-446.

7. Carstens, M. R. "Accelerated Motion of a Spherical Particle". Trans. Am. Geophys. Un. Vol. 33, No. 5, Part 1. Oct. 1952, pp. 713-721.

8. Brooks, Norman H. Discussion of Reference 7. Trans. Am. Geophys. Un. Vol. 34, No. 6, December 1953, pp. 947-950.

9. von Karman, Th. "Turbulence and Skin Friction". Jour. Aero. Sci. Vol. No. 1. Jan. 1934. pp. 1-20.

10. Vanoni, Vito A. "Velocity Distribution in Open Channels". Civil Engineering. Vol. 11, No. 6, June 1941, pp. 356-357.

11. Rouse, Hunter. "Modern Conceptions of the Mechanics of Fluid Turbulence." Trans. Am. Soc. Civ. Engrs. Vol. 102, 1937, p. 534.

12. Lane, E. W. and Kalinske, A. A. "Engineering Calculations of Suspended Load". Trans. Am. Geophys. Un. Vol. 22, 1941, pp. 603-607.

13. Lane, E. W. and Kalinske, A. A. "The Relation of Suspended to Bed Material in Rivers". Trans. Am. Geophys. Un. Part IV, Vol. 20, 1939, pp. 637-641.

14. Kalinske, A. A. and Hsia, C. H. "Study of Transportation of Fine Sediments by Flowing Water". Univ. of Iowa Studies in Engrg. Bull. No. 29, 1945.

15. Pien, C. L. "Investigation of Turbulence and Suspended Material Transportation in Open Channels". Doctoral dissertation. Univ. of Iowa, 1941.

16. Einstein, H. A. "The Bed-Load Function for Sediment Transportation in Open Channels." U. S. Dept. of Agr., Soil Conservation Service. Tech. Bull. No. 1026, September 1950.

17. Rouse, Hunter. "Elementary Mechanics of Fluids". J. Wiley & Sons, New York. 1946.

18. Dryden, H. L. and Schubauer, G. B. "Use of Damping Screens for the Reduction of Wind Tunnel Turbulence". Jour. Aero. Sc. Vol. 14, No. 4, April 1947, pp. 221-228.

19. Schiller, L. "Handbuch der Experimentalphysik". Akademische Verlagsgesellshaft, M.B.H., Leipzig, 1931. Vol. 4, part 1. p. 505.

20. McNown, John, and Malaika, Jamil. "Effects of Particle Shape on Settling Velocity at Low Reynolds Numbers." Trans. Am. Geophys. Union. Vol. 31 No. 1, Feb. 1950, pp. 74-82.

21. McNown, John, and Lin, Pin-Nam. "Sediment Concentration and Fall Velocity." Proc. 2nd Midwest Conf. on Fluid Mechanics. Ohio State Univ. 1952, p. 401-411.

22. Vanoni, Vito A. "Experiments on the Transportation of Suspended Sediment by Water". Thesis presented to the Calif. Inst. of Tech. Pasadena, Calif. in 1940, in partial fulfillment of the requirements for the degree of Doctor of Philosophy.

23. Otto, Geo. H. "A Modified Logarithmic Probability Graph for the Interpretation of Mechanical Analysis of Sediments". Jour. of Sedimentary Petrology. Vol. 9, No. 2, 1939. pp. 62-76.

24. White, C.M. "The Equilibrium of Grains on the Bed of a Stream". Proc. Royal Soc. of London, Vol. 174, Series A, No. 958, Feb. 1940, pp. 322-338.

25. Lane, E.W. "Progress Report on Studies on the Design of Stable Channels by the Bureau of Reclamation". Proc. Am. Soc. Civ. Engrs. Vol. 79, Separate No. 280, September 1953.

26. "Sedimentation Studies in Open Channels — Boundary Shear and Velocity Distribution by the Membrane Analogy, Analytic, and Finite-Difference Methods". U. S. Bureau of Reclamation. Structural Laboratory Report No. SP-34, August 5, 1952. Denver, Colorado.

27. von Karman, Th. "Some Aspects of the Turbulence Problem". Proc. Fourth Intern. Congr. for Appl. Mech., Cambridge, England, 1934, pp. 54-91.

28. Keulegan, Garbis, H. "Laws of Turbulent Flow in Open Channels". Research paper 1151. Jour. of Research, National Bureau of Standards, Vol. 21, 1938, pp. 707-741.

29. Liepmann, H. W., and Dhawan, S. "Direct Measurement of Local Skin Friction in Low-Speed and High-Speed Flow". Proc. First U. S. National Congress for Appl. Mech. p. 869. 1952.

30. Rouse, Hunter. "Elementary Mechanics of Fluids". J. Wiley & Sons, New York. 1946.

31. Einstein, H. A. "Formulas for the Transportation of Bed Load". Trans. Am. Soc. Civ. Engrs. Vol. 107, 1942. pp. 561-577.

32. Johnson, J. W. "The Importance of Side-Wall Friction in Bed-Load Investigations." Civil Engineering, Vol. 12, No. 6, June 1942, pp. 329-331.

33. Haywood, O. G. "Flume Experiments on the Transportation by Water of Sands and Light-Weight Materials". Submitted in 1940 to the Massachusetts Inst. of Tech. at Cambridge, Mass. in partial fulfillment of the requirements for the Degree of Doctor of Science.

34. Leopold, Luna B. and Maddock, Thomas, Jr. "The Hydraulic Geometry of Stream Channels and Some Physiographic Implications." Geological Survey Professional Paper 252. U. S. Dept. of the Interior. 1953. 57 pp.

35. Hill, R. A. Discussion of "Permissible Canal Velocities", by S. Fortier and F. C. Scobey. Trans. Am. Soc. Civ. Engrs. Vol. 89, 1926, pp. 961-964.

36. Lane, E. W., Carlson, E.J. and Hanson, O.S. "Low Temperature Increases Sediment Transportation in Colorado River". Civil Engineering. Vol. 19, No. 9, Sept. 1949, pp. 45-46.

37. Straub, Lorenz G. "Terminal Report on Transportation Characteristics of Missouri River Sediment". Univ. of Minn. St. Anthony Falls Hydraulic Lab. in cooperation with The Missouri River Division, Corps of Engrs. U. S. Army. M.R.D. Sediment Series No. 4, April 1954.

38. Einstein, Hans A. and Barbarossa, Nicholas L. "River Channel Roughness". Trans. Am. Soc. Civ. Engrs. Vol. 117, 1952, pp. 1121-1146.

39. Blench, Thomas. "Regime Theory for Self-Formed Sediment-Bearing Channels". Trans. Am. Soc. Civ. Engrs. Vol. 117, 1952, pp. 383-408.

40. Lane, E. W. and Eden, E. W. "Sand Waves in the Lower Mississippi River". Western Soc. of Engineering. Vol. 45 No. 6, December 1940, pp. 281-291.

41. Missouri River Division, U.S. Corps of Engineers. "Sediment Transportation Characteristics Study". First Interim Report, Appendix D, Topographic Maps, Omaha, Neb., Feb. 1952.

42. von Karman, Th. "Sand Ripples in the Desert". Technion Yearbook. 1947.

43. Anderson, Alvin G. "The Characteristics of Sediment Waves Formed by Flow in Open Channels." Proc. 3rd Midwestern Conf. on Fluid Mechanics, 1953. pp. 379-395.

44. Langbein, W. B. "Hydraulic Criteria for Sand-Waves". Trans. A.G.U. Part II, 1942. pp. 615-621.

45. Craven, John P. "The Transportation of Sand in Pipes - I. Full-Pipe Flow". Proc. Fifth Hydraulics Conf. State Univ. of Iowa, Studies in Engrg. Bulletin 34. No. 426, pp. 67-76. 1952.

46. Morris, Henry N. "A New Concept of Flow in Rough Conduits". Proc. Am. Soc. Civ. Engrs. Vol. 80. Separate No. 390. Jan. 1954.

47. Vanoni, Vito A. "Some Effects of Suspended Sediment on Flow Characteristics". Proc. Fifth Hydraulics Conf. State Univ. of Iowa. Studies in Engineering, Bulletin 34 No. 420, pp. 137-158.1952.

48. Missouri River Division, U. S. Corps of Engineers. "Notes on the Turbulence Function k". Omaha, Nebr. November 1953.

49. Laursen, E. M. Discussion of Reference 47. Proc. Fifth Hydraulics Conf. State Univ. of Iowa. Studies in Engineering, Bulletin 34, No. 420, pp. 155-6. 1952.

50. Page, F., Jr., Schlinger, W.G., Breaux, D.K., and Sage, B.H. "Temperature Gradients in Turbulent Gas Streams - Point Values of Eddy Conductivity and Viscosity in Uniform Flow between Parallel Plates". Industrial and Engineering Chemistry. Vol. 44, No. 2. Feb. 1952, pp. 424-430.

APPENDIX A

SUMMARY OF NOTATION

The following summary omits, for simplicity, definitions of some letters of secondary importance which appear only a few times in a single section. A typical example of such a quantity is A_2, cross sectional area of the Venturi meter.

The page numbers listed refer to the page on which each symbol is first used or defined.

		Page
a	= distance from stream bed to some arbitrary reference level	10
A	= cross sectional area of the stream	97
A_b	= part of cross sectional area assigned to the bed	113
A_w	= part of cross sectional area assigned to the walls	113
b	= width of a rectangular channel	110
B	= constant defined by Eq. 1.31	14
c	= total concentration of suspended sediment, (time average at a point, expressed in dry weight per unit volume)	6
c_a	= concentration at $y = a$	10
c_b	= concentration of sediment in the bed (dry weight per unit volume)	20
c_{md}	= concentration at mid-depth ($y = d/2$)	10
$\bar{C}$	= G/Q = sediment discharge concentration	128
d	= depth of flow	8
D	= grain size	20
D_g	= geometric mean grain size	92
D_s	= mean sedimentation diameter for a mixture	90
D_{s_i}	= mean sedimentation diameter for a sieve fraction	88

Page

f	= Darcy-Weisbach friction factor	
	= $8\,(u_*/\bar{u})^2$ for two-dimensional flow	27
	= $8\,(U_*/U)^2$ for three-dimensional flow	111
f_b	= $8\,(U_{*b}/U_b)^2$ = bed friction factor	116
f_w	= $8\,(U_{*w}/U_w)^2$ = wall friction factor	117
F	= $U/\sqrt{gd}$ = Froude number	77
g	= acceleration due to gravity	
G	= total sediment discharge or transportation rate	128
h	= representative dune height	166
H	= $(d - y)/y$	9
H_a	= $(d - a)/a$	14
$I_1(z,\eta_o)$	= integral defined by Eq. 1.51	26
$I_2(z,\eta_o)$	= integral defined by Eq. 1.52	26
$J_1(z,\eta_o)$	= integral defined by Eq. 1.48	25
$J_2(z,\eta_o)$	= integral defined by Eq. 1.49	26
k	= von Karman universal constant	9
m	= $du/d(\log_{10}y)$ = slope of velocity profile	101
n	= roughness coefficient in Manning flow equation	112
p	= wetted perimeter of the stream	97
p_b	= wetted perimeter of bed section	113
p_w	= wetted perimeter of wall sections	113
q	= $\bar{u}d$ = discharge per unit width	25
q_s	= suspended sediment discharge (or transportation rate) per unit width	23
Q	= total discharge	52

		Page
r	= A/p = hydraulic radius	97
r_b	= A_b/p_b = bed hydraulic radius	113
r_w	= A_w/p_w = wall hydraulic radius	113
R	= $4U\,r/\nu$ = Reynolds number for the channel	116
R_w	= $4U_w\,r_w/\nu$ = Reynolds number for wall sections	117
S	= slope of the energy line for the stream	76
T	= water temperature	
u	= stream velocity (time average at a point)	7
u_{max}	= maximum velocity	9
$\bar{u}$	= average profile velocity (i.e., average in a vertical plane parallel to direction of flow; in Chap.V and VI at the centerline)	24
U	= mean velocity in the channel	76
U_b	= mean velocity in bed section	115
U_w	= mean velocity in wall sections	115
u_*	= $\sqrt{\tau_o/\rho}$ = shear or friction velocity	9
u_{*m}	= maximum shear velocity (center of bed)	109,123
U_*	= $\sqrt{\bar{\tau}_o/\rho}$ = $\sqrt{grS}$ = shear velocity for whole channel	101
U_{*b}	= $\sqrt{\bar{\tau}_o/\rho}$ = $\sqrt{gr_bS}$ = shear velocity for bed alone	109
U_{*w}	= $\sqrt{\bar{\tau}_w/\rho}$ = $\sqrt{gr_wS}$ = shear velocity for wall alone	110
w	= settling velocity of sand particles (weighted arith. mean, Chap. IV, VI)	90
w_i	= mean settling velocity for a sieve fraction	90
$W(y)$	= weighted arithmetic mean of w at level y (Chap.I only)	12
W_a	= $W(a)$	13
y	= distance from the bed of the stream	6
y_o	= lower limit of integration for suspended sediment discharge	25

		Page
$z = \frac{w}{\beta k u_*}$	= exponent in suspended load equation	9
$Z(y) = \frac{W(y)}{\beta k u_*}$		12
Z_a	= $Z(a)$	16
β	= ϵ_s / ϵ_m	7
γ	= unit weight of water = ρg	97
ϵ_m	= eddy viscosity (or turbulent diffusion coefficient for momentum)	7
ϵ_s	= turbulent diffusion coefficient for sand particles	6
$\bar{\epsilon}_s$	= average value of ϵ_s over the depth	19
η	= y/d	25
η_o	= y_o / d	25
λ	= average dune wavelength	167
ν	= kinematic viscosity of fluid (water)	20
ρ	= mass density of fluid (in most cases water)	7
σ	= standard deviation of w	13
σ_g	= geometric standard deviation of the grain size	94
τ	= shear stress in the fluid	7
τ_o	= shear stress at the boundary	8
$\bar{\tau}_o$	= average shear stress on the entire boundary	97
$\bar{\tau}_b$	= average shear stress on the bed	108
$\bar{\tau}_w$	= average shear stress on the walls	108
$\Phi(w,y)$	= frequency distribution for settling velocity at level y	11

APPENDIX B

Discussion* of

"Accelerated Motion of a Spherical Particle" by M.R. Carstens (7)

The notation used in the attached reprint follows the notation of Carstens, and differs in some respects from the notation used in the rest of this thesis. The definitions of the symbols used here are as follows:

A = damping coefficient (Carstens)

a = $a(t)$ = displacement of a fluid parcel, taken as a known function.

a_o = amplitude of motion of fluid parcel

$\dot{a} = \frac{da}{dt}$, $\ddot{a} = \frac{d^2a}{dt^2}$ and $\dddot{a} = \frac{d^3a}{dt^3}$.

d = diameter of spherical particle

G = $G(t)$ = forcing function defined by Eq. 24.

g = acceleration due to gravity

K = constant defined by Eq. 26

k = apparent mass factor

M_o = mass of sphere

M = mass of displaced fluid

s = constant defined by Eq. 25

t = time

t_1 = dummy time variable

x = $x(t)$ = particle displacement

x_o = amplitude of particle motion

---

*Reprinted from Trans. Am. Geophys. Union. Vol. 34, No. 6, Dec. 1953, pp. 947-949.

$\dot{x} = \frac{dx}{dt}$, $\ddot{x} = \frac{d^2x}{dt^2}$, $\dddot{x} = \frac{d^3x}{dt^3}$

w = settling velocity of sphere in still fluid

α = phase angle

a_0, a_1, a_2, a_3 = constants defined by Eq. 26

$\beta = \epsilon_s / \epsilon_m$

γ = constant defined by Eq. 25

ϵ_m = turbulent diffusion coefficient for momentum, (or kinematic eddy viscosity)

ϵ_o = turbulent diffusion coefficient for fluid particles

ϵ_s = turbulent diffusion coefficient for solid particles

η = dummy variable in Eq. 27

μ = dynamic viscosity of fluid

ρ = mass density of sphere

σ = constant defined by Eq. 26

ω = frequency

DISCUSSION OF

"ACCELERATED MOTION OF A SPHERICAL PARTICLE"
by M. R. CARSTENS

[Trans., v. 33, pp. 713-721, 1952]

Norman H. Brooks (Department of Civil Engineering, California Institute of Technology, Pasadena, Calif.)--In considering the accelerated motion of spheres in a viscous fluid, the author has restricted himself to consideration of only simple harmonic motions of the fluid field and the sphere. The author's equation of motion (Eq. 11) for a suspended sphere is true only when the solution yields a relative displacement (x - a) which is sinusoidal in time. Otherwise, the apparent mass factor k, and the damping coefficient A have no meaning, because they are both based on the Stokes solution for an oscillating sphere given in LAMB [1945, see References at end of published paper, p. 721]. Both k and A are functions of the circular frequency ω as they are defined by (1), (2), and (3).

As an example of the inadequacy of (11) for general purposes, one may consider the effect of adding the gravity force $-(M_o - M)g$ to the right side of (11). Using $a = a_o \sin\omega t$, the solution will be just as given in (12) except for an added term; thus we get

$$x = x_o \sin(\omega t + \alpha) - [(M_o - M)g/A]\, t$$

The superposed settling velocity appears to be $(M_o - M)g/A$ where A depends on ω.

This is clearly incorrect, because the settling velocity has a constant value w which is independent of the frequency ω. This follows directly from the fact that the Navier-Stokes equations are linear in pressure and velocity when all velocity product terms (that is, convective acceleration terms) are neglected, according to the Stokes approximation. Thus the solution $x_1 = -wt$ can be superimposed on any other solution (which the author correctly did subsequently in deriving ϵ_s).

TCHEN [1947, chap. 4 and 5] has obtained a general equation of motion which is not based upon

any presuppositions about the solution and might be given in place of (11). Tchen started with the integro-differential equation for the rectilinear accelerated motion of a sphere derived by BASSETT [1888, p. 291] and BOUSSINESQ [1903, p. 238]. Again all velocity product terms were neglected. In the author's notation this equation, including the gravity term, may be written as

$$(M_0 + M/2)\,\ddot{x} = -3\pi\mu d\left[\dot{x} + (d/2\sqrt{\pi\nu})\int_{t_0}^{t} dt_1\, \ddot{x}(t_1)/\sqrt{t-t_1}\right] - (M_0 - M)\,g \quad \ldots\ldots\ldots (21)$$

where the entire system is at rest until the instant $t = t_0$. For convenience t_0 may be taken as $-\infty$. From this, Tchen derived the equation of motion for a small sphere in a moving fluid

$$(M_0 + M/2)\,\ddot{x} = (3/2)\,M\ddot{a} - 3\pi\mu d\left\{\dot{x} - \dot{a} + (d/2\sqrt{\pi\nu})\int_{-\infty}^{t} dt_1\,[\ddot{x}(t_1) - \ddot{a}(t_1)]/\sqrt{t-t_1}\right\} - (M_0 - M)\,g \quad \ldots\ldots (22)$$

He solved this equation for the case of simple harmonic fluid motion and obtained the same result as the author's (15).

By skillful manipulations which eliminated the integral term involving $\ddot{x}$, Tchen arrived at the following linear second-order differential equation for $\dot{x}$

$$\dddot{x} + 2K\ddot{x} + (K^2 + \sigma^2)\,\dot{x} = G(t) \quad \ldots\ldots\ldots\ldots\ldots\ldots (23)$$

where

$$G(t) = -\alpha_0 w + \alpha_0 \dot{a}(t) + \alpha_1 \ddot{a}(t) + \alpha_2 \dddot{a}(t) - \alpha_3 \int_0^{\infty} dt_1\, \dddot{a}(t - t_1)/\sqrt{t_1} \quad \ldots\ldots (24)$$

The various coefficients in (23) and (24) may be conveniently defined in terms of the two constants

$$\gamma = 12\,\nu/d^2, \quad s = 3\rho/(2\rho_s + \rho) \quad \ldots\ldots\ldots\ldots\ldots\ldots (25)$$

and are as follows

$$\left.\begin{aligned} \alpha_0 &= \gamma^2 s^2 \\ \alpha_1 &= \gamma s\,(1 - 2s) \\ \alpha_2 &= s \\ \alpha_3 &= (\sqrt{3\gamma/\pi})\,s\,(s - 1) \\ K &= \gamma s\,(1 - 3s/2) \\ \sigma^2 &= \gamma^2 s^2 - K^2 = 3\gamma^2 s^3\,(1 - 3s/4) \end{aligned}\right\} \quad \ldots\ldots\ldots\ldots (26)$$

Also w, the Stokes settling velocity, is given by the familiar formula

$$w = g\,(\rho_s - \rho)\,d^2/18\mu$$

The general integral solution of (23) is

$$\dot{x}(t) = (1/\sigma)\int_0^{\infty} d\eta\, e^{-K\eta} \sin\sigma\eta\, G(t - \eta) \quad \ldots\ldots\ldots\ldots\ldots (27)$$

Equation (27) will give the correct particle velocity $\dot{x}(t)$ for any arbitrary fluid velocity $\dot{a}(t)$, provided only that the convective acceleration terms are small, as was originally assumed.

In the derivation of (19) for ϵ_m, the author implies that ϵ_m is identical with the coefficient of diffusion of fluid particles (let this be called ϵ_0). Fluid particles or molecules in solution are transported bodily in a fluid element, and, except for a relatively insignificant amount of molecular diffusion, they are carried with the fluid element wherever it goes. But, on the other hand, momentum

is continually being transferred from one fluid element to its neighbors by pressure differentials and viscous shear. Thus the momentum carried by a parcel of fluid may be expected to vary continuously during its excursion from one point to another. TAYLOR [1932, p. 685] pointed out the variability of momentum due to pressure fluctuations as a weakness of Prandtl's momentum transfer theory when he advocated his vorticity transfer theory to obviate this difficulty. BURGERS [1951, chap. 5] considers the viscous transfer of momentum between adjacent elements more important than the pressure forces in his derivation of the diffusion coefficient for momentum.

Because of these two special factors impeding momentum transfer, this writer believes that it is quite reasonable to presume that the diffusion coefficient for momentum (ϵ_m) is less than the diffusion coefficient for particles of the fluid itself (ϵ_0).

Consequently, the author would be nearer to the truth to give (20) as

$$\epsilon_s/\epsilon_0 = (x_0/a)^2 \quad \ldots\ldots\ldots\ldots\ldots\ldots\ldots\ldots (28)$$

Thus, for sediment in water, $\epsilon_s/\epsilon_0 < 1$ (since $x_0 < a_0$ for $\rho_s > \rho$), but since $\epsilon_m/\epsilon_0 < 1$ also, it is not all clear when $\beta = \epsilon_s/\epsilon_m$ is greater than or less than one.

But, whether or not (19) should give the diffusion coefficient for momentum (ϵ_m) or fluid particles (ϵ_0), there is some question about the validity of the way in which the author has tried to derive diffusion coefficients from the equation of motion of a suspended particle. The argument the author follows on page 719 is based on the concept of a discontinuous mixing process with the use of some sort of mixing length, and with the assumption that the fluid elements carry the same concentration of sediment as the mean concentration at the starting point. This Prandtl type of approach is often satisfactory for engineering purposes where the interest is in some average bulk property like concentration of sediment. However, it is hardly a good framework in which to utilize detailed information about the behavior of individual particles. At best, one can talk only of a loosely defined "average behavior" at some representative frequency of a simplified type of motion; and, after all, if a body of fluid simply oscillates up and down with $a = a_0 \sin\omega t$, so that the motion of particles in the fluid is $x = x_0 \sin(\omega t + \alpha) - wt$, there is certainly no turbulent diffusion. Diffusion occurs only because the turbulent velocities of a fluid element are not periodic in any simple sense.

To make use of the equations of motions of a small particle in suspension (23) to (26), it seems more reasonable to consider diffusion as a continuous process, expressing the diffusion coefficients in terms of integrals of Lagrangian correlations. TCHEN [1947, chap. 4 and 5] used this approach and with (27) calculated the integral of the Lagrangian correlation for the sphere velocity in terms of the same integral for the velocity of the fluid surrounding the particle. Neglecting the effect of gravity, the integrals are equal for any general type of turbulent motion.

Tchen's results are reported in detail by BURGERS [1951, chap. 5] who carries the development still further. Results of theirs which differ from the author's are summarized very briefly here. (1) $\epsilon_s \doteq \epsilon_0$ if the particles generally stay well within their respective fluid elements so that the relative motion can be adequately described by (27). This is true regardless of the type or frequency of the fluid oscillations. This assumption is probably quite accurate for silt and clay in suspension. (2) Actually $\epsilon_s < \epsilon_0$ only by virtue of the fact that sediment particles slip from one fluid element into another in the course of their motion. The amount of this slippage and the ratio ϵ_s/ϵ_0 depends on the nature of the motion and size of the fluid elements carrying the sediment; this information cannot be deduced from the equation of motion which simply relates x to a. (3) $\epsilon_m < \epsilon_0$, because of the role of viscous forces transferring momentum between fluid elements. (4) $\epsilon_s > \epsilon_m$ ($\beta > 1$) and $\epsilon_s < \epsilon_m$ ($\beta < 1$) are both physically plausible cases. For very fine material it is reasonable to expect $\epsilon_s > \epsilon_m$, because $\epsilon_s \doteq \epsilon_0$.

Hence this writer is unable to accept (20) which implies that β is always less than unity for particles heavier than the fluid.

References

BASSETT, A. B., A treatise on hydrodynamics, Deighton, Bell and Co., Cambridge, v. 2, 1888.

BOUSSINESQ, J., Theorie analytique de la Chaleur, Gauthier-Villars, Paris, v. 2, 1903.

BURGERS, J. M., Lecture notes on turbulent fluid motion, California Institute of Technology, Pasadena, Calif., 1951.

TAYLOR, G. I., The transport of vorticity and heat through fluids in turbulent motion, Proc. R. Soc., A, v. 135, 1932.

TCHEN, CHAN-MOU, Mean value and correlation problems connected with the motion of small particles suspended in a turbulent fluid, Med. 51, Lab. Aero Hydrodynam., Technische Hogeschool, Delft, 1947.

Erratum: In Eq. 28, a should read a_0.

APPENDIX C

MODIFICATION OF SIDE-WALL CORRECTION EQUATIONS FOR DIFFERENT BED AND WALL SECTION VELOCITIES

The derivation of the side-wall correction equations given below parallels the derivation in Chap. V, Sec. C (2), pages 116-120, with the addition of the parameter U_w/U, the ratio of the wall section velocity to the over-all average velocity. The notation used here is exactly the same as that given on page 116. The assumptions are the same except that U_w/U is assumed to be some known value not equal to one. Starting at the bottom of page 117, the more general derivation would be as follows:

For smooth walls, f_w will be a function only of the Reynolds number for the wall,

$$R_w = \frac{4\, U_w r_w}{\nu}$$

Inasmuch as r_w is still unknown, R_w will be rewritten as

$$R_w = R \frac{r_w}{r} \frac{U_w}{U} \tag{9.01}$$

Furthermore, from Eqs. 5.29 and 5.30

$$U_{*w}^2 = g r_w S = \frac{f_w}{8} U_w^2 \tag{9.02}$$

$$U_*^2 = grS = \frac{f}{8} U^2 \tag{9.03}$$

Hence,

$$\frac{r_w}{r} = \frac{f_w}{f} \left(\frac{U_w}{U}\right)^2 \tag{9.04}$$

and from Eq. 9.01, putting all the unknowns on the left,

$$\frac{R_w}{f_w} = \frac{R}{f} \left(\frac{U_w}{U}\right)^3 \tag{9.05}$$

$\frac{R_w}{r_w}$ can be calculated by this equation, and f_w can be read from the curve in Fig. 17 (page 119).

Now, compatibility of the bed and wall sections with the total section requires that

$$A = A_b + A_w \tag{9.06}$$

and

$$UA = U_b A_b + U_w A_w \tag{9.07}$$

If $r = A/p$ is substituted into Eq. 9.03,

$$A = \frac{p f U^2}{8gS} \tag{9.08}$$

Similarly,

$$A_w = \frac{p_w f_w U_w^2}{8gS} \tag{9.09}$$

and

$$A_b = \frac{p_b f_b U_b^2}{8gS} \tag{9.10}$$

Substituting Eqs. 9.08 to 9.10 into Eqs. 9.06 and 9.07, and cancelling the common factor, 8gS, the results are:

$$pfU^2 = p_b f_b U_b^2 + p_w f_w U_w^2 \tag{9.11}$$

$$pfU^3 = p_b f_b U_b^3 + p_w f_w U_w^3 \tag{9.12}$$

Rearranging,

$$\frac{f_b}{f}\left(\frac{U_b}{U}\right)^2 = \frac{p}{p_b} - \frac{p_w}{p_b}\frac{f_w}{f}\left(\frac{U_w}{U}\right)^2 , \tag{9.13}$$

$$\frac{f_b}{f}\left(\frac{U_b}{U}\right)^3 = \frac{p}{p_b} - \frac{p_w}{p_b}\frac{f_w}{f}\left(\frac{U_w}{U}\right)^3 \tag{9.14}$$

The two unknowns are f_b/f and U_b/U. By cubing Eq. 9.13, squaring Eq. 9.14 and making the quotient, the solution for f_b becomes

$$f_b = f \frac{p}{p_b} \frac{\left[1 - \frac{p_w}{p} \frac{f_w}{f} \left(\frac{U_w}{U}\right)^2\right]^3}{\left[1 - \frac{p_w}{p} \frac{f_w}{f} \left(\frac{U_w}{U}\right)^3\right]^2} \qquad (9.15)$$

The value of U_b/U may also be found by dividing Eq. 9.14 by Eq. 9.13.

By analogy with Eq. 9.04

$$\frac{r_b}{r} = \frac{f_b}{f} \left(\frac{U_b}{U}\right)^2 \qquad (9.16)$$

Hence, the right hand side of Eq. 9.13 is also an expression for r_b/r; that is,

$$r_b = r\left[\frac{p}{p_b} - \frac{p_w}{p_b} \frac{f_w}{f} \left(\frac{U_w}{U}\right)^2\right] \qquad (9.17)$$

The shear velocity for the bed, U_{*b}, may now be found from the relation

$$U_{*b} = \sqrt{gr_b S} \ .$$

The problem is now essentially solved. Any other quantities, such as A_b or r_w can easily be found from the various fundamental relations. In all the foregoing derivation, the subscripts b and w may be interchanged if so desired.

To compare these equations with the simplified equations given in Chap. V (pages 116-120), consider the same example, Run 28. It will be assumed that $U_w/U = 0.9$, a value which has been found to be reasonable. (Cf. Fig. 10, page 180).

The results are as follows:

Run 28	f_b	r_b ft	U_{*b} ft/sec
Assuming $U_w/U = 1.0$ (Chap. V)	.088	.244	.138
Assuming $U_w/U = 0.9$	.0875	.249	.140
	f	r	U_*
Without using any side-wall correction (values for whole channel)	.062	.172	.116

In comparing the results with the average values for the whole channel, it is obvious that the side-wall correction is necessary to get values of f_b and U_{*b} which are representative of the sand bed alone, but it appears that taking the simple case of $U_w/U = 1.0$ is quite sufficient.

From Eq. 9.17 it may be deduced that the biggest difference between the two values of r_b obtained using $U_w/U = 0.9$ and 1.0 will occur when p_w/p and f_w/f are relatively large. Run 29 is an extreme case and yields the following results (see Table 7, page 127, for basic data):

Run 29	f_b	r_b ft	U_{*b} ft/sec
Assuming $U_w/U = 1.0$	.019	.178	.103
Assuming $U_w/U = 0.9$	.0185	.192	.107
	f	r	U_*
Whole channel	.0180	.171	.101

Again the differences are small, partly because the side-wall correction is small anyway. Since for this extreme case the difference in the U_{*b} values found by the two methods is only 4 per cent, it may be concluded that the

U_{*b} values by the simple method based on $U_w/U = 1.0$ will not differ by more than 4 per cent from the values found by the equations in this appendix using $U_w/U = 0.9$ for any of the experimental runs with sand bed.

APPENDIX D

TABULATION OF POINT CONCENTRATION AND VELOCITY MEASUREMENTS FOR RUNS WITH SMOOTH BED

The following tables give the basic data from which the velocity and concentration profiles given in Chap. V, Sec. B (2) and Chap. VI, Section C were drawn. Since the tables herewith include only data which have not already been presented in tabular form in the text, the reader is referred to Tables 7, 9, 11, and others, for many items such as discharge, slope, temperature, friction factor, and sediment discharge.

In the column headings, y is the distance from the bed, u is the point velocity, and c is the point concentration. In most instances the values of c reported are the average concentrations for groups of three consecutive samples. For more details on the procedure used to measure u and c, refer to Chap. III, Sections E and G (1). The distance from the centerline is taken as positive on the north side of the centerline, or on the right when one faces upstream. The station number is the distance in feet from the upstream end of the flume.

Data for the following runs are reported in the tables:

Clear flow: Runs C1, C2, C3, C4, and C6.

0.16 mm Sand: Runs 2, 3, 4, 6, and 7.

0.10 mm Sand: Runs 21 and 29.

TABLE 15

Velocity Measurements

Run C1

(Clear Flow)

Station 27, d = .232 ft

Dist. from centerline, ft	+.005	-.045	.055	-.095	.105	-.195	.205	-.295	.305	-.395	405	.410	.415	.420	.425
Dist. from nearest wall, ft	.431	.391	.381	.341	.331	.241	.231	.141	.131	.041	.031	.026	.021	.016	.011
y = dist. from bed, ft	u = velocity, ft/sec														
.008				2.79		2.67		2.47		2.37					
.013	3.10			3.02		2.81		2.65		2.53					
.018				3.15		2.93		2.74		2.66					
.023	3.34														
.028				3.33		3.12		2.88		2.80					
.048	3.68	3.63	3.63	3.55	3.57	3.31	3.33	3.11	3.12	2.97	2.88	2.84		2.63	
.068				3.72		3.44		3.27		3.03					
.073	3.88														
.098	4.03			3.87		3.62		3.44		3.07					
.148	4.16	4.13	4.13	4.04	4.08	3.82	3.87	3.67	3.70	3.08	3.01	2.95	2.86	2.76	2.60
.178	4.16			4.02		3.84		3.66		3.05					
.208	4.12			3.94		3.71		3.45		2.97					
.213	4.11														
.218				3.89		3.65		3.34							

Table 16

Velocity Measurements

Run C2
(Clear flow)
Station 27, d = .171 ft

y ft	Dist. from center-line, ft	u ft/sec
.010	0	2.64
.015	0	2.80
.020	0	2.93
.030	0	3.08
.050	0	3.29
.070	0	3.44
.100	0	3.62
.125	0	3.69
.140	0	3.72
.150	0	3.72
.100	+.050	3.61
.100	+.100	3.57
.100	+.200	3.38
.100	-.050	3.58
.100	-.100	3.51
.100	-.200	3.36

Table 17

Velocity Measurements

Run C3
(Clear flow)
Station 24, d = .115 ft

y ft	Dist. from center-line, ft	u ft/sec
.010	0	2.12
.015	0	2.24
.020	0	2.34
.030	0	2.49
.050	0	2.66
.070	0	2.78
.100	0	2.86
.070	+.050	2.77
.070	.100	2.77
.070	.200	2.78
.070	-.050	2.78
.070	-.100	2.77
.070	-.150	2.78
.070	-.200	2.80
.070	-.250	2.76
.070	-.300	2.61

Table 18

Velocity Measurements

Run C4

(Clear Flow)

Station 24, d = .225 ft
Centerline

y ft	u ft/sec
.010	1.32
.015	1.39
.020	1.47
.030	1.54
.050	1.66
.070	1.74
.100	1.84
.150	1.93

Table 19

Velocity Measurements

Run C6

(Clear Flow)

Station 20, d = .179 ft

Dist. from centerline, ft	0	-.100	-.200	-.300	-.360	-.400	-.419
Dist. from wall, ft	.439	.339	.239	.139	.079	.039	.020
(y = Dist. from bed, ft)	u = velocity, ft/sec						
.010	2.60	2.54	2.43	2.28		2.14	2.00
.020	2.86	2.77	2.69	2.50	2.43	2.37	2.18
.030				2.62			
.040	3.14	3.02	2.94	2.73	2.71	2.61	2.33
.080	3.45	3.36	3.23	3.05	2.98	2.70	2.41
.120	3.63	3.52	3.38	3.23		2.69	
.160	3.64	3.53	3.33	3.10	2.91	2.61	2.33
.168	3.63	3.50	3.27	3.00			

TABLE 20

Velocity and Concentration Measurements

Run 2
Station 31, d = .284 ft

y ft	Dist. from Centerline ft	Dist. from wall ft	u ft/sec	c gr/l
.010	0	.435	1.53	
.015	"	"	1.70	
.016	"	"		14.5
.020	"	"	1.83	
.021	"	"		9.57
.030	"	"	1.96	
.036	"	"		3.37
.050	"	"	2.17	
.056	"	"		1.59
.075	"	"	2.31	
.109	"	"	2.49	
.115	"	"		0.290
.159	"	"	2.63	
.165	"	"		0.104
.209	"	"	2.66	
.215	"	"		0.028
.246	"	"		0.019
.267	"	"		0.010
.269	"	"	2.59	
.109	-.050	-	2.49	
"	+.050	.385	2.47	
"	.100	.335	2.39	
"	.200	.235	2.20	
"	.300	.135	2.11	
"	.350	.085	2.08	
"	.380	.055	1.98	
"	.400	.035	1.85	
"	.410	.025	1.76	
"	.415	.020	1.72	
"	.420	.015	1.64	

TABLE 21

Velocity and Concentration Measurements

Run 3
Station 25.5, d = .243 ft

y ft	Dist. from Centerline	u ft/sec	c gr/l
.011	0	1.34	12.72
.016	"	1.56	-
.021	"	1.65	5.02
.031	"	1.83	2.78
.061	"	2.14	0.86
.121	"	2.41	0.166
.161	"	2.49	-
.201	"	2.52	0.024
.231	"	2.54	0.014
.061	-.100	2.12	0.81
.061	+.100	2.08	-
.061	+.050	2.15	-

TABLE 22

Velocity and Concentration Measurements

Run 4
Station 25.5, d = .236 ft

y ft	Dist. from Centerline	u ft/sec	c gr/l
.007	0	1.34	-
.012	"	1.60	18.13
.017	"	1.72	11.79
.027	"	1.88	6.72
.057	"	2.21	2.25
.117	"	2.55	0.508
.157	"	2.70	-
.197	"	2.72	0.077
.217	"	2.71	0.043
.057	-.100	2.15	2.28
.057	-.050	2.20	-
.057	+.050	2.20	-

TABLE 23

Velocity and Concentration Measurements
Run 6

Station 25, d = .195 ft
Centerline

y ft	u ft/sec	c gr/l
.011	1.48	16.7
"	1.60	-
.016	1.76	11.0
.021	1.66	-
.021	1.81	-
.021	1.88	-
.026	1.85	4.56
"	2.01	-
.031	1.98	-
"	2.00	-
.041	1.98	2.04
"	2.03	-
"	2.06	-
"	2.09	-
.051	2.15	-
"	2.18	-
.061	2.24	0.98
"	2.30	-
"	2.33	-
.101	2.49	0.227
"	2.51	-
.141	2.51	0.112
"	2.72	-
.161	2.72	0.054

Note: Fluctuations in velocity were caused by large waves on the water surface, which travel up the channel very slowly. The position of the Pitot tube relative to the wave crests and troughs was not recorded.

TABLE 24

Velocity and Concentration Measurements

Run 7

Station 25, Centerline
d = .243 ft

y* ft	u, ft/sec: Under trough of surface wave	Under crest of surface wave	Ave. of trough and crest	Position rel. to waves not recorded	c gr/l
.011	-	-	-	1.64	18.7
.012	1.36	1.54	1.45	-	-
.016	-	-	-	1.76	12.85
.017	1.76	1.64	1.70	-	-
.021	-	-	-	1.89	5.23
.021	-	-	-	1.83	-
.022	1.85	1.78	1.81	-	-
.031	-	-	-	1.98	3.01
.031	-	-	-	2.00	-
.032	2.05	1.93	1.99	-	-
.061	-	-	-	2.20	0.60
.061	-	-	-	2.23	-
.062	2.28	2.18	2.23	-	-
.121	-	-	-	2.47	0.092
.122	2.56	2.42	2.49	-	-
.161	-	-	-	2.62	-
.162	2.72	2.51	2.62	-	-
.201	-	-	-	2.58	0.010
.201	-	-	-	2.69	-
.201	-	-	-	2.70	-
.202	2.78	2.50	2.63	-	-
.202	2.74	-	-	-	-
.221	-	-	-	2.68	-
.221	-	-	-	2.51	-

There were large water surface waves, which traveled slowly upstream, causing fluctuations in the velocities.

*Since the bed is slightly wavy, with fluctuations in elevation of ± .002 ft, y, the distance from the bed, is calculated on the basis of the mean bed elevation.

TABLE 25

Velocity and Concentration Measurements

Run 21

Station 25, d = .236 ft

y ft	Dist. from Centerline	u, ft/sec				c gr/l
		Under trough of surface wave	Under crest of surface wave	Water Surf. Momentarily Smooth	Mean	
.011	0	1.53	1.44	1.50	1.50	28.5
.016	"	1.61	1.58	1.58	1.59	21.1
.016	"			1.60		
.021	"	1.76	1.63	1.69	1.70	18.2
.031	"	1.93	1.79		1.86	13.0
.031	"		1.80			
.061	"	2.21	2.14		2.18	6.65
.101	"	2.48	2.37		2.44	2.94
.101	"		2.41			
.141	"	2.70	2.58	2.64	2.64	
.161	"					0.78
.181	"	2.73	2.62		2.68	
.211	"	2.72	2.64		2.68	0.19
.101	+.100	2.45		2.39	2.39	3.15
.101	+.100			2.38		
.101	-.100	2.45	2.35	2.38	2.38	3.18

There were large water surface waves, which traveled upstream very slowly, causing fluctuations in the velocities.

TABLE 26

Velocity and Concentration Measurements

Run 29

Station 25.5, Centerline
d = .280 ft

Dist. from centerline, ft	0*	0*	+.100	-.100	+.200	-.200	+.300	-.300	-.360	+.400	-.400	-.420
Dist. from nearest wall, ft	.435	.435	.335	.335	.235	.235	.135	.135	.075	.035	.035	.015
y'_b = point gage read. of sand bed, ft	.055	.054	.054	.055	.055	.056	.055	.056	.052	.045	.047	.047
y' = gage reading, ft	u = point velocity, ft/sec											
.067	1.46	1.50		1.50		1.41		1.34			1.50	
.072	1.58	1.59		1.56		1.51		1.44			1.60	
.077	1.65	1.69		1.67		1.62		1.54			1.63	
.087	1.79	1.80		1.81		1.75		1.66	1.72		1.70	1.51
.117	2.10	2.09	2.08	2.09	2.03	2.03	1.91	1.93	1.94	1.76	1.79	1.58
.157	2.36	2.35		2.33		2.27		2.22	2.08		1.86	1.64
.217	2.60	2.61	2.61	2.60	2.55	2.54	2.32	2.36	2.08	1.77	1.81	1.64
.277	2.64	2.65	2.64	2.60	2.60	2.59	2.33	2.37	2.09		1.85	1.66
.300	2.61											
.320	2.56	2.56		2.51		2.43		2.21	2.05		1.83	1.68
		c = point concentration, gr/l										
.067		23.5										
.072		17.7										
.077		14.8										
.087		11.1										
.117		5.53										
.157		2.73		3.00		3.14		2.91			2.84	
.217		0.787										
.277		0.103										
.320		0.031										

*Separate profiles on different days

TABLE 27

Concentration Measurements by Sieve Fractions

Run 29

Centerline, d = .280 ft
Station 25.5

y' = gage reading, ft		.072	.087	.117	.157	.217	Sed Disch. Samples
y = distance above bed, ft		.018	.033	.063	.103	.163	
c = concentration gr/l		17.7	11.1	5.53	2.73	0.787	3.45
150 sieve:	p_i %	8.19	6.67	4.57	3.60	1.67	5.92
	c_i gr/l	1.45	0.74	0.25	0.10	0.013	0.20
170 sieve:	p_i %	30.3	23.3	23.8	18.3	9.74	25.1
	c_i gr/l	5.36	2.58	1.32	0.50	0.076	0.86
200 sieve:	p_i %	37.0	41.3	36.8	34.8	27.3	34.5
	c_i gr/l	6.55	4.58	2.04	0.95	0.215	1.19
250 sieve:	p_i %	10.7	12.0	13.3	14.6	14.9	11.4
	c_i gr/l	1.89	1.33	0.74	0.40	0.117	0.39
Pan:	p_i %	13.3	16.3	21.4	28.6	46.1	22.6
	c_i gr/l	2.36	1.81	1.18	0.78	0.363	0.78